Max-Planck-Institut für Kolloid- und Grenzflächenforschung

Utilization of Graphitic Carbon Nitride in Dispersed Media

Dissertation

zur Erlangung des akademischen Grades

Doktor der Naturwissenschaften (Dr. rer. nat.)

In der Wissenschaftsdisziplin „Kolloid- und Polymerchemie“

eingereicht an der

Mathematisch-Naturwissenschaftlichen Fakultät

der Universität Potsdam

von

Baris Kumru

Potsdam-Golm, im Oktober 2018

Published online at the
Institutional Repository of the University of Potsdam:
https://doi.org/10.25932/publishup-42733
https://nbn-resolving.org/urn:nbn:de:kobv:517-opus4-427339

Table of Contents

1. Introduction

From the dawn of civilization, humans have depended on wood fires followed by fossil fuels as their primary energy supply. However, a steadily increasing demand has created awareness that the sustainability of this model is not possible as the sources are rapidly depleting. In addition, the side effects arising from fires and fossil fuel consumption have been exposed, such as a drastic increase in atmospheric CO_2 concentration.[1] As the problems surmounted, research into alternative and sustainable energy source that is environmentally benign was necessitated. As a result, the awesome and enigmatic power of the sun was turned to once again, as it always has since the beginning of Homo erectus epoch. The metaphors retrieved from the sun have differed through ages. Firstly, it was worshipped as a supernatural entity in ancient Egypt[2] and Sumeria[3] as a significant part of their religion. However, later on, the desire to comprehend orbits of the planets and stars placed the sun as an object instead of God-like entity. Observing planetary motion provided hypotheses related to the changing of the seasons and cosmic events.[4] Essential scientific clues were retrieved by the studies of numerous scientists, notably, Newton, Herschel, Planck and Fraunhofer, which showed rays from the sun are made up of many colors with different energies creating optical spectrum.[4]

It was realized that sunlight can be transferred into energy via utilization of semiconductors, and innumerable of innovations came to follow. Of tremendous importance has been the silicon- and TiO_2-focussed research, but other metal-containing materials such as CdS has been investigated as well. However, the necessity to significantly increase the yield couple with the inherent toxicity of utilizing metal-based semiconductors initiated the search for other materials. Graphitic carbon nitride (g-CN) has since been discovered having the benefits of being metal-free in composition and can be synthesized from abundant and low cost precursors. Diversified applications of g-CN as a heterogeneous catalyst have being presented, however functionality and processability of g-CN must be enhanced for the synthesis of ideal energy-harvesting devices in the future.

Humankind’s innate drive toward development, innovation, explaining seemingly inexplicable events, and designing devices has facilitated today’s technology level. Indeed there were many challenges and obstacles on the way, but humanity has always found a way to proceed even in the

face of adversity. Considering the very short time humans have spent on Earth, the transition from sleeping in caves to skyscrapers, from local limited resources to globalization and an industrial era have been achieved. Similar breakthroughs have occurred in healthcare, i.e. the plague, once killing millions of people, can now be treated with antibiotics. Novel disease treatments have increased average lifetime profoundly. Further, current healthcare studies are overcoming substantial hurdles: It is likely tissue engineering will soon facilitate the synthesis of artificial organs, where synthetic materials will present both mechanical and biological performance similar to natural tissues. Hydrogels, crosslinked hydrophilic polymer networks, are promising as synthetic materials for tissue engineering as high water content of hydrogels are similar to biological tissues. Being mechanically weak under regular synthesis conditions, hydrogel reinforcement can be applied in order to fabricate hydrogels with diverse mechanical features. The synthesis of appropriately reinforced hydrogels will be the first step in manufacturing advanced healthcare materials.

In the present thesis, the applications of g-CN in dispersed media utilizing visible light will be emphasized and the potentials from bio based applications to energy harvesting will be investigated.

2. Background and Motivation

2.1. Carbon Nitride: A Futuristic Semiconductor for Photo-based Applications

Scientific understanding of sunlight has triggered the research about semiconductors, materials which can be employed to transform visible light into energy. Absorption in the visible light range and decent band gap properties are determining factors for semiconductors, providing photoexcitation which allows facilitating chemical processes. Materials like Si or TiO_2 were studied to enhance the knowledge about chemistry and fabrication of energy harvesting devices.[5] In addition, various metal including semiconductors (such as ZnO, CdS, Ta_3N_5, GaP) were reported which expanded the library of semiconductors with different photophysical properties.[6] Despite the fact that reported materials have effective early stage results, several problems regarding manufacturing, long-term efficiency and sustainability are still present.

The search for sustainable semiconductors encountered carbon nitride (CN), a synthetic polymeric structure based on carbon and nitrogen atoms.[7] The metal-free structure is based on repeating units of 'melems' where tri-s-triazine units are connected via nitrogen bridges in defect-rich polymeric structure with slight negative surface charge (Figure 1.1).[8] Theoretically, it was foreseen that novel polymer has 5 different crystal phases with graphitic phase is the most stable allotrope, called graphitic-CN (g-CN).[9] The ideal composition consists of 3C:4N ratio and synthesis procedure is based on condensation of nitrogen-rich precursors at high temperatures under inert atmosphere. Subsequently, properties of the polymeric structure were investigated. It showed excellent stability up to 630 °C, even in air, being non-volatile at high temperatures while total decomposition occurs at 750 °C with no remaining residues.[10] Similar to graphite, stacking due to π-π interaction between sheets causes insolubility in solvents.[10] Thus, it provides characteristic X-ray diffraction (XRD) pattern, which presents two peaks around 13° and 27° due to intraplanar distance of holes and interplanar stacking.[6] However, due to incomplete condensation, defects exist in the final structure.[11]

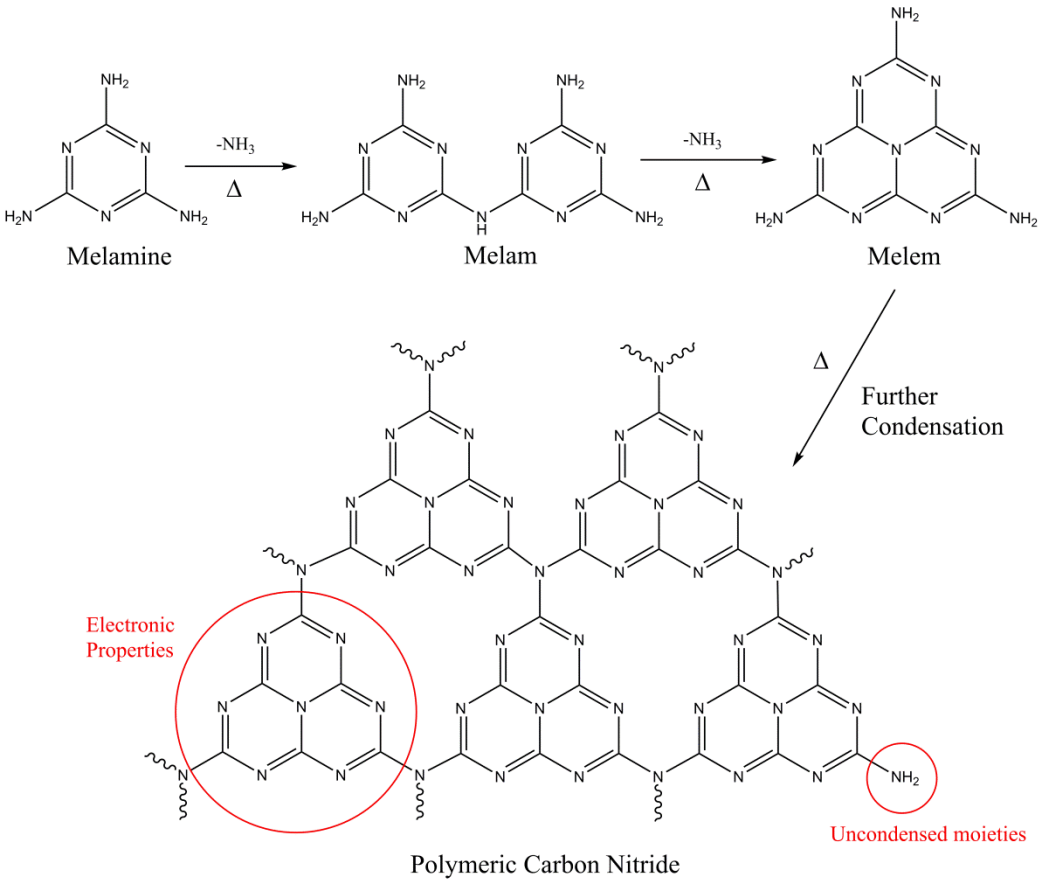

Figure 1.1. Synthesis and structure of polymeric carbon nitride through melamine (nitrogen-rich precursor) via condensation.

Renaissance for the g-CN material began with the investigation of optical properties. Conventional g-CN was shown to be a semiconductor with maximum absorbance at 420 nm which is consistent to its pale yellow color. g-CN also shows blue emission and creates photocurrent in photoelectrochemical cells.[12] Even though appealing properties of g-CN created thriving research, g-CN had some drawbacks such as low dispersibility, high charge recombination rate, low conductivity etc.[6] Apart from the aforementioned properties of g-CN, tunability of physical and chemical properties prolonged the attention as drawbacks might be eliminated with proper modifications in future. Compared to traditional metal semiconductors which have defined composition and structures, g-CN can be tailored to alter the chemical and photophysical properties. Such properties can be considered as porosity, crystallinity, elemental ratio, surface charge, absorption and dispersibility. Modification of g-CN, which can be applied as pre- or post-modification, has elicited many new features for g-CN materials facilitating promising results for variety of photoinduced applications. Diverse nitrogen-rich precursors can

be qualified as g-CN 'monomers', and interestingly changes in the final g-CN products are obtained. Precursors such as melamine, dicyandiamide, urea, guanidine hydrochloride and precursors with additional elements such as thiourea can be employed for g-CN synthesis. Therefore, it is possible to tune the final C:N ratio and photon absorption properties as well as introducing new elements such as sulfur and boron.

For example, utilizing cyanuric acid with melamine and barbituric acid as supramolecular complex monomer for g-CN synthesis shows significant red shift of absorption in final g-CN product.[13] In addition, barbituric acid insertion forms *in situ* in-plane heterojunctions which increases solar absorption yield and charge separation.[13] Direct copolymerization of barbituric acid with dicyandiamide shows similar increase in absorption in final g-CN product via partial replacement of NH_2 groups with methylene, which presents the flexibility of g-CN modification via organic protocols.[14] Employing urea with oxamide results in precursor complex which is crosslinked through hydrogen bonding. Subsequent polycondensation for g-CN synthesis provides a clear absorption above 465 nm which can be ascribed to enhanced n-π^* transition of g-CN.[15]

Morphology control was observed when cyanuric acid-melamine complex was utilized as g-CN precursor. Resulting ordered hollow carbon nitride structures presented reduced fluorescence intensity and improved photocatalytic activity via hole transport pathway.[16] Copolycondensation with precursors including more elements provide doped carbon nitride, e. g. ammoniotrihydroborate (BNH_6) with dicyandiamide yields boron defects on g-CN which reduces the band-gap and fabricates more suitable material for H_2 evolution due to increased photon absorption.[17] Salt-mediated synthesis using potassium salts facilitates a novel kind of carbon nitride (K-PHI) via potassium as template for formation of g-CN with enhanced bandgap properties. Resulting material with heptazine imide as repeating polymeric units presents both photophysical and crystal structure-porosity difference compared to traditional g-CNs.[18] Nitrogen rich precursors with phenyl pendant group can effectively introduce phenyl domains to g-CN sheet after polycondensation, providing significantly increased luminescence behavior due to increased aromaticity on the edges.[19] Not only precursor composition, also condensation temperature can alter g-CN properties. Thus, temperature effect for formation of g-CN from melamine precursor was investigated, which g-CN samples showed differences in crystallinity at low (around 450 °C) temperatures and formation of pure graphitic phase above 550 °C.[20] g-CN

products yielded via thiourea condensation at different temperatures were examined together with photocatalytic activity, similarly products at lower condensation temperatures were not satisfying. However increasing condensation temperatures above 500 °C improves the polycondensation degree and enhanced electron delocalization on aromatic sheets supported by sulfur moiety, thus promoting photoredox properties.[21]

As g-CN was exhibited as heterogeneous catalyst, increased porosity results in enhanced activities. Porosity engineering of g-CN can be achieved via soft or hard templating methods. Utilization of block copolymers such as Triton X-100[22] or ionic liquids such as 1-ethyl-3-methylimidazolium (EMIM)[23] provides well organized g-CN nanostructures with increased pore size. However during condensation, thermal breakdown of the pore templates causes impurities which results in significant amounts of residual carbon in final g-CN structure.[24] Using hard templates such as SBA 15, hierarchical mesoporous g-CN can be obtained with high surface area and interlinked mesopores, which can simultaneously be transformed into metal-carbon composites via reactive templating.[25]

Not only molecular structure and composition, but band gap engineering of g-CN remains a hot topic as it is related to overall efficiency in photocatalytic-energy harvesting applications. First of all, it is important to understand the photophysical concepts of semiconductors. g-CN with filled valence band (VB) and vacant conduction band (CB) exhibits a band gap. Excitation of g-CN with light transfers an electron from VB to CB creating a positively charged hole on VB and negatively charged e^- on CB. Efficient oxidation and reduction can be achieved when the charges are separated and recombination is prohibited (Figure 1.2). As pure g-CN has high recombination rate, g-CN can be engaged to create heterojunctions for manufacturing of advanced catalysts. Employing a material with dissimilar bandgap values to g-CN facilitates new electronic structure, where the interface of semiconductors plays the most important role for efficiency. Commonly it is stated that efficiency of overall photocatalytic process highly depends on the interface, which can induce charge transfer or recombination process.[26]

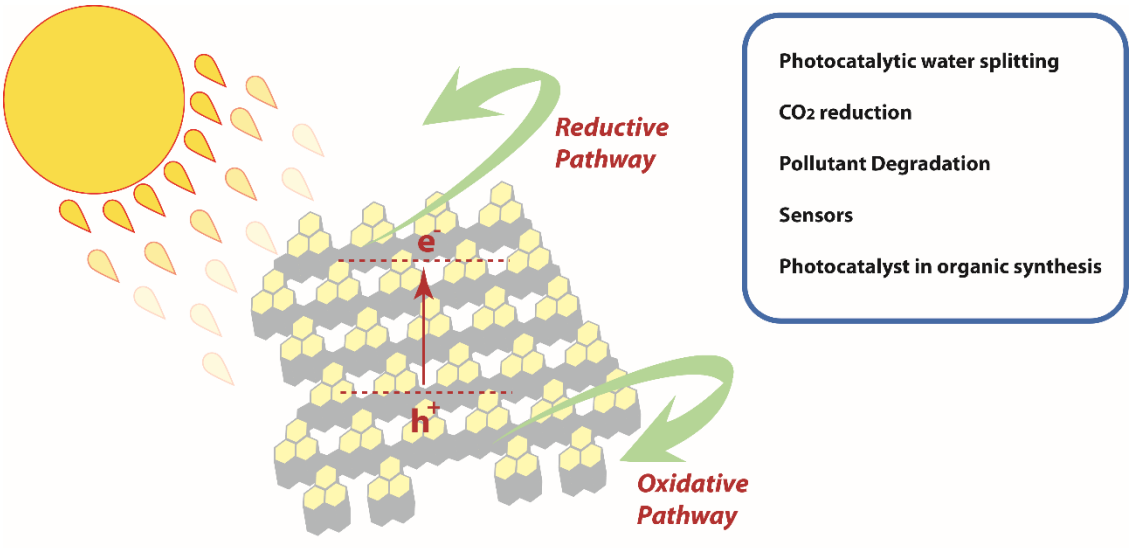

Figure 1.2. Excitation of g-CN and some applications employing g-CN as heterogeneous photocatalyst.

Photocatalytic water splitting is one of the many appealing applications of g-CN heterojunctions. In such a way water is split into hydrogen and oxygen elements in three steps, i) light absorption creates electron-hole pairs in semiconductor, ii) migration of charge carriers to surface, iii) electrons in CB can reduce H^+ to H_2 while hole can oxidize water to O_2.[27] Various metal-g-CN heterojunctions were reported utilizing materials such as TiO_2,[28] Ag_2O,[29] CdS,[30] WO_3[31] targeting different possible pathways for photochemical processes. As an example, formation of g-C_3N_4-TiO_2 yolk-shell composite was investigated for its photochemical activity in water splitting and dye degradation. Enhanced activity compared to pure g-C_3N_4 was observed, which is due to migration of excited electrons on g-CN to CB of TiO_2 resulting in degradative pathway and positive hole of g-CN triggers oxidative pathway.[28] *p*-type semiconductor Ag_2O particles on surface of *n*-type semiconductor g-CN possess matched energy band structure, which promotes multielectron migration pathway (e^- and h^+ transfer from g-CN to Ag_2O). Thus, photocatalytic activity due to elevated charge separation is improved.[29] Formation of metal-free heterojunction structures utilizing carbon-based materials raises significant attention due to electron storage properties and conductivity.[32]

A ruthenium complex on g-CN performs very well for CO_2 reduction to formic acid as final product at ambient conditions.[33] Excited g-CN electrons on CB migrate to the Ru complex which promotes reductive pathway, and hole of g-CN reacts with sacrificial electron donor. In contrast, photocatalytic system composed of g-CN, cobalt complex and triethanolamine (TEOA) improves

charge separation rate, which endows significantly increased CO_2 photoreduction to CO and H_2 in water-acetonitrile mixture.[34] g-CN can also be utilized for dye degradation, as an example study showed that photoexcited g-CN electrons in CB can reduce the dissolved oxygen to create superoxide radical, which can oxidize sulfamethazine on the g-CN surface.[35] Thus, organic pollutants in water can be oxidized employing mesoporous g-CN under visible light. Oxidation of 4-chlorophenol was investigated, and it was shown that radical species formed via g-CN (H_2O_2, $^{\cdot}OH$, $^{\cdot}O_2$-, $^{\cdot}OOH$) serve for photocatalytic oxidation of pollutants.[36] g-CN is a highly active heterogeneous photocatalyst that provides outstanding applications, especially with proper modifications.

For further expansion of applications, especially the areas of optoelectronics or solar cells, encountered a solid obstacle. Even though g-CN was shown to be a striking heterogeneous catalyst, processing of bulk g-CN is problematic due to colloidal instability of g-CN. At this point it is necessary to discuss the aspects regarding the stability of colloidal systems. Colloids can simply be defined as dispersed particles in a medium where they do not dissolve. It is possible to find colloids in daily life, i.e. milk, mayonnaise and blood.[37] Colloids can be considered to be prepared via two different approaches; namely dispersion and condensation.[38] Dispersion is based on either applying mechanical energy (such as ultrasonication) or additives (such as surfactants) to form a colloidal system. Condensation method is commonly utilized for aerosols and emulsions to condense small dissolved molecules into larger colloidal particles.[37]

The stability of particles in dispersion can be explained with thermodynamic aspects of the system and is related to the minimum total free energy.[38] As random collision of particles take place (Brownian motion), factors such as temperature, pressure, solvent properties and concentration affect the colloidal stability. Dispersion is a kinetic system and interaction of particles might lead to sedimentation. Thus, atoms or molecules being separated from the dispersing media leading to formation of heterogeneous mixture.[37] The main forces which influence interaction of particles are attractive (van der Waals-London) and repulsive (electrostatic and steric) forces.[38] Stable colloids comprsie a system where no sedimentation or aggregation is observed (when repulsive forces are stronger than attractive forces) and generally defined with time scale, i.e. dispersion is stable for some hours or days (Figure 1.3).

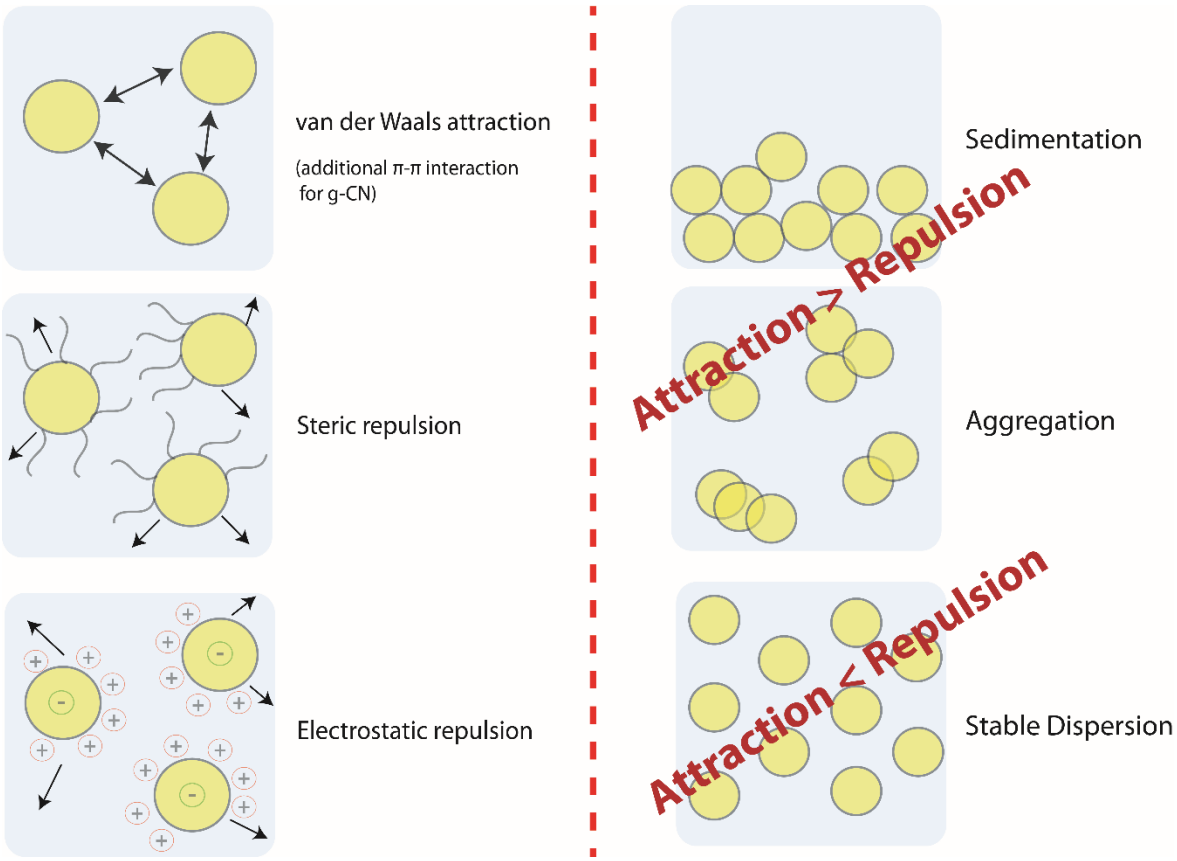

Figure 1.3. Main attractive and repulsive forces on colloidal particles and terms arising for colloidal systems.

Fluctuations in electron density create temporary dipole moment on particles, which create attractive potential energy. Arising from quantum mechanical considerations, movement of electrons promote interim change in dipole moment of particles, via reversing the direction of charge and creating attractive forces over time average.[39] Such an alternation generates energy which is much higher than gravitational potential energy of particles, which leads to van der Waals attractions of colloids.[39] Repulsive forces can be divided into electrostatic and steric forces. Using macromolecules (usually non-charged) adsorbed on particle surface facilitates steric force and therefore steric stabilization.[37] Upon attraction of two particles with macromolecules absorbed on the surface, osmotic effect increases concentration and solvent pushes itself to interface resulting in loss of entropy. In order to balance the entropy, particles move apart, which prevents sedimentation or aggregation.[38] Electrostatic stabilization arises from Coulombic repulsion between charged particles. Counter ions and surface charge form electric double layer (EDL), thickness of double layer and surface potential at Stern layer (size of particles as well) are main factors which determine electrostatic stabilization. Zeta potential

measurement is helpful to estimate the colloidal stability of the system via providing information about magnitude of electrostatic potential of the particles.[38]

Colloidaly stable g-CN dispersion is the main requirement for successful photovoltaic and optoelectronic applications of g-CN. Therefore, some researchers showed interest in g-CN functionalization for facile processing of g-CN. g-CN sheets contain strong van der Waals interactions which promotes sheet accumulation, and etching g-CN sheets with strong acid was one of the approaches for exfoliation based dispersion preparation. For example, bulk g-CN powders can be oxidized via $K_2Cr_2O_7$-H_2SO_4 mixture to yield dispersible and porous g-CN structures, but such harsh oxidizing conditions are not favorable for applications.[40] Employing montmorillonite as exfoliator in ultrasonication forms highly dispersed g-CN sheets in water, however the presence of high amount of montmorillonite fixed on the g-CN surface (1:1 w/w) can be undesirable for some practical applications.[41] Stable g-CN nanosheets in water were created with oxygen plasma method via protonating hydroxylamine groups on the surface of g-CN, however once again modification conditions limit the applicability.[42] Discussed reports were focused on dispersibility of g-CN in aqueous media providing in-situ dispersibility with additives. However applicability was limited. Employing low amounts of g-CN and long ultrasonication times (more than 24 hours) can be considered as another approach,[43] it yields pure g-CN dispersions however scaling or industrial manufacturing is challenging as well.

A promising application for luminescent g-CN might be bioimaging, which requires highly dispersible and colloidaly stable g-CN particles. Low condensation temperature for g-CN formation is the synthetic approach of g-CN based quantum dots (QD). Inhibiting tri-s-triazine sheet polycondensation at low temperature provides small sheets or dots formation, with highly uncondensed moieties (NH_2 and OH edges) presenting hydrophilic character. For example, human urine was employed as a precursor for the synthesis of fluorescent g-CN at 200 °C.[44] Resulting g-CN showed water dispersibility and colloidal stability due to formation of g-CN QDs with much less polycondensation degree compared to traditional g-CN. Similarly, mixing urea and sodium citrate in different ratios and polycondensation at 180 °C in autoclave results in formation of g-CN QDs with high fluorescence, where the PL emission can be readily shifted via variation of precursor ratios.[45] Aforementioned applications combined water dispersible g-CN QDs with luminescent properties of g-CN. PL mechanism of g-CN was expected to be related to π-π^* transition, however recent studies showed that PL arises from the interaction of lone pair of

nitrogen atoms with polymeric structure (π) of carbon nitride.[46] Not only water dispersions of g-CN QDs, but also highly condensed g-CN powders can benefit from luminescent properties. Highly fluorescent g-CN powder was synthesized from urea and trimesic acid precursors at 500 °C which can be employed for fingerprint imaging. In that report, doping g-CN with phenyl groups was shown to shift the emission spectra of g-CN to green light, and object imaging can be achieved very precisely.[47]

As the interest for optical properties of g-CN has developed, interest for g-CN thin films has increased collectively as uniform thin films are main requirements for solar energy harvesting devices. Two important studies have shown that synthesis of doped g-CN on FTO films can be utilized for photovoltaics[48] and light emitting diodes (LED).[49] Film synthesis was conducted via polycondensation of g-CN precursor over FTO under inert atmosphere. However, high film thickness, reproducibility and processability are the main problems, yet the studies have elucidated the potential of g-CN. Unlike previous applications which were conducted in aqueous environment, such systems require either high colloidal stability of g-CN particles over a variety of organic solvents for solution based processing, or costly instruments for vapor phase processing via physical or chemical vapor deposition. For both approaches, unfortunately there is no solid background yet.

Considering the future development of society, energy issues would be solved via effective utilization of sun as the main energy source. Shifting from heavy metal containing systems to metal-free and sustainable energy harvesting devices creates opportunities and challenges at the same time. g-CN was found to have many advantages compared to other semiconductors, and tunability of g-CN created enormous scope in the field, with variety of applications from water splitting to bio imaging. Remarkable performance of g-CN in heterogeneous systems is effectively being utilized and more and more research is being presented, however expansion of knowledge for the chemistry of g-CN is not linear in that sense. There is a whole new world waiting for g-CN, which is based on dispersible systems. Many key applications such as photovoltaics and energy harvesting will depend on colloidaly stable dispersions of g-CN, especially in organic solvents. Additionally, durable dispersions of g-CN should base on the bulk g-CN properties instead of in-situ additives to afford pure dispersions. All of these factors should be considered together with exciton stability, suitable interface formation, absorption and charge

delocalization properties of g-CN. Understanding the working mechanism of g-CN and adjusting the material properties indeed will be the main factor for designing the future.

2.2. Carbon Nitride in Polymer Chemistry: State of the Art

Properties of g-CN were also appealing for polymer chemistry, there is an increasing number of publications since 2015 which intensify the applications of g-CN in polymers. The first report was from Yagci, Wang and Antonietti, showing visible light photoactivity of g-CN combined with photopolymerization.[50] Utilization of mesoporous g-CN with co-catalyst for free radical polymerization of methyl methacrylate (MMA) in organic media was reported. The experimental set-up was typical for free radical polymerization, g-CN was utilized as heterogeneous photoinitiator and tertiary amine as co-initiator in the system. Polymerization was successfully attained, with typical free-radical polymerization kinetics. Proposed mechanism was based on the excitation of g-CN via visible light and electron-hole formation, followed by i) oxidation of tertiary amines creating positive charge and radical by hole, ii) radical on tertiary amine initiates polymerization, iii) electron created via photoexcitation reacts with positively charged tertiary amine (Figure 1.4).[50]

Two years later, g-CN was utilized in photochemically controlled atom transfer radical polymerization (ATRP) for precise control of polymer molecular weight. g-CN was employed with copper (II) species, ligand, MMA monomer, ATRP initiator and photoinduced polymerization was investigated.[51] Polymerization was achieved in controlled manner with low molecular dispersity, and living character of polymerization due to functional end groups on polymer chains was indicated via chain extension. The mechanism was based on photoexcitation of g-CN which forms electrons and holes. Electrons in CB promote reductive pathway via reducing copper (II) to ATRP active copper (I) species which can initiate the controlled polymerization, and photoexcitation based mechanism was verified via light on-off experiments (Figure 1.4). Utilization of visible light and ease of g-CN separation after reaction provides satisfactory route for polymer synthesis.[51] A similar route was applied for photoinduced azide-alkyne cycloadditions, where photoexcited g-CN electrons promote reductive pathway. Coupling of variety of organic molecules containing azide and alkyne groups with high efficiencies were demonstrated via triazole ring formation via g-CN mediated in situ reduction of Cu (II) species to active Cu (I) catalyst.[52] Additionally, photo induced electron/energy transfer (PET) reversible addition−fragmentation chain transfer (RAFT) polymerization employing g-CN was reported.[53]

Similarly, formation of excited electrons upon irradiation of g-CN was followed by interaction with special RAFT agents initiating controlled polymerization (Figure 1.4). Benign polymerization conditions and low molecular dispersity along with chain extension was reported for methyl acrylate (MA), butyl acrylate (BA) and *N*,*N*-dimethylacrylamide (DMA). g-CN was also reported to reduce dissolved O_2 in the reaction medium therefore polymerizations can be achieved without deoxygenation or monomer purification. Tertiary amines were needed as co-initiator.[53] Overall, g-CN was successfully utilized as heterogeneous catalyst for polymerization and coupling reactions in organic media.

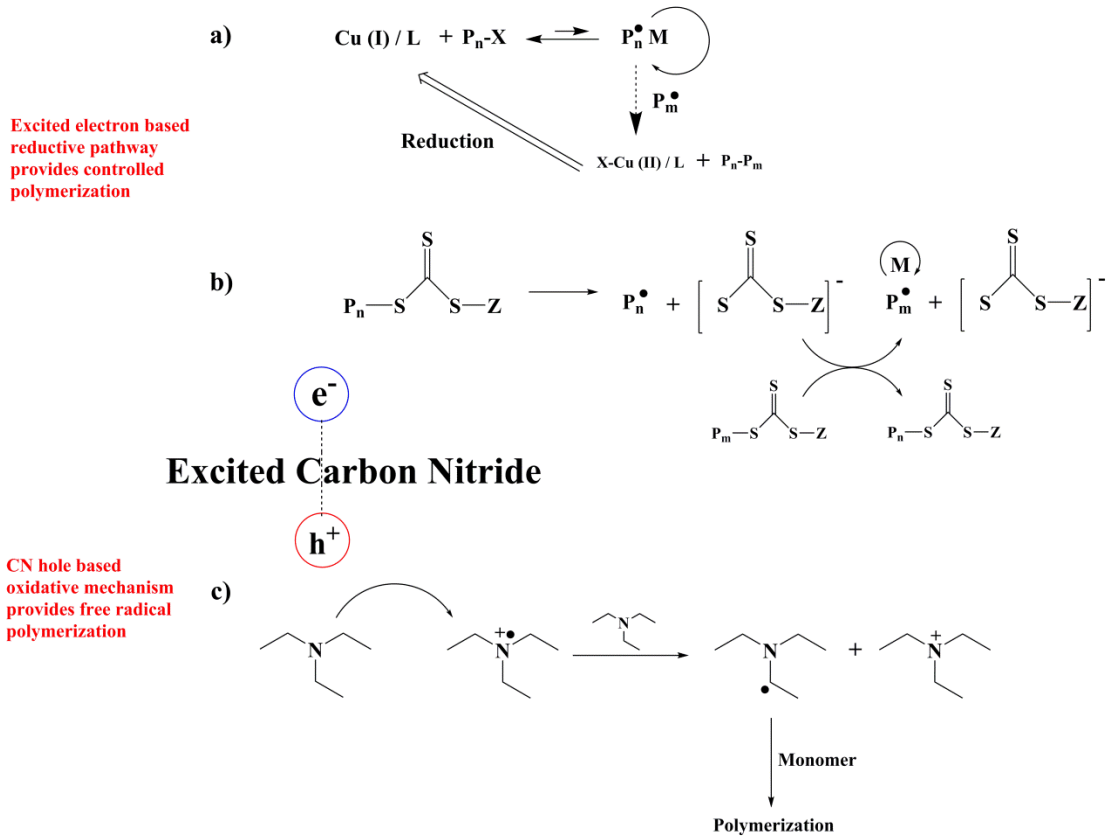

Figure 1.4. Proposed radical formation and polymerization mechanism via photoexcitation of g-CN in organic media, **(a)** ATRP, **(b)** RAFT and **(c)** free radical polymerization mechanisms.

Not only in organic media, organic-water 'interface' applications of g-CN were also investigated. g-CN was demonstrated to perform as Pickering emulsion stabilizer, which is an emulsion stabilized via addition of solid particles.[54] The structure of g-CN consists of hydrophobic conjugated framework (tri-s-triazine rings) and hydrophilic non-condensed groups, such an amphiphilic character drives g-CN to the interface of aqueous-organic mixtures. g-CN behaves as

colloidal surfactant which allows dispersion of hydrophobic carbon materials such as graphite and carbon nanotubes.[54] When organic phase is filled with styrene monomer, g-CN stabilized uniform styrene droplets were formed in water, and polymerization of styrene was conducted via radical species initiating at 70 °C. Uniform size distribution and smooth surface for polystyrene (PS) latex with embedded (non-covalent) g-CN was exhibited, the left-over g-CN on the outer surface was simply removed via centrifugation. PS microspheres with well-defined size distributions were obtained for fabrication of photonic crystals.[55]

In addition, applications of g-CN in aqueous media were investigated. Hydrolysis of g-CN under aqueous alkaline conditions promotes exfoliated g-CN fiber formation. A CO_2 stream generates hydrogel formation via assembly of g-CN fibers, and resulting 3D network was utilized for dye absorption. Furthermore, sol-gel transition of a hydrogel was demonstrated, i. e. hydrogel could be converted to uniform dispersion via N_2 stream.[56] g-CN assembly approach was followed for the formation of g-CN aerogels. Salt templated g-CN nanoparticles containing highly uncondensed hydrophilic edges were dispersed in water. Hydrogel formation was observed over long periods of standing due to assembly of g-CN nanoparticles, and subsequent freeze drying resulted in aerogel formation. Pure g-CN aerogel was endowed with high photocatalytic activity.[57] Co-assembly of g-CN with peptides presented highly creative application. Fmoc-diphenylalanine peptide has aromatic interactions and hydrogen bonding, which leads to high tendency for self-assembly in aqueous solutions. Dispersions of g-CN were mixed with Fmoc-diphenylalanine, which spontaneously undergoes hydrogel formation due to hydrogen bonding and enhanced π-π stacking. Non-covalent hydrogel was a model for light harvesting photosynthesis scaffold, excitation of g-CN and enzymatic energy conversion through peptide was an example for light responsive redox biocatalysis.[58]

As g-CN has high thermal stability, embedding g-CN in polyacrylamide hydrogel for gel electrophoresis was investigated. g-CN dispersion was mixed with acrylamide monomer, crosslinker and gelation was achieved by radical initiation via redox couple. Existence of g-CN significantly increased thermal conductivity of the gel and band resolution of electrophoresis, which is promising for improved separation efficiency.[59] A similar strategy was followed for the synthesis of g-CN embedded polyacrylamide-acrylic acid hydrogel. The composite hydrogel was prepared by radical polymerization via redox couple, in aqueous solution containing g-CN

nanosheets, monomers and crosslinker. High fluorescence, which is served by g-CN, was employed as fluorescent probe of Ag^+ species.[60]

Covalent attachment of g-CN to polymeric hydrogel network was also investigated. Aqueous g-CN dispersion containing monomer and crosslinker can be irradiated with visible light. In this case, g-CN acts as photoinitiator, and covalently connects to polymer network. Presented study showed the photocatalytic activity of resulting g-CN based hydrogels, demonstrating dye degradation kinetics, however reinforcement due to g-CN was not investigated.[61] As g-CN sheets are two dimensional structures, radicals form on opposing surfaces upon visible light excitation. Therefore, g-CN also has crosslinker character in addition to photoinitiation. Such phenomenon was examined via irradiating aqueous g-CN dispersion containing only monomer (*N*-isopropyl acrylamide), providing soft hydrogels with tunable turbidity.[62] Oxidative polymerization of aniline in g-CN dispersion introduces polyaniline formation between g-CN nanosheets. Composite hydrogel with g-CN-polyaniline heterojunction was demonstrated as photocatalytic platform for dye degradation in aqueous media.[63] Mixture of g-CN dispersion with sodium alginate promotes formation of a viscous liquid which can be 3D printed. Addition of $CaCl_2$ solution crosslinks alginate units, and Au nanoparticles were loaded for heterojunction formation with g-CN. Patterned aerogel membrane were fabricated via supercritical drying of hydrogel, which can be implemented for solar wastewater remediation.[64] Phenyl doped g-CN was previously reported due to its fluorescent properties. Physical mixing phenyl doped g-CN with a class of water soluble π conjugated polymers, such as poly[(9,9-bis(6′-((N,N,N-trimethylammonium)hexyl)-2,7-fluorene)-co-4,7-di-2-thienyl-2,1,3-benzothiadiazole] dibromide, facilitates full-color emission materials for cell imaging.[65] Polyethylene glycol (PEG) groups were attached on oxidized g-CN surface, covalently via mesyl groups. Resulting water dispersible nanodots were utilized for metal-free cell bioimaging probes.[66] Mixing bulk g-CN with ionic liquids (IL) under hydrothermal conditions result in exfoliated g-CN sheets. IL fixed on g-CN surface triggers subsequent reversible hydrogel formation, which was explored for gas sensing applications.[67]

As summary, integration of g-CN into polymer chemistry has started in 2012 and has shown significant increase since 2016. Besides presenting alternative routes for prevalent reactions (such as controlled polymerizations), novel approaches such as emulsion stabilization were demonstrated as well. g-CN can be applied in organic media, at the organic-water interface and

aqueous media showing diverse properties. Photoexcited g-CN electrons were employed through reductive mechanisms in organic media, utilizing g-CN as heterogeneous catalyst in controlled polymerization and azide-alkyne coupling reactions. Well defined latex particles can be obtained via g-CN as emulsion stabilizer, which is embedded in final polymer particles presenting optical properties. In aqueous media, hydrogel formation with g-CN found variety of applications, from photocatalysis to sensing. Drying g-CN based hydrogels establishes g-CN aerogel synthesis, which similarly can be utilized as photocatalytic scaffolds. Modified g-CN particles dispersed in aqueous media were shown as bioimaging agents. Despite the field is relatively new, understanding g-CN based reaction mechanisms and perceiving possible modifications via polymer chemistry are a promising avenue for improving g-CN properties.

2.3. Biological Tissues and Hydrogels: Strong Relation

Throughout history, much before than discovery semiconductors or utilization of fossil fuels, human health has been one of the major topics. Since the first days of human evolution, human beings always tried to offer solutions regarding health problems.[68-70] Early ages passed via understanding the causes of diseases for prevention. Later on 'intervention' has started, meaning diseases were tried to be cured with ancient methods such as primitive instruments or herbal mixtures.[71-73] Years of biological research provided background about human tissues and their structure.[74] Human tissues have characteristic properties which evolved over millions of years to perform a task.[75] Differences in water content or biochemical ingredients endow variety of mechanical properties in natural tissues.[76] Human tissues can be considered as mechanical wonders, i.e. skin and articular cartilage. Yet, mimicking skin and articular cartilage via synthetic materials is one of the main challenges in healthcare research.

As the largest organ of the human body, skin serves as a barrier for pathogenics, dehydration and ultraviolet (UV) light.[77] Skin is composed of two distinct layers, the epidermis and dermis, approximately every 20 days skin is renewed. Skin contains high amount of water (more than 80 %) with moderate flexibility and extreme stability under load. When skin is damaged, i.e. the barrier is ruined, human body becomes vulnerable against pathogens, which results in immediate and serious infections. Wounds can be classified as acute and chronic, based on the time to heal.[78] Acute wounds usually heal between 8-12 weeks with minimal scarring, and the primary causes are friction, tear or abrasion of skin. Chronic wounds, however, are not healed beyond 12 weeks and generally observed with other diseases.[79-80] Defenseless skin must be well protected during

healing periods and major injuries. Especially burns or deep cuts, require more specialized materials for protection called wound dressings.[81] Wound dressings should be oxygen permeable, antibacterial and contain water to mimic the functions of skin on minimum level.[82-83] Indeed it should be affordable, and application should not restrict the daily life activities of patient during healing period.[84] As it is applied onto skin, skin-like feeling should bring extra comfort for utilization of wound dressings.[85] Burns, for example, cause wounds that might be critical regarding burn degree, and require special treatment as the skin is damaged and dehydrated at the same time.[86] Considering the high numbers of serious burns (1.2 million in United States per year) and chronic skin ulcers (6.5 million in United States), wound dressings created an enormous market with 15 billion dollars per year in United States alone.[87]

Regarding skin, another interesting and highly creative application was suggested recently, called 'wearable electronics'.[88] High demand of personalized medication created innovative approaches which would promise personalized treatment to individual patients.[89] As discussed previously, skin was one of the main inspirations for such a development. Human body is composed of electrolytes which can be imagined as moderately conductive network.[90] Touching, for example, is sensed via ultrafast delivery of electrostatic interactions to the brain.[90] Therefore, common literature investigates wearable electronics based on conductive networks with high flexibility with well tensile properties.[91] Such a design relies on tracking physiological signals arising from skin and transfer into digital signals.[92] In such a way, the health status of a patient can be monitored continuously over long periods. Therefore possible risks can be diagnosed immediately and specific treatment would be presented.[93] It has been foreseen that such a market will grow to 1 trillion dollars in 2020 as world population is getting older, and smart solutions would improve the lifestyle of many human beings.[94] Overall, fabrication of skin like materials remains as one of the hottest topics both in academic research and healthcare market.

Considering human tissues, also articular cartilage should be discussed, which can be found in joints. Articular cartilage is a mechanical masterpiece which consists of 70% water and collagen type II fibers. It can bear enormous cyclic loads from the human mobility in daily life, i.e. walking or running (around 8 MPa).[95] Such a system would have significant wear problems, thankfully Nature provided a smart solution which allows movement of human beings. The secret for the extraordinary mechanical performance with fatigue resistance over long periods was not only the toughness of articular cartilage, but also introduction of lubricant properties.[96] Joint is

composed of charged proteoglycans in synovial fluid which provide ultra-low friction during the load. Therefore long-term performance to articular cartilage is granted. However, increased lifetime expectancy caused discovery of new problems which probably did not exist previously. Especially articular cartilage starts having wear problem with aging, which reduces mobility and decreases life standards. [97] As a result, joint replacement became one of the typical treatments regarding healthcare; however it is not so straightforward. Current technology suggests ultrahigh molecular weight polyethylene (UHMWPE) alloys for joint replacement surgery, though long term usage is not possible and surgery needs to be applied regularly.[98] An innovative solution is required for joint replacement to provide long term stability and minimized application effort, ideally even without surgery.[99] Developments in biology revealed the compositions and functions of natural tissues. Unlike early ages, humankind has progressed considerably for disease treatments, however new problems require new answers. Skin and articular cartilage are just some examples of natural tissues where permanent solutions and synthesis of synthetic replicas would significantly increase life quality of humans.

In recent years a novel class of materials was established, so called 'hydrogels'. Hydrogels consist of crosslinked hydrophilic polymer chains forming 3D networks with high water absorbance capacities. Thanks to the crosslinked nature, hydrogel networks do not dissolve in water, but swell.[100] Indeed such definition resembles biological tissues, which contains significant amounts of water embedded in 3D networks. Later on, considerable attention was observed for hydrogel research to provide a spectrum of materials that are similar to natural tissues.[101] Following the hydrogel definition, simple synthesis conditions were not satisfactory to provide functionalities to hydrogels, therefore different synthetic approaches were investigated. As the research expanded, highly functional hydrogels are introduced via utilization of chemical advances. Before starting the classification of hydrogels, it is important to talk about crosslinking. Crosslinking enables connection of polymeric chains in the network. Thus it is responsible of many parameters such as elasticity, toughness, insolubility and increased glass transition (T_g) temperatures.[102] A first classification can be carried out according to the nature of crosslinking, namely chemical hydrogels and physical hydrogels.[103] Chemical crosslinking indicates covalent bonding that forms the polymer network, which can be applied utilizing chain growth polymerization, addition and condensation as well as gamma ray polymerizations.[102] Chain growth polymerization proceeds via monomers attaching to active side of growing polymer chain

one at a time.[104] In hydrogel synthesis, free radical polymerization is favored over ionic polymerization due to feasibility. Free radical polymerization begins with radical formation, an initiator forming active radicals due to decomposition from heat or light.[105] Radical is added from initiator to monomer, which initiates the polymerization. Addition of monomers to the active site advances the chain length by each addition, which is called propagation. Terminal monomer carries the active site for the addition of next monomer. The propagation of the polymer chains ends with termination or disproportionation. Termination is when active radicals, either on chains or small molecules combine. Disproportionation results in one double bond formation in one chain.[105] Figure 1.5 shows the linear growth of the polymer chain with one active double bond. If the monomer contains more than one active double bond, i.e. crosslinker, it connects polymer chains and therefore crosslinks the structure (Figure 1.5). Oxygen moieties in solutions or stabilizers terminate or slow down chain propagation.

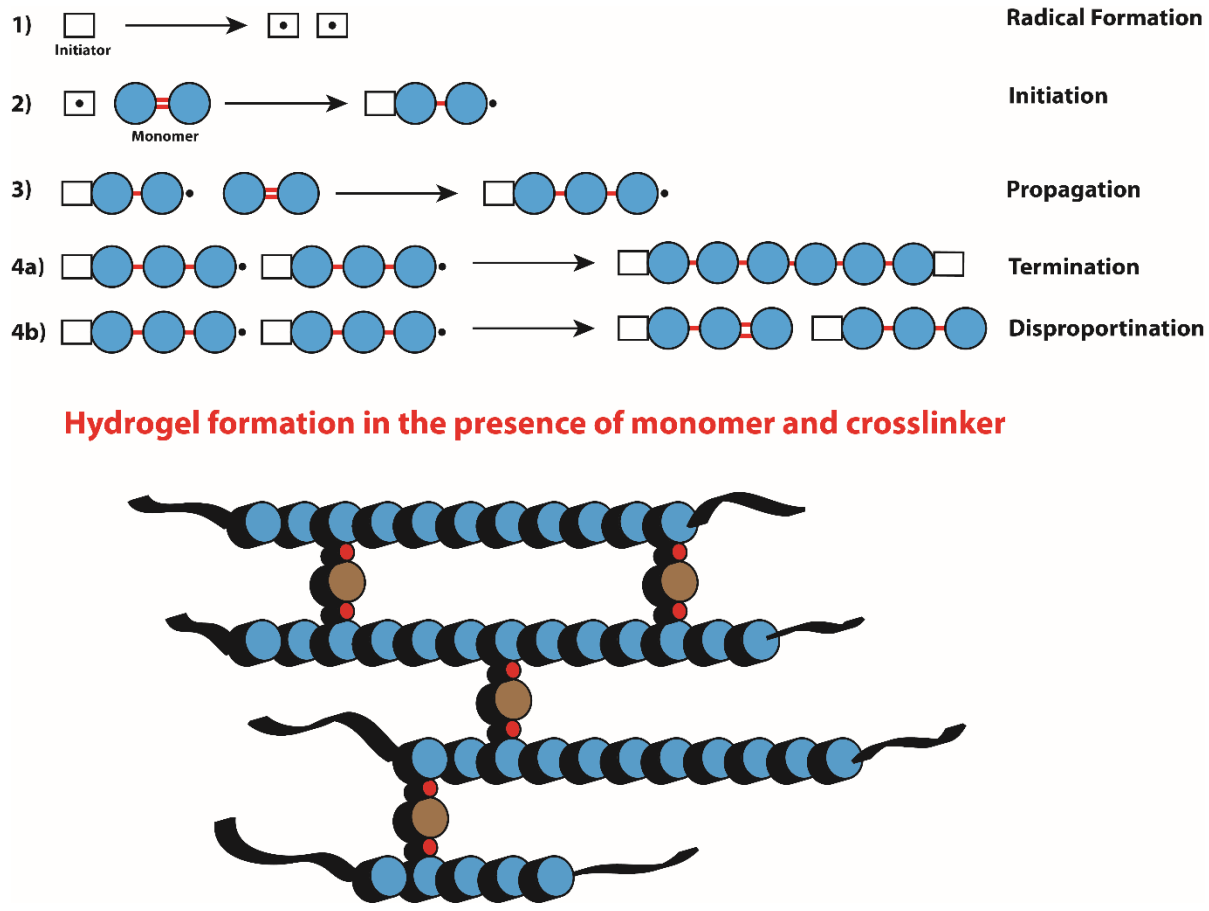

Figure 1.5. Mechanism for radical polymerization and scheme showing hydrogel formation.

Addition polymerization process is completed in three steps as chain initiation, propagation and termination. Chain reaction adds new monomer units to growing chain through double bonds. As a summary, chemical hydrogels are formed via covalent crosslinking, bond is irreversible and stable against degradation.

Physical crosslinking indicates crosslinking via physical interactions instead of covalent bond formation. Physical interactions which are employed for hydrogel synthesis are ionic interaction, hydrogen bonding, hydrophobic interaction, crystallization and π-π interaction.[106] Aforementioned interactions are weaker but dynamic compared to covalent bonding, therefore physical hydrogels are generally considered reversible.[107] Charge interactions may be introduced via utilizing charged polymer and oppositely charged small molecule as linker, or via utilization of oppositely charged polymer chains leading hydrogel formation. As gelation and de-gelation is pH dependent, such hydrogels can be tailored to have specific performance at different pH.[108] Hydrogen bonding offers strong interaction between molecules e.g. hydrogels can be fabricated via dissolved polyvinyl alcohol (PVA) linear polymers in defined concentrations.[109] In addition, some natural biocompatible materials such as sugars, cellulose and hyaluronic acids form significant amounts of hydrogen bonds, which enable formation of hydrogels via hydrogen bond interactions.[110-111] Hydrophobic interactions require hydrophilic and hydrophobic domains in polymer chains, thus hydrogel formation generally depends on temperature and concentration. Poloxamer (PX) is ABA type triblock copolymer composed of poly (ethylene oxide) (PEO) as hydrophilic and poly (propylene oxide) (PPO) as hydrophobic core, and hydrogel synthesis from dissolved PX can be achieved via controlling temperature and concentration.[112] Stereocomplexation is based on employing similar molecules with different stereochemistry, such as D- and L- polylactide. Difference in tacticity induces strong interaction resulting in hydrogel formation.[113] Materials with strong aromaticity benefits from π-π interactions for hydrogel synthesis. For example graphene, with high aromaticity and sheet like structures assembles at certain concentrations yielding hydrogels.[114] Physical crosslinking provides dynamic non-covalent interactions to hydrogel network, and presents variety of properties to hydrogels. Overall, crosslinking is the most important factor to present non-solubility to hydrogel network, which can be applied via various methods.

Once the hydrogel is formed, swelling plays an important role for the performance of the material. As hydrogels contain hydrophilic domains, water absorption through hydrogel matrix

starts when dry hydrogel is in contact with water. Primary bound water initiates swelling by moving through hydrophilic domains in hydrogel network. Secondary bound water defines the interface of hydrophobic domain and water in hydrogel network.[106] Most of the swelling models are based on Fick's diffusion law, as infiltration of water into hydrogel network is diffusion driven. Expanding typical equation with mass transport, Equation 1 is used to calculate swelling kinetics (c: concentration of diffusing species, D: diffusion coefficient, ϑ: convective velocity of solvent).[115] Swelling ratio is defined via Equation 2 which is based on the mass of dry (W_d) and swollen (W_s) hydrogel samples. Crosslinking polymer chains form porosity in hydrogels and porosity is related to swelling performance of hydrogels. Porosity can be calculated using equation 3 employing absolute ethanol as eluent (M_1 and M_2 stands for mass of hydrogel before and after immersion, ρ is density of absolute ethanol and V is volume of hydrogel).[116] Not only swelling capacity, but also retention plays an important role in some applications, even in agricultural sciences.[117] Equation 4 shows calculation of water retention (WR_t) using swollen mass (W_s), dry mass (W_d) and mass at different exposure times (W_p).[116]

1. $\frac{\partial c}{\partial t} = D\frac{\partial^2 c}{\partial x^2} - \frac{\partial}{\partial x}c\vartheta$

2. $Swelling\ Ratio = \frac{W_s - W_d}{Wd} \times 100$

3. $Porosity = \frac{M_2 - M_1}{\rho V}$

4. $WR_t = \frac{W_p - W_d}{W_s - W_d}$

Equation 1.1. Equations regarding swelling of hydrogels.

After discussing two of the most important parameters for hydrogels, namely crosslinking and swelling, further classifications can be assessed according to the components employed. Variety of hydrophilic components can be utilized for hydrogel synthesis, which can be natural or synthetic according to the origin.[118] Natural monomers possess biocompatible identities and common natural components for hydrogel synthesis are chitosan, collagen, fibrin, chitin, cellulose, gelatin and hyaluronic acid derivatives.[119] Hydroxyl and amino functionalities in natural components serve for hydrophilicity, however high molecular weight and limited chemistry restrains synthesis conditions. On the other hand, synthetic monomers represent a

significant class of materials with variety of functionalities. Common monomers are poly (ethylene glycol) (PEG) based acrylates, lactic acid, caprolactone, *N*-vinyl pyrrolidone, acrylamide (AAm), *N*,*N*, dimethyl acrylamide (DMA), *N*-isopropyl acrylamide (NIPAM), hydroxy ethyl methacrylate (HEMA) and some charged monomers such as 3-sulfopropyl methacrylate potassium salt (SPMA) and [2-(methacryloyloxy)ethyl] trimethylammonium chloride.[119] Various functionalities and ease of processing present advantages for the utilization of synthetic monomers. Further investigation of parameters such as biocompatibility and cell viability forms a platform for possible tissue engineering applications in the future.

Arising from their chemical nature, some monomers with specific functional groups or physical characteristics provide a stimuli responsive property to hydrogels. Therefore stimuli responsive (smart) hydrogels have gained significant attention in research.[120] Response to the environment can be triggered via different factors, e. g. pH, temperature, electric field or light.[120] As response arises from chemical nature, in practice triggering can be applied over many cycles, resulting in physical changes of hydrogels such as elongation, expansion, folding, bending and shrinking. In mechanics, response of hydrogels is based on elastic deformation, meaning physical change (deformation) can be recovered.[121] Such a response of hydrogels can be employed for smart drug delivery platforms,[122] actuators[123] and self-healing hydrogels.[124] Hydrogels containing acidic or basic groups possess pH responsive character, arising from interaction with ions in solution. pH responsive hydrogels can be of interest for smart drug delivery platforms, as pH difference in parts of the body can be a stimulus. One example utilizes drug loaded poly (*N*,*N*′-dimethyl aminoethyl methacrylate) (PDMAEMA) based polybase hydrogel for targeted drug delivery to solid tumor (weak acid). Changing pH from neutral to acidic range protonates the functional groups of hydrogel which triggers the release of loaded cargo drug in desired area.[125] PNIPAM is known for its lower critical solution temperature (LCST) close to body temperature. Change in temperature triggers a considerable volume change of PNIPAM based hydrogels. Such an expansion or shrinking of hydrogel (due to change in hydrophobicity with temperature as stimuli) can similarly be utilized in drug delivery systems.[126] Temperature stimuli can be employed for designing in-situ gelling systems, injectable solution at room temperature undergoes gelation once injected to body. Some hydrogels such as polyelectrolyte hydrogels can respond to electric field, showing change in hydrogel volume. In addition to drug delivery, such a system can be employed to synthesize artificial muscles which resemble natural systems.[127] As muscle

movement is based on electrical conductivity, hydrogel showing physical change with electric field can be promising for the future in soft robotics.[127] Light responsive hydrogels respond to different wavelengths of light and can be applied to display units and optical switches. Mechanism is based on change in molecular conformation via light irradiation, e.g. in the case of azobenzene and derivatives. Altering conformation changes the molecular polarity, therefore hydrogels with such functional groups present physical change via light irradiation.[128]

As summary, changes in environment can trigger response in hydrogels via certain stimuli, which promotes the concept of active materials for variety of applications. Implementing architectural designs to hydrogels promises that the deformation can be controlled in a tailor-made style. Such innovative designs present hydrogels which can walk,[129] open up like flowers,[130] or lift a load.[131] Combining the chemistry of hydrogels with current technologies such as 4D printing, hydrogels have no limit in physical movements.[132] Actuation of hydrogels revealed the possibility to synthesize actuating networks similar to natural tissues. However, hydrogels should fulfill the mechanical properties of biological tissues.

Understanding biological tissues, scientists were inspired to work on tissue engineering and treat diseases innovatively. Chemical approaches led to formation of hydrogels which are similar to biological tissues. Since then, hydrogels with diversified functionalities were presented. However, one of the most important properties of hydrogels is mechanical performance. Ideas to mimic skin-like soft structures or cartilage-like tissues require meeting specific mechanical criteria from hydrogels. Simple synthetic approaches yield hydrogels which in general fail to meet these mechanical criteria, therefore an important step for advancing in hydrogels is proper reinforcement.

2.4. Reinforced Hydrogels: Chemical Methods for Reinforcement

Biological tissues possess diverse mechanical properties, thus hydrogels are expected to show similar performance. Excellent mechanical performance should be performed despite high water contents, unfortunately, fragility of hydrogels causes strong limitation for possible load-bearing applications.[133] Diverse mechanical properties are accessible for hydrogels via reinforcements, which can be applied by different synthetic approaches. Some of the well-studied methods are interpenetrating networks (IPN) and nanocomposite reinforcements.

IPNs are based on the crosslinking of more than one network within each other.[134] The methodology can be extended to synthesize double network (DN) or triple network (TN) hydrogels. The synthesis can be divided into two approaches, e.g. sequential or simultaneous. In sequential formation, inner crosslinked network, which is preferred to be rigid, is synthesized in the first step. The first polymerization is followed by swelling primary hydrogel network with precursors of the secondary network and subsequent gelation (Figure 1.6).[133] In simultaneous formation, precursors of both networks exist in the same solution however crosslinking is applied via orthogonal triggers.[134] Single network hydrogels are generally brittle as they contain voids. The strength of IPN hydrogels relies on the formation of secondary network within the voids of the first network, which decreases the void and increases the polymer concentration of resulting hydrogel.[135] The first network absorbs precursors of the secondary network which endows rigid inner core, and the secondary network is preferred to be more elastic.[136] Rigid inner network provides the toughness and stress absorption whereas elastic secondary network allows better stress dissipation.[137] It is also possible to discuss the nature of crosslinking in IPN approach, which can be chemical or physical as discussed previously. As an example, ionic crosslinking can be applied to crosslink alginate units in alginate-polyacrylamide (PAAm) double network resulting in highly flexible and tough hydrogels.[138] Covalently crosslinked hydrogel based on poly (2-acrylamido,2-methyl,1-propanesulfonic acid) (PAMPS) as first network and PAAm as secondary network also showed outstanding mechanical performance. Resistance against compression and high fracture energy clearly indicates the strength of combination of networks in contrast to single networks.[139] As the resulting hydrogels from this approach are extremely tough, utilization of charged monomers provide tough and lubricant hydrogels, one-step closer to mimic articular cartilage.[140-141]

Indeed characterization methods require strong background in mechanics, and some basic introduction in deformation and fracture mechanism is needed. Deformation can be described as a change in material due to applied force. Such a change can be reversible (recoverable) or irreversible (non-recoverable), so called elastic deformation and plastic deformation, respectively. As the natural tissues withstand different types of forces, applied forces for mechanical tests are tensile (pulling), compression (pressing) and shearing. Strength of the material is defined as the resistance to applied directional force without plastic deformation, which results in compression strength or tensile strength.[142] Typical mechanical tests

(compression and tensile) apply defined forces until fracture of the materials, and monitor the progress via stress-strain curves. From the graph, elastic and plastic deformation range can be concluded, and related elastic moduli (Young's modulus, E_{mod}) can be calculated from the slope of the curve in elastic deformation range.

Toughness is material's resistance to fracture when stress is applied, and can be calculated via integration of the stress-strain curve.[142] Fatigue is defined as weakening of the material over repeatedly applied force. As natural tissues withstand enormous amounts of cyclic forces, investigation of cyclic tests (compression and tensile) provides an appropriate estimation for the fatigue resistance of hydrogel materials.[142] Rheology is an active method to understand flow mechanics of hydrogels. Measurement provides two independent modulus values, namely storage modulus (G') and loss modulus (G''). G' represents elastic behavior of material and G'' represents viscous behavior. When $G'>G''$, it can be concluded that the material has gel character, contrarily material shows viscous liquid character when $G'<G''$.[143] Modulus measurements with changing strain provide a hint about the nature of reinforcement (shear thinning etc.), and modulus measurements against changing frequency show the stability of the network.[143] As a summary, the described mechanical measurements provide an insight into hydrogel structure and properties as well as comparison of mechanical properties of hydrogels and natural tissues.

Utilization of nanoparticles in hydrogel synthesis leads to enhanced mechanical properties as well as more functionality. Such a system consists of polymeric hydrogel network and embedded or chemically linked nanoparticles (Figure 1.6). Commonly employed nanoparticles can be classified as polymeric, carbon-based, and inorganic.[101] Polymeric nanoparticles represent materials such as dendrimers, core-shell particles and micelles. Dendrimers have highly branched polymeric structures and would provide better stress handling in hydrogels, at least theoretically. For example, poly (glycerol-succinic acid) dendrimers on PEG core were investigated. Changing dendrimer concentration significantly influences hydrogel stiffness and hydration kinetics.[144] Highly branched (5^{th} generation) poly (amine ester) (HPE) modified with photocrosslinkable groups were incorporated in hydrogels, which allows the tuning of mechanical properties as well as drug delivery capacity.[145] Utilization of carbon-based materials in hydrogels, such as carbon nanotubes (CNT) or graphene would have potential for conductive hydrogel synthesis due to their electrical conductivity and rigid structures.[146] However, incorporation of carbon-based materials

as reinforcer is problematic due to their strong hydrophobic nature (strong π-π interactions) causing dispersion problems in aqueous media.[101] First of all, the surface of these materials has to be modified with functional groups such as $–NH_2$, -OH and –COOH to customize hydrophilicity and dispersibility.[147] –COOH functionalized CNTs were employed for reinforcing gelatin methacrylate (GelMA) hydrogels. Reinforcer generates fractal-like nanostructures and enhances mechanical performance, as well as increases cell viability of resulting hydrogel.[148] Similarly, graphene is oxidized to graphene peroxide (GpO) which can be utilized for PAAm hydrogel synthesis. Resulting reinforced hydrogel shows significant increase in tensile properties which can be utilized to fabricate elastomeric scaffolds.[149]

Inorganic nanoparticles represent materials such as hydroxyapatite (nHA), silica, clay, titanate and TiO_2. Choice of mineral based materials arises from their presence in body, therefore favoring biological responses.[150] Two inspiring publications from Aida and coworkers show that there is apparently no limit in nanocomposite reinforced hydrogels. Employing clay with dendritic molecular binder provides soft, self-healable, skin-like hydrogel with high amounts of water and good mechanical performance.[151] Second one presents the utilization of magnetic field for manufacturing anisotropic hydrogels. Titanate nanosheets were shown to align in the direction of applied magnetic field, thus titanate dispersion with hydrogel precursors was utilized. Subsequent gelation in such environment results in reinforced anisotropic hydrogels, which show mechanical response depending on the direction of applied load.[152] Covalent bonding of nanoparticle to polymer network presents different results compared to utilization of nanoparticles as physical filler as the crosslinking density differs. Even in some cases, employing nanoparticles as physical fillers do not improve mechanical properties at all.[153] Covalent bonding of reinforcer to polymer network provides extra crosslinking points, therefore enables a stress transfer between polymer and nanoparticle resulting in enhanced mechanical properties.[101] For example, irradiation of titanate nanosheet forms hydroxy radical from water. Then the polymerization is initiated from titanate surface and covalently reinforced hydrogel explains the enhanced mechanical performance.[152] Being part of free radical polymerization, such an approach is also part of photochemical grafting. When a semiconductor material absorbs light, it forms excitons and holes which promote radical formation in aqueous solution. Polymer growth is initiated from inorganic surface with slight radical transfer to aqueous media.[154]

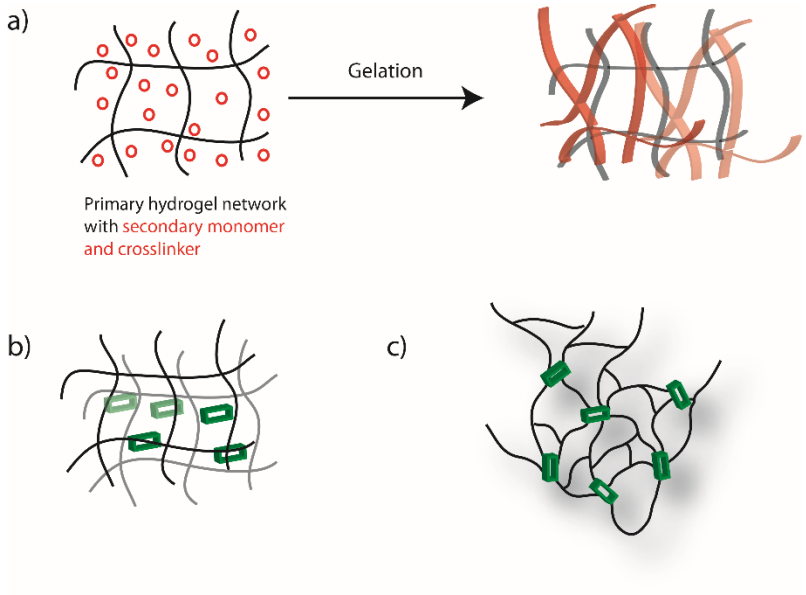

Figure 1.6. Scheme showing common reinforcement methods, **(a)** IPN strategy, **(b)** nanoparticle embedded reinforcement, **(c)** nanoparticle initiated covalent reinforcement.

As summary, reinforcement of hydrogels can be achieved via network engineering or nanoparticle integration. IPNs generally form reinforced tough hydrogels which makes them prime candidates for joint replacement materials. Nanoparticle materials can initiate the gelation or be embedded in hydrogel network, both cases resulting in reinforced hydrogels. Not only reinforcement, but also novel functionalities are accessible via utilization of nanoparticles in hydrogel synthesis. Interdisciplinary cooperation of chemistry, biology and mechanics will design hydrogels of the future, and tissue engineering will tailor the hydrogel materials for daily use. Yet, the background from macromolecular chemistry is needed for facile, accessible and cheap hydrogel reinforcement methods to meet the mechanical properties of natural tissues.

2.5. Motivation of the Thesis

The necessity to alter world's energy source has boosted the studies about semiconductors, materials which can transform sun light into energy. The sustainability problem of metal-containing semiconductors was responded via metal-free semiconductor g-CN, which can be synthesized from abundant precursors. g-CN has been heavily investigated as heterogeneous catalyst, presenting promising results for diversified applications. However, processability of g-CN must be enhanced significantly for integration in solar cells and optoelectronics, therefore g-CN based organic dispersions will reveal next generation energy harvesting devices.

Chapter 2

As hydrogels are promising replacements for natural tissues, tissue engineering and synthesis of artificial tissues primarily require mechanical performance from synthetic hydrogels. Aqueous dispersions of g-CN were studied for hydrogel formations, however reinforcing effect of g-CN in hydrogels has never been investigated. Focusing on the reinforcement, utilization of g-CN as reinforcer and visible light initiator might synthesize inspiring materials for tissue engineering.

This thesis will try to extend the borders of applications of g-CN and employs a combination of g-CN, visible light and simple chemistry to create variety of advanced materials solely based on g-CN in dispersed media.

3. Outline

This thesis investigates the applications of g-CN in dispersed media for fabrication of materials. It addresses the following questions:

Can g-CN be utilized as a photoinitiator and reinforcer in the synthesis of hydrogels? Chapter 4 shows the utilization of various g-CNs with different properties in a one pot, photoinitiated hydrogel synthesis. g-CN will be discussed as a photoinitiator and reinforcer at the same time. The strength of the final hydrogels in the presence of 0.6 wt.% g-CN will be related to the physical properties of g-CN to understand the toughening mechanism. In addition, mechanistic questions, related to bond formation and radical transfer will be answered in order to expand the scope of g-CN utility in aqueous media, monomers and gelation.

Can the amount of g-CN in hydrogel synthesis be increased? The limiting factor for g-CN solid content in hydrogel synthesis is attributed to poor water dispersibility of g-CN. Chapter 5 presents a method to increase g-CN content up to 4 wt.% via a co-solvent method. A 1:1 water:ethylene glycol (EG) mixture provides suitable conditions to disperse higher amounts of g-CN. In the next step, the mixture is utilized in a one-pot, photoinitiated hydrogel synthesis yielding tough organohydrogels. The EG can be removed by immersing the organohydrogels in water providing pure hydrogels. Storage moduli of the resulting hydrogels depend significantly on g-CN content. Simple photopatterning employing home-made masks is introduced which enables the synthesis hydrogels with a specific design.

How to enhance the dispersibility of g-CN? Chapter 6 will demonstrate the enhanced dispersibility arising from bulk g-CN properties. In order to increase g-CN dispersibility in aqueous and organic media, a one-pot photoinduced grafting of olefinic molecules has been designed. The choice of non-propagating molecules helps to preserve bulk g-CN photophysical properties while increasing the dispersibility. The introduction of -SO_3H functionality for aqueous dispersions, 1-decene for organodispersions and -NH_2 for pH-driven dispersibility is presented.

How does g-CN surface chemistry affect hydrogel properties? Chapter 7 shows hydrogel formation from surface-functionalized g-CN. Inspired by the effect of a negative charge on hydrogel toughening as presented in Chapter 4, -SO_3H-functionalized g-CN will be employed for

hydrogel synthesis. Altering the monomers and composition manifests extremely compressible and soft hydrogels with tissue-adhesive, shock-resistance and cut-resistance properties with no toxicity and a skin-like feeling.

Can g-CN be formulated for stable aqueous dispersions? Chapter 8 presents a g-CN 'prepolymer' which can be utilized in hydrogel synthesis. Grafting hydrophilic monomer to g-CN in a water-EG mixture results in highly viscous, but still injectable network. Prepolymer can be mixed with a secondary monomer and crosslinker (without an additional initiator) to synthesize tough hydrogels. Colloidal stability of the prepolymer allows utilization of charged monomers, which was not possible in g-CN-based dispersions before. As an example, the synthesis of a superhydrophilic and tough hydrogel is demonstrated employing a prepolymer and a negatively charged monomer.

Can g-CN be dispersed in organic media? Finally, Chapter 9 shows that by modifiying g-CN with vinyl thiazole provides ultrastable and pure g-CN dispersions in organic media. Vinyl thiazole groups grafted on the edge of g-CN particles facilitate electrostatic stabilization in organic media as the negative charge delocalizes onto the thiazole edges so g-CN sheet remains positively charged, thus, creating donor–acceptor-type structure. Dispersions can be prepared in 20 seconds and stored for weeks. As the sheet exfoliation is highly efficient, for the first time it is possible to create transparent g-CN coatings. Moreover, organic g-CN dispersions can be employed as ink to print g-CN onto paper using commercial inkjet printers.

4. Reinforced Hydrogels via Carbon Nitride Initiated Polymerization [a]

4.1. Overview

The presented Chapter focuses on the utilization of g-CN as visible light photoinitiator and reinforcer for the synthesis of hydrogels with enhanced mechanical properties via a one pot, visible light initiated process. Relation of mechanical strength to g-CN properties (such as electronegativity, surface area etc.) was investigated. Moreover, the mechanism of hydrogel formation was elucidated and role of g-CN in the system. The presence of 0.6 wt.% g-CN leads to a reinforcing effect compared to reference hydrogel, and pH sensitivity of hydrogels due to negatively charged g-CN.

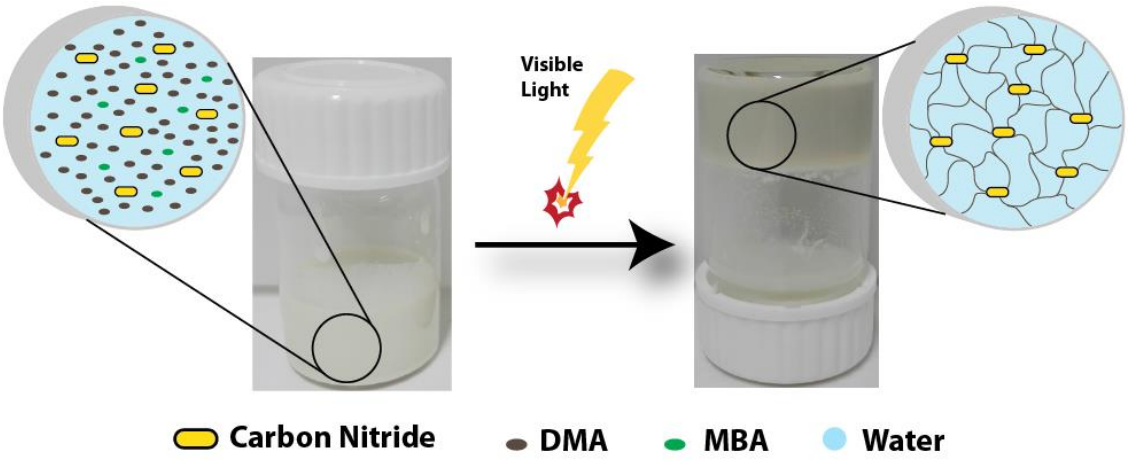

Figure 4.1. Hydrogel precursors with dispersed g-CN particles and formation of hydrogel after visible light treatment with covalent bonding of g-CN to polymer network.

[a] Terms of use: This chapter was adapted with permission from B. Kumru, M. Shalom, M. Antonietti and B. V. K. J. Schmidt, "Reinforced Hydrogels via Carbon Nitride Initiated Polymerization"; *Macromolecules*, **2017**, 50 (5), 1862-1869. Copyright 2017 American Chemical Society.

4.2. Results-Discussion

At first, different types of graphitic carbon (g-CN) nitride were synthesized from different monomers; such as cyanuric acid-melamine (CM), cyanuric acid-melamine-barbituric acid (CMB 0.1 and CMB 0.25), cyanuric acid-2,4-diamino-6-phenyl-1,3,5 triazine (CMp) and from crystalline urea (u-CN) with proper heating conditions under N_2 protected atmosphere (See Appendix-Experimental).[13, 16, 155-156] Main characterizations of synthesized g-CNs are presented in Figure 4.2 and Table 4.1.

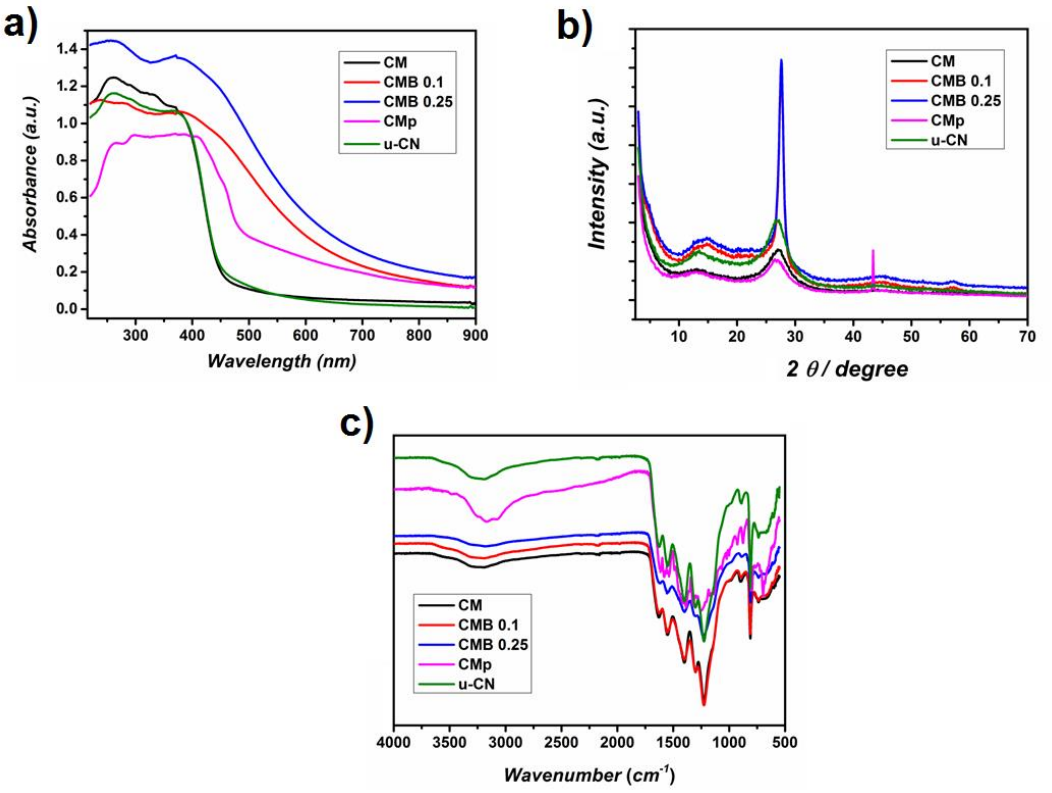

Figure 4.2. Solid state analysis of synthesized g-CNs, **(a)** UV-Vis spectra, **(b)** XRD profile and **(c)** FT-IR spectra.

g-CNs show overall absorption in the visible light is observed in the range of 250-500 nm with differences in absorption intensity due to different precursors (Figure 4.2a). Powder XRD profile shows two main peaks at 13° and 27° which present the formation of graphitic structure of carbon nitride (Figure 4.2b) and FT-IR features the common vibration bands of g-CN (Figure 4.2c).

Table 4.1. Properties of g-CNs and gelation times.

g-CN type	Surface Area (m^2/g)[a]	Zeta Potential (mV)	C:N ratio[b]	Gelation Time
CM	108.0	-38.5	0.6025	1 hour
u-CN	63.6	-40.9	0.5920	1.5 hour
CMB 0.1	80.3	-28.3	0.6652	4.5 hours
CMB 0.25	27.6	-26.7	0.6746	8 hours
CMp	34.7	-24.1	0.9146	8 hours

[a]obtained via porosimetry and the BET method, [b]obtained by elemental analysis.

In order to form g-CN based hydrogels, first g-CN was dispersed in water. Subsequently, monomer and crosslinker were added to the dispersion and nitrogen was flushed through the system. The gel formation was initiated by illuminating the mixture with a 50 W white LED until gelation was achieved.

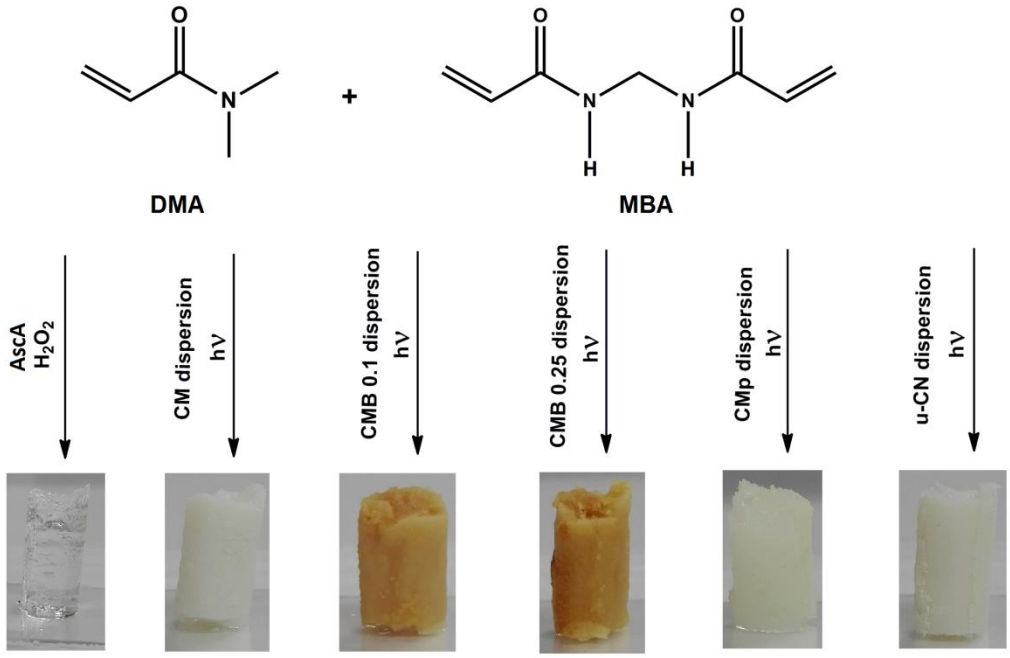

Figure 4.3. Overview over hydrogel formation via visible light irradiation, reactants and exemplary pictures of resulting hydrogels.

g-CN is photoactive material under visible light irradiation, and 0.6 wt.% g-CN content by weight is enough to accomplish the gelation, while the total solid content including monomer and

crosslinker is 11 wt.%. This underlines the nanoscopic dispersion of the g-CN, as the average distance between sheets has to be bridged by a polymer to create a gel. For comparison, a reference hydrogel was prepared utilizing hydrogen peroxide-potassium persulfate (KPS) redox couple initiation. From Table 4.1 it can be concluded that the gelation times decrease with increased surface area of g-CN. Nevertheless, not only the surface area affects the gelation rate. As seen from Table 4.1, u-CN has lower surface area than CMB 0.1, yet much faster gelation is observed. To explain this phenomenon other values have to be taken into account. It seems that a better dispersion and photoactivity as well as lower C:N ratio also lead to improved gelation.

From a mechanistic point of view the main question is the role of g-CN in the system. First, it was investigated whether the polymerization reaction is driven by the formation of radicals. The radical scavenger hydroquinone was added to the reaction medium, and complete inhibition of gelation was observed. It is assumed that the radicals are formed on the g-CN surface upon illumination. Furthermore, in the presence of oxygen, a ~3 fold longer gelation time was observed, which is due to the photoreaction of the catalyst with oxygen, which thereby acts as an inhibitor and/or transfer agent for the polymerization. Another important question is how g-CN is integrated into the hydrogels. Previous reports regarding the utilization of g-CN as catalyst in photopolymerization and controlled atom transfer radical polymerization (ATRP) stated that g-CN remains unchanged as utilization of co-initiator led to radical transfer from g-CN to the co-initiator and thus initiation in solution.[50-52] The co-initiators used so far were basic amines, where the nitrogen atom was responsible of reacting with the radical formed on the g-CN surface. To prove the direct participation of g-CN in the hydrogelation, the system was altered to exclude molecules with nitrogen atoms. Thus, monomer and crosslinker were changed to PEGMEMA and PEGDMA (Figure 4.4). Indeed the nitrogen free system also yielded hydrogels, indicating that initiation of the polymerization for hydrogel formation can happen at the g-CN surface directly without necessity of any soluble co-initiator.

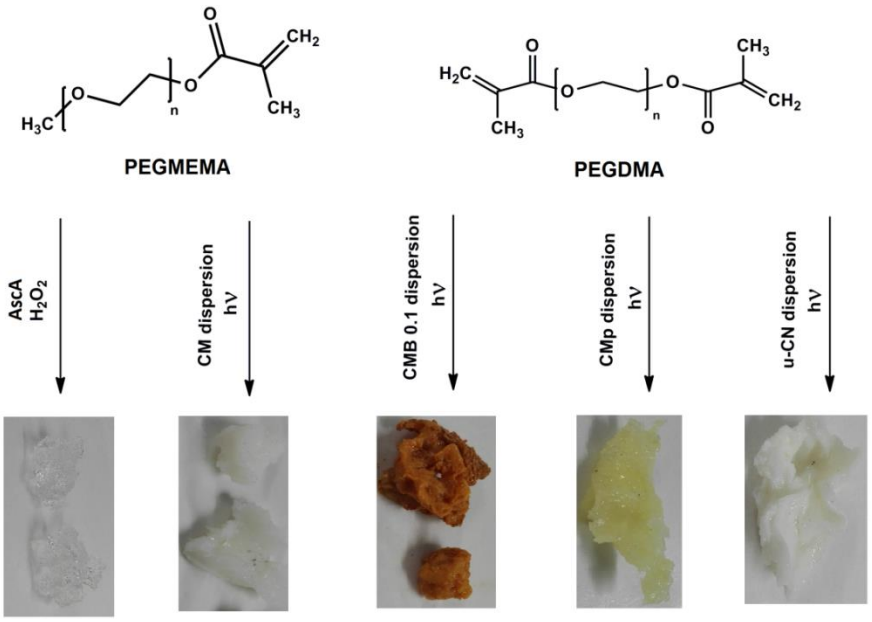

Figure 4.4. Non-nitrogen containing monomers utilized for g-CN initiated hydrogelation and images of resulting hydrogels.

The stable incorporation of g-CN into the hydrogel is another indication that the reaction initiates on the g-CN surface. As seen via solid UV-Vis spectroscopy in Figure 4.5 the reference DMA gel absorbs light between 260-400 nm. The g-CN derived hydrogel u-CN shows strong absorption in a similar range as the respective g-CN precursor. Furthermore, the other g-CN derived hydrogels show the same resemblance between the powders and corresponding hydrogels in the UV-Vis spectra (Figure A1). Imaging via cryo-SEM for g-CN derived DMA hydrogels shows the microscopic structure of hydrogel networks (Figure A2-7).

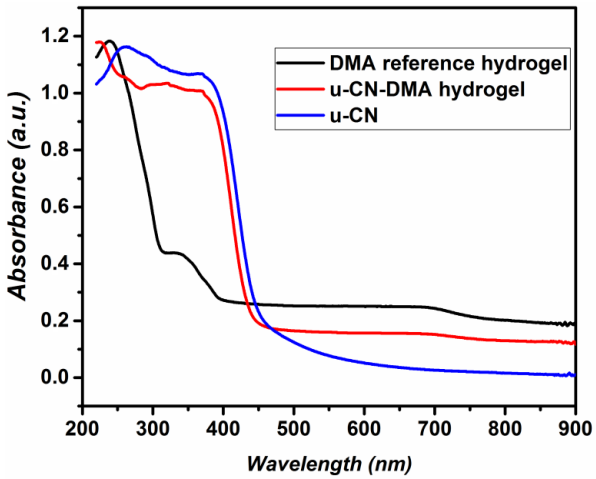

Figure 4.5. Solid state UV-vis spectra of reference DMA hydrogel compared with u-CN derived DMA hydrogel and native u-CN.

Radicals can be generated on the surface of the g-CN which also acts as anchoring points for the monomer. Ideally chain growth starts from surface of g-CN particle and ends at the surface of other g-CN particle (or by recombination with another surface generated polymer chain), this provides more crosslinking density throughout the network. By those mechanisms, g-CNs acts as a colloidal crosslinker as well. In order to investigate the relative effect of g-CN as a crosslinking unit, gelation was performed without the addition of molecular crosslinker. After 5 hours, a softer but insoluble material was obtained, which appeared to be a hydrogel. Rheology measurements show that it has a more viscoelastic character, as shown in Figure 4.6.

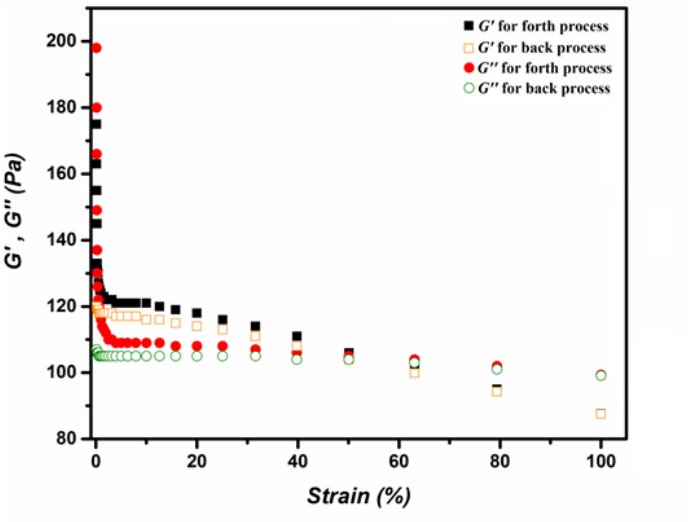

Figure 4.6. Rheological properties of CM-DMA hydrogel without commercial crosslinker, with storage (*G'*) and loss moduli (*G''*) against changing strain on constant angular frequency, back (open) and forth (filled) process.

As the g-CN initiator is a stiff polymeric filler, it also acts as a potential reinforcing agent in the hydrogels, providing extra strength. Interestingly, the mechanical properties of the hydrogels are directly related to the g-CN concentration. In general, g-CN derived hydrogels show much higher storage modulus (*G'*), around 40 times, and loss moduli (*G''*) compared to the reference hydrogel (Figure 4.7, Figure A8-13). In spite of the relative low concentration of filler particles, this increase is remarkable and underlines an altered cross-linking topology.

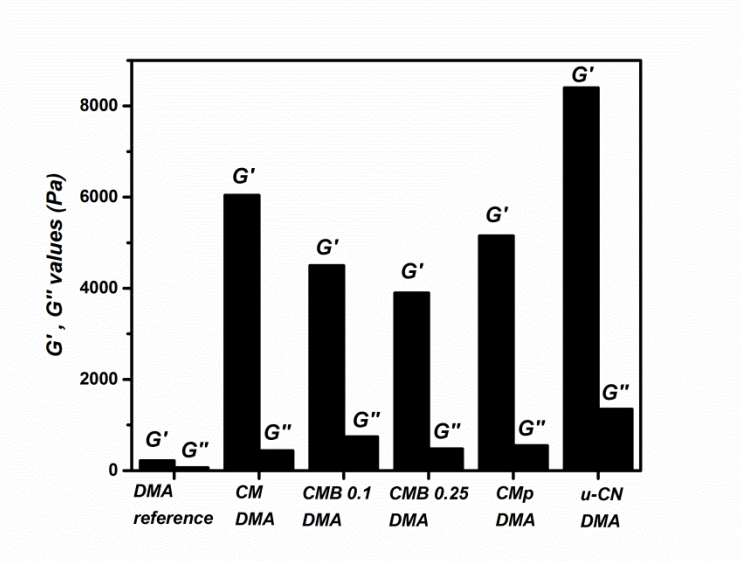

Figure 4.7. Comparison of average storage (*G'*) and loss modulus (*G''*) values of reference and g-CN derived DMA hydrogels at 0.1% strain.

While the reference DMA hydrogel has *G'* values around 240 Pa, g-CN reinforced hydrogels have *G'* values in a range of 3800 to 8300 Pa. Storage moduli can be directly related to the mechanical strength of the hydrogel. The significant difference in hydrogel strength can be, by the model of rubber elasticity, quantitatively attributed to an increased number of mechanically active crosslinking points in the hydrogels. By the incorporation of the solid nanofillers, also a better distribution of stress in the network is possible that may be one of the reasons for increased stability even under extreme deformations (no gel fracture).[157] In addition, repulsion of negatively charged g-CNs in the hydrogel system may add to the higher moduli as reported by Aida and coworkers in the case of negatively charged titanate nanosheets in hydrogels.[152] Compared to titanate nanosheets, incorporation of g-CN promises a wider optical absorption range and adjustable electronic character via the variation of g-CN species. Moreover, g-CN possesses increased negative surface charge than titanate nanosheets. Comparing the different types of CN by the resulting values of *G'*, it is obvious that zeta potential has the strongest influence on the mechanical strength compared to other parameters such as surface area, C/N ratio (Figure 4.8). For example, u-CN with the lowest zeta potential g-CN, has the highest value of *G'* while the second lowest zeta potential belongs to CM that has the second highest *G'* value. In turn, the hydrogel made from CMp, which has the highest C:N ratio, medium zeta potential and low surface area shows higher values of *G'* than CMB for instance. CMp was chosen also

due to possibility to modify its properties easily. Overall, one can conclude that g-CN with high negative surface charge leads to the formation of stronger hydrogels.

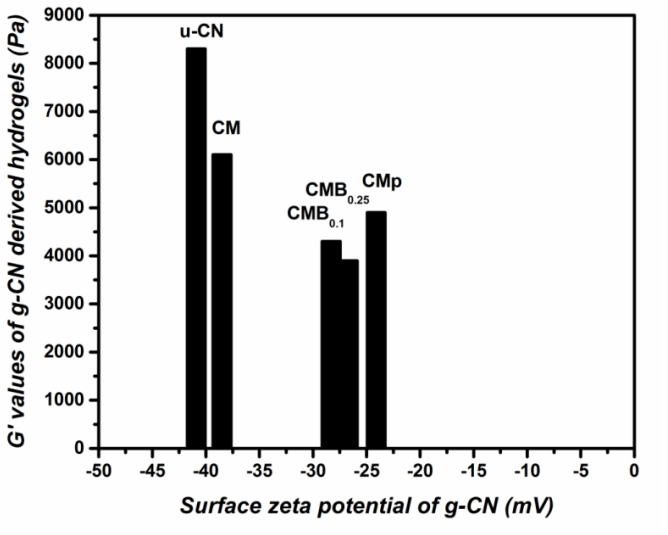

Figure 4.8. Connection between surface zeta potentials of g-CN types and storage moduli (*G'*) values of hydrogels derived from g-CNs at 0.1% strain.

The light absorption properties of g-CN hydrogels were also investigated. Freeze dried reference hydrogel was put into a g-CN dispersion and left to swell. Very small change in UV-Vis spectra and no change in rheology were observed, which means that g-CN can hardly infiltrate the hydrogel once the hydrogel is formed. Formation of u-CN embedded hydrogel via redox initiation in the dark leads to hydrogels with *G'* around 3000 Pa at 0.1% strain (Figure 4.9b). Thus, u-CN is incorporated even without any photoinitiation, however creating a weaker gel due to dangling chains. Compared to the reference gel without g-CN addition, already this mode of incorporation results in a significantly improved mechanical strength. Nevertheless, g-CN initiation and thus introduction of additional topological crosslinks via g-CN further enhances the mechanical strength significantly.

The effect of g-CN incorporation can be nicely observed via strain dependent rheological measurements. For the reference DMA hydrogel without g-CN incorporation a slight decrease of *G'* with increasing strain is observed (from 227 Pa at 0.1% strain to 174 Pa for 100% strain), which is the common shear thinning effect observed for polymer samples (Figure 4.9a). Addition of g-CN without covalent incorporation into the gel structure leads to an increase in the storage moduli (*G'*) compared to reference hydrogel and a more significant strain dependence of the

modulus (from 2865 Pa at 0.1% strain to 1042 Pa for 100% strain for u-CN derived hydrogel). In addition to the shear thinning effect of the polymer network itself, the embedded g-CN sheets cause significant shear thinning due to alignment of the g-CN sheets upon shear stress (Figure 4.9b). The strain dependent decrease of *G'* is well-known for hydrogels that include inorganic support as in the hydrogel two different networks are formed, a soft polymeric and a rigid inorganic network from sheet-sheet contacts.[158] Furthermore, yield stress is observed as the system does not return to the initial value of *G'* at 0.1% strain. The yield stress stems from the required energy to align the g-CN sheets in the hydrogel when stress is applied. More importantly, the covalent incorporation of g-CN increases the mechanical strength further. Moreover, a significant shear thinning effect is observed (from 8320 Pa at 0.1% strain to 3060 Pa for 100% strain), which can be explained by the alignment of g-CN sheets with the application of strain stress. In addition, the yield stress coupled with the shear thinning effect can be observed by the non-fully reversible dependency of *G'* with strain, which is a typical effect for reinforced hydrogels (Figure 4.9c).

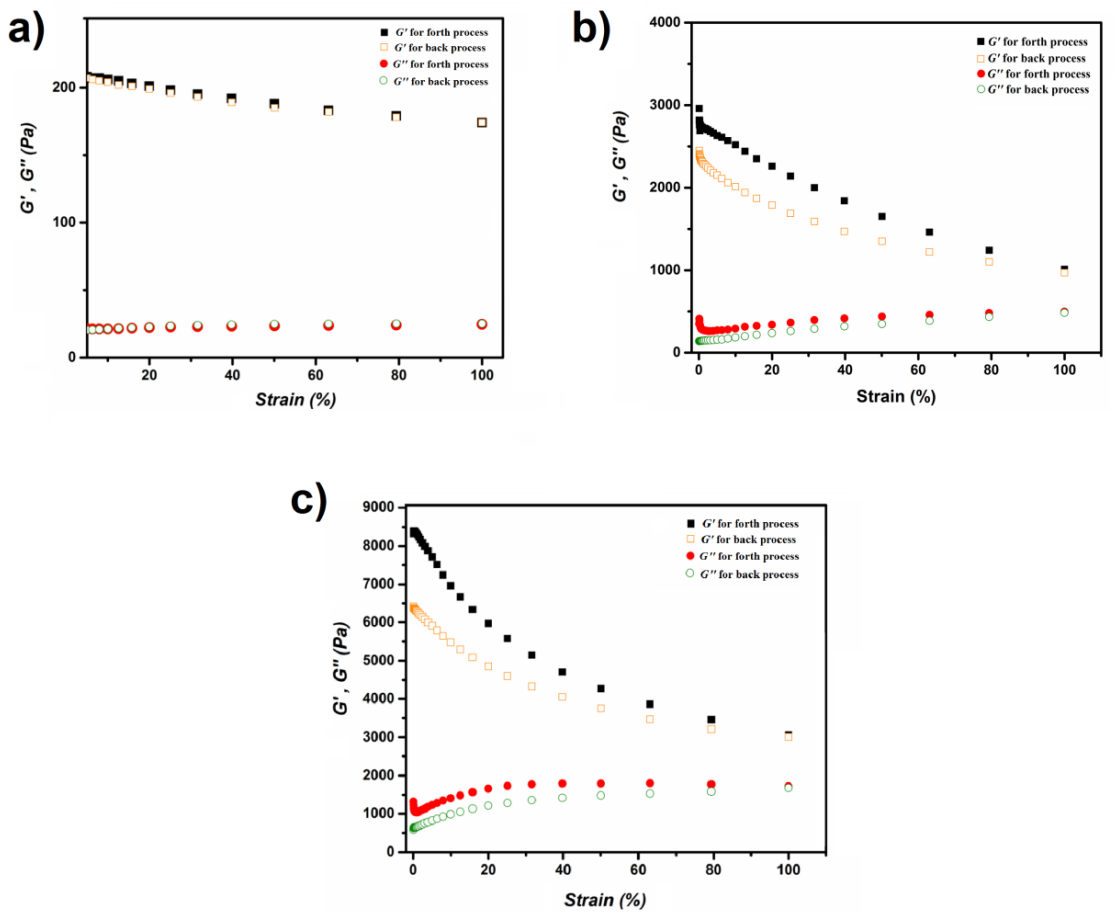

Figure 4.9. Comparison of storage (*G'*, black and orange) and loss modulus (*G''*, red and green) values of **(a)** reference, **(b)** u-CN embedded without covalent bonding and **(c)** u-CN derived DMA hydrogels against strain, back (open) and forth (filled) process.

XRD profiles and FT-IR results of g-CN derived hydrogels show the related peaks from both DMA polymeric network and from g-CN (Figure A14-15). Due to the high water content of hydrogels, observation of order from XRD profiles is challenging. However, highly crystalline g-CNs as CMp still lead to signals in the XRD profiles from hydrogels.

Swelling is one of the most important properties of hydrogels. Addition of solid structures like g-CN is expected to decrease the swelling ratio of hydrogel as the number of crosslinking points increases. Figure 4.10 shows the swelling behavior of freeze dried hydrogel samples in the custom made set up and the swelling ratios calculated by the mass change of swollen and dry hydrogel.

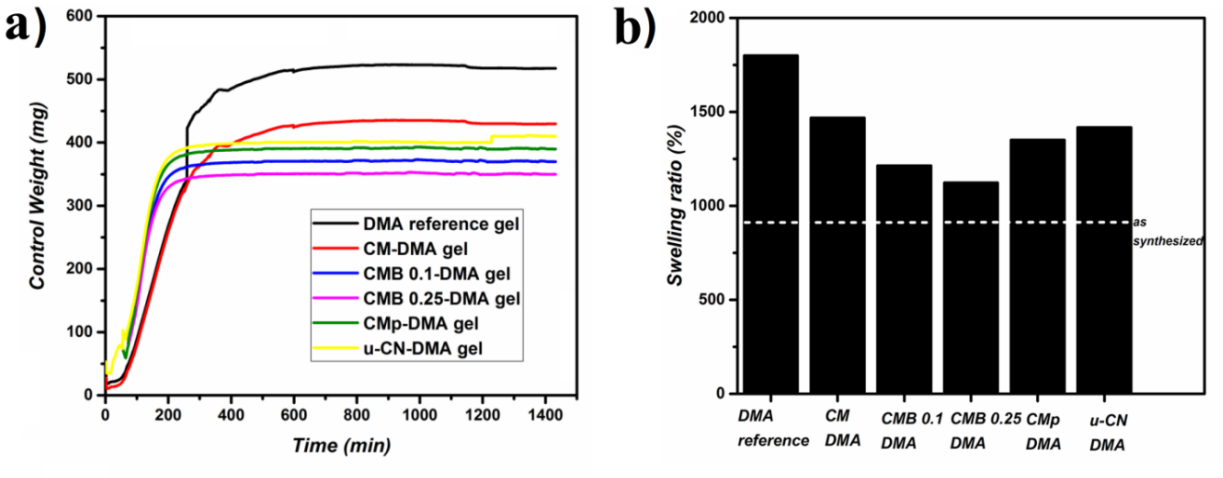

Figure 4.10. (a) Swelling behavior and **(b)** swelling ratios at equilibrium of hydrogel samples with a white dashed line at 900% referring to the as synthesized state.

Obviously, the reference gel demonstrates much higher swelling compared to g-CN derived hydrogels. For the reference gel swelling by a factor of 2 is observed, while for the g-CN derived swelling factors of around 1.2 to 1.7 as compared to the state of synthesis are observed. The swelling behavior is again in-line with the expectation for reinforced hydrogels as the presence of g-CN leads to additional covalent crosslinking points and tectonic sheet-sheet contacts that lead to decreased swelling properties. As g-CNs entail a surface charge, swelling was also performed in acidic/basic media, but no significant change was observed, which proves that the swelling property is mainly controlled by the crosslinking density and less by colloidal interactions (Figure A16).

Nevertheless, the swelling medium should affect the mechanical strength of g-CN based hydrogels. In order to investigate the effect of pH onto mechanical strength, freeze dried u-CN derived DMA hydrogels were left to swell in basic (0.5 M) and acidic (0.5 M) medium. Rheology results (Figure 4.11a and b) show a relation between pH of the swelling medium and strength of hydrogels which makes hydrogels pH dependent.

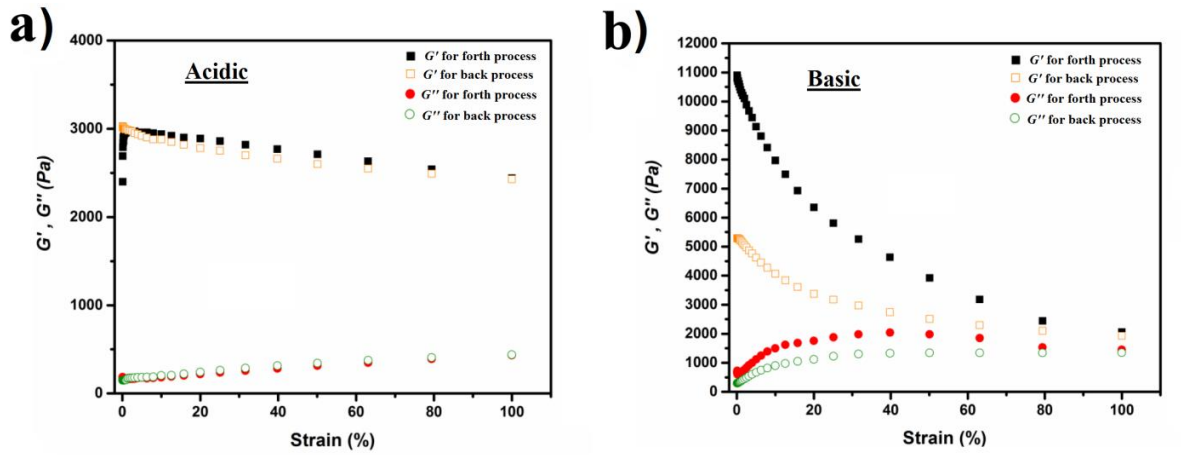

Figure 4.11. Storage modulus (*G'*, black and orange) and loss modulus (*G''*, red and green) values of u-CN assisted hydrogel swollen in **(a)** acidic and **(b)** basic medium, against strain, back (open) and forth (filled) process.

The initial *G'* value for pure water swollen u-CN assisted DMA hydrogel drops from 8300 to 3000 Pa when it is swollen in acidic medium (Figure 4.11a), yet it decreases only in minor amount with increased strain. Apparently, the amount of protons in the gel networks can change the order of the surface zeta potential of g-CN, which causes a significant decrease in the mechanical strength. On a microscopic level the effect can be explained via screening of negative charges at the edges of g-CN and weakened sheet-sheet interactions constituting the stacked-card house structure. Correspondingly, the gels show a weak sheer thinning effect and less strength. However, swelling in basic medium leads to an increase in mechanical properties (Figure 4.11b), showing a strong dependence on the strain. The decrease of *G'* at high strain becomes significant (around 2500 Pa) and back process loses significant amount of strength. In contrast to acid treatment, addition of base leads to further deprotonation of the charges at the edges of g-CN. Therefore, sheet-sheet interactions are expressed more strongly. Thus, indeed a significant shear thinning effect and increased strength at 0.1% strain are observed. Overall, the g-CN derived hydrogels show pH dependency due to the incorporation of charged g-CN moieties.

As discussed above, using g-CN as photoinitiator and reinforcer yields strong hydrogels. Connection of polymeric network to g-CN layer causes improved distribution of stress throughout the hydrogel network. The strength of the hydrogels seems to be governed most significantly by surface electronegativity of g-CN, probably due to repulsion of layers upon compression. Covalent incorporation of g-CN as a crosslinker yields stronger materials than

physically dispersed g-CN in the hydrogel. Providing random anchoring points decreases the swelling properties of hydrogels but not significantly. Since g-CN is highly charged, g-CN derived DMA hydrogels are pH dependent due to interactions of ions with the surface of g-CN. Therefore, g-CN surface charges are screened that lead to less g-CN sheet-sheet interactions and a decreased reinforcement.

4.3. Conclusion

In the present Chapter g-CN was utilized as photoinitiator for hydrogel formation that can significantly increase the mechanical strength of the obtained hydrogels (up to 8300 Pa with 0.6 wt.% g-CN content and 11 wt.% solid content in total). The g-CN reacts as initiator and reinforcing agent in the one pot, photoinduced DMA gelation process. Utilization of visible light for the gelation makes reaction conditions mild and convenient. Mechanical strength of g-CN derived hydrogels was found to be directly related to the surface zeta potential values of g-CNs. Covalent incorporation of g-CN in the hydrogel was found to be significant for the advanced mechanical properties, as blending hydrogels with g-CN in a non-covalent way led to a significant decrease of the mechanical strength. Swelling properties of hydrogels do not change in acidic or basic media but pH has significant effect on the mechanical properties. The latter accentuates that the g-CN is acting as a crosslinker. This work opens the possibility to utilize g-CN based hydrogels with tunable mechanical properties for a number of advanced applications, such as instrumentation of their photocatalytic properties.

5. Tough High Modulus Hydrogels Derived from Carbon Nitride via an Ethylene Glycol Co-solvent Route [a]

5.1. Overview

Previous Chapter demonstrated the possibility to utilize g-CN as visible light photoinitiator and reinforcer in hydrogels. However low dispersibility of g-CN (0.6 wt. %) is an obstacle in the fabrication of tough hydrogels. In the presented Chapter, routes to increase g-CN content for the synthesis of tough hydrogels were investigated. Employing water:EG mixture as dispersing medium, g-CN showed much better dispersibility up to 4 wt.%. The dispersion was utilized for hydrogel synthesis after addition of monomer and crosslinker to obtain organohydrogels under visible light. Immersing intermediate organohydrogel into water yields pure hydrogels with remarkable mechanical properties. In addition, utilization of visible light enables patterned organohydro-and hydrogels via photomasks.

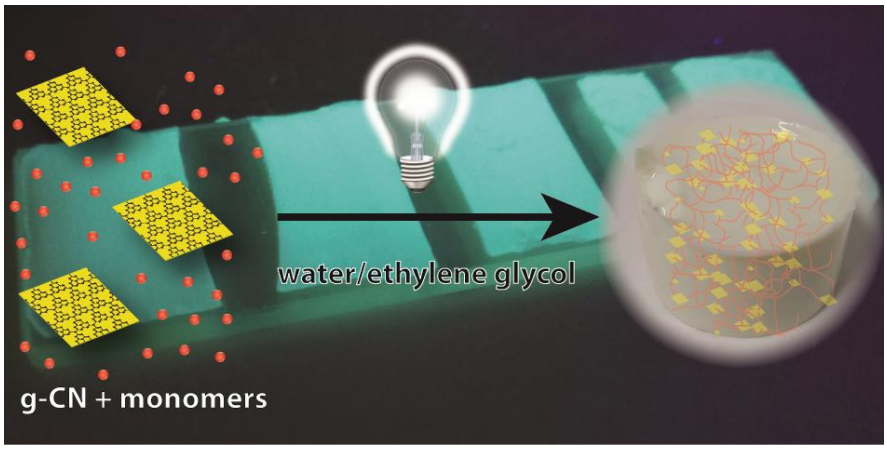

Figure 5.1. Schematic view for the synthesis applied in this chapter.

[a] Terms of use: This chapter was adapted with permission from B. Kumru, V. Molinari, M. Shalom, M. Antonietti and B. V. K. J. Schmidt, "Tough high modulus hydrogels derived from carbon-nitride via an ethylene glycol co-solvent route"; *Soft Matter*, **2018**, 14, 2655-2664 Published by The Royal Society of Chemistry and is licensed under CC BY 3.0.

5.2. Results-Discussion

In order to conduct photoinitiated gel formation, g-CN was synthesized according to previous reports utilizing cyanuric acid-melamine as precursor.[16] As g-CN has low dispersibility in aqueous media, hydrogels with g-CN incorporation above 0.6 wt.% were not accessible so far.[159] Addition of surfactants (1 wt. %) yields good dispersions after ultrasonication for 20 minutes, however sedimentation takes place within 10 minutes for 2 wt. % g-CN in water (Figure A17). In order to increase dispersibility and colloidal stability of g-CN, utilization of a co-solvent in addition to water was investigated. Addition of common water miscible solvents such as acetone, alcohols and *N*-methyl-2-pyrrolidone had negative effects on g-CN dispersibility leading to immediate precipitation. Interestingly, addition of ethylene glycol (EG) to water in a ratio of 1:1 *w*/*w* significantly increased the dispersibility of g-CN while variation in EG:water ratio showed negative effect for the preparation of dispersions. Utilization of pure EG as dispersion medium for g-CN was reported in the literature in order to synthesize doped g-CN quantum dots, where experimental investigations reported that upon ultrasonication C-N bond between melem units break and EG acts as radical scavenger, yielding smaller sized particles[160] or recently for the formation of thin g-CN films.[161] A similar effect was reported for hexagonal boron nitride nanosheet dispersions.[162] The reason for enhanced dispersibility is two-fold.[163] First of all, polar solvents are effective in exfoliation of carbon nitride sheets via intercalation in the stacked structure and hydrogen bonding. Moreover, an efficient exfoliation can be obtained when surface energies of solvent and carbon nitride are in a similar range, which is the case for EG. The co-solvent approach allows the preparation of dispersions with solid contents of g-CN up to 4 wt.%. Higher contents of g-CN led to non-uniform dispersions containing non-dispersed solid particles after ultrasonication. Therefore, dispersions containing 2, 3 and 4 wt.% g-CN were prepared via ultrasonication for further studies. To avoid side reactions, initial dispersions were prepared without monomer and crosslinker. A visual inspection of the formed dispersion was performed before and after ultrasonication of mixtures (Figure 5.2) showing uniform dispersions that could be utilized for the photocrosslinking step.

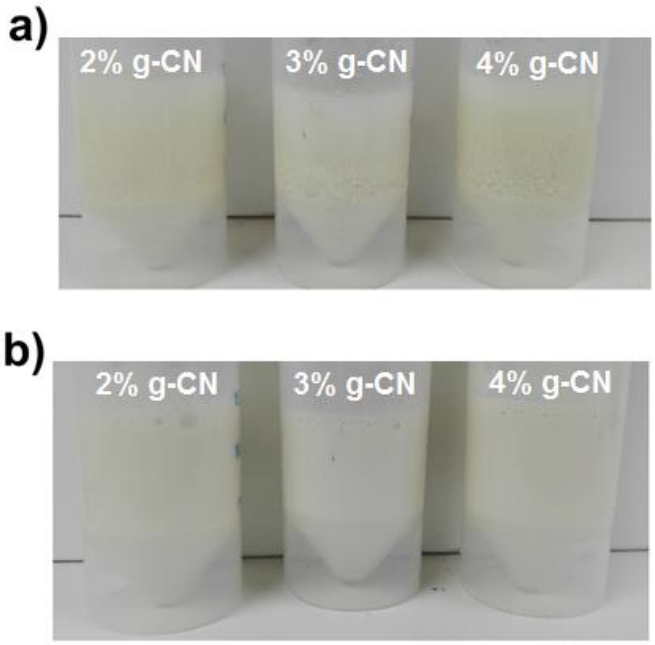

Figure 5.2. (a) 2, 3 and 4 wt.% (from left to right) g-CN in water:EG mixture before ultrasonication and **(b)** 2, 3 and 4 wt.% (from left to right) g-CN dispersions in water:EG after ultrasonication for 40 minutes.

The stability of dispersions was confirmed via the absence of sedimentation of g-CN particles over 4 hours, where sedimentation occurs at g-CN concentrations above 4 wt.%. Thus, a maximum of 4 wt.% g-CN was added to ensure dispersion throughout hydrogel formation, which is described in the following section. In the next step, the formed g-CN EG-water dispersions were used for gel formation (Figure 5.3).

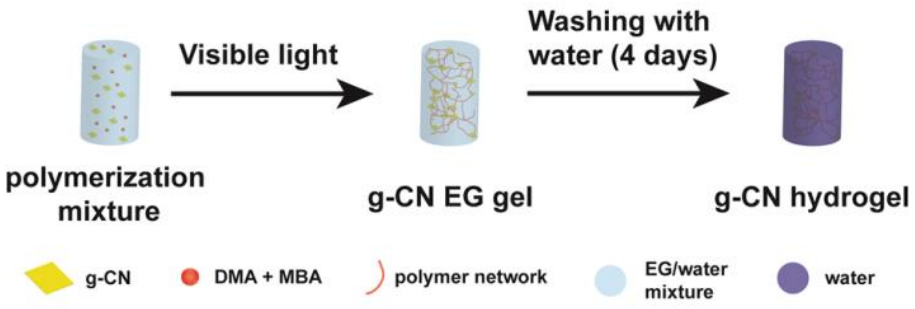

Figure 5.3. Overview for EG gel formation via visible light irradiation and washing of hybrid gel network to obtain pure hydrogels. (DMA: *N*,*N*-dimethylacrylamide; MBA: *N*,*N*-methylenebisacrylamide; EG: ethylene glycol)

For that, monomer and crosslinker were added, nitrogen was flushed through the mixtures, and polymerization was initiated *via* illumination with two 50 W white LED sources. Due to the photoactivity of g-CN, complete gelations were achieved in less than 1 h. Compared to the literature[159, 164] a significantly faster gelation rate was observed that is attributed to the increased amount of g-CN in the system. Furthermore, a reference DMA EG gel crosslinked with MBA was synthesized using KPS-H_2O_2 redox couple (1 wt. %) as a radical initiator. In order to investigate the mechanical properties, rheology measurements of EG gel samples were performed (Table 5.1, Figure 5.4a and A18), e.g. 4 wt.% g-CN EG hybrid gel has a remarkable *G'* value of 645 ± 1.6 kPa at 0.1% strain. In the presence of g-CN, gels show significantly increased *G'* values due to the reinforcement effect from g-CN when compared to the reference gel (Figure A19). Very typical for such systems, increasing amounts of g-CN improve the *G'* values at low strain but cause more significant shear thinning at high strains. Frequency dependent rheology measurements in the presence of EG did not show significant change in the region between 0-10 rad s^{-1}, (Figure A18), as well as 4% g-CN EG gel and 4% g-CN hydrogel between 1-100 rad s^{-1} (Figure 5.4c).

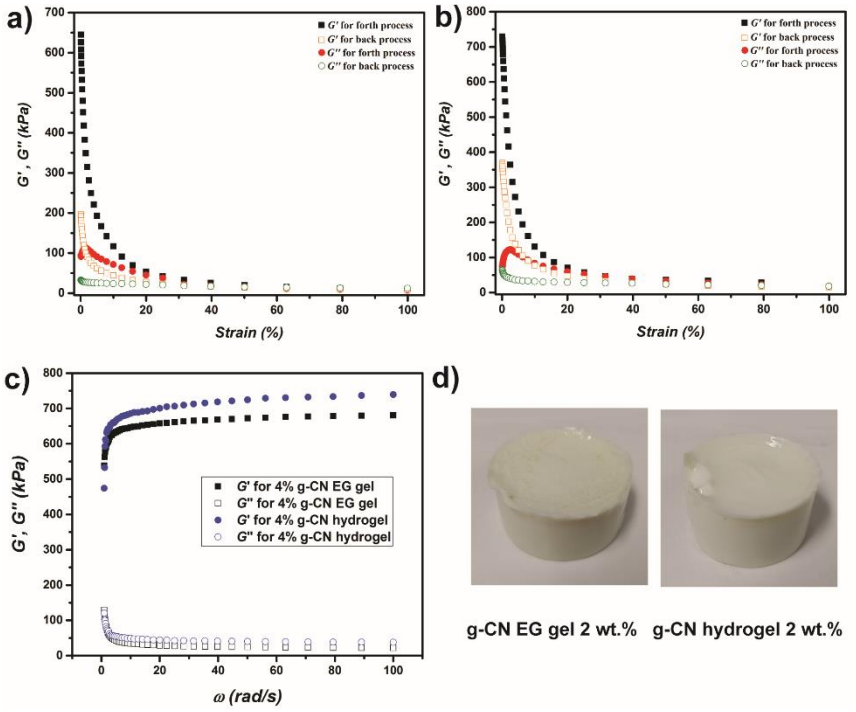

Figure 5.4. Comparison of storage (*G'*, black and orange squares) and loss modulus (*G''*, red and green circles) of **(a)** 4 wt.% g-CN EG and **(b)** 4 wt.% g-CN hydrogel against strain, back (open) and forth (filled) process, **(c)** *G'* and *G''* values of 4 wt.% g-CN EG gel and 4 wt.% hydrogel against frequency with constant strain (0.1%) and **(d)** images of free standing g-CN derived gels.

As discussed previously,[159] the utilization of g-CN as initiator leads to the formation of radicals on its surface and chain growth starts from g-CN surface. Hence, g-CN acts as colloidal crosslinker in the system. In order to study the effect in the co-solvent approach, polymerization was performed for 2 wt.% g-CN EG gel system without external crosslinker (MBA) addition. After 4 hours, a highly viscoelastic liquid that has gel character as shown via rheology was obtained (Figure 5.5). For this system *G'* value of 2.0 ± 0.005 kPa and *G''* values of 0.5 ± 0.001 kPa at 0.1% strain were obtained, suggesting that in the presence of EG, g-CN also acts as crosslinker and yields relatively strong gels compared with non-g-CN based reference gel even without addition of a crosslinker.

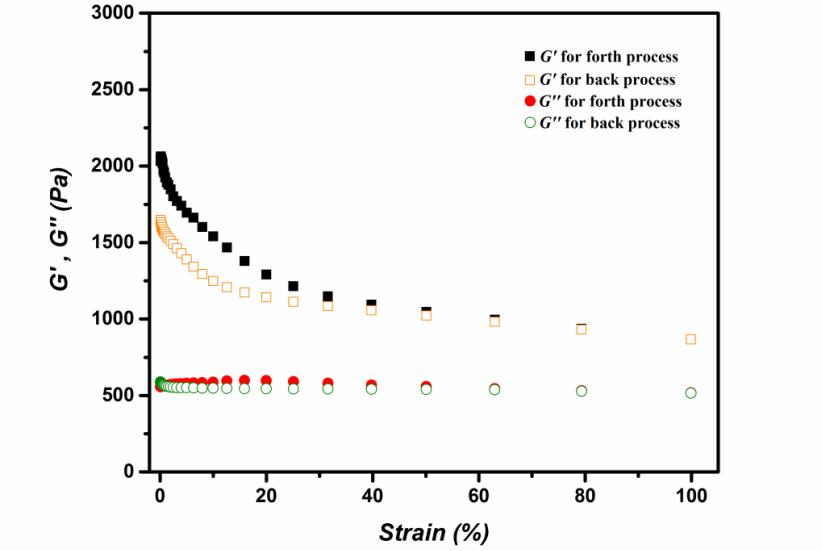

Figure 5.5. Rheology result of 2 wt.% g-CN EG gel without commercial crosslinker, storage (*G'*, black and orange squares) and loss modulus (*G''*, red and green circles) against strain, back (open) and forth (filled) process.

To confirm the statement, control reactions were performed. Gel formation does not take place in the presence of redox initiator and g-CN in dark but without MBA. This clearly indicates the necessity of light irradiation to form gels via attachment of polymeric chains to g-CN. Moreover, redox couple initiation without MBA addition does not yield crosslinked systems, in a similar way as irradiation of just monomer and crosslinker without radical source does not yield a hydrogel. The addition of radical scavengers such as hydroquinone completely inhibits gel

formation, which points to the radical mechanism of gel formation. As shown in Chapter 4, the effect of covalent bonding on reinforcement was investigated via performing gelation reactions with related g-CN amounts with redox initiators in dark (Figure 5.6).

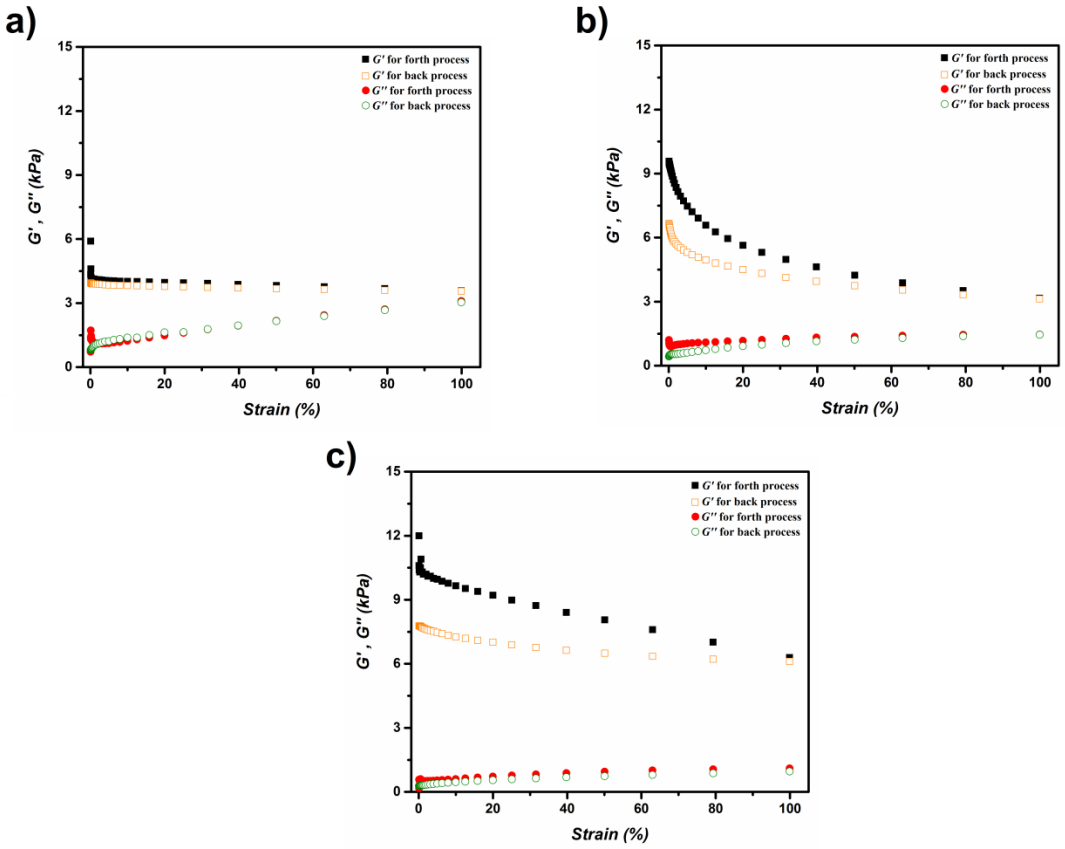

Figure 5.6. Comparison of storage (*G*', black and orange squares) and loss modulus (*G*'', red and green circles) of **(a)** 2 wt.% and **(b)** 3 wt.% and **(c)** 4 wt.% g-CN EG gels initiated via redox in the dark, against strain, back (open) and forth (filled) process.

Therefore, g-CN remains as unreacted particles buried in the gel network. Dramatic decrease in *G*' values for all concentrations were observed, up to 98%. Clearly covalent reinforcement plays an important role to yield g-CN based strong hydrogels.

Table 5.1. Overview of the storage moduli (*G*') and loss moduli (*G*'') values of g-CN EG gels and hydrogels at different strains.

Sample	*G*' at 0.1% strain (kPa)	*G*'' at 0.1% strain (kPa)	*G*' at 20% strain (kPa)	*G*'' at 20% strain (kPa)
2 wt.% g-CN-EG gel	96.5 ± 0.2	18.1 ± 0.05	11.7 ± 0.03	9.9 ± 0.02
3 wt.% g-CN-EG gel	460 ± 1.2	75 ± 0.19	58.1 ± 0.15	41.6 ± 0.10
4 wt.% g-CN-EG gel	645 ± 1.6	93.7 ± 0.23	53.2 ± 0.13	45 ± 0.11
2 wt.% g-CN hydrogel	88.3 ± 0.2	20.4 ± 0.05	25.8 ± 0.06	20.4 ± 0.05
3 wt.% g-CN hydrogel	430 ± 1.1	35.1 ± 0.09	78.4 ± 0.20	45 ± 0.11
4 wt.% g-CN hydrogel	729 ± 1.8	74.4 ± 0.19	70.7 ± 0.18	59.7 ± 0.15

The removal of EG from hybrid gels was performed via solvent exchange as previously reported for other solvents.[165] Hybrid gels were washed with water via immersion and frequent solvent exchange, which yields swollen hydrogels in a convenient way. No particles were observed in solution during washing process which hints to a covalent bonding of g-CN and polymeric network. The solvent exchange of EG was monitored via FT-IR measurements of freeze-dried samples after various periods of time. Rheology measurements of hydrogels without EG were performed (Figure A20) to assess the effect of EG incorporation on mechanical properties (Table 5.1). Storage moduli similar to EG gels were obtained, e.g. 4 wt.% g-CN hydrogel has a *G*' value of 729 ± 1.8 kPa at 0.1% strain. Again, significant shear thinning behavior was evident as *G*' values decrease in all samples as strain increases. In any case, the reference DMA hydrogel possesses significantly lower *G*' values of 0.3 kPa at any strain compared with the g-CN reinforced hydrogels. Redox initiated g-CN hydrogels possess much lower *G'* and *G''* values at any strain, by showing an increase in *G*' values with increased g-CN concentration (Figure A21). Therefore, strength of hydrogel also depends on the incorporated g-CN amount itself. Overall, covalent incorporation of g-CN in hydrogels provides increased mechanical strength due to reinforcing effect of g-CN, which can be attributed to increased number of mechanically active crosslinking points and an increased repulsion between g-CN layers upon compression.

Decrease of *G*' with increasing strain is a common effect when inorganic supports are used.[166] The hydrogels are composed of 2 different networks, namely the polymeric network and the inorganic network from sheet-sheet interaction. Upon increased strain, shear-induced deformation of these networks occurs and *G*' decreases.[158] In particular, sheet-sheet interactions (strong π-π interaction between g-CN sheets due to aromatic repeating units of g-CN)[167] are broken due to the shear stress, leading to alignment of g-CN sheets with the shear flow. Thus, shear thinning is observed. At high g-CN concentration the mechanical properties of the gel increase due to the enhanced sheet-sheet interaction. At the same time more pronounced strain dependency of storage and loss moduli are obtained. The non-linear increase of *G*' with increasing g-CN content might be due to significantly enhanced sheet-sheet contacts in the gels with higher g-CN amount. Accordingly, the storage modulus rapidly decreases with strain the most for gels with the highest amount of g-CN as the interactions of g-CN is broken due to shear force. In EG hybrid gels, the decrease in *G*' is more significant than for hydrogels. Moreover, lower *G*' values were observed for hydrogels compared to EG hybrid gels, which is due to weakened charge dissociation in EG gels. After significant increase of strain, the sheet-sheet interaction network is disturbed and a stable network could not be formed again on the time scale of the back process. A comparison of *G*' values for both systems at 0.1% and 10% strain shows that except for 4 wt.% g-CN systems, EG gels possess higher *G*' values at very low strains and hydrogels possess higher *G*' values at higher strains (after around 4% strain) (Figure A22), which can be explained with the decreased charge dissociation and sheet-sheet interactions in EG gels that lead to a stronger strain dependency.

Another hydrogel property of key importance is compressibility with stress and durability in cyclic compression. Classical hydrogels as soft polymeric networks often fail upon gentle compression due to a loss of mobility of the entanglements of chains and poor distribution of applied stress, and the then broken system is useless in tissue repair. However, reinforced hydrogels are expected to dissipate the stress through the reinforcer more effectively, and increased compression stress can be usually applied before failure of the crosslinked structure.

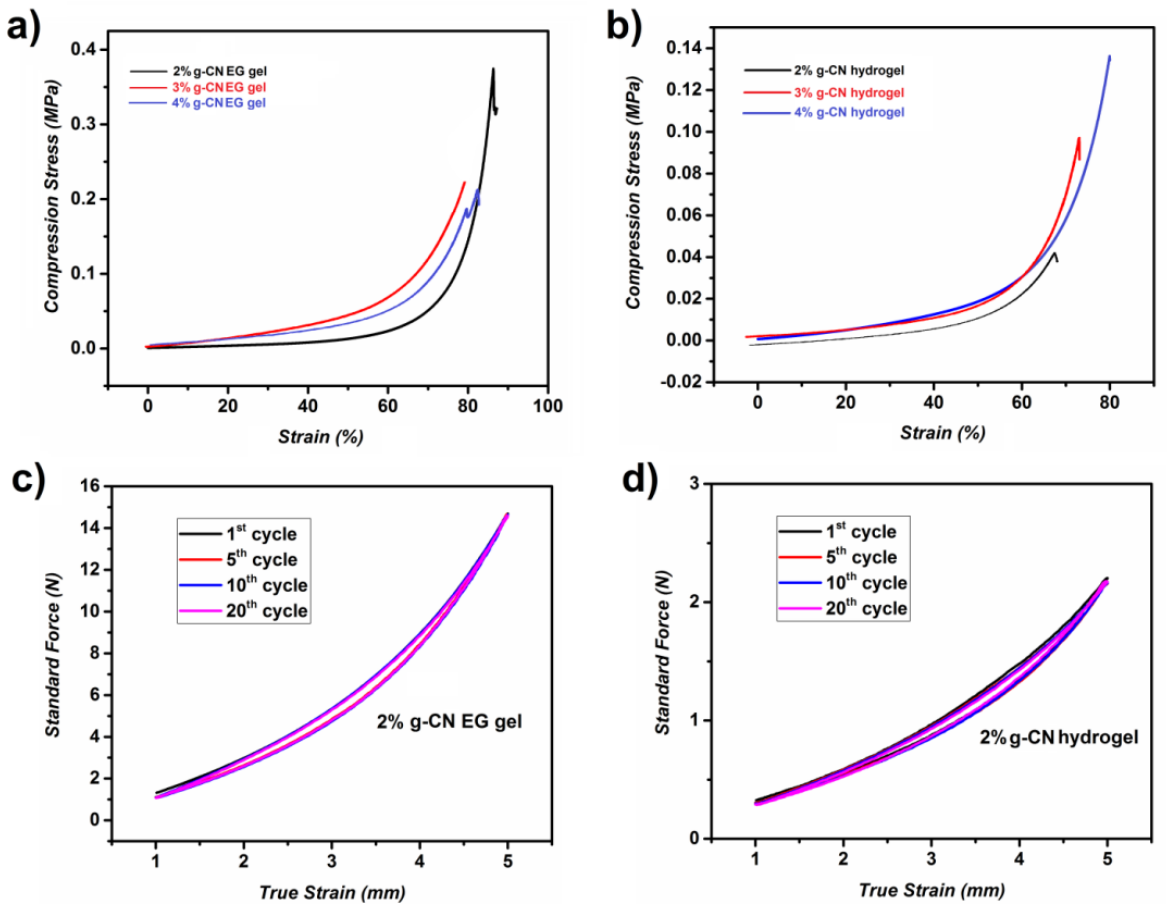

Figure 5.7. Compression test results of **(a)** EG gels and **(b)** hydrogels and cyclic compression graphs of **(c)** 2 wt.% g-CN EG gel and **(d)** 2 wt.% g-CN hydrogel for 20 cycles.

g-CN derived hybrid gels and hydrogels show excellent compression properties (Figure 5.7 and Table 5.2). Especially, EG hybrid gels show high elongation at break values, e.g. 84% for 2 wt.% g-CN EG gel. Moreover, compression tests show that 2 wt.% g-CN EG gel possesses the highest compression modulus (E_{mod}) of 9.45 MPa compared to the other EG gel samples. In addition, 2 wt.% g-CN EG gel shows the highest strength in the series with an average fracture stress of 316 kPa. Increased amounts of EG lead to decreased charge dissipation of g-CN sheets, which provides more flexibility to the gels.[168]

Table 5.2. Overview of compression test results of EG gels and hydrogels.

Sample	Strain at which E_{mod} was calculated (%)[a]	Average E_{mod} (MPa)	Average fracture strain (%)	Average fracture stress (kPa)
2 wt.% g-CN-EG gel	72-73	9.45 ± 0.9	84	316 ± 57
3 wt.% g-CN-EG gel	71-72	7.70 ± 0.2	81	199 ± 62
4 wt.% g-CN-EG gel	64-65	6.45 ± 0.9	74	210 ± 46
2 wt.% g-CN hydrogel	56-57	1.27 ± 0.5	67	39 ± 21
3 wt.% g-CN hydrogel	56-57	3.10 ± 0.2	66	83 ± 20
4 wt.% g-CN hydrogel	58-59	3.55 ± 0.7	68	86 ± 42

[a] E_{mod} was calculated at strain values equal to 10% before break of specimen via the slope of the stress-strain curve.

After removal of EG from the system, lower compression moduli and fracture strain values are observed. In contrast to EG gels, the hydrogels show an improvement in compression modulus as g-CN content increases, and the 4 wt.% g-CN hydrogel is the strongest hydrogel with 3.55 MPa compression modulus value. Moreover, hydrogels show less strength as indicted by the average fracture stress of 39 to 86 kPa. In comparison, EG gels possess much higher fracture stress and compression modulus values than hydrogels, possibly due to less charge dissipation of g-CN sheets. Absence of EG also results in lower flexibility and causes lower strain at fracture values for hydrogels. Thus, calculation of compression modulus values was performed at different elongations (Table 5.2).

To investigate the fatigue resistance of EG gels and hydrogels, consecutive cyclic compression tests were performed. Standard force was recorded against true strain, which is the absolute change in plate distance, with an elongation of 50%. A total of 20 compression cycles were conducted for each sample of EG gels and hydrogels. Overall, cyclic compression showed no significant non-recoverable damages for all hybrid gel and hydrogel samples (Figure 5.7 and A23-26). Recovery of the initial strength shows that after compression, alignment of a non-damaged polymeric network and reinforcer was achieved successfully leading to the same behavior as the initial synthesized structures. In comparison with hydrogels, EG gels show higher net force upon compression. Reversible recovery profiles are important for applicability of covalently bound reinforced hydrogels as broken crosslinking points cannot be regenerated after

compression. Therefore, it can be concluded that direct covalent bonds between g-CN and polymeric network are strong enough to bear compression at elongations of up to 50%. Moreover, the gels have the capacity to recover their original structure without any energy loss in the system even after 20 consecutive compression cycles. As summary, tough and mechanically stable hydrogels could also be formed via covalent reinforcement.

The swelling ratio defines the capacity of 3D crosslinked hydrophilic networks for water uptake, which is an important property of hydrogels. Addition of solid reinforcers, such as clays and titanates, lead to decreased water uptake in the system due to hydrophobic interactions.[169] Moreover, increasing number of crosslinks lead to restrictions in the swelling as lengths of chain segments decrease accordingly, which limits elongation of the gel. Hence, a challenging aspect for reinforced hydrogels is the preservation of the swelling property of the material, while enhancing mechanical properties at the same time. In the present case, swelling behaviour of gels and hydrogels were calculated via using the equation given in appendix from the masses of dry samples from freeze-drying and swollen samples after immersing dried samples in water (Figure 5.8).

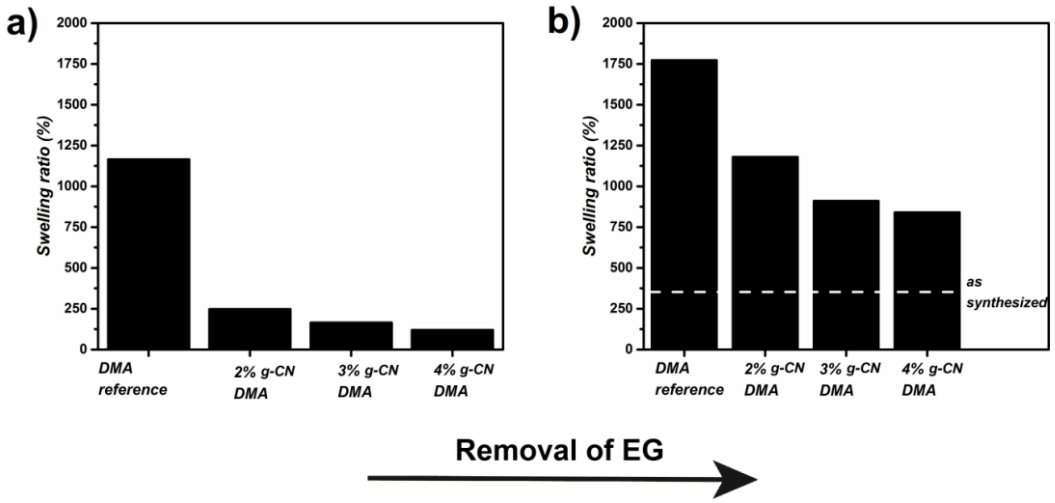

Figure 5.8. Swelling ratios at equilibrium in water after 24 hours of **(a)** EG gels after freeze drying (40 % remaining EG) and **(b)** hydrogels after freeze drying.

After the freeze drying process, EG is still present in the gel network occupying the pores. Quantification via TGA of freeze dried g-CN EG gel samples indicates that samples contain around 40 wt.% EG after freeze drying, assuming no residual water in samples after freeze drying and mass loss up to 150 °C is due to EG (Figure A27). Consequently, molecular water uptakes of

EG gel samples with respect to the overall weight are expected to be lower than for hydrogel samples due to remaining EG after freeze drying. Thus, swelling ratios of 250 to 150% were observed for EG gels. In the case of hydrogel samples, higher swelling ratios are obtained, e.g. 1100% for 2 wt.% g-CN hydrogel. Nevertheless, reference hydrogels show an increased swelling by a factor of 2 compared to g-CN-derived hydrogels as g-CN provides increased crosslinking density. g-CN has characteristic absorption bands in the UV-Vis range (Figure A28), and g-CN derived EG gels and hydrogels show similar absorption profiles which points towards g-CN incorporation in the gels as well as unaltered photophysical properties (Figure A29).

Due to the fact that g-CN is active under visible light, sunlight is also an efficient source to initiate gelation. Hence, a vial containing the polymerization mixture was put outside on a sunny day and during 1 hour gelation was completed showing the facile approach of g-CN initiated gelation (Figure 5.9).

Figure 5.9. (a) EG-based g-CN dispersion for gelation was put on a balcony receiving direct sun, **(b)** complete gel formation after 1 hour.

As gelation is achieved via visible light, spatially controlled polymerization was investigated as well, i.e. photopatterning (Figure 5.10a). Illumination of certain parts in the system yields gels with patterned shapes. To illustrate the concept, the polymerization mixture was poured into a plastic dish, covered with a patterned mask and irradiated directly from the top while keeping the

temperature of the mixture stable in order to avoid heat-assisted polymerization. In order to evaluate the approach, different patterns were used and partial illumination resulted in desired structures of free standing gels (Figure 5.10b). In a half-illuminated system, the illuminated half forms gel and the other half remains liquid. Moreover, symbols from deck of cards were patterned via various masks as presented in Figure 5.10c and A30. Further investigation regarding photopatterning was conducted via formation of patterned thin gels on the surface of glass slides (Figure 5.10d).

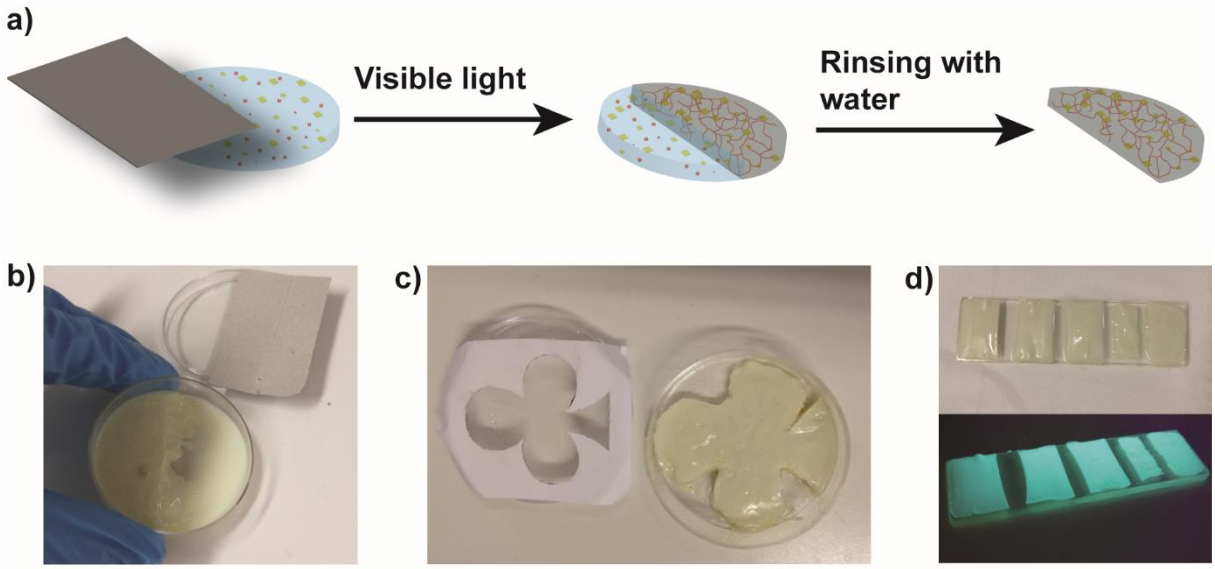

Figure 5.10. Spatial control of hybrid gel formation: **(a)** schematic overview, **(b)** formation of a self-standing half-circle after rinsing with water, **(c)** formation of a self-standing club shape after rinsing with water and **(d)** photopatterning of stripes on a glass slide after rinsing with water.

Another feature is photopolymerization around preformed gels that allows formation of a singular network after a previous gelation. First, a thick gel was created and put into plastic petri dish, where the dish was filled with monomer mixture around precursor gel network. After gelation was completed, the system yielded a single gel network which can be seen from the difference in thickness (Figure 5.11). Overall, patterning and formation of single networks after second gelation may be a hint for future applications in additive manufacturing technologies.

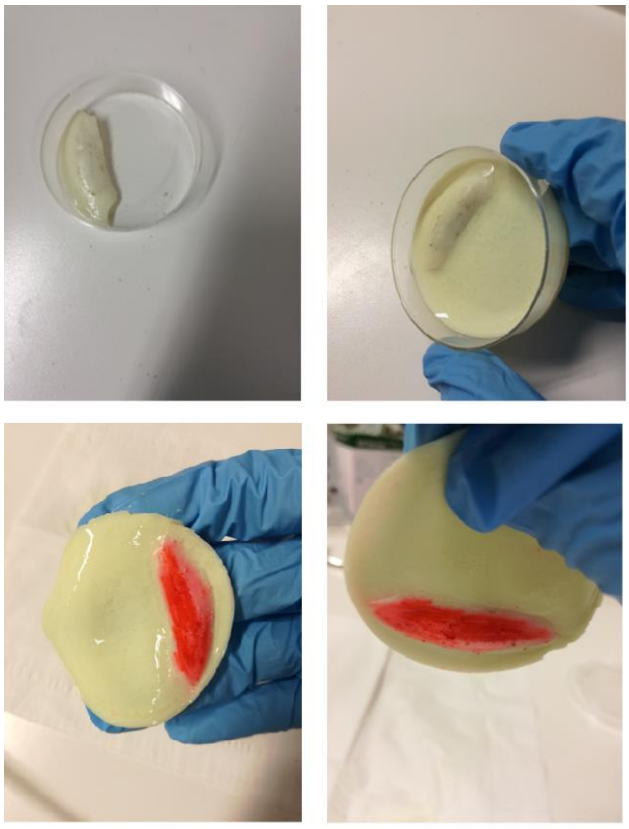

Figure 5.11. Formation of an initial gel network and subsequent gelation around initial gel. The initial gel was colored for visualization.

In order to broaden the scope of gel formation, the gelation was performed within structured scaffolds with near-medical application profile. Flexible, thin, porous, but robust structures like thin lab tissue paper were utilized as a matrix for gel formation, with the final goal to have a thin sliceable supported hydrogel, e.g. for wound coverage. Thus, tissue paper was soaked with the initial EG mixture and treated with visible light. After 1 hour, the tissue paper was taken and washed with deionized water continuously for the removal of unreacted monomers. Finally, a pale yellow tissue was obtained. Under UV light, it is possible to observe fluorescence on the tissue due to g-CN incorporation. In contrast a reference sample tissue remains dark (Figure 5.12). Such photoactive tissue/hydrogel hybrids might be a promising material for photocatalytic applications like artificial photosynthesis or as antimicrobial surface via photocatalytic generation of biocidal reactive oxygen species.

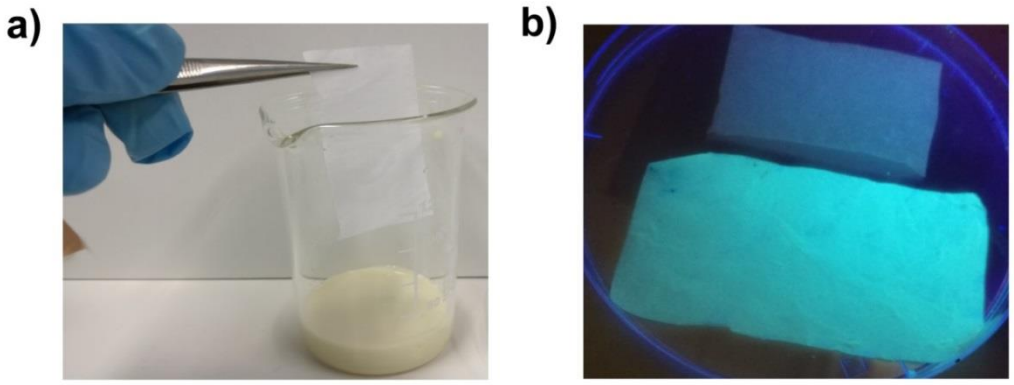

Figure 5.12. (a) Soaking thin tissue paper with EG-based CM dispersion, **(b)** after polymerization and washing, tissue glows under UV light due to g-CN incorporation whereas reference tissue remains dark.

Moreover, applications as cartilage or tendon replacement are in reach, as the presented novel materials have compressive moduli in a similar order as mentioned natural tissues,[170-171] e.g. storage moduli of 880 kPa and compression moduli of 0.08 – 2.1 MPa for cartilage. In such a way application as components for intervertebral disc implants are expected, especially when additive manufacturing methods such as 3D printing are utilized. Nevertheless, biocompatibility of the formed hydrogels has to be assessed in order to facilitate biology or medicine related applications.

5.3. Conclusion

The presented chapter described a procedure how significantly increased amounts of g-CN nanosheets (up to 4 wt.%) could be stabilized in aqueous monomer mixtures to form hybrid hydrogels. The g-CN can subsequently be utilized as photoinitiator and reinforcer for gel formation under visible light in a one pot process. EG together with water was used as a co-solvent to enhance dispersibility of g-CN. The EG-containing hybrid gels could be transformed into hydrogels via simple solvent exchange. Both types of networks show remarkable storage moduli (up to 650 kPa for hybrid gels and 720 kPa for hydrogels) and compression moduli (up to 9.45 MPa for gels and 3.45 MPa for hydrogels), i.e. are of the order of cartilage or tendon. Cyclic compression tests of both gels and hydrogels after 20 consecutive cyclic compressions state recovery of the initial state without energy loss. Moreover, application of spatially controlled optical patterning was investigated via simple, home-made photomasks.

6. Enhanced Dispersibility of Graphitic Carbon Nitride Particles in Aqueous and Organic Media via a One Pot Grafting Approach [a]

6.1. Overview

This chapter has been published and results and figures are taken from it.[172] Chapters 4 and 5 have provided information about the role of g-CN upon visible light treatment during hydrogel formation. These valuable pieces of information have shown that radicals are created on the surface of g-CN sheets when illuminated. Therefore in the presented chapter one-pot visible light induced grafting approach was investigated. Olefinic molecules which do not propagate were chosen as grafted moieties in order to avoid polymerization reactions. Introduction of functionalities (such as SO_3H and decene) lends to extremely enhanced sheet exfoliation in aqueous and organic media resulting in stable g-CN dispersions. Thus, the solid content of g-CN dispersion can be increased significantly, along with facile dispersion preparation and colloidal stability of the systems. Functional groups such as NH_2 can be anchored to surface showing pH dependent dispersibility in aqueous media. Moreover, fluorophilic character can be introduced via grafting fluoro functional molecules.

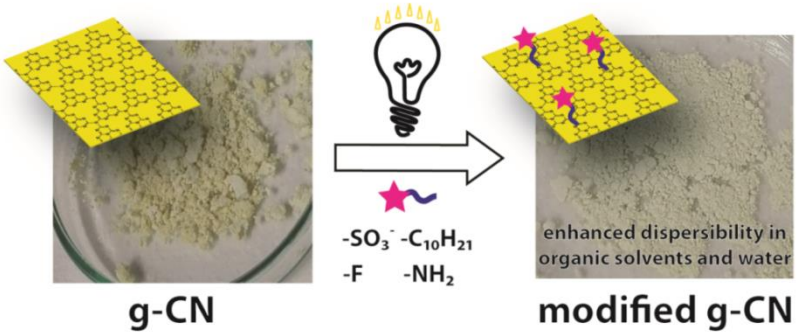

Figure 6.1. Schematic view for the modifications applied in current chapter.

[a] Terms of use: This chapter was adapted with permission from B. Kumru, M. Antonietti and B. V. K. J. Schmidt, "Enhanced Dispersibility of Graphitic Carbon Nitride Particles in Aqueous and Organic Media via a One-Pot Grafting Approach"; *Langmuir*, **2017**, 33 (38), 9897-9906. Copyright 2017 American Chemical Society.

6.2. Results-Discussion

Inspired by recent work on g-CN photoinitiation for hydrogel formation,[61, 159] it is attempted here to utilize radicals on the g-CN surface for modification: radicals are formed on the surface of g-CN via visible light, and various functionalities are integrated. In order to suppress polymerization, functional non-propagating allyl compounds were utilized as depicted in Figure 6.2.

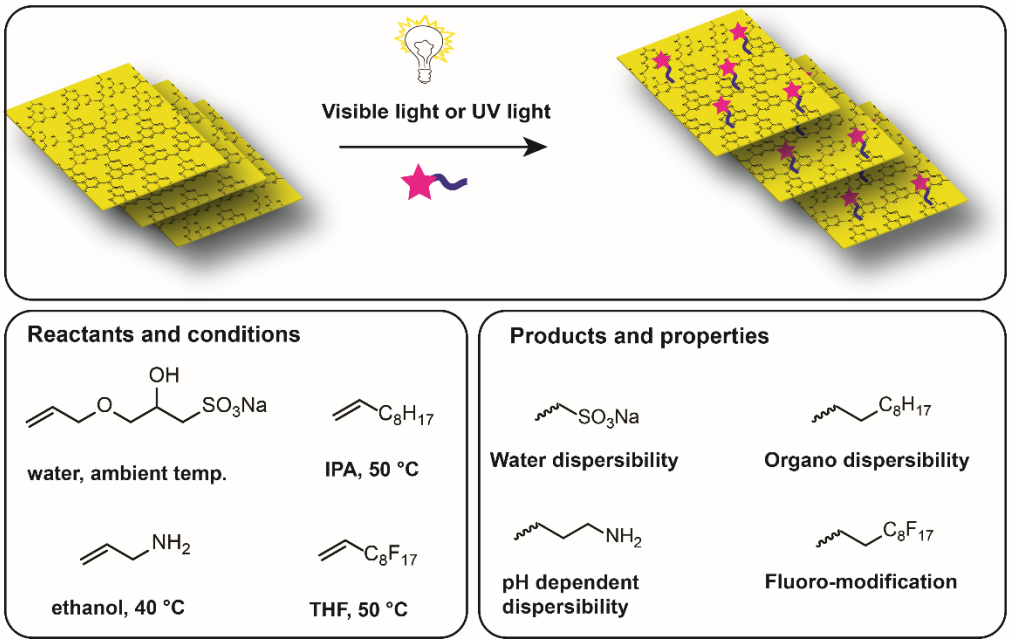

Figure 6.2. Overview for g-CN modifications based on light induced grafting. (IPA: isopropanol, THF: tetrahydrofuran)

To perform photoinduced g-CN functionalizations, allyl containing molecules were chosen as the formation of stable radicals and suppressed propagation leads to single radical additions. A one pot visible light induced grafting method was utilized to integrate allyl compounds onto the surface of g-CN (noted as CM in the chapter). Hydrophilic grafting via 3-Allyloxy-2-hydroxy-1-propanesulfonic acid sodium salt solution (AHPA) molecule (50 mg CM and 20 wt.% AHPA solution in water) increases negative charge as well as S, O and Na atoms on the g-CN structure. Table 6.1 shows the initial analysis results of unmodified and AHPA modified CM by the means of particle size, zeta potential and elemental analysis. Particle size measurements and zeta potential measurements were performed in aqueous dispersion. As grafting time increases particle sizes decreases from 2448 nm to 1468 nm (number average). As grafting with AHPA introduces additional negative charges to the CN structure increased repelling force between

layers might be caused. Therefore decreased particle sizes are observed in the case of CM-AHPA. Grafting onto the surface also causes a spacing effect, which may be another reason for smaller particle size as grafting time increases. Moreover, a significant increase in negative zeta potentials was also observed over the course of the grafting reaction due to grafted sulfonic acid groups from AHPA molecule, while unmodified CM has a zeta potential of -27.5 mV a change up to -53.5 mV is observed via increase of negative surface charges. Longer reaction times provide increased grafting densities, as shown by the sulfur content observed via elemental analysis and more stable zeta potentials occurs at the same time (Figure 6.3).

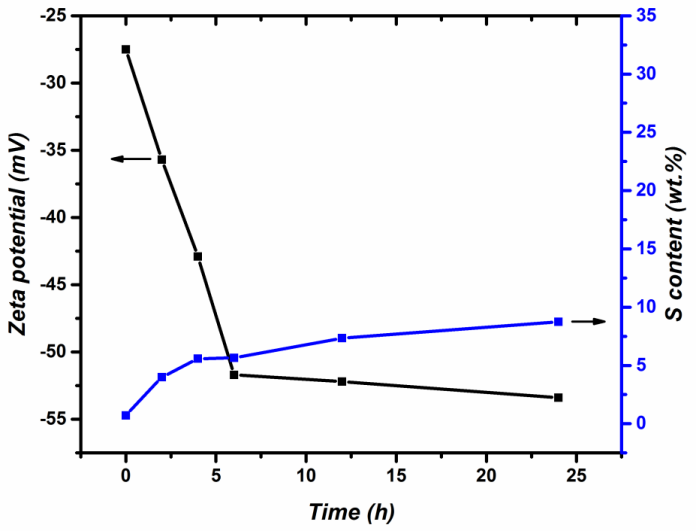

Figure 6.3. The relation of grafting time with sulfur content and zeta potential of modified CMs.

The double bond activity of AHPA is sufficient to achieve grafting at ambient temperature via visible light induction, and as can be compared from the sulfur amount, it is possible to increase the sulfur content by a factor of 10 after 24 hours of reaction, namely from 0.7 % up to 8.74 wt.%. Assuming a sheet model consisting of g-CN sheets with complete grafting of an AHPA layer, a sheet thickness can be estimated from the elemental analysis data acquired from the sample with the highest grafting density. Considering the length of AHPA the maximal overall coating thickness can be estimated to be two times 1.2 nm for the top and the bottom of the hybrid sheet. The theoretical S weight content for the AHPA layer is 14.7 wt.%. Therefore, the overall hybrid sheet thickness can be estimated to be maximal 4.1 nm for the grafted structure, which leaves 1.7 nm for the inner g-CN part. Theoretical assumption calculated via S weight content also fits with the height profiles from AFM results (Figure A31). Thus, this functional delamination can be regarded as very effective.

Table 6.1. Properties of unmodified and AHPA modified CMs. (reaction parameters: 50 mg CM, 1 g 40 wt.% AHPA solution in water, 1 g deionized water, visible light, ambient temperature).

Sample	Time	D_n (nm)[a]	Zeta Potential (mV)	S content (wt.%)[b]	C/N Ratio[b]
CM		2448	-27.5	0.712	0.6025
CM- AHPA2	2 h	2105	-35.7	3.997	0.8478
CM- AHPA4	4 h	1944	-42.9	5.574	0.8518
CM- AHPA6	6 h	1712	-51.7	5.648	0.9125
CM- AHPA12	12 h	1610	-52.2	7.345	1.0997
CM- AHPA24	24 h	1468	-53.4	8.743	1.2244
CM-AHPA ref.[c]	12 h	2278	-27.6	0.697	0.6032

[a] DLS measurements were performed in water (0.05 wt.%) and intensity weighted diameters are presented, [b] obtained via elemental analysis, [c] reference based on mixing of the reactants without visible light irradiation and subsequent purification

In order to exclude physical adsorption of AHPA to the surface, reference experiments were performed. The reference reaction was based on mixing of reactants without visible light irradiation and subsequent purification. After 12 hours the same purification steps were applied as for the irradiated samples and the obtained material was characterized via elemental analysis (Table 6.1). However no change was observed for the non-irradiated samples, which indicates that reaction proceeds on surface of g-CN through photoexcitation. Moreover, the reference experiment suggests that AHPA is grafted to the surface instead of simple physical adsorption. Addition of radical scavenger such as hydroquinone also inhibits the reaction as no change in elemental analysis was observed, which indicates a radical mechanism for the grafting reaction. No change was observed in elemental analysis and particle size while mixing just CM in water under visible light irradiation. AHPA grafted CM was also put into D_2O and mixed thoroughly for 2 hours, then filtered, and ^{1}H-NMR spectra of the solution were taken as shown in Figure A32. Existence of only solvent peak states that the AHPA molecule is grafted to the surface chemically instead of being adsorbed in the pores of CN and that the applied purification method is sufficient to remove any unreacted starting material.

In order to observe the effect of concentration on grafting experiments, variations in allyl compound concentration were conducted as explained in experimental part. Compared to the initial attempted concentration of 20 wt.% of AHPA, a lower concentration of 10 wt.% as well as an increased concentration of 40 wt.% was utilized (Table A1). The obtained results match with the results retrieved from time dependent grafting, e.g. smaller sized particles and decrease in zeta potential values are obtained for increased AHPA concentrations. Moreover, less concentrated medium (10 wt.%) leads to decreased sulfur content compared to higher concentration as expected (3.68 wt.%). Also, as expected, it is possible to graft increased amounts of AHPA on g-CN with higher concentration of allyl compound (40 wt.%) as shown by elemental analysis and the increase of the weight percentage of sulfur atom (up to 9.28 wt.%).

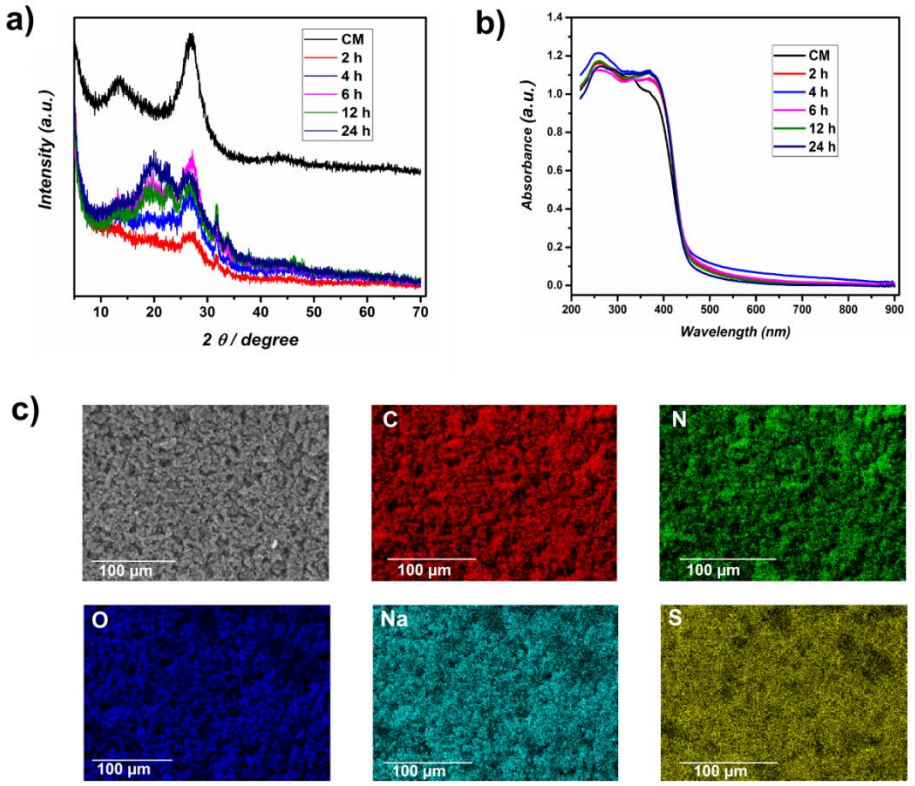

Figure 6.4. (a) XRD profiles of unmodified and AHPA modified CM, **(b)** solid UV-Vis spectra of unmodified and AHPA modified CM and **(c)** elemental mapping of CM-AHPA24 via EDX.

XRD profiles show a change in peak positions (Figure 6.4a), which may be due to a potential positioning of the positively charged sodium atom between layers. The region between 17-20 degrees can be assigned to the layer-layer stacking and increase in these peaks after modification can be the result of weak scattering due to delamination. Solid UV-Vis spectra follow the same pattern as unmodified CM with a slight increase in the region between 350-430 nm (Figure 6.4b)

suggesting preservation of activity towards photocatalytic applications. Elemental mapping via EDX of CM-AHPA24 (Figure 6.4c) indicates the existence of oxygen, sulfur and sodium atoms throughout the surface originating from grafted AHPA molecules. Therefore a homogenous grafting of AHPA on this length scale can be assumed. FT-IR spectra of CM and AHPA as well as AHPA modified CM (Figure A33) can be utilized to identify the grafted species. After modification, all the dominant peaks of CM are still present, with a slight new peak at 2900 cm^{-1} and 1050 cm^{-1}, which can be attributed to asymmetric CH_2 stretching and sulfoxide bond respectively.

For the introduction of organosoluble moieties, 1-decene was grafted to the surface of CM. Initial experiments were performed at ambient temperature at a 1-decene concentration of 50 wt.% in IPA. Even though the dispersion quality in organic solvents increased, changes in the molecular structure could not be proven, which might be due to low double bond activity of 1-decene leading to a low grafting density at ambient temperature. To increase the grafting density, experiments were conducted at 50 °C as delineated in the experimental part. Particle size, zeta potential of elemental analysis of unmodified CM compared to 1-decene modified CM (Table 6.2) confirm successful grafting under the altered conditions. DLS measurements in acetone dispersion showed decreased particle sizes with increasing reaction times, which can be due to anchoring of long chain molecule to the surface of CM. Zeta potential measurements were performed in acetone dispersion, which is a complicated task. Moreover, the results show only insignificant differences to unmodified CM, which has to be considered carefully. In our opinion the observation of only minor changes in zeta potential might be due to the polar aprotic solvent acetone, which is an uncommon solvent for zeta potential measurements due to its poor properties in the stabilization of charged particles. The carbon:nitrogen ratio increases over reaction time, which is an indication of aliphatic grafting. Only small changes in hydrogen weight percentage could be observed (from 1.923% up to 2.377 wt.%). The illustrated relation between reaction time, particle size, zeta potential, H amount and C/N ratio can be found in Figure A34.

Table 6.2. Properties of unmodified and 1-decene modified CMs. (reaction conditions: 50 mg CM, 1 g 1-decene, 1 g IPA, visible light, 50°C).

Sample	Time	D_n (nm)[a]	Zeta Potential (mV)	H content (wt.%)[b]	C/N Ratio[b]
CM		2581	-4.6	1.923	0.6013
CM-Decene2	2 h	2377	-5.1	2.203	0.6431
CM-Decene4	4 h	2215	-5.5	2.272	0.6840
CM-Decene6	6 h	2098	-7.0	2.345	0.7056
CM-Decene12	12 h	1968	-7.2	2.361	0.7372
CM-Decene24	24 h	1896	-7.5	2.377	0.7582
CM-Decene ref.[c]	12 h	2365	-4.6	1.905	0.6024
[a] DLS measurements were performed in acetone (0.05 wt.%) and intensity weighted diameters are presented, [b] obtained via elemental analysis, [c] reference reaction based on mixing reactants without visible light irradiation and subsequent purification					

XRD profiles of CM and 1-decene modified CMs follow a similar pattern and show only small differences in peak intensities (Figure 6.5a). The differences in XRD profiles can be attributed to slight distortion of the g-CN framework. Moreover, solid UV-Vis spectra of 1-decene modified CM show similar absorption bands as unmodified CM. Therefore, one of the most important features of g-CN, namely light absorption in the visible range, is retained in the modified product (Figure 6.5b). As expected, EDX shows no significant changes as no new elements are introduced. In order to check if there was any physical adsorption, 1-decene modified CM was put into $CDCl_3$ and mixed for 2 hours. It was then filtered and ^{1}H-NMR spectrum was taken, which showed only the solvent peak (Figure A35). Moreover, a reference sample was prepared without light irradiation but the same purification, which showed only insignificant differences from untreated CM. Thus, the efficiency of the washing process can be stated as well as physisorption of 1-decene can be excluded.

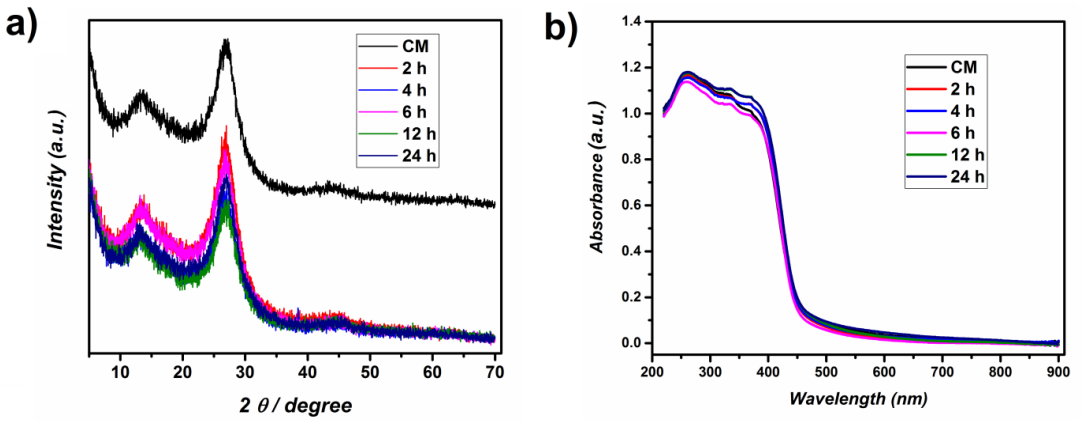

Figure 6.5. (a) XRD and **(b)** solid UV-Vis spectra of unmodified and 1-decene modified CM.

Photoluminescence spectra of CM, AHPA modified CM and 1-decene modified CM follow the exact same pattern, which indicates preservation of CM photoproperties in the grafted products (Figure A36a). Moreover, the appearance of the modified material is very similar to the starting material, where modified samples became a bit paler compared to the unmodified CM (Figure A36b), due the "dilution" with organic compounds.

Mechanistic studies for photodegradation process via g-CN have been reported. Irradiation of g-CN results in electron excitation and hole formation. Interestingly, either hole oxidation or photoreduction can take place depending on the counter molecule. Methyl orange (MO) degradation via g-CN is attributed to photoreduction process with a hole oxidation providing a minor contribution where Rhodamine B (RhB) degradation solely conducted via hole oxidation.[173-174] The mechanism suggested in literature for g-CN with double bonds under visible light is based on the theory of formation of OH radicals and related to valance band values of possible intermediate species.[62] Regarding the mechanism of grafting, the most probable pathway seems to be radical recombination. Upon irradiation electrons in the valence band of g-CN can be excited leading to an exciton state with adjacent electron hole. Subsequently, the formed radical can react with the respective ene in a radical addition. Finally, the leftover other radical on the surface can recombine with the radical formed at the ene after radical addition, which leads to a new covalent bond between g-CN surface and the ene molecule. Whether the first addition to the ene stems from the electron hole or the excited electron can only be speculated at the current point. As the utilized enes are quite electron-rich it is likely that the first addition originates from the formed electron hole on the g-CN surface, i.e. the grafting agent is first oxidized, then recombines to close the photocatalytic cycle.

In order to observe the effects of hole formation and excited electrons on grafting, several control experiments were performed via addition of triethanolamine as hole scavenger or hydrogen peroxide as electron scavenger for AHPA grafting as explained in appendix (Chapter 11). Interestingly, after 4 hours of reaction, slight increase in sulfur amounts, yet significantly lower grafting compared with CM-AHPA4 was observed, and no grafting took place when both hydrogen peroxide and triethanolamine were present (Table A2). These results suggest that grafting can also be achieved via only electron hole or excited electron based mechanism resulting significantly lower grafting rate, and efficient grafting may take place via a process combining both mechanisms. Hole can abstract electron from double bond leaving cation and radical on the molecule. The cationic part can be anchored to excited electron resulting in grafting. For the mechanism from excited electron; formation of hydroxyl radical (either from water or oxygen after chain reactions) is an essential step. Hydroxyl radical can perform addition to double bond leaving another radical on the molecule. For grafting to g-CN, this path is questionable as no possible anchoring points exist. In a recent article investigating mechanism of water splitting with g-CN, it was theoretically shown that water molecule forms a complex with heptazine rings of g-CN and after irradiation and abstraction. A radical formation takes place on heptazine ring[175], which can couple with the radical formed via excited electron route and results in grafting as well.

Dispersion Properties

Sulfonic acid group is known to be an excellent hydrophilic functional group.[176] Therefore, the introduction of sulfonic acid functionality to g-CN is expected to result in enhanced dispersibility in water. To test dispersibility of the AHPA modified CM, various conditions were tried. Pure CM precipitates directly from water and requires long times of sonication (as much as 24 hours) for the formation of uniform dispersions. However, CM AHPA is immediately dispersible in water even *via* gentle shaking by hand. To prepare the CM dispersion in water, even after 30 minutes of sonication, still most of the CM is present at the bottom of the vial as depicted in Figure 6.6a. On the other hand CM-AHPA disperses in water after 5 minutes of sonication (Figure 6.6b), and the dispersion is uniform, and solid particles are not visible in the system. In order to check the stability of water dispersion, the sedimentation of CM and CM-AHPA (1 wt.% in water, both sonicated for 5 minutes), was investigated. In the case of AHPA modified CM the

solid particles are still dispersed in water phase after 3 days (Figure 6.6c), while CM sediments completely after 8 h.

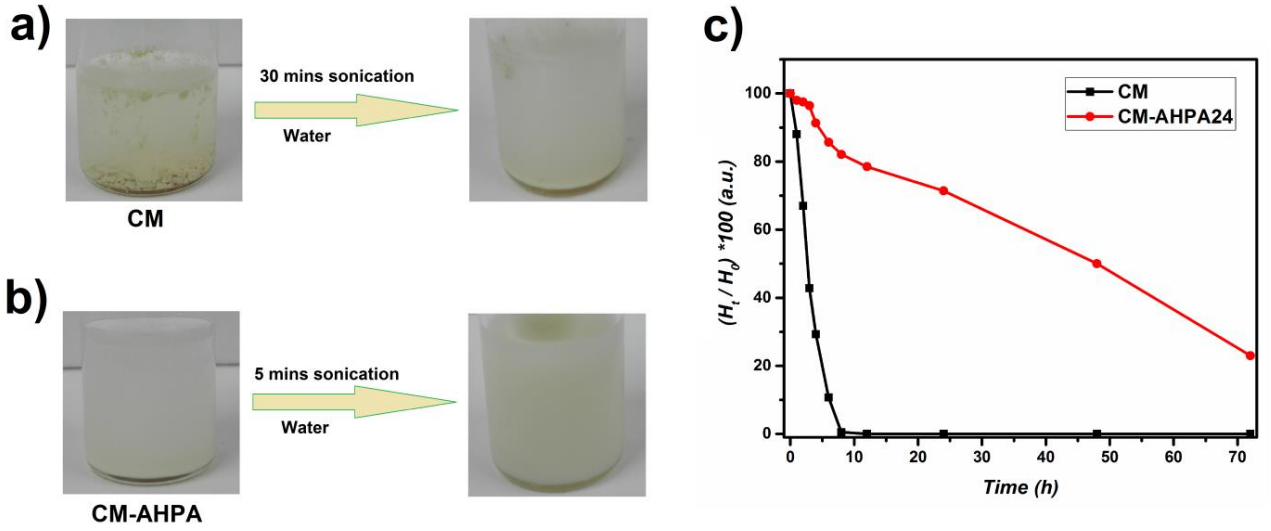

Figure 6.6. (a) CM in water before and after 30 minutes sonication, **(b)** AHPA modified CM in water before and after 5 minutes sonication, **(c)** sedimentation graph of unmodified and AHPA modified CM in water over 3 days.

To analyze the sedimentation process, initial heights of dispersions (H_0) as well as the heights of the dispersed phases in specific time intervals (H_t) were measured to yield a sedimentation graph as shown in Figure 6.6c. Moreover, sedimentation images of CM and AHPA modified CM over defined times can be found in Figure 6.7.

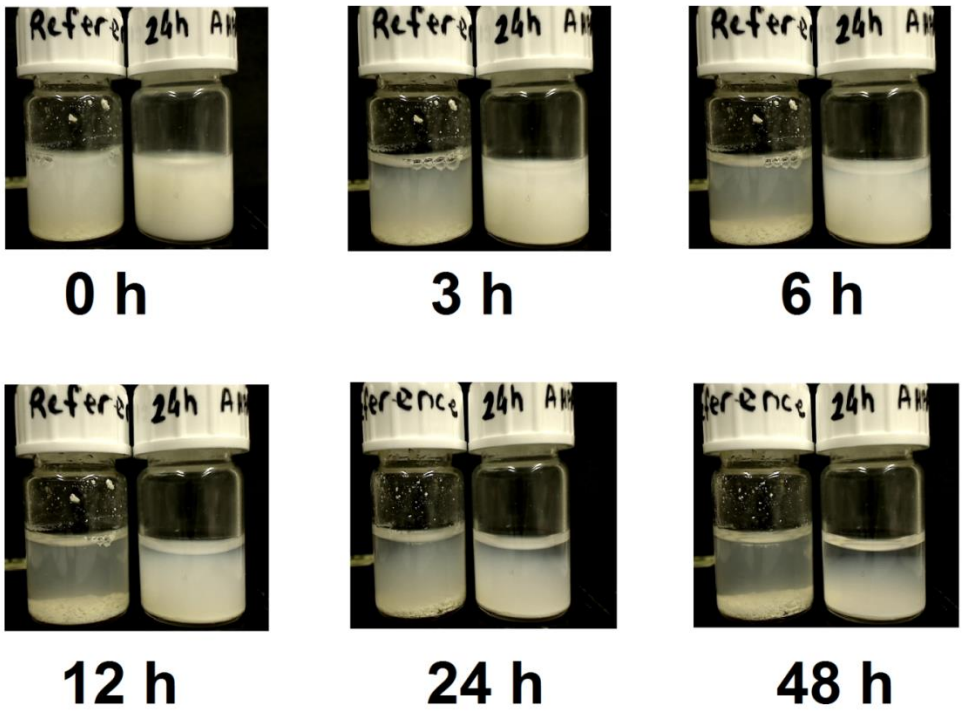

Figure 6.7. Sedimentation images of reference (left vial) and CM-AHPA (right vial) water dispersions over time.

All these results confirm the stability of CM-AHPA dispersion along with benign dispersion preparation. Dispersions of AHPA modified CM from control experiments with hole or electron scavengers also show stability over 3 hours (Figure A37a), where the product from both electron and hole scavenger reaction has poor dispersibility comparable to non-modified g-CN (Figure A37b). In addition, only small amounts of non-modified g-CNs can be dispersed (as low as 0.05 wt.%). In contrast, the hydrophilic character of AHPA modified CM also allows to disperse increased amounts of g-CN in water. Therefore, enhanced activity per volume of g-CN might be the case. Overall, grafting of sulfonic acid groups onto the surface of g-CN improved the dispersion properties of g-CN in water significantly. Dispersions can be prepared in shorter times, are stable over much longer periods, and increased amounts of g-CN can be introduced into dispersion, which is of significant interest for various applications of g-CN.

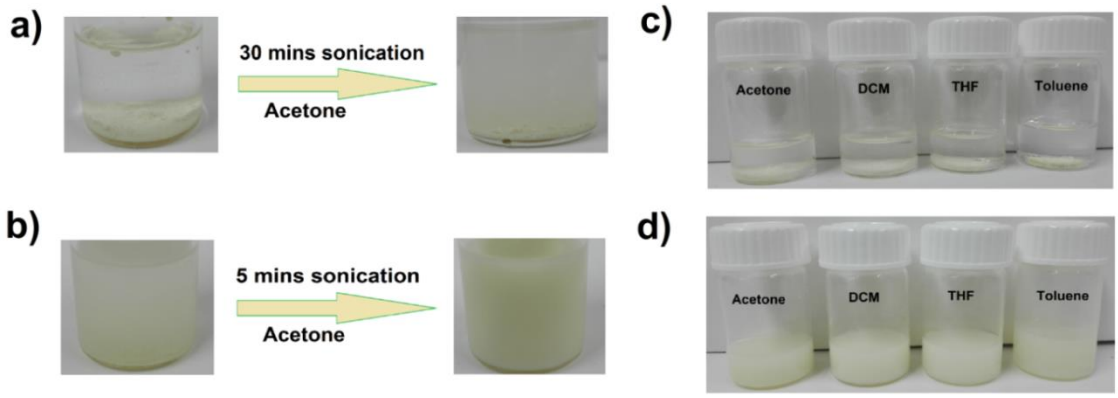

Figure 6.8. (a) CM in acetone before and after 30 minutes sonication, **(b)** 1-decene modified CM in acetone before and after 5 minutes of sonication, **(c)** 1-decene modified CM in 4 different organic solvents before sonication **(d)** 1-decene modified CM in 4 different organic solvents after 10 minutes sonication (0.8 wt.%).

Some applications such as organic coupling require organic solvent as medium. However, g-CN entails usually poor organic dispersibility. Therefore, the medium chain alkene 1-decene was used to improve the dispersion in organic media. In the case of CM, only poor dispersibility in organic solvents exists, e.g. in acetone before and after 30 minutes of sonication, where most of the material remains non-dispersed (Figure 6.8a). On the other hand 1-decene modified CM yields good dispersions in acetone after 5 minutes sonication (Figure 6.8b). The 1-decene modified CM stays dispersed over a significantly longer period than unmodified CM (Figure 6.9).

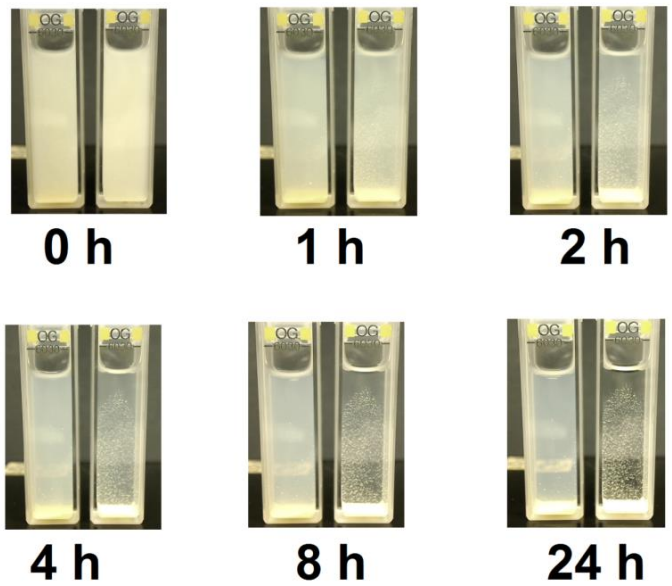

Figure 6.9. Sedimentation images of CM-Decene (left cuvette) and CM reference (right cuvette) acetone dispersions over time. Dispersions were prepared by 10 minutes sonication.

The images of unmodified and 1-decene modified CM dispersions in acetone and their sedimentation over distinct periods confirm the partial stability of 1-decene modified CM dispersions in acetone. Other common organic solvents were also investigated as shown in Figure 6.8c-d. The addition of 1-decene modified CM to acetone, DCM, THF and toluene leads in all the examined cases to uniform dispersions after 10 minutes of sonication. Moreover, it could be shown that the solid content of CM-decene could be increased up to 2 wt.% in organic dispersions. Overall, grafting with 1-decene enhances the organic character of g-CN which is beneficial for the preparation of organic dispersions and might be useful for a variety of applications.

Introduction of Functionalities

In order to show the generality of the approach, functionalities were introduced as well, namely amine and fluoro functionalities via allylamine and perfluoro-1-decene, respectively. Possessing an amino group, allylamine can be protonated in acidic conditions, which leads to cationic, but pH sensitive materials. On the other hand fluorinated 1-decene might lead to fluorophilic materials. In addition, the fluorinated molecule allows easy detection of grafting as fluorine is a marker atom. Reactions were performed in a one pot procedure under visible light (see Appendix for experimental details). Allylamine grafting was achieved in ethanol at 40 °C, and fluoro-modification was performed in THF at 50 °C. Initial results did not show a significant size change or altered zeta potential values (Table 6.3). However, increased C/N ratios were observed in both cases. As g-CN has better absorption in the UV range, grafting with 1-decene or perfluoro-1-decene was also investigated via UV light irradiation at a wavelength of 395 nm. It was concluded that grafting via UV light is indeed more effective with enes that show otherwise low activity, which is in line with the already discussed recombination mechanism that is most likely the basis for the grafting reaction. In the case of UV light induced grafting, also lower reaction temperatures can be utilized (Table A3).

Table 6.3. Properties of unmodified, allylamine and perfluoro decene modified CMs.

Sample	D_n (nm)[a]	Zeta Potential (mV)	C/N Ratio[b]
CM	2448	-27.5	0.6025
CM-AA	2265	-28.9	0.7433
CM-F	2198	-6.4 (in acetone)	0.6617
CM-AA reference[c]	2376	-26.9	0.6112
CM-F reference[c]	2407	-4.7 (in acetone)	0.6054

[a] DLS measurements were performed in acetone (0.05 wt.%) and intensity weighted diameters are presented, [b] obtained by elemental analysis results, [c] reference reaction based on mixing reactants without visible light irradiation and subsequent purification

Elemental mapping of perfluoro decene grafted CM clearly indicates the existence of fluorine atoms on the surface (Figure 6.10a).

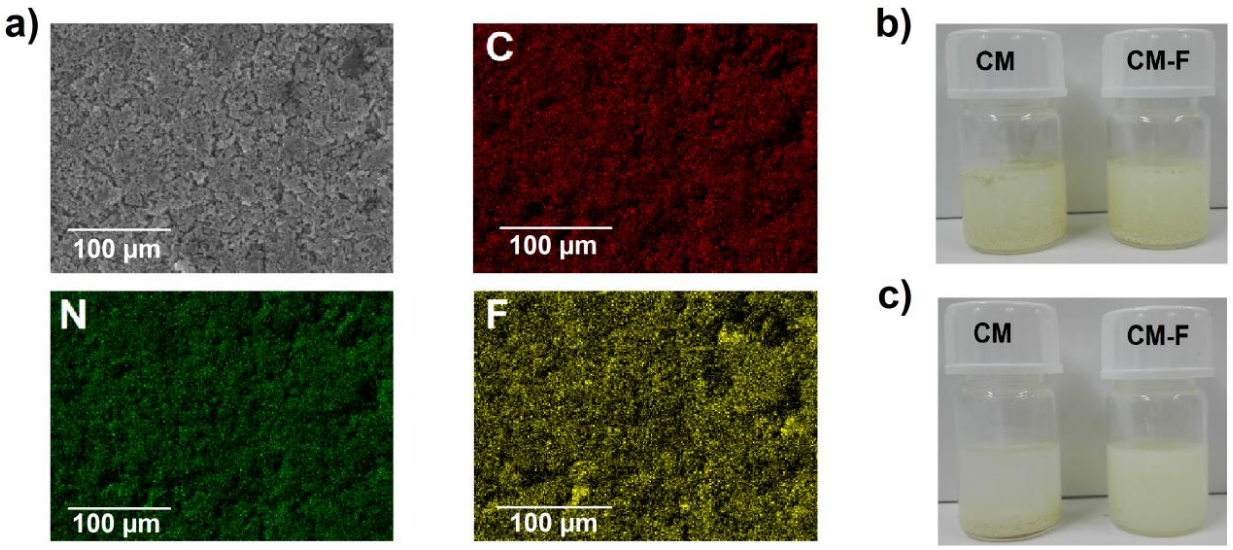

Figure 6.10. (a) Elemental mapping of perfluoro decene grafted CM via EDX, **(b)** CM and fluoro modified CM (CM-F) in hexafluorobenzene before sonication, **(c)** CM and CM-F in hexafluorobenzene after 30 minutes sonication.

Introduction of fluorine atoms provides fluorophilic character to g-CN, which allows dispersibility in fluorosolvents. For example hexafluorobenzene was used as solvent and 0.4 wt.% non-modified and fluoro modified CM were dispersed (Figure 6.10b-c). Sonication for 30 minutes does not lead to dispersion of non-modified CM as almost all of the material remains

non-dispersed at the bottom of the vial. A similar result was observed when CM-decene was utilized in hexafluorobenzene. On the other hand CM-F has better dispersion properties and yields a uniform dispersion. However it is important to note that sedimentation of this dispersion starts after 5 minutes and sediments completely after 1 hour. Theoretically the increased density of hexafluorobenzene should slow sedimentation down. Nevertheless, fast sedimentation was observed that might be due to the low dielectric constant of the solvent hexafluorobenzene, which promotes Hamaker forces between the sheets. Yet, it is easy to re-disperse the material even via gentle shaking by hand. Therefore the fluoro grafted material can be of great interest as a catalyst within fluorinated solvents under continuous mixing.

pH Dependent Dispersion

Allylamine functionality was introduced to illustrate the option of a pH dependent dispersibility in aqueous media. In acidic pH (pH=4), allylamine modified CM yields uniform dispersions via protonation of amino groups. On the other hand increasing the pH of the medium to the basic range (pH=9) causes immediate precipitation of solid particles due to deprotonation of amino groups (Figure 6.11). Re-acidification of the medium leads to uniform dispersions once again, so the dispersion process is reversible. In aqueous media, allylamine modified CM shows high pH sensitivity and can be effective when acidic conditions are needed. Moreover, ease of separation after base addition makes this material highly beneficial for pH dependent reaction media and recycling of the catalytic material. Another attractive application that might be accessible via ionically modified CM is anion-cation-driven layer-by-layer deposition, which is a method that generates well defined superstructures on surfaces and in dispersion.[177-178]

Figure 6.11. Allylamine modified CM in water (1 wt.%) at acidic pH (pH=4), observation of immediate precipitation after base addition (pH=9), complete sedimentation after standing for 2 hours and redispersion after re-acidification (pH=4).

6.3. Conclusion

Overall, visible light induced, one pot grafting approach for g-CN for enhanced dispersion features was introduced, while keeping the photoproperties of g-CN unchanged. Using molecules with allylic double bonds avoids monomer polymerization and provides a monolayer dispersion stabilization. Sulfonic acid group of AHPA provides excellent hydrophilicity and grafting 1-decene provides significant organo dispersibility for g-CN. These changes result in minimal times for redispersion preparation, higher dispersion stability and increasing the possible highest solid content (e.g. or hybrid formation) of dispersed systems significantly. It is also possible to introduce pH dependent dispersion stability on CM *via* allylamine groups or fluorophilic character by integrating perfluoro-1-decene molecule. The presented method can help to expand the whole g-CN field as dispersibility is a substantial aspect for heterogeneous catalysis systems.

7. Extremely Compressible Hydrogel via Incorporation of Modified Graphitic Carbon Nitride [a]

7.1. Overview

Herein, the fabrication of hydrogels with extreme compressibility and skin-like features is presented. For this purpose, sulfonic acid modified carbon nitride (g-CN-AHPA) is utilized as visible light photoinitiator and covalent reinforcer for hydrogel synthesis. Hydrogels with 2 wt.% g-CN-AHPA content and a water content around 90 wt.% show unusual compressibility upon temporary deformation into a thin and flat form and remain undamaged after stress removal. Cyclic compressibility proves the durability of the covalently reinforced system. Interestingly, the hydrogels possess tissue adhesive properties, shock resistance, flexibility, cut resistance and little to no toxicity. Overall, a novel hydrogel system featuring remarkable mechanical properties and easy fabrication via visible light irradiation is reported.

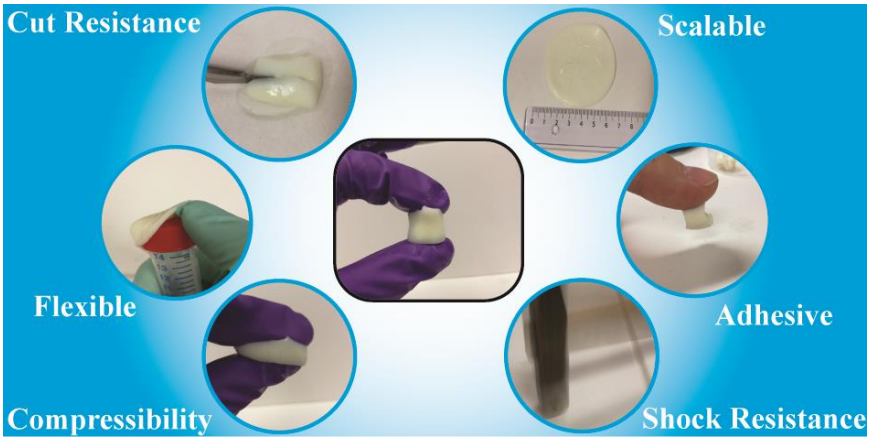

Figure 7.1. Scheme showing the properties of g-CN-AHPA based hydrogel.

[a] Terms of use: This chapter was adapted with permission from B. Kumru, V. Molinari, R. Dünnebacke, K. G. Blank, and B. V. K. J. Schmidt, 'Extremely Compressible Hydrogel via Incorporation of Modified Graphitic Carbon Nitride', *Macromol. Rapid Commun.*, **2019**, 40 (4), 1800712. Copyright 2019, John Wiley and Sons.

7.2. Results-Discussion

Chapter 6 showed the surface functionalization of g-CN via sulfonic acid groups (g-CN-AHPA), which provides enhanced dispersibility of g-CN in aqueous media. From the hydrogel synthesis point of view, preparing g-CN aqueous dispersion with high solid content would be of interest to examine the effect of g-CN surface on mechanical properties of resulting pure hydrogels. Therefore, g-CN-AHPA was synthesized via cyanuric acid-melamine complex and surface modification as reported in literature.[16, 172] Modification of g-CN with AHPA was confirmed via elemental analysis and zeta potential (Table A4), as well as EDX mapping in SEM (Figure A38) and spectroscopy (Figure A39). In the next step, different concentrations of g-CN-AHPA were employed for one pot, visible light induced synthesis of hydrogels with acrylamide (AAm)/ DMA monomer mixtures (3:1) with MBA crosslinker in water (Figure 7.2, Table 7.1).

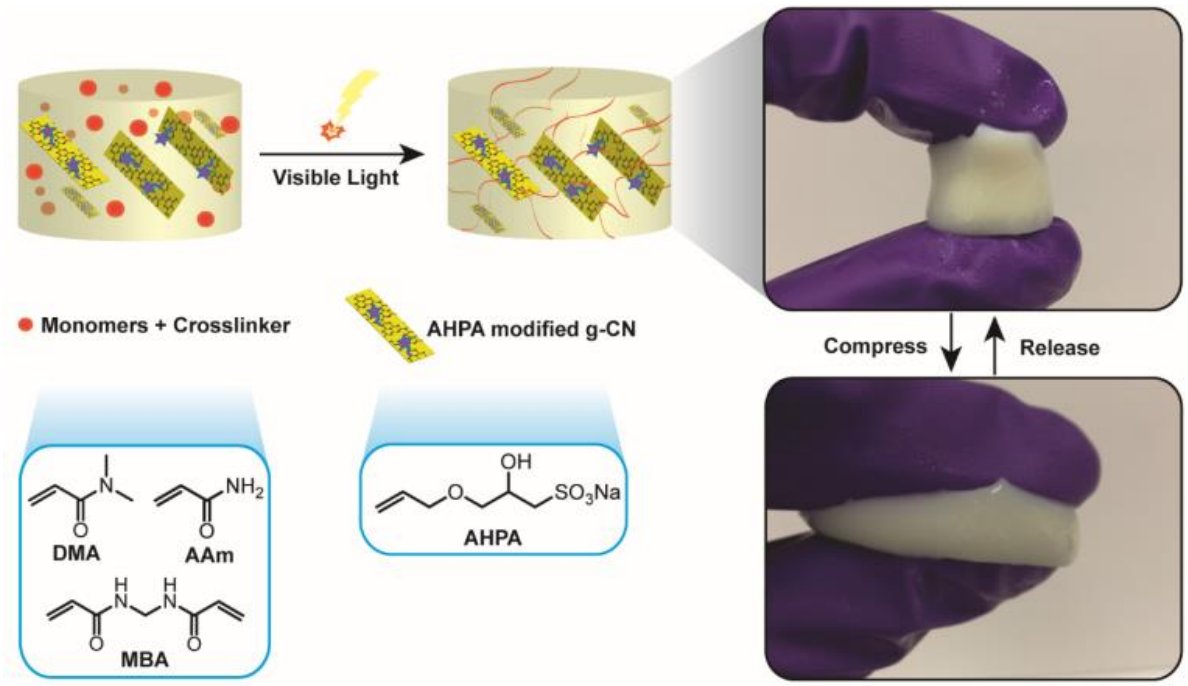

Figure 7.2. Overview for the synthesis of g-CN-AHPA hydrogel and images of final hydrogel product.

Even though the employed g-CN content is relatively higher compared to previous chapters, gelation is achieved over 4 hours, which might be due to the fact that some active sides of g-CN were anchored with sulfonic acid groups during surface modification.

Hydrogels with water contents between 87% and 92% were synthesized and characterized via rheology.

Table 7.1. Overview of mechanical properties of g-CN-AHPA hydrogels.

g-CN-AHPA content (wt.%)	**Water content (wt.%)**	***G'* (Pa)[c]**	***G''* (Pa)[c]**	***G'* (Pa)[d]**	**Change in *G'* after back process (%)[c]**	**E_{mod} (MPa)[e]**
0.35[a]	99	469	69.4	387	-13	0.41
1[b]	91	584	130	645	15	0.92
2[b]	90	114	44.1	123	14	1.63
3.5[b]	89	5840	1300	6450	17	10.76
5[b]	87	44300	3940	27100	-42	0.21

[a]composed of 0.45 wt.% AAm, 0.15 wt.% DMA and 0.05 wt.% MBA, [b]composed of 6 wt.% AAm, 2 wt.% DMA and 0.03 wt.% MBA [c]at 0.1% strain, [d]at 20% strain, [e]calculated at 10% strain before the break or at 10% before maximum strain.

The formed materials are in gel state at any strain (storage moduli (*G'*) > loss moduli (*G''*)) and *G'* values show a slight increase with increased frequency (Figure 7.3). Materials show a decrease in *G'* values with increasing strain due to shear thinning effect, which is more pronounced with high g-CN-AHPA content (5 wt.%, 38% decrease in *G'* value at 20% strain). The softest hydrogel with the lowest *G'* value is 2 wt.% g-CN-AHPA hydrogel, however it shows excellent recovery in *G'* and *G''* values at any strain (Figure 7.3a). Upon rotational compression in the rheometer, self-standing 2 wt.% g-CN-AHPA hydrogel shows an outstanding compressibility, remaining undamaged after removal of stress.

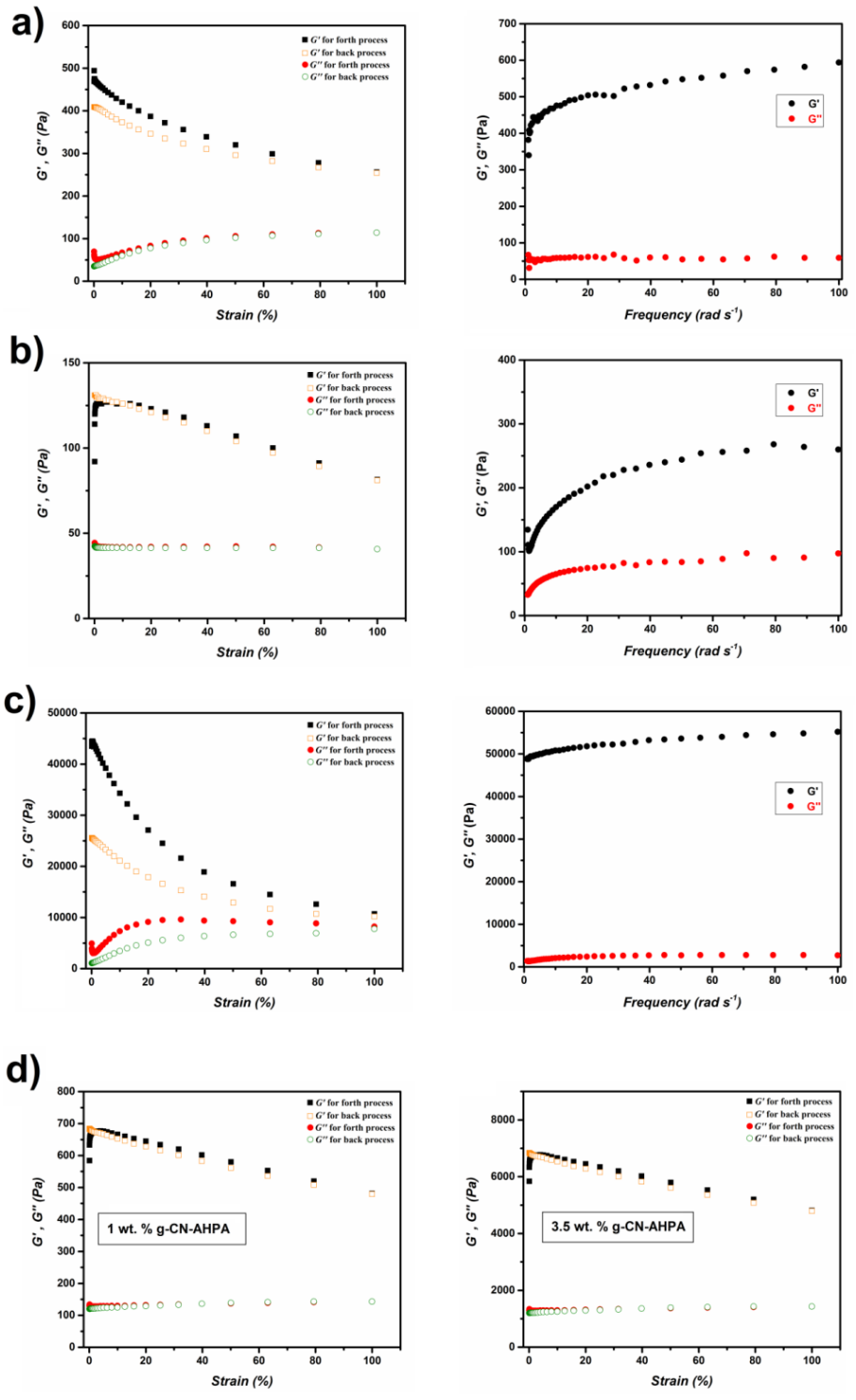

Figure 7.3. Comparison of storage and loss modulus values of **(a)** 0.35 wt.% g-CN-AHPA, **(b)** 2 wt.% g-CN-AHPA and **(c)** 5 wt.% g-CN-AHPA hydrogels against strain (left, *G'* values are black and orange squares and *G''* values are red and green circles, back (open) and forth (filled) process) and frequency (right), **(d)** storage and loss modulus values of 1 wt.% g-CN-AHPA (left) and 3.5 wt.% g-CN-AHPA hydrogels.

Solid state analysis shows the incorporation of g-CN-AHPA into the hydrogels (Figure A40), e.g. UV-Vis spectra of freeze dried hydrogels follow the characteristic absorption of g-CN-AHPA (220-480 nm). XRD shows signal around 27°, which is assigned to the typical aromatic interlayer stacking of g-CN sheets and intensity correlates with the incorporated amount of g-CN-AHPA. In addition, FT-IR results show bands from both g-CN (bands between 1630-1230 cm^{-1} from C=N and C-N stretching) and monomers (around 1750 and 2900 cm^{-1} as carbonyl and N-H stretching). SEM image of freeze dried 2 wt.% g-CN-AHPA and relative elemental mapping clearly shows the incorporation of sulfur atoms arising from sulfonic acid group of g-CN-AHPA which is homogenously distributed through the porous hydrogel network (Figure A41).

Mechanical Properties of Hydrogels

Subsequently, compression tests were performed for more information on the mechanical properties of hydrogels. Interestingly, 0.35 wt.%, 1 wt.% and 5 wt.% g-CN-AHPA containing hydrogels show mechanical failure at low forces (around 80 N) and resulted in cracking under compression (Figure 7.4b). The intermediate hydrogel with 3.5 wt.% g-CN-AHPA shows resistance up to 600 N but breaks at a strain around 50%. Remarkably, 2 wt.% g-CN-AHPA containing hydrogel showed excellent compressibility even at forces of 800 N. The soft material shows almost no resistance for compression up to 70% strain but shows significant response at high strain values (~800 N) remaining undamaged after removal of stress (Figure 7.4b-c). The cylindrical shaped material shows remarkable elastic properties as it transforms into thin and flat form upon strong compression. The original shape is immediately retained after removal of stress (Figure 7.4e), even when the stress is not equally received. Herein, another important factor to discuss is absorption of the applied stress. In most of the known hydrogel systems non-uniform stress causes dramatic damage via unequal stress distribution, which is in contrast to the presented g-CN-AHPA hydrogel.

Elastic modulus values showed quite low results for 0.35, 1 and 5 wt.% g-CN-AHPA hydrogels, while 2 wt.% and 3.5 wt.% g-CN-AHPA hydrogel possess highest elastic modulus values (Table 7.1). These calculations were performed at 10% strain before the break or at 10% before maximum strain. However, 2 and 3.5 wt.% g-CN-AHPA hydrogels possess different compression profiles as they show a non-gradual increase. Therefore, elastic moduli values were also calculated right before the break, which follow the same trend as 10% before the break.

Especially 2 and 3.5 wt.% g-CN-AHPA hydrogels show very high elastic moduli (64.1 and 68.7 MPa, respectively) (Table A5). 2 wt.% g-CN-AHPA hydrogel is flexible enough under compression and can withstand forces up to 800 N, even when the force is received non-uniformly. Due to physical changes upon compression (regardless of initial shape and surface area), rough calculation of compressive strength value for presented hydrogel is approximately 18 MPa, which is remarkable for a covalent hydrogel, especially when compared to systems with non-covalent reinforcements and having the high water content of the presented hydrogel in mind.[179-183] The mechanical performance of the hydrogel is clearly in the range to meet the criteria for tough cartilage-joint systems where the average cyclic stress ranges from 6 MPa up to 14 MPa with daily activities like walking or running.[184-185] One important, distinct characteristic of the presented hydrogel lies beneath its softness, which allows improved stress load distribution compared to though hydrogels.

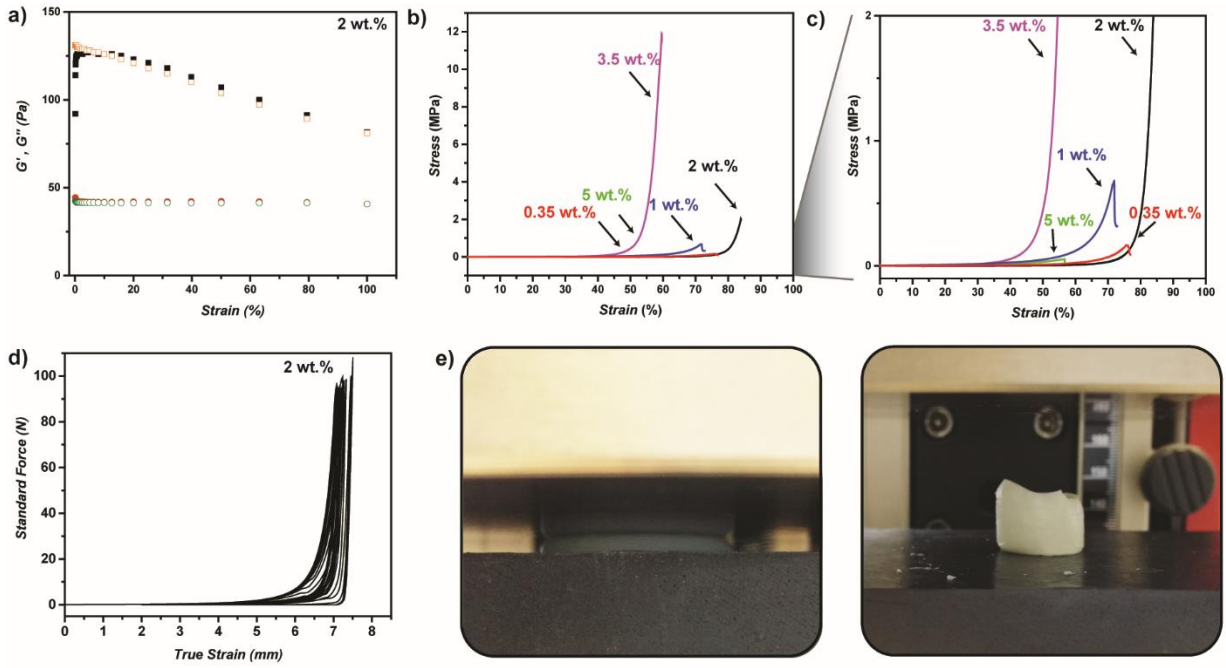

Figure 7.4. (a) Rheology results of 2 wt.% g-CN-AHPA hydrogel (black squares: *G'* forth process; orange squares: *G'* back process; red circles: *G''* forth process; green circles: *G''* back process), **(b)** Compression test results of g-CN-AHPA hydrogels (red: 0.35 wt.%; blue: 1 wt.%; black: 2 wt.%; violet: 3.5 wt.%; green: 5 wt.%), **(c)** magnification of compression test results of g-CN-AHPA hydrogels, **(d)** cyclic compression (50 cycles) test results of 2 wt.% g-CN-AHPA hydrogel and **(e)** images of 2 wt.% g-CN-AHPA hydrogel during (left) and after (right) compression.

Cyclic compression of 2% g-CN-AHPA hydrogel at high forces shows recovery of the material properties, which proves the durability of the hydrogel system (Figure 7.4d). Durability of a material containing a covalently bonded reinforcer is an important factor, as possible damages are non-healable. The 2% g-CN-AHPA hydrogel shows excellent performance at 100 N of applied force, going from completely thin and flat structure back to original shape for at least 50 cycles, which is a clear statement for the fatigue resistance of the material.

Physical Properties and Toxicity Investigation of Hydrogels

2 wt.% g-CN-AHPA hydrogel has other interesting properties as well, e.g. it is quite resistant against compression with scalpel (Figure 7.5a), remaining undamaged even after repetitive compressions. For such a soft and covalently reinforced hydrogel, resistance to compression with sharp materials shows the strength of the network. In addition, the hydrogel is also flexible enough to cover surfaces such as polypropylene (PP) caps (Figure 7.5b) or bending the circular shaped hydrogel around a finger.

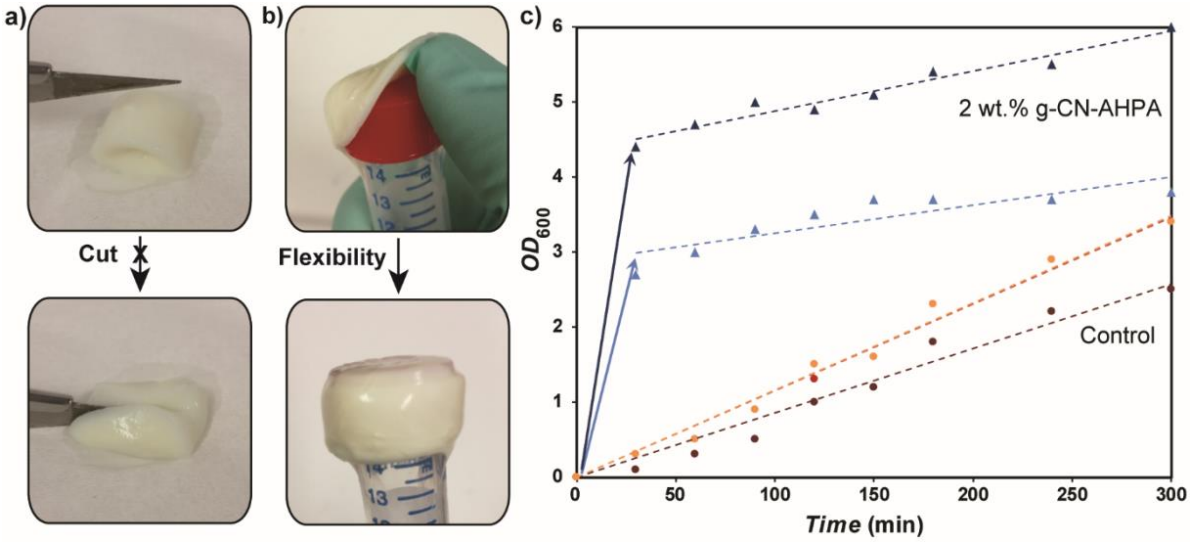

Figure 7.5. 2 wt.% g-CN-AHPA hydrogel **(a)** under compression with blade, **(b)** hydrogel covering the poly(propylene) (PP) cap of a centrifuge tube, **(c)** bacteria growth tests, showing an increase in the optical density at 600 nm (OD_{600}) in the presence of hydrogels (blue data: 2 wt.% g-CN-AHPA hydrogels; orange/red/brown data: control samples).

In order to elucidate future applications in the biomedical field, first investigations regarding toxicity of the present hydrogels were conducted as toxic effects might arise from residual

unreacted monomer moieties or the incorporation of g-CN. To test for possible toxicity, bacterial cultures (*E. coli*) were grown in the presence of hydrogel pieces, added to the culture medium right after synthesis without purification. Bacterial growth curves were compared to a negative control where no hydrogel was added (Figure 7.5c). In the samples containing the hydrogel, the optical density at 600 nm (OD_{600}) increases sharply during the first 30 min and insoluble aggregates appear in the culture medium. This was attributed to g-CN leaching out of the hydrogel into the culture medium. Afterwards, a steady increase in the OD_{600} value is observed. When compared to the negative control, the growth rate is decelerated in the presence of hydrogel. However, the bacteria are able to divide at a constant rate. Thus, it was tentatively concluded that the investigated hydrogels are non-toxic and that the decelerated growth rate most likely originates from the release of g-CN, which can be removed with thorough washing.

The presented hydrogel strongly adheres to tissue, e.g. to skin after gentle touch (Figure A42). Skin-like feeling and bioadhesive properties may be of interest for biomedical applications, such as wound dressings and surgical sealants.[186-187] The hydrogel does not only adhere to skin, but also to a variety of surfaces such as glass, metal, paper and PP (Figure 7.6).

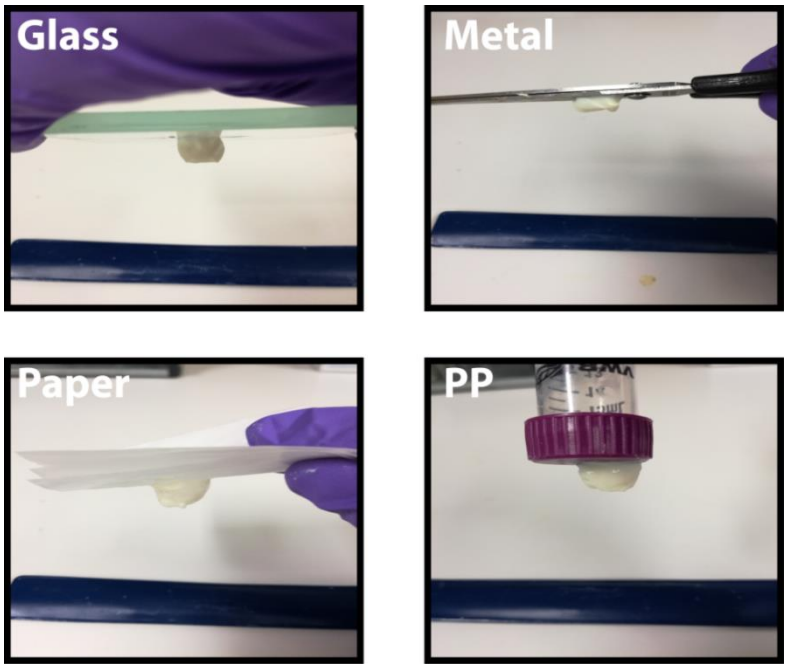

Figure 7.6. Adhesion of 2 wt.% g-CN-AHPA hydrogel onto various surfaces.

During compression experiments, the force is applied at a gradual rate, giving the material the chance to absorb the stress with time. In a shock-type compression, stress is received non-gradually and immediately, which is a property that needs to be improved for hydrogels.[188] To

visualize shock absorption, the present hydrogel was hit with a 3 kg weight hammer, and no sign of fracture was observed.

Swelling in water is an important property of hydrogels. Usually, addition of reinforcer (such as clay) decreases water uptake due to increased crosslinking density and hydrophobic interactions.[169] Hence, it is a challenging task to improve mechanical and preserve swelling properties of hydrogels simultaneously. For the swelling properties, interestingly 2 wt.% g-CN-AHPA showed the highest swelling ratio with 2476% (Figure A40-d), yet still showing similar rheology profile and compressibility to the one right after gelation (Figure 7.7a). The preservation of mechanical properties in the presence of high amounts of water is a significant feature of the presented hydrogel material. 5 wt.% g-CN-AHPA swells the least (254%) due to higher amount of reinforcer and increased crosslinking, and 0.35 wt. % g-CN-AHPA has a swelling ratio of 1750%, which is still considerably high for hydrogel systems. Interestingly, swelling in acidic or basic media significantly affects the hydrogel structure. In the case of 2 wt.% g-CN-AHPA hydrogel swelling in 0.1 M HCl and 0.1 M NaOH solutions, rheology of both swollen hydrogels showed a significant decrease in *G'* and *G''* values, yet showing similar strain dependency (Figure A43a-b). Swelling ratio in basic media is almost 3 times higher than in acidic media (3855% to 1310%) (Figure A43c), which can be attributed to the incorporated sulfonic acid group.

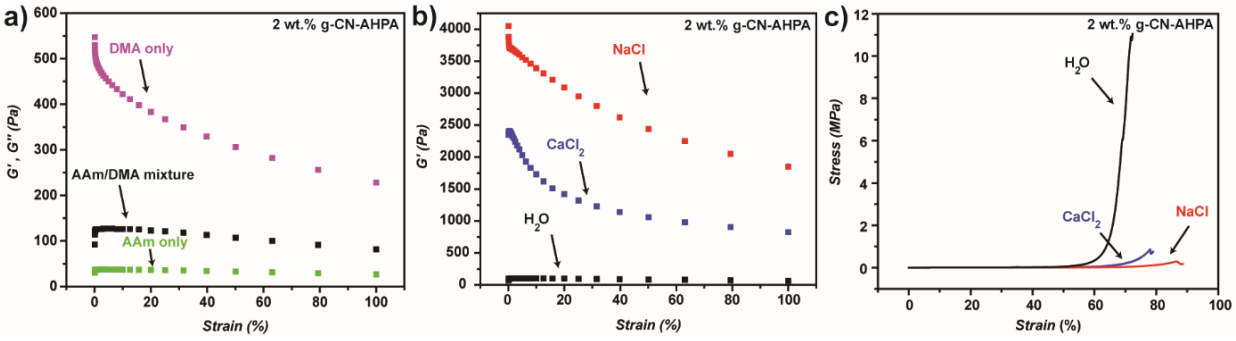

Figure 7.7. (a) Rheology of 2 wt.% g-CN-AHPA hydrogel from different monomers (black squares: AAm/DMA mixture; violet squares: pure AAm; green squares: pure DMA), **(b)** Rheology fully swollen 2 wt.% g-CN-AHPA hydrogel (black squares: in water; red squares: NaCl solution; blue squares: $CaCl_2$ solution) and **(c)** compression profiles of fully swollen 2 wt.% g-CN-AHPA hydrogels (black line: in water; red line: NaCl solution; blue line: $CaCl_2$ solution).

To gain a deeper understanding of the toughening mechanism of 2 wt.% g-CN-AHPA hydrogel reference materials were fabricated. First of all, a comparison with hydrogels formed from a

single monomer was investigated. 2 wt.% g-CN-AHPA hydrogel from AAm shows a soft rheology profile with good recovery (*G'* 30 Pa at 0.1% strain). On the other hand, hydrogel from DMA is almost five times stronger than the 3:1 monomer mixture (550 Pa at 0.1% strain), while a significant strain dependency and a yield stress of approximately 150 Pa is observed (Figure 7.7a, A44). The utilization of monomer mixtures increases *G'* values of hydrogel compared to AAm hydrogel (effect from DMA) in addition a preserved recovery profile is obtained (effect from AAm). However, hydrogels from individual monomers break at gentle compression. Performed control experiments provide a hint for the necessity of using monomer mixtures with certain g-CN-AHPA ratio, which leads to a softening of the gel and a significant decrease in shear thinning behaviour. Thus, the applied compression force can be effectively distributed over the whole network.

As shown in compressions tests, there was a non-linear increase in *G'* and *G''* values with increased g-CN-AHPA content, which may be due to amplified sheet-sheet interactions. Similar to the optimum monomer ratio there is also an optimum amount of g-CN-AHPA incorporation to balance between stiffness of the hydrogel and elasticity. Conclusively the negative charge on the g-CN surface plays an important role for reinforcement.[159] Thus, swelling of 2 wt.% g-CN-AHPA hydrogels in salt solutions (0.2 M in NaCl or $CaCl_2$) was performed. Compared with the water swollen hydrogel, swelling in salt media significantly increases *G'* and *G''* values by gaining highly shear thinning behavior, which may be due to possible cluster formation, originating from cation of salt-anion on g-CN-AHPA surface interaction (Figure A45).[189] However, hydrogels swollen in salt solution are easy-to-break upon compression at forces around 100 N (Figure 7.7c). Also, the elastic moduli values decrease in salt swollen hydrogels, compared to the water swollen reference (1.15 MPa for fully water swollen, 0.64 MPa for NaCl swollen and 1.47 MPa for $CaCl_2$ swollen hydrogel). Preserving negative charge on g-CN surface inside the hydrogel possibly plays the most important role for the extreme compressibility due to strong repulsion of negatively charged sheets upon stress. Decreasing g-CN-AHPA content increases polymer network density per sheet, which may hinder the repulsion of sheets upon stress. Oppositely, increasing g-CN-AHPA content decreases the polymer network density per sheet, and π-π interactions of g-CN sheets become more pronounced and provide toughness (increased *G'* values), yet still fail to improve compression upon stress.

7.3. Conclusion

Overall, novel reinforced soft hydrogel materials were reported. The hydrogels feature outstanding mechanical properties such as compressibility, cut and shock resistance as well as tissue adhesive properties with moderate flexibility. Sulfonic acid modified g-CN is utilized as photoinitiator and covalent reinforcer under visible light for one pot hydrogel synthesis. Different concentrations of g-CN-AHPA can be introduced while retaining high amounts of water (up to 99 wt.%). A weight content of 2 wt.% g-CN-AHPA leads to hydrogels that possess excellent compressibility above 800 N with around 18 MPa compressive strength and show elastic behaviour without loss for 50 cycles at 100 N loading. The presented hydrogels show similar resistance when the stress is received non-uniformly. It is believed that the presented hydrogel can be of great interest in bioapplications such as soft tissue engineering, wound healing, joint replacement and surgical sealant. Due to the skin-like soft feeling, g-CN-AHPA hydrogel might replace PDMS in wearable electronics in the near future.

8. Polymer Grafted Graphitic Carbon Nitride as Precursors for Reinforced Lubricant Hydrogels[a]

8.1. Overview

Chapter 7 focussed on soft but extremely compressible skin-like hydrogel. In the present chapter synthesis of tough and cartilage-like hydrogels utilizing g-CN is presented. g-CN prepolymer was synthesized via grafting of DMA polymer chains on g-CN surface in water:EG mixture via visible light. The resulting gel-like viscoelastic liquid can serve as precursor for hydrogel synthesis, via mixing with secondary monomer, crosslinker and water to yield tough organohydrogels without external photoinitiator. Utilization of charged monomers allows fabrication of lubricant hydrogels with various mechanical properties. Organohydrogel intermediates can be transformed to pure hydrogels via washing with water as depicted in Chapter 5.

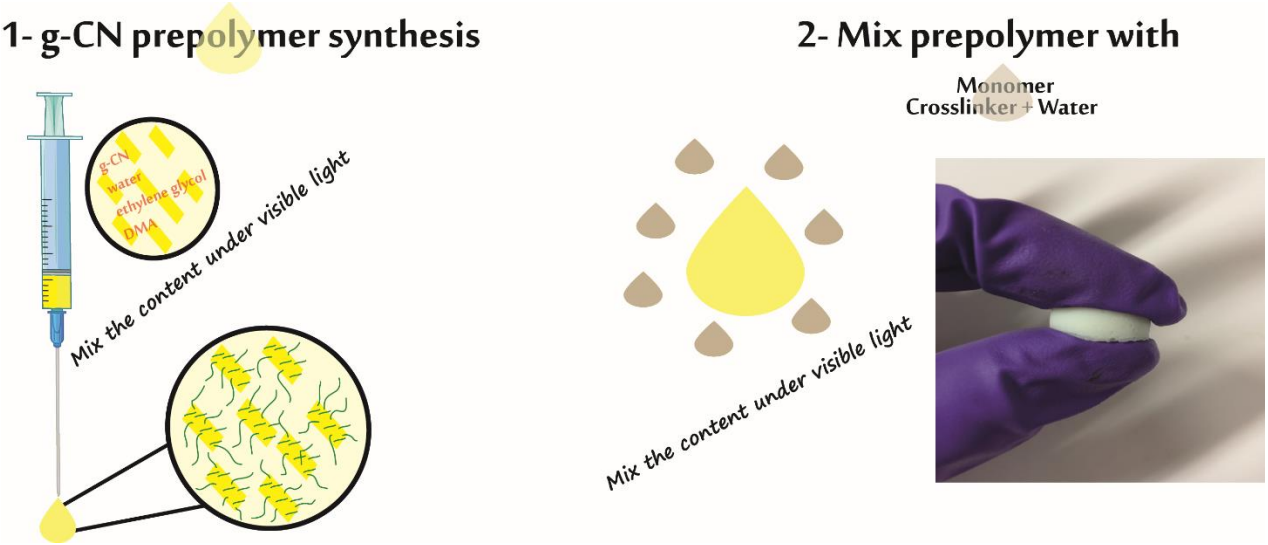

Figure 8.1. Overview for the synthesis of tough hydrogels via g-CN prepolymer.

[a] Terms of use: This chapter was adapted with permission from B. Kumru, V. Molinari, M. Hilgart, F. Rummel, M. Schaeffler and B. V. K. J. Schmidt, 'Polymer Grafted Graphitic Carbon Nitride as Precursors for Reinforced Lubricant Hydrogels" manuscript submitted.

8.2. Results-Discussion

Chapters 4 and 5 showed that g-CN forms radicals on the surface during visible light illumination, and that the 2-D sheet like structure provides crosslinking points for polymeric network. Combining this information with enhanced dispersibility of g-CN in water-EG mixture, g-CN 'prepolymer' was synthesized via adding DMA monomer to g-CN water-EG dispersion and irradiation with visible light. To investigate prepolymer formation, irradiation was applied for different time intervals (1, 3, 6 and 12 h) and rheology profiles were investigated. Storage moduli values (*G'*) increased dramatically over increased reaction times, i.e. more than 100 times between 1 h and 12 h reaction time, yet showing similar strain dependency (Table 8.1, Figure 8.2a, Figure A46-48). The increase can be attributed to grafting and growth of polyDMA chains on surface of g-CN particles. In order to prove aforementioned effect, a prepolymer was prepared with double amount of DMA, irradiated for 3 hours, and its rheology was investigated (Figure A49). In a comparison with the previous recipe, increasing organic content in the prepolymer formulation resulted in much stronger material that exhibits a 10 fold increase in *G'* value. It is important to note that increasing g-CN amounts (more than 3 wt.%) in prepolymer synthesis afford stiff organohydrogels that cannot be further employed as precursor material.

Table 8.1. Storage and loss moduli values of prepolymers with viscosity (summarized from rheology experiments).

Prepolymer type	**Irradiation time (h)**	**Storage moduli (*G'*, Pa) at 0.1 % strain**	**Loss moduli (*G''*, Pa) at 0.1 % strain**	**Viscosity (Pa*s) at 1 s^{-1} shear rate**
g-CN pre1h[a]	1	267	41	0.88
g-CN pre3h[a]	3	11100	870	5.32
g-CN pre6h[a]	6	28200	2370	23.9
g-CN pre12h[a]	12	36050	2340	163
g-CN 2pre3h[b]	3	118000	9500	770

[a]composed of 2 wt.% g-CN, 45 wt.% water and EG, 8 wt.% DMA, [b] composed of 2 wt.% g-CN, 41 wt.% water, 41 wt.% EG, 16 wt.% DMA

As grafting takes place, not only *G'* values, but viscosity of the prepolymer is also expected to change. For longer irradiation times, higher viscosity of the prepolymer is obtained as indicated

from viscosity measurements (Table 8.1, Figure A50-54). Especially, doubling the concentration of DMA monomer resulted in more than a 100 fold increase in viscosity. The increment is attributed to polymer formation and grafting to g-CN surface. Further, evaluation of *G'* values with changing frequency were investigated for g-CN pre3h (which was chosen for hydrogel synthesis in upcoming part), which showed a slight increase in *G'* values with increasing frequency, confirming stable covalent incorporation (Figure 8.2b).

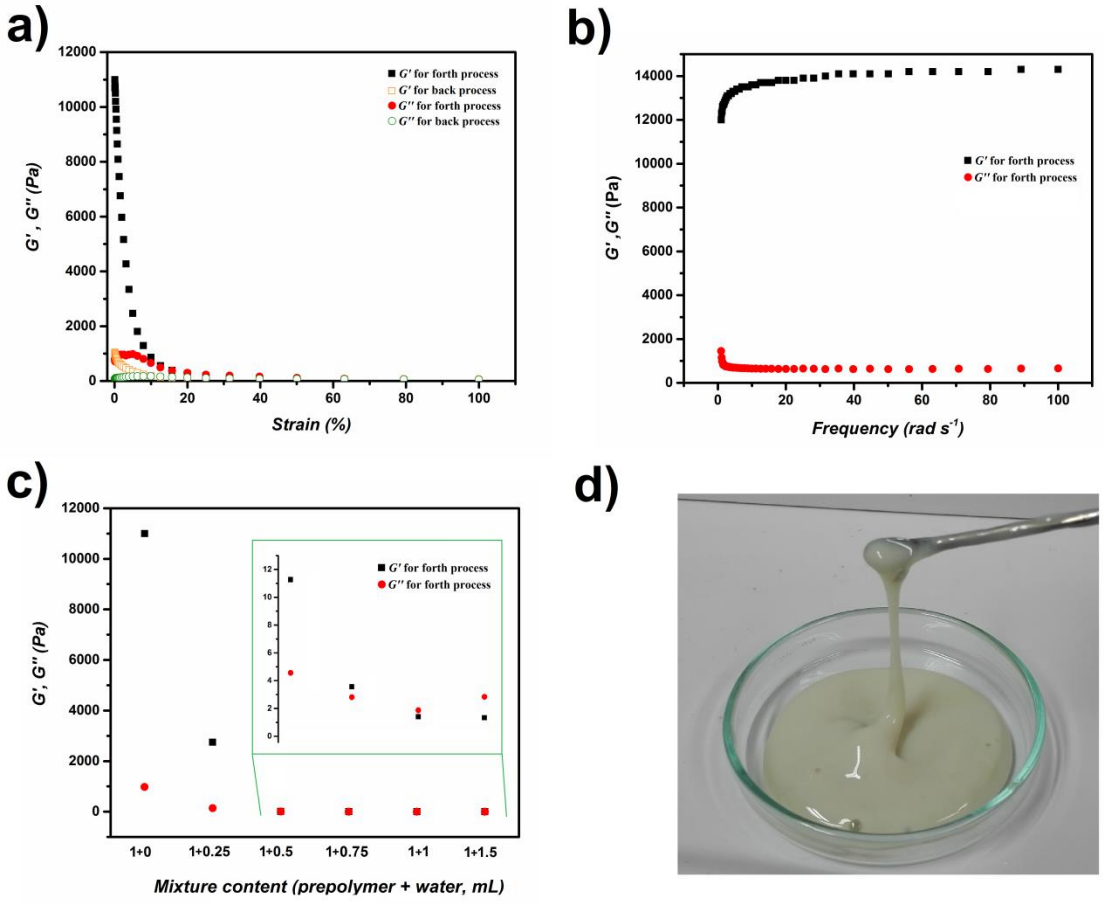

Figure 8.2. Storage and loss moduli values of g-CN pre 3h **(a)** against strain and **(b)** against frequency, **(c)** storage and loss moduli values of g-CN pre 3h and its dilution at 0.1 % strain, **(d)** image of g-CN pre 3h.

One of the main aspects was to study the stability of the prepolymer along with its rheological profile. As prepolymer formation is based on grafting hydrophilic polymers on g-CN surface, no sedimentation was observed in g-CN based prepolymer over 2 months standing, which is highly advantageous for practical applications. Addition of water to prepolymer is expected to result in changes in rheological profile and a transition from gel to sol state. Dilution with water at

different ratios was performed to determine the transition from gel to sol. As expected, addition of water caused significant decrease in *G'* values, and the transition to *G''>G'* was observed at 1:1 dilution (Figure 8.2c, Figure A55-59). Furthermore, TEM and TGA investigations were performed on g-CN pre 3h, showing the dispersed g-CN particles (Figure 8.3a), mass loss profile due to evaporation of water-EG solvents (up to 150 °C) and loss of organic network (around 420 °C), as g-CN shows no decomposition up to the highest applied temperatures (Figure A60). Overall, a homogenous, highly disperse (Figure 8.2d), injectable (Figure 8.3b) and highly stable g-CN based viscoelastic prepolymer was formulated and employed for the exemplary hydrogel formation in the next step. g-CN pre3h was utilized as precursor in the following synthesis procedures.

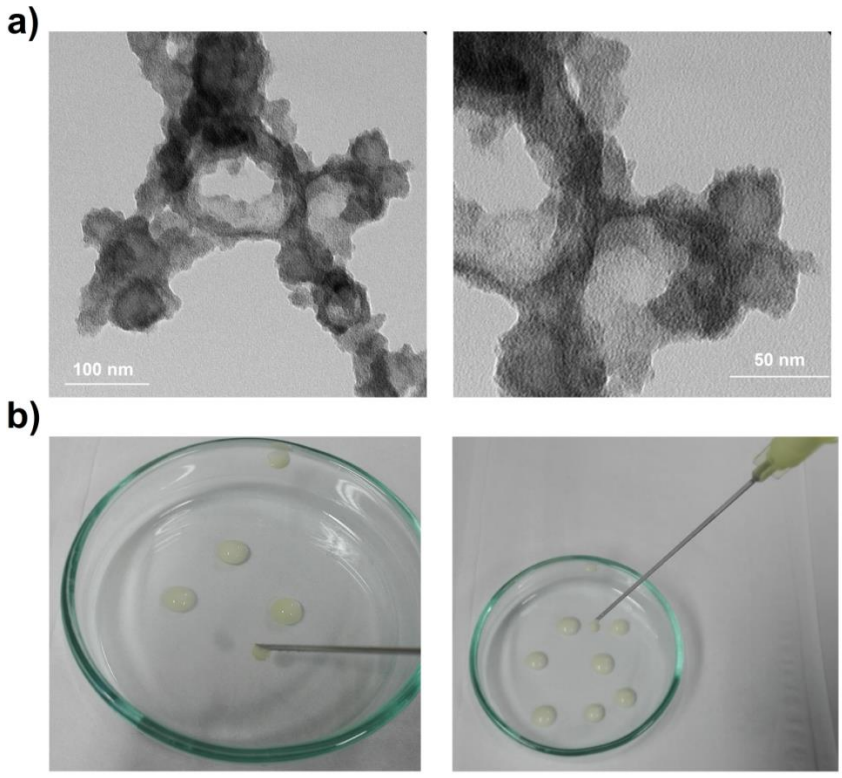

Figure 8.3. (a) TEM images of g-CN pre3h, **(b)** image showing the injectibility of g-CN pre3h.

Hydrogel synthesis using g-CN prepolymer was chosen as an exemplary application which was inspired from double network chemistry.[190] The previous chapters reported the integration of g-CN particles as reinforcer and visible light photoinitiator in hydrogel synthesis, yet the synthesis of mechanically tough hydrogels was not possible. Here, a prepolymer was utilized as precursor

and photoinitiator which can be mixed with monomer and crosslinker, yielding double network-like hydrogels. As the first network constitutes a non-solid viscous prepolymer, resulting hydrogels can be better considered as semi-IPN systems. It is also important to note that the g-CN prepolymer is not dispersible in organic solvents, owing to its hydrophilic character. As there might be countless possibilities, arising from adjusting water content, monomer content, monomer type and crosslinker amount, hydrogels with 3 different concentrations (touA, touB, touC, touRef) were synthesized to show viability of the approach (Appendix 11.2.5, Table 8.2).

Table 8.2. Amounts of precursor, water, monomer and crosslinker for exemplary organohydrogel synthesis.

Sample	Precursor (g-CN pre3h) amount (wt.%)	Water amount (wt.%)	DMA amount (wt.%)	MBA amount (wt.%)
touA	25	25	47.5	2.5
touB	32.5	32.5	32	3
touC	22	38	38	2
touRef	25[a]	25	47.5	2.5

[a]Control solution (450 mg EG, 450 mg water and 80 mg DMA) was utilized

The main feature of g-CN prepolymer is the photoactivity of g-CN particles that can initiate a second photopolymerization without adding extra photoinitiator. Simply, the prepolymer was mixed with water, monomer (DMA) and crosslinker (MBA) with different concentrations, and organohydrogel formation took place via short term visible light irradiation (circa 20 minutes). A control solution was utilized for reference hydrogel synthesis to imitate the g-CN prepolymer. EG can easily be removed from organohydrogel network *via* water immersion affording pure hydrogels as discussed in Chapter 5. In the next step, both organohydrogels and hydrogels were characterized via mechanical compression test (Figure 8.4, Figure A61, Table 8.3).

Table 8.3. Elastic modulus values of tough organohydrogels and hydrogels.

Specimen	E_{mod} (-10% before break, MPa)	Elongation (-10% before break, %)	E_{mod} at break (MPa)	Elongation at break (%)	Maximum stress (MPa)
tou Ref	1.17	34	1.51	44	0.36
touA	11.9	24	13.74	34	2.67
touB	3.04	20	4.29	30	0.79
touC	6.01	22	7.37	32	1.51
tou Ref hydrogel	0.94	42	0.72	52	0.14
touA hydrogel	9.94	21	14.53	31	2.36
touB hydrogel	4.40	14	7.75	24	1.07
touC hydrogel	0.51	17	0.59	27	0.12

g-CN incorporated organohydrogels showed significant increase in E_{mod} values compared to the reference organohydrogel. touA withstands against highest standard force, while increasing water amount in organohydrogel synthesis yielded weaker products. Compared to reference organohydrogel, g-CN based organohydrogels started to deform at less elongation. touA organohydrogel (with the highest organic content) shows highest E_{mod} (11.9 MPa) as expected and increasing water amount decreases E_{mod} to 6 MPa.

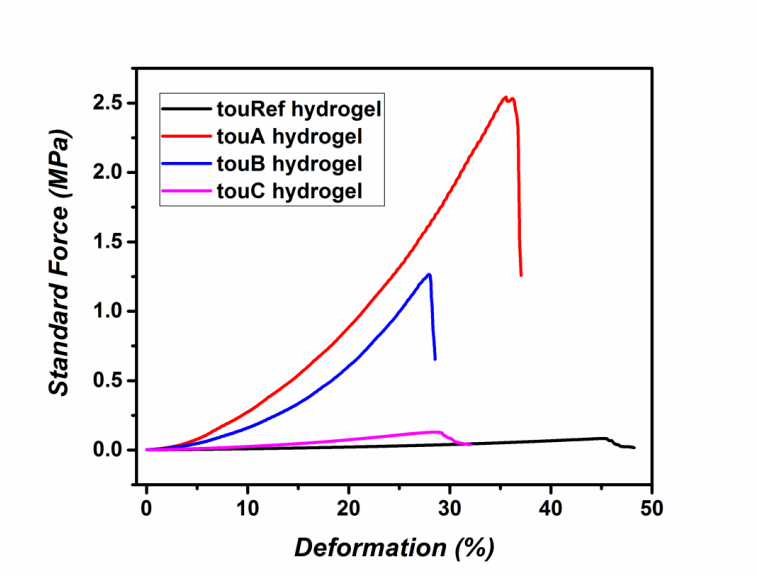

Figure 8.4. Compression test results of swollen reference hydrogel and g-CN prepolymer based hydrogels with different compositions.

Similar compression tests were also performed on related hydrogel products having similar swelling ratios. Deformation at less elongation was also observed for g-CN based hydrogels compared to reference hydrogel. For the case of swollen hydrogels, touA hydrogel showed the highest E_{mod} values, and surprisingly placement of hydrogels in terms of E_{mod} was similar to parent organohydrogels. Hydrogels yielded from organohydrogels with higher water amount were much weaker. A range of mechanical properties can be accessible with the present hydrogels via variation of composition which would allow mimicking mechanical properties of natural tissues in the future.

Extending the functionality of hydrogels beyond toughness has been of interest so far. Inspired from composition of articular cartilage, lubricity should accompany the toughness for fabrication of functional hydrogels. Lubricity could be achieved via utilization of charged monomers in hydrogels. Extensive research has been conducted and charged monomers were investigated to provide lubricity in hydrogel systems. Significant knowledge about friction mechanism between charged monomer and water interface was obtained. Previous attempts to utilize charged monomers in g-CN dispersions failed as colloidal stability of g-CN in water diminishes upon addition of ions to the system. Herein, novel g-CN based prepolymer provides excellent colloidal stability so that studying lubricity of g-CN based hydrogels is enabled via utilization of negatively charged 3-Sulfopropyl methacrylate potassium salt (SPMA) monomer. Exemplary

synthesis conditions were selected employing prepolymer and monomer mixtures as explained in Appendix (11.2.5) and summarized in Table 8.4 (lubA, lubB, lubC, lubRef).

Table 8.4. Compositions of lubricant and blank hydrogels.

Sample	Precursor (g-CN pre3h) amount (wt.%)	Water amount (wt.%)	DMA amount (wt.%)	MBA amount (wt.%)	SPMA amount (wt.%)
lubA	20	40	20	1.5	18.5
lubB	20	40	38.5	1.5	-
lubC	24	48	-	1.8	26.2[b]
lubRef	20[a]	40	20	1.5	18.5

[a]Control solution used to synthesize reference organohydrogel, [b]limited to 1.2 g instead of 1.8 g due to solubility.

g-CN prepolymer based monomer mixtures were illuminated via visible light, and gelation was achieved in 1 hour. EG can easily be removed via water immersion or 2 times washing-freeze drying process. Later on, organohydrogels and hydrogels were characterized via compression test for mechanical properties (Figure 8.5a-b, Figure A62).

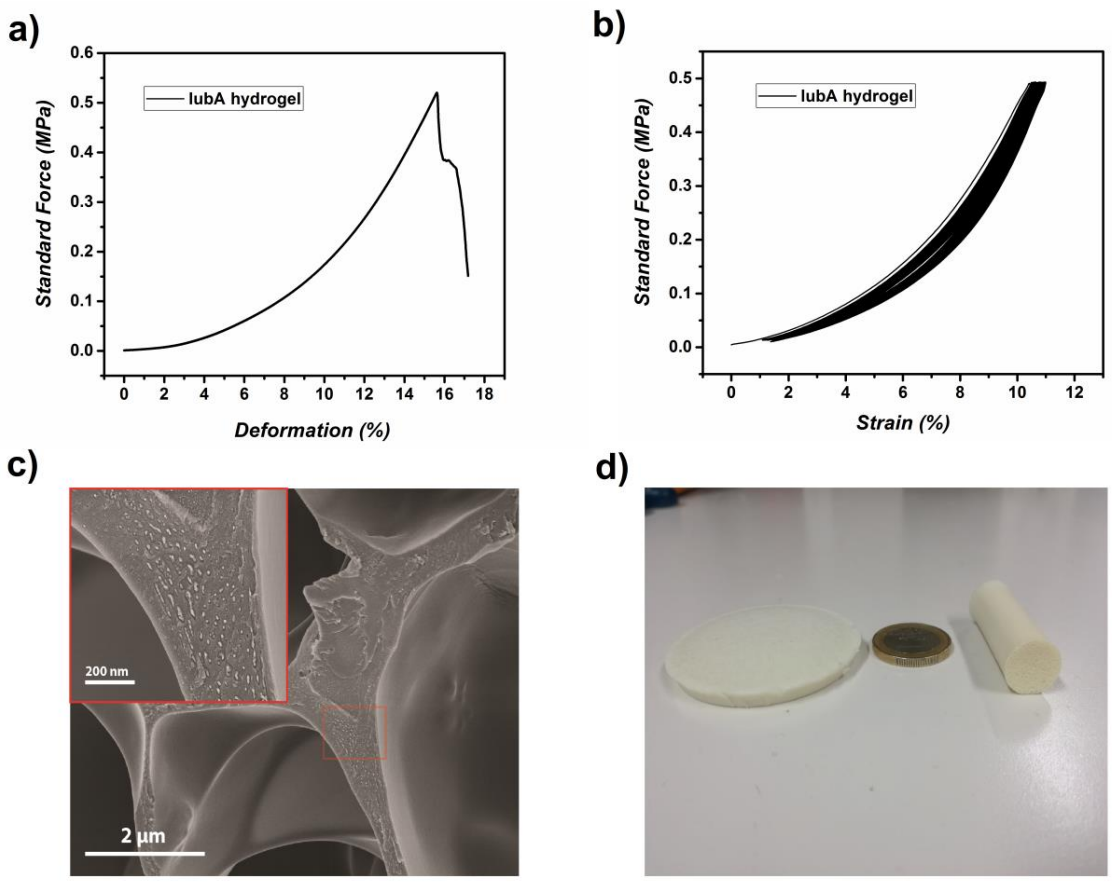

Figure 8.5. (a) Compression and **(b)** cyclic compression (100 times) profiles of lubA hydrogel, **(c)** SEM image of freeze dried lubA hydrogel and **(d)** images of lubA hydrogel fabricated in different shape and size.

Investigating the compression of organohydrogels, lubB which consists of only DMA as secondary network shows the highest E_{mod} values (around 3.1 MPa) and lubC (consists of only SPMA as secondary network) shows the lowest (around 1.27 MPa). Performance of lubA, by the means of E_{mod} value, falls exactly between them (around 2.52 MPa) which combines satisfactory mechanical properties for organohydrogels with possible lubricant features (Table 8.5).

Table 8.5. Elastic moduli values of lubricant organohydrogels and hydrogels.

Specimen	E_{mod} (-10% before break, MPa)	Elongation (-10% before break, %)	E_{mod} at break (MPa)	Elongation at break (%)	Maximum stress (MPa)
lub Ref	0.66	18	1.83	28	0.29
lubA	2.52	23	2.47	33	0.79
lubB	3.10	22	5.49	32	0.96
lubC	1.27	57	1.69	67	0.38
lub Ref hydrogel	1.01	19	1.68	29	0.30
lubA hydrogel	1.51	3	7.96	13	0.47
lubB hydrogel	4.75	18	27.75	28	1.28

After EG is removed from the organohydrogel networks, further investigations were performed to understand the mechanical properties of pure hydrogels. Pure lubA hydrogel consists of 2 different monomers, namely DMA and SPMA. DMA was chosen for toughness adjustment and SPMA was chosen for lubricity adjustment. Compression test results of hydrogels showed similar profile to tough hydrogels as depicted in Chapter 5. lubRef hydrogel is quite weak compared to hydrogels based on g-CN incorporation, which clearly shows the reinforcer role of g-CN in the system (Figure 8.5a, Figure A63). It is important to note that lubC hydrogel which contains SPMA as secondary network was not self-standing, while compression test result in Figure A63c shows it can resist high amount of load. However it cracks in the beginning of compression and graph shows the compression of individual pieces. In addition, lubB hydrogel can withstand highest amount of load as expected and lubA hydrogel has a performance in between. Average elastic moduli values of hydrogels present the order of strength (Table 8.5). First of all, compared to lubRef hydrogel, lubA hydrogel loses elongation capacity. lubB shows the highest E_{mod} values at any elongation, and lubA presents much higher E_{mod} values at break compared to reference. Compression tests suggest the necessity to include g-CN as reinforcer and DMA as mechanical adjuster in composite hydrogel system. Lubricity effect from SPMA will be discussed in next

paragraph. As durability against continuous compression is important in cartilage like systems, cyclic compression was performed on lubA hydrogel (Figure 8.5b). Cyclic compression was performed at maximum load before break and showed no fracture after 100 cycles showing the durability of synthesized hydrogel. SEM image of freeze dried lubA hydrogel shows highly porous network with smooth surface in large scale. After magnification, particles with size around 40 nm can be observed within polymeric network showing incorporation of g-CN particles in the hydrogel network (Figure 8.5c). Visible light initiation and synthesis from abundant and accessible chemicals allow scale-up synthesis conditions where lubricant hydrogels can be synthesized in any shape and size such as disc-like or cylinder-like (Figure 8.5d).

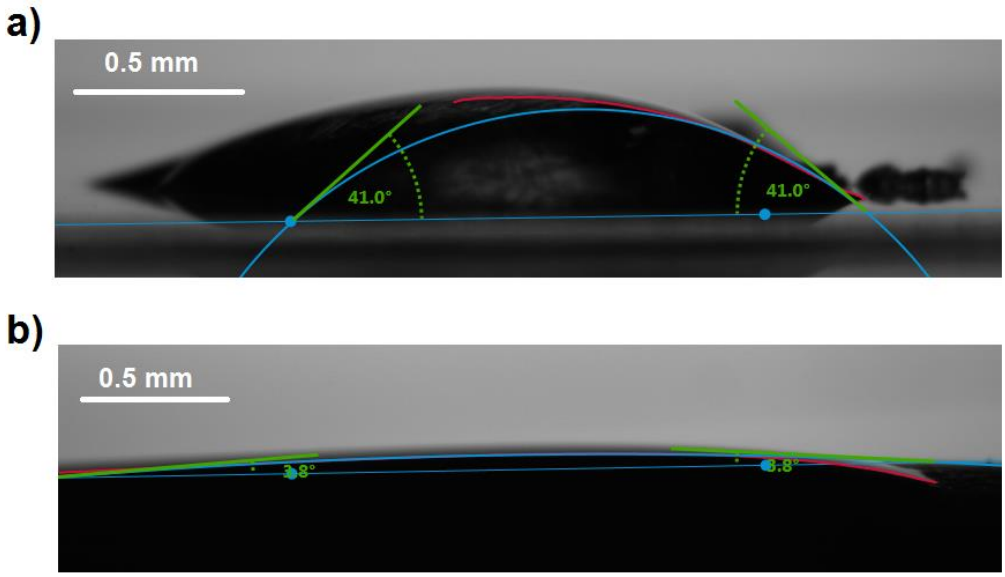

Figure 8.6. Water contact angle measurements of swollen **(a)** lubA reference hydrogel and **(b)** lubA hydrogel.

As SPMA polymer is known to possess superhydrophilic properties, water contact angles of reference and g-CN based hydrogels were investigated (Figure 8.6). As expected, superhydrophilic character was observed for lubA hydrogel showing the existence of g-CN does not affect water interaction and uptake in hydrogel system. Lubricity arises from the charged polymer brushes and water interaction, therefore the superhydrophilic nature of lubA is promising for low friction coefficients. However, lubricity mechanism and friction coefficient experiments are still being conducted.

8.3. Conclusion

Herein, g-CN was introduced in dispersed systems via synthesis of g-CN based prepolymer. Injectable prepolymer was synthesized via visible light irradiation and possesses high stability over long periods as well as facile processing. As an exemplary application, g-CN based prepolymer was employed as first network in hydrogel synthesis yielding tough hydrogels where g-CN acts as reinforcer and photoinitiator. The colloidal stability of the g-CN based prepolymer allows introduction of charged monomers, as well as it yields tough and lubricant hydrogels via photoinitiated reaction without external initiator. Initial attempts to synthesize g-CN based cartilage-like, tough and lubricant hydrogels were successful, and further attempts to investigate lubricity, accelerate the gelation rate and bio related studies might reveal photo polymerization based injectable cartilage formation which would entirely change the treatment for such problems from periodical and painful surgeries to affordable and facile injection method.

9. Electrostatic Stabilization of Carbon Nitride Colloids in Organic Solvents Enables Stable Dispersions and Transparent Homogeneous CN-Films for Optoelectronics [a]

9.1. Overview

Stable g-CN dispersion in organic media is of increasing need for potential applications. In order to solve this problem, phenyl modified g-CN (CMp) was covalently modified with methyl vinyl thiazole (vTA) groups via a visible light induced grafting approach. Even though the structure is neutral, in organic solvents it delocalizes negative charges on the rim while the sheets remain positively charged. Such a phenomenon provides electrostatic stabilization in organic solvents. Thus, stable dispersions can be prepared in 20 seconds and stored over weeks. Reasonable sheet size (both thickness and width) of modified g-CN in organic dispersions provide transparent film casting with high luminescence. In addition, for the first time, dispersions can be employed as inks for inkjet printers resulting in printing of pure g-CN.

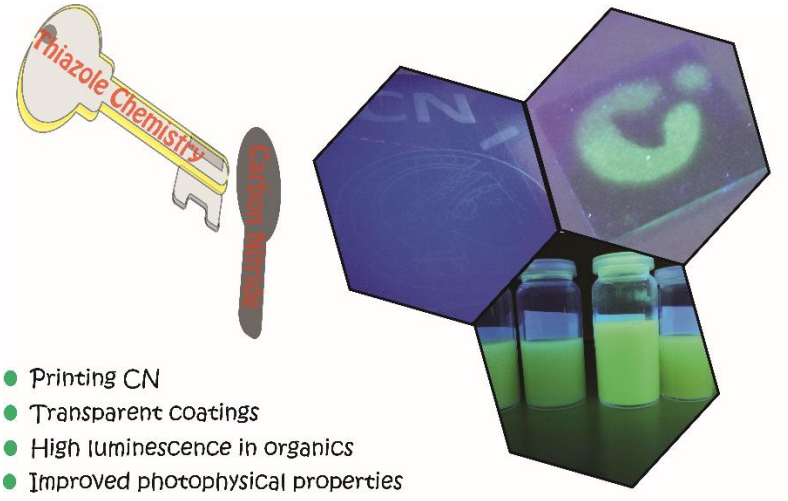

Figure 9.1. Summary of the chapter with properties of resulting modified g-CN.

[a] Terms of use: This chapter was adapted with permission from B. Kumru, D. Cruz, T. Heil, B. V. K. J. Schmidt and M. Antonietti, "Electrostatic Stabilization of Carbon Nitride Colloids in Organic Solvents Enables Stable Dispersions and Transparent Homogeneous CN-Films for Optoelectronics"; *J. Am. Chem. Soc.*, **2019**, 140 (50), 17532-17537. Copyright 2019, American Chemical Society.

9.2. Results-Discussion

CMp is a carbon nitride structure with phenyl as functionalities at the edges. It has small sheet size as well as luminescent properties and was synthesized as described in literature.[19] Before modification on CMp, vTA polymerization was probed. vTA is commonly employed in food industry, and there are only few articles investigating its polymerization after quarternization for final poly (ionic liquid) products.[191-192] Radical polymerization of pure vTA monomer was performed in order to understand its propagation activity, typical free radical polymerization was conducted under inert atmosphere with vTA monomer and AIBN as initiator at 90 °C for 24 hours. However, effective polymerization was not observed under the investigated reaction conditions. Only small portion of product was obtained as possible polymer of vTA (less than 1 % yield) indicating low conversion. SEC of obtained product indeed showed a polymer from radical polymerization (*Đ*: 1.92, M_n: 1700 g/mol), which was supported by ^{1}H NMR spectra as vinylic hydrogen peaks were not observed around 5.4, 5.4 and 6.7 ppm (Figure 9.2). Peak at 8.5 ppm indicates the hydrogen from thiazole ring and peak at 2.4 ppm arises from methyl group of vTA. However, extremely low yields in traditional polymerization conditions showed unfavorable propagation property of vTA monomer. Similar results were obtained for photopolymerization attempt over 24 hours via Irgacure 2959 as photocatalyst. It is therefore assumed that visible light induced photochemical grafting at ambient temperature in 3 hours results only in very short functional oligo vTA sites on CMp.

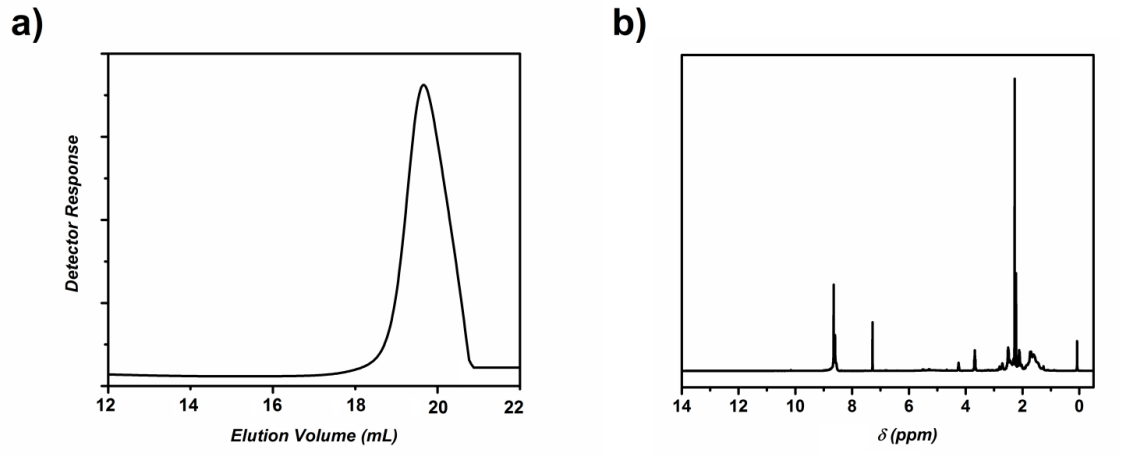

Figure 9.2. (a) SEC trace and **(b)** ^{1}H NMR spectra of vTA polymerization product.

For the modification, CMp was mixed with vTA and irradiated with visible light for 3 hours under continuous stirring. The so obtained CMp-vTA showed excellent dispersibility in organic media, resulting in colloidally stable dispersions in a variety of solvents which can be stored at least up to two weeks (Figure 9.3).

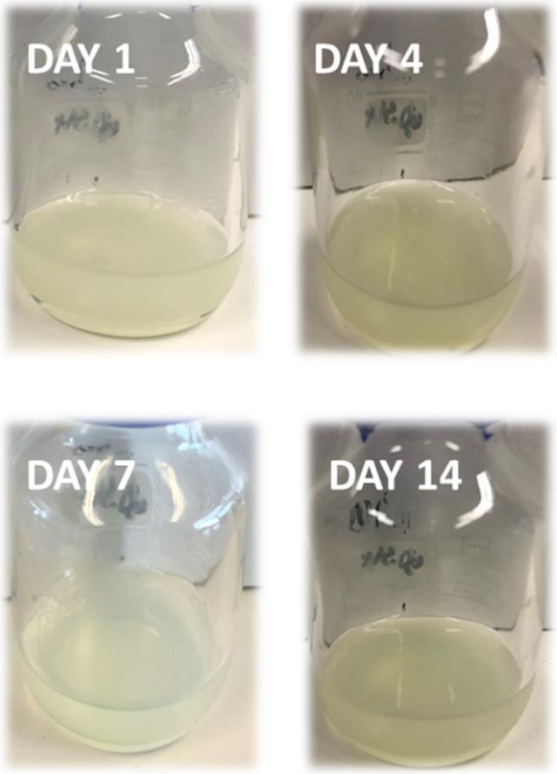

Figure 9.3. Digital images of CMp-vTA dispersion (30 mg CMp-vTA in 20 mL DMF) over 2 weeks.

The dispersions were prepared after only 20 seconds sonication. Together with the high dispersibility, strong luminescence was observed in CMp-vTA organic dispersions under UV light (Figure 9.4a). Subsequently, possible coating application employing colloidally stable dispersion was investigated. CMp-vTA was dispersed in chloroform and spray coated on glass. Glass substrate was washed with ethanol and dried prior to coating, spray coated from top while substrate was heated to 80 °C from below. Spray coating of CMp-vTA was applied utilizing simple mask patterning (glass substrate half-covered), resulting in totally transparent coating

pattern where the structure is only revealed by its photoluminescence under UV light (Figure 9.3b).

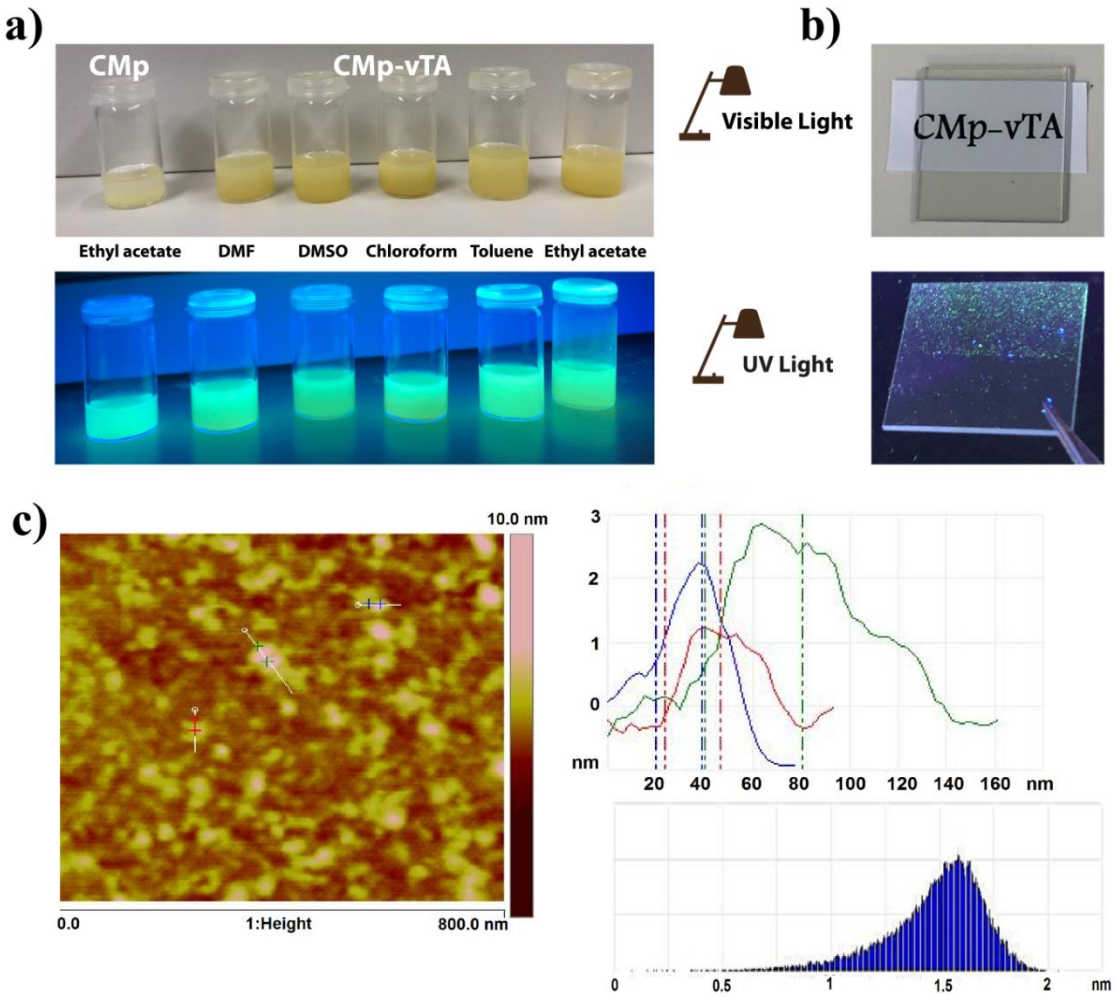

Figure 9.4. (a) CMp and CMp-vTA dispersions in some common organic solvents and dispersions under UV light (same order as visible light), **(b)** image showing the glass substrate after spray coating of CMp-vTA particles in visible and UV light, **(c)** AFM profile of spray coated glass substrate, 3 particles in detail and average thickness distribution.

Such a transparent coating hints to small and thin particles, therefore AFM was performed to study particle properties on glass substrate. AFM pictures show densely packed particles with primary particle thickness of 1.2 nm and an in-planar extension of 20 – 40 nm, i.e. the dispersion after functionalization is about perfect (Figure 9.4c). It is of importance to underline that presented dispersions are free of any additives such as surfactants and thereby very pure. The inherent colloidal stability arises from the sample itself. As coating is such a reliable process, it

can be applied for more than 1 cycle resulting in coatings with variety of thicknesses (from 1.3 nm to 4.2 nm) (Figure A64). On the other hand, dispersions in some solvents such as water and THF are not stable which causes relatively quick sedimentation, and particle size in these dispersions are much larger and thicker (Figure A65).

This surprising stability in organic media is a key to many possible applications in the future, and it was important to understand the reason behind the stability. We therefore analyzed the surface potential of the particles by a streaming potential analyzer, and the results are summarized in Table 9.1. Interestingly, even in organic solvents a comparably high particle charge was found, and particle charge correlates well with the dielectric constant of the respective solvent (Figure 9.5).

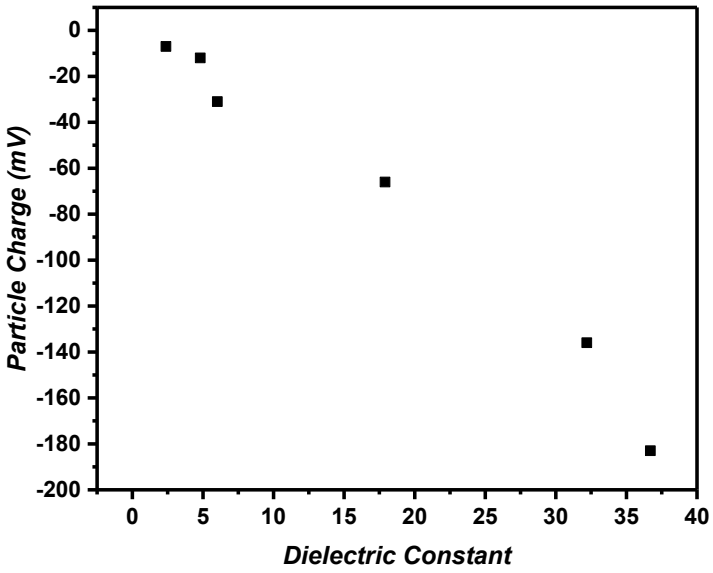

Figure 9.5. Correlation between particle charge and dielectric constant of solvent for CMp-vTA (solvents: toluene, chloroform, ethyl acetate, isopropyl alcohol, NMP and DMF).

The measured values are all negative, with surprisingly high absolute values going up to -183 and -305 mV. It is foreseen that such high numbers have never been reported before. Especially in solvents which do not allow ion dissociation, such as isopropanol or ethylacetate, it contradicts textbook knowledge that the particles are still highly charged.

Table 9.1. Particle charges of modified and non-modified g-CNs in different organic solvents ordered according to dielectric constants (measured by particle charge detector, values are in mV).

	DMF	*N*-methyl pyrrolidone	IPA	Ethyl acetate	Chloroform	Toluene
CMp	-70	-44	-28	-5	between 0 and -1	between 0 and -1
CMp-vTA	-183	-136	-66	-31	-12	-7
CMB	-82	-	-	-	-	-
CMB-vTA	-305	-	-	-	-	-

For extending the borders of vTA modification, carbon nitride from cyanuric acid-melamine-barbituric acid (CMB) was synthesized and modified with vTA in similar approach. Electrostatic stabilization was also found for CMB-vTA i.e. the observed effects can be generalized regardless of the type of parental g-CN.

The possibility of the thiazole modification with other carbon nitrides was also explored, while the electronic influences and the Donor-Acceptor type (D-A) sheet activation seem to be rather general, the ultimate dispersion to small colloidal plates obviously relies on the existence of small primary sheets in the masterbatch. Carbon nitride sheets can be very large, and small sheets are typically mostly obtained by structure terminating copolymerization additives to create edges, such as the described phenyl-substitution. All systems are nevertheless electrostatically stabilized even in organic solvents, where Coulomb stabilization is only known for plasmas and aerosols with permanent not-balanced charges. The only explanation for such a charging is that the particles are electrically neutralized inside the conjugated sheets. The Donor-Acceptor structure (DA) provided by the thiazole functionalization creates a polarity pattern which is core-shell-type (or better: plane-edge type, Figure 9.6).

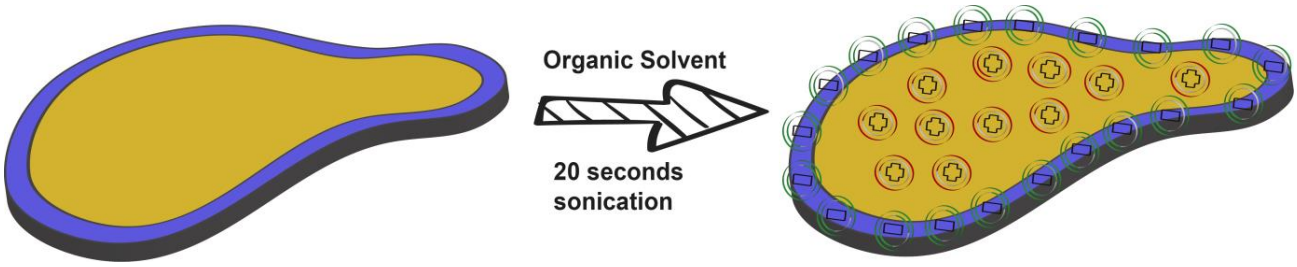

Figure 9.6. CMp-vTA sheet and charge delocalization in organic solvents via simple sonication.

Such organic-organic heterojunctions are of increasing relevance in materials chemistry, for instance in solid heterojunction devices for organic photovoltaics[193] and photon upconversions.[194] In the present context, it is worth mentioning that Yuan et al. used carbon-carbon heterojunctions for the additive-free electrostatic dispersion of nanocarbons,[195] however only in water.

Formation of simultaneously polarized sheets is also expected to result in stable aqueous dispersions, very surprisingly sedimentation in aqueous dispersion was observed. Very high zeta potentials can be assumed to trigger counterion condensation, in this case water splitting into hydronium and hydroxyl ions. Therefore the pH of water and CMp-vTA water dispersions were measured. The change in pH was quite low in number (7.06 for water and 7.16 for CMp-vTA in water), but there was an obvious decrease in proton number in solution (increase in basicity). As dispersion included only small amount of CMp-vTA (30 mg in 6 mL water), using logarithmic concentration formula of pH roughly showed that 1 mg CMp-vTA interacts with $1*10^{-7}$ moles of H^+ in distilled water, this is one H^+ per 6 nm x 6 nm.

Another very surprising aspect of these materials is their ability to restack when simply solvent casted from organic solution after evaporation of the solvent. Figure 9.7a shows the XRD data of CMp and CMp-vTA, and the graphitic stacking remains after modification and solvent restacking. Two characteristic peaks around 13° and 27° represents g-CN with intraplanar and interplanar stackings. Changes in XRD profile were only observed by processing from a bad solvent or shock precipitation, which results in new peak formations indicating changes in crystalline packing (Figure A66). From the fact that the stacking distance is similar to the primary stacking distance before modification, it can also be concluded that the thiazole modification only occurs at the edges, as any in-plane substitution would increase the gallery height or create disorder in the packing.

For light absorption, CMp-vTA powder presents an increased light absorption compard to CMp (Figure 9.7b). Moreover, photoluminescence lifetime is slightly increased when compared to the parent material (from 30 nanoseconds to about 44 nanoseconds, Figure 9.7c). Ultraviolet photoelectron spectroscopy shows about the same bandgap, with both HOMO and LUMO slightly moved to higher stability and more positive values (Figure 9.7d). Tauc plots derived from UV absorption of CMp and CMp-vTA are presented at Figure A67 where the bandgap values were calculated. A long-range UPS spectrum of CMp-vTA clearly shows a new band formation higher than 15 eV (higher binding energy cutoff (HBEC) area) (Figure A68).

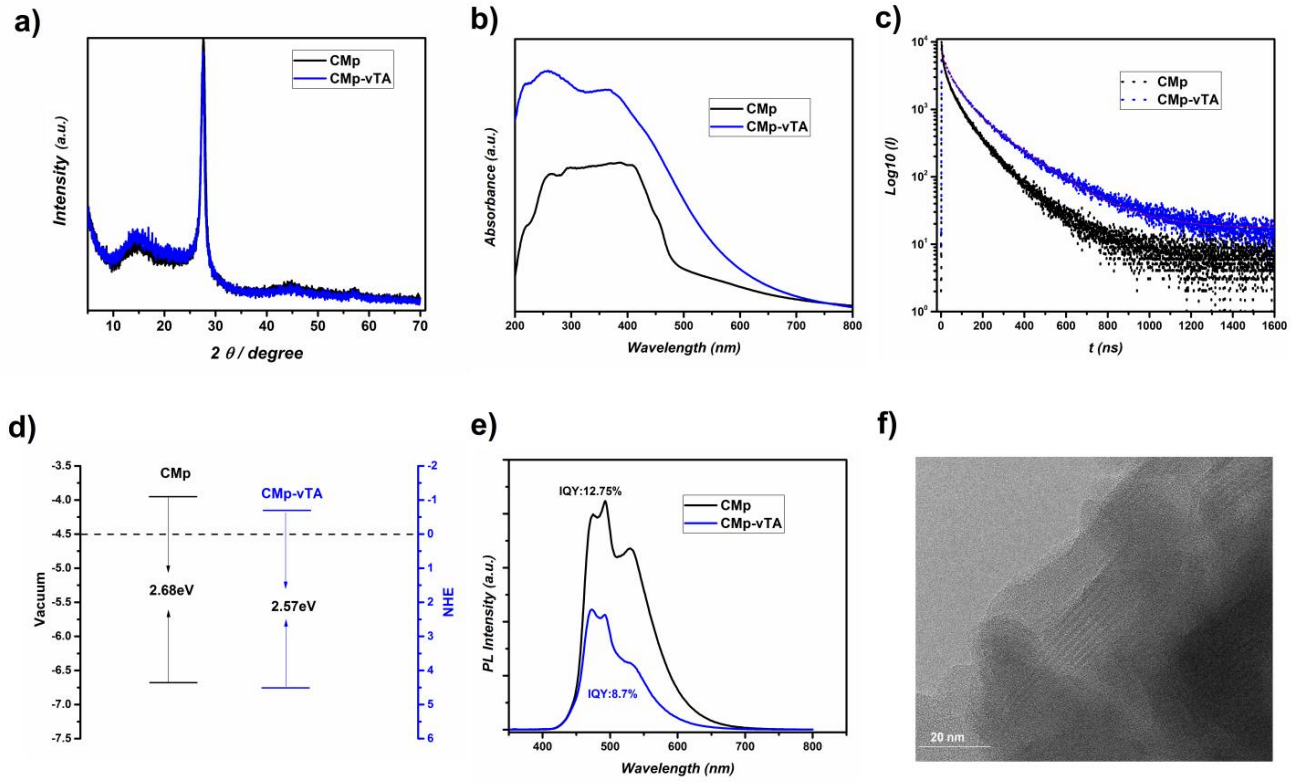

Figure 9.7. (a) XRD profiles, **(b)** powder UV-Vis spectra, **(c)** time resolved photoluminescence spectra, **(d)** optical bandgap and **(e)** PL spectra of CMp and CMp-vTA, **(f)** HR TEM image of CMp-vTA dried from ethyl acetate dispersion.

PL emission spectra of CMp and CMp-vTA show that CMp-vTA has lower internal quantum efficiency (IQE, 12.75% for CMp and 8.7% for CMp-vTA, with 1% error estimate from instrument) (Figure 9.7e). PL emissions with changing excitation wavelength was recorded for CMp, CMp-vTA, CMB and CMB-vTA samples and show the excitonic stability of vTA modified particles regardless of the parental g-CN type (Figure 9.8). More detailed information on the structure of CMp-vTA particles was obtained via HR TEM images (Figure 9.7f) where it

shows a nice lamellar in-plane microphase structure (with repeats of around 3±0.3 nm) similar to surfactant or block copolymer assembly, and the stripes indicate phenyl rich and phenyl poor domains in CMp-vTA. Such patterns can also be observed in particles from bad solvent dispersions (Figure A69).

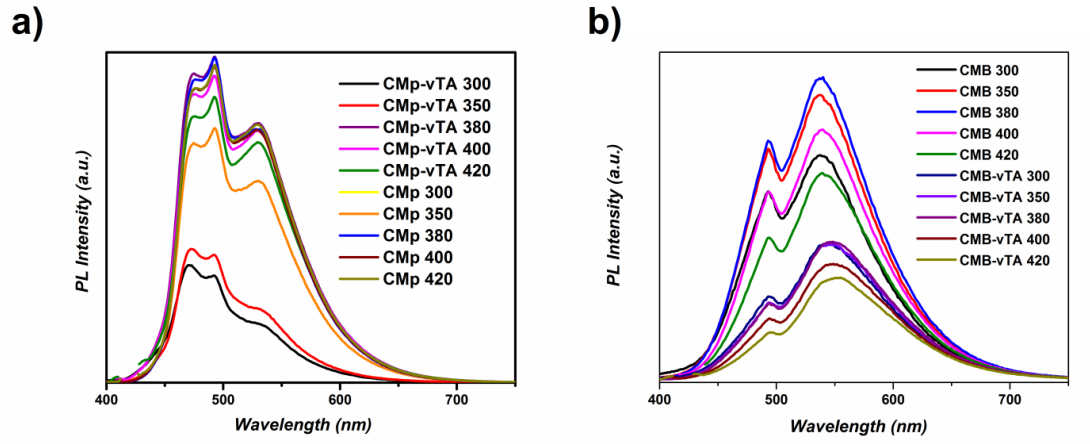

Figure 9.8. PL spectra with different excitation wavelengths for (a) CMp and CMp-vTA, (b) CMB and CMB-vTA.

FT-IR spectra were investigated for CMp and CMp-vTA, however both spectra show similar results, which can be attributed to comparably low amount of grafted vTA compared to CMp (Figure 9.9).

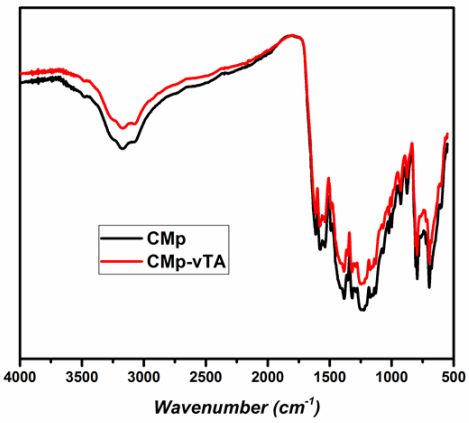

Figure 9.9. FT-IR spectra of CMp and CMp-vTA.

Therefore, combustive elemental analysis was performed to quantify the amount of grafting, which shows around 4 wt.% vTA grafting to CMp (Table 9.2).

Table 9.2. Combustive elemental analysis results of CMp and CMp-vTA.

	N (%)	**C (%)**	**S (%)**	**C/N**
CMp	50.43	43.16	0.461	0.855
CMp-vTA	42.98	46.59	3.134	1.0838

The nature of the charge separation is easily unraveled by using XPS on the transparent films. While both the highly resolved N- and C- K-edges are rather typical for phenyl-modified carbon nitride (Figure 9.10), the S-edge of the thiazole moiety moved by about 2 eV to lower binding energies, i.e. the sulfur in the thiazole structure is much more electron rich: D-A- charge transfer from CMp to every thiazole took place.

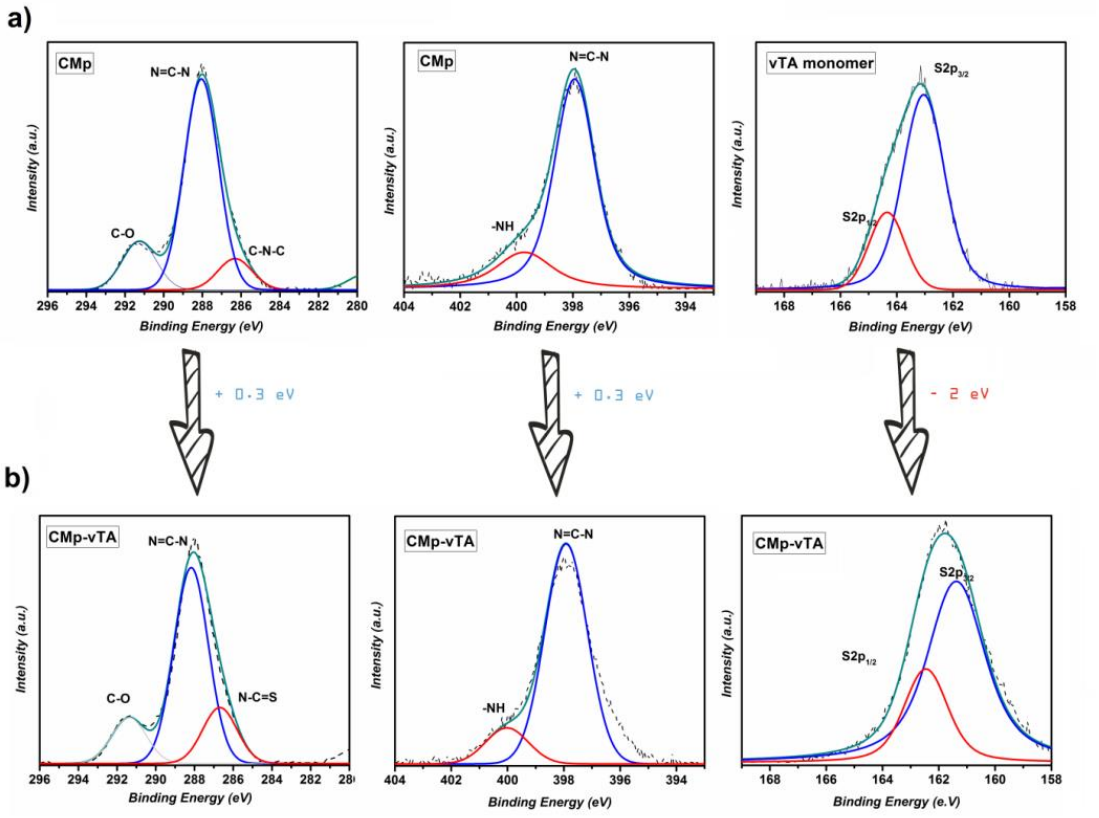

Figure 9.10. (a) XPS survey of CMp (C1s and N1s) and vTA monomer (S2p) and **(b)** XPS survey of CMp-vTA (C1s, N1s and S2p).

The corresponding positive countercharge is of course more delocalized and thereby more minute, but indeed positive partial charges in XPS at the tertiary nitrogen positions were observed (shift about 0.3 eV). These observations nicely quantify the proposed model shown in Figure 9.4. As expected, S2p element in non-modified CMp was not observed (Figure 9.11a). C1s and N1s survey of vTA monomer were presented in Figure 9.11.

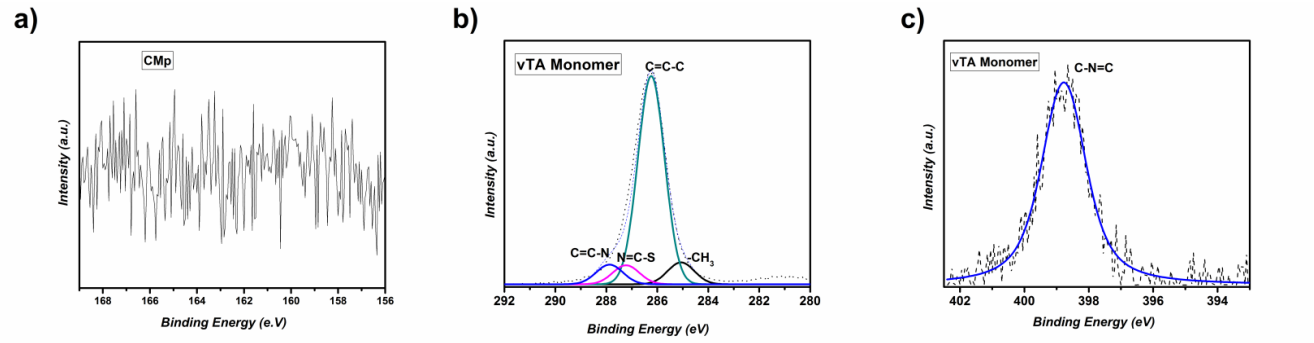

Figure 9.11. XPS survey of (a) CMp S2p, (b) vTA monomer C1s and (c) vTA monomer N1s.

The value of such solvent processable 2D-semiconductors can of course not be underestimated. Indeed, one of dispersions (CMp-vTA in ethyl acetate) was put in the cartridge of a standard ink-jet printer and printed (2 times over same side) 'CN' and Max Planck Society Minerva logo as a highly luminescent patterns array (Figure 9.12). Such an easy processing of carbon nitride is reported for the first time and easily allows printing any design and pattern for affordable costs.

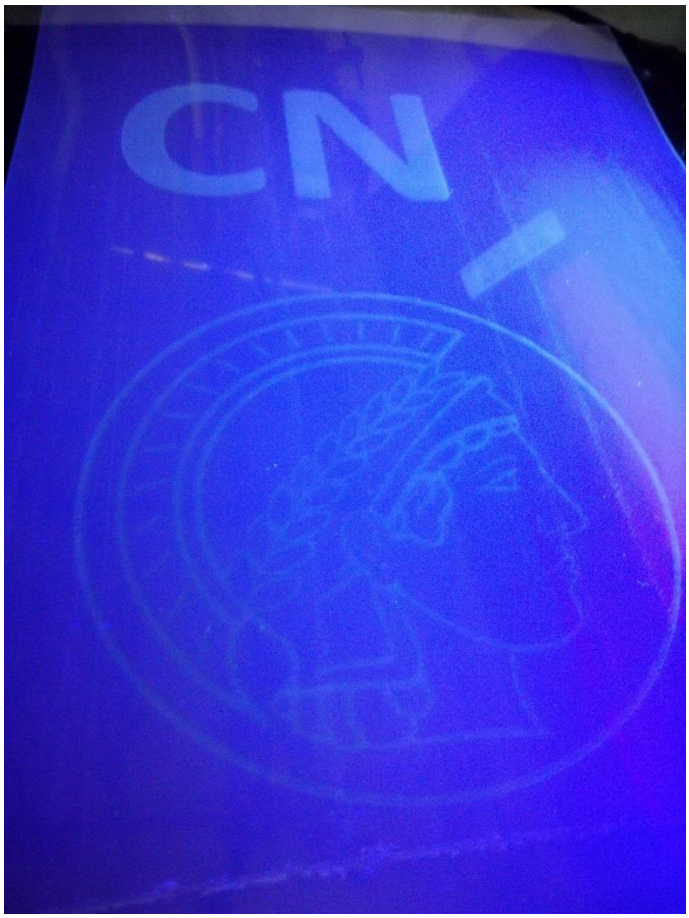

Figure 9.12. Image of CMp-vTA under UV irradiation after printing from commercial inkjet printer.

9.3. Conclusion

To conclude, the modification of phenyl doped carbon nitride with thiazole blocks at the rim was demonstrated. Modified 2D conjugated layers lead to a Donor-Acceptor-in-plane charge transfer structure, which allows spontaneous dispersion in polar organic solvents. Contrary to textbook expectations, these dispersions are stabilized by a strong Coulomb repulsion, which is in low dielectric constant solvents even stronger than in water and not screened by the dissociated charges.

Due to the additive free nature of such modified carbon nitride sheets, pure bulk materials can be casted from the dispersions, e.g. as very flat, reflective and transparent films which are in addition highly luminescent. XPS data allows to prove the postulated charge transfer with the heterojunction structure, which is no less than -2 eV at the sulfur positions, compensated by smaller shift on the conjugated carbon nitride network which goes at specific positions to + 0.3

eV relative charge strength. Beside dispersibility in organic solvents, also photophysical properties were enhanced via introduction of vTA groups, such as increased photoluminescent lifetime and enhanced light absorption. Effort has been spent on better understanding of the mechanism and showed pieces of possible applications in the current project. The present work is an important step for the simple handling of transparent and flat carbon nitride by solvent based technologies, such as ink jet printers. Current work is related to the use of the described dispersion for the synthesis of hybrid materials, as lumiphores in ultramicroscopy, and for electron buffer layers in perovskite solar cells.

10.Conclusion and Outlook

The ultimate goal of this thesis was to investigate g-CN in dispersed media and elucidate applications of such dispersions utilizing visible light.

The first part of this thesis investigated different types of g-CNs and their possible utility in visible light photoinitiation and reinforcerment in hydrogel synthesis. Indeed hydrogels have shown significant reinforcement in the presence of g-CN (0.6 wt. %). Detailed studies have shown that reinforcement is governed by the surface charge of g-CN. Namely more negatively charged g-CN species provide more reinforcement to hydrogels. Mechanistic studies for photoinitiated hydrogel formation via g-CN were conducted (mixing under light, mixing in the dark, g-CN embedded in the hydrogel). Indeed covalent reinforcement was observed which confirmed radical formation on the surface of g-CN upon irradiation, whereas embedding g-CN in hydrogel network without covalent bonding showed a completely different reinforcement profile. Overall, g-CN sheets were presented as visible light photoinitiators and covalent reinforcers in one pot hydrogel synthesis.

Due to the low dispersibility of g-CN in aqueous media, the first project was limited to 0.6 wt. % g-CN incorporation. As reinforcement showed promising results, increasing g-CN content was the primary objective of second part. Of the different compositions assayed, a water–ethylene glycol (EG) mixture presented the most suitable combination to increase g-CN content in a dispersion. A 1:1 water:EG mixture can disperse up to 4 wt. % g-CN, which was later employed for hydrogel synthesis. Indeed a higher amount of initiator (g-CN) resulted in significantly faster gelation time under visible light providing an organohydrogel intermediate. Subsequently, EG can be removed from an organohydrogel network by immersion in water which yields pure hydrogels. Both organohydro- and hydrogels showed good mechanical properties under compression with E_{mod} values similar to tough biological tissues. Cyclic compression tests presented the fatigue resistance of reinforced hydrogels. Compared with hydrogels from the previous part, G' values have increased up to 100 times, presenting the significant reinforcing effect of g-CN sheets. As gelation is photoinduced, simple photopatterning was applied to yield patterned hydrogels, which indicates the radical formation on illuminated regions and no significant radical transfer to dark areas. Physically, the size of gels can be extended by adding a monomer solution and subsequent photoinitiated gelation around the primary gel, forming a

stable single network. Such tough hydrogels can be interesting for additive manufacturing due to ease of processing and worthy mechanical performance.

The third part of the thesis investigated enhanced dispersibility of g-CN particles in aqueous and organic media arising from bulk properties. The literature shows that g-CN dispersions in aqueous media can be enhanced by acid etching, surfactant addition and long ultrasonication periods, yet no detailed study was performed for organic media. However, most of the conditions for dispersion enhancement are followed by limitations to potential applications due to the addition of additives. Inspired by the initial work, radical formation on g-CN was employed for photoinduced grafting on a g-CN surface. Allylic molecules which do not propagate were chosen in order to preserve the photophysical properties of g-CN. The introduction of a -SO_3H group yielded improved water dispersibility and decene functionality added organo dispersible character to g-CN. -NH_2 groups can be introduced to create pH-dependent g-CN water dispersions and –F groups offer fluorophilic character. Enhanced dispersibility (up to 10 wt.% in aqueous and 2 wt.% in organic media) was accompanied with colloidaly stable dispersions which can be prepared *via* simple sonication for 10 minutes. Visible light-induced functional group grafting on g-CN surface is reported as a versatile method for increased g-CN dispersibility in aqueous and organic media.

The effect of surface chemistry of g-CN for hydrogel synthesis was investigated. Employing -SO_3H-modified g-CN (g-CN-AHPA), water dispersions can easily be formed and employed for hydrogel synthesis. The resulting hydrogel was extremely compressible despite its high water content and softness. A g-CN–AHPA hydrogel is impervious to compression, even at 800 N, showing a temporary physical change to a thin and flat form under stress, but retains its original shape after the source of stress is removed. In addition, the hydrogels presented cut resistance, shock resistance, moderate flexibility and tissue adhesive properties with no toxicity and a skin-like feeling.

Another option to increase g-CN dispersibility is to graft of polymer chains. g-CN ‘prepolymer’ was synthesized utilizing hydrophilic polymer photografting in a water:EG mixture. Viscoelastic prepolymer presenting extreme colloidal stability can be mixed with secondary monomers and crosslinkers to yield extremely tough hydrogels. g-CN particles can initiate radical formation twice, first in prepolymer synthesis and secondly in initiation of gelation. Injectable prepolymer and its colloidal stability allowed for the study of charged monomers with g-CN for the first time, resulting in tough and lubricant hydrogels. The benign experimental conditions and facile

synthesis demonstrates that g-CN based hydrogels can mimic the mechanical properties of biological tissues.

The last part of this thesis provides a possible solution to a long-term question of well-dispersed g-CN in organic media. Employing a photografting approach to g-CN, vinyl thiazole groups were introduced to g-CN. Interestingly, modified g-CN showed extreme stability in organic solvents stabilized via electrostatic interactions. Dispersions in organic media can be prepared in 20 seconds and stored up to some weeks. The surprising fact was the charge delocalization on g-CN sheets in organic solvents where the negative charge migrates to the thiazole edges creating D–A-type structures. Such a fine dispersion was utilized to create patterned transparent coatings that can be observed under UV illumination. Further, the dispersion can be filled in a cartridge and pure g-CN can be printed copy paper using a commercial inkjet printer. Novel properties governed by modification with thiazole edges create a unique platform for the processing of g-CN.

Overall, this thesis addresses novel applications of g-CN beyond heterogeneous catalysis. The research presented here can be summarized globally as “the dispersion of g-CN”. A g-CN and visible light duo were at the core of all presented chapters, either via initiation of polymerization for hydrogel reinforcement or through grafting functional groups onto a g-CN surface as a post-modification approach for enhanced dispersibility. Research centering on aqueous dispersions and hydrogel formation shows hydrogels with various mechanical properties, which are similar to biological tissues and are accessible via utilization of g-CN as a visible light photoinitiator and reinforcer. Investigation of g-CN dispersions in organic media was explored using a simple photografting method, resulted in enhanced dispersibility of g-CN particles in organic media. Each study revealed more insight into g-CN behavior in the presence of allylic molecules upon visible light treatment, which expanded the limits of fabrication of g-CN based materials. Simplicity of the experiments and accessible chemicals lead to facile synthesis and modifications which can be scaled up or conducted at any institution.

In the near future, g-CN reinforced hydrogels may become prime candidates in nanocomposite hydrogel research as numerous materials are accessible via simple synthetic conditions utilizing g-CN. Undoubtedly, the employment of g-CN-reinforced hydrogels in tissue engineering is a must to create potential biomaterials of the future, such as artificial cartilage, wound dressings or soft tissue platforms. Diversifying the synthesis of g-CN-based hydrogels would allow for covalently-layered hydrogel synthesis from which muscle-like materials can be designed.

Furthermore, the formation of stable organic g-CN dispersions will eliminate the biggest obstacle in other potential applications of g-CN such as a doping layer in solar cells and optoelectronics. Significant steps in the synthesis of transparent films and printing pure g-CN not only feature the necessary conditions (stable dispersions) for applications, but also provide advanced manufacturing routes. This thesis is therefore just the beginning of more to come, and indeed it provides a bridge between the emerging research areas of tissue engineering, energy harvesting and catalysis. Thus, it can be surmised that g-CN in dispersed media compromise a Midas touch to current material science.

11.Appendix

11.1. Materials

All materials were used as purchased unless noted otherwise. **1-decene** (94%, Sigma Aldrich), **1*H*,1*H*,2*H*-perfluoro-1-decene** (99%, Alfa Aesar), **2,2′-Azobis(2-methylpropionitrile)** (AIBN, 98%, Sigma Aldrich), **2,4-diamino-6-phenyl-1,3,5 triazine** (97%, Sigma Aldrich), **3-Allyloxy-2-hydroxy-1-propanesulfonic acid sodium salt solution** (40% *w/w,* AHPA, Sigma Aldrich), **3-Sulfopropyl methacrylate potassium salt** (SPMA, 98 %, Sigma Aldrich), **4-methyl 5-vinyl thiazole** (vTA, 97%, Kosher, Sigma Aldrich), **acetone** (HPLC grade, Sigma Aldrich), **acrylamide** (AAm, 98% GC grade, Sigma Aldrich), **allylamine** (98%, Sigma Aldrich), **aluminum oxide basic** (Al_2O_3, Sigma Aldrich), **barbituric acid** (99%, Alfa Aesar), **calcium chloride** ($CaCl_2$, 97%, Alfa Aesar), **chloroform** (anhydrous, 99%, Sigma Aldrich), **cyanuric acid** (98%, Sigma Aldrich), **deuterated chloroform** ($CDCl_3$, Sigma Aldrich), **deuterium oxide** (D_2O, Sigma Aldrich), **dichloromethane** (DCM, anhydrous 99.8%, Sigma Aldrich), **dimethyl sulfoxide** (DMSO, anhydrous 99.9%, Sigma Aldrich), ***E. coli* Turbo bacteria** (New England Biolabs), **ethyl acetate** (EA, HPLC grade, 99.5%, Alfa Aesar), **ethylene glycol** (EG, 99%, Fluka), **hexafluorobenzene** (99%, Alfa Aesar), **hexane** (anhydrous, 95%, Sigma Aldrich), **hydrochloric acid solution** (HCl, 0.1 M, Sigma-Aldrich), **hydrogen peroxide** (30%, Sigma Aldrich), **isopropyl alcohol** (IPA, 99.7%, Sigma Aldrich), **melamine** (99%, Sigma Aldrich), ***N*,*N*-dimethylacrylamide** (DMA, 99%, TCI and Acros), ***N*,*N* dimethylformamide** (DMF, anhydrous 99.8%, Sigma Aldrich), ***N*,*N*'-methylenebis(acrylamide)** (MBA), **Pluronic F127** (Sigma Aldrich), **poly(ethylene glycol) methyl ether methacrylate 300** (PEGMEMA, Sigma Aldrich), **poly(ethylene glycol) dimethacrylate 750** (PEGDMA, Sigma Aldrich), **potassium hydroxide** (KOH, Sigma Aldrich), **potassium persulfate** (KPS, Sigma Aldrich), **sodium chloride** (NaCl, 99%, Sigma Aldrich), **sodium hydroxide solution** (NaOH, 0.1 N, Sigma-Aldrich), **tetrahydrofuran** (THF, 99%, Sigma Aldrich), **Triton X 305 solution** (70 wt.% in water, Sigma Aldrich), **toluene** (anhydrous, 99.8%, Sigma Aldrich), **urea** (99 %, crystalline, Alfa Aesar). DMA, PEGMEMA and PEGDMA were passed through basic alumina column prior to use. Visible light irradiation was performed via two 50 W LED chips (Foxpic High Power 50 W LED Chip Bulb Light DIY White 3800LM 6500 K) connected to a self-made circuit and cooling system. UV light irradiation was performed via 5 W LED stripes (Chili-Tec, CLS-100UV)

containing 30 UV SMD LEDs (type 5050, λ = 395 nm). Tissue paper samples were cut from Kimtech Science brand tissue paper. Glass slides were washed with ethanol and dried at 60 ºC before spray coating. Photomasks for spray coating were prepared *via* carving out the Max Planck Institute of Colloids and Interfaces logo. Spray coating with nitrogen flux and hot plate geometry were custom made which allows controlling g-CN dispersion flux through glass samples with controlled heating. Printing was performed using Canon Pixma iP7250 commercial printer and loading CMp-vTA ethyl actetate dispersion into ink cartridge.

11.2. Synthesis Procedures

11.2.1. Synthesis of materials described in Chapter 4

Preparation of CM: 1.0 g of cyanuric acid (C) and 1.0 g of melamine (M) were mixed with 40 mL distilled water and shaked overnight. After centrifugation at 5000 rpm for 5 minutes, a precipitate was dried at 60 °C under vacuum overnight. The dried product was transferred into a capped crucible and placed to oven with N_2 atmosphere at 550 °C for 4 hours, with a heating rate of 2.3 °C /min.[16]

Preparation of CMB 0.1: 1.0 g of cyanuric acid (C), 0.1 g barbituric acid (B) and 1.0 g of melamine (M) were mixed with 40 mL distilled water and shaked overnight. After centrifugation at 5000 rpm for 5 minutes. The precipitate was dried at 60 °C under vacuum overnight. The dried product was transferred into a capped crucible and placed to oven with N_2 atmosphere at 550 °C for 4 hours, with a heating rate of 2.3 °C /min.[13]

Preparation of CMB 0.25: 1.0 g of cyanuric acid (C), 0.25 g barbituric acid (B) and 1.0 g of melamine (M) were mixed with 40 mL distilled water and shaked overnight. After centrifugation at 5000 rpm for 5 minutes. A precipitate was dried at 60 °C under vacuum overnight. The dried product was transferred into a capped crucible and placed to oven with N_2 atmosphere at 550 °C for 4 hours, with a heating rate of 2.3 °C /min.[13]

Preparation of CMp: 1.3 g of cyanuric acid (C) and 1.8 g of 2,4-diamino-6-phenyl-1,3,5 triazine (Mp) were mixed with 50 mL distilled water and shaked overnight. After centrifugation at 5000 rpm for 5 minutes. A precipitate was dried at 60 °C under vacuum overnight. The dried product is transferred into a capped crucible and placed to oven with N_2 atmosphere at 450 °C for 2 hours, with a heating rate of 2.3 °C /min.[19]

Preparation of u-CN: 4.5 g of urea is weighed into a capped crucible and placed to oven with N_2 atmosphere at 550 °C for 4 hours with a heating rate of 2.3 °C/min.[156]

Synthesis of *N*,*N*-Dimethylacrylamide Reference Hydrogel: 9.2 g of distilled water, 0.8 g DMA and 0.06 g MBA crosslinker were mixed in a 20 mL glass vial. 0.1 g KPS was added to the mixture and mixed until dissolution. Addition of 0.5 mL 50% hydrogen peroxide was utilized to start the radical formation in the system. The glass vial was capped immediately after the

hydrogen peroxide addition was completed. The reaction was left to stand for 1 hour until complete gelation occured. The gel was removed from the vial and transferred into a beaker with 40 mL distilled water; where it was left there to stand for 2 days for purification by changing the water daily.

Synthesis of Carbon Nitride Derived *N*,*N*-Dimethylacrylamide Hydrogels: 9.2 g distilled water and 60 mg of related carbon nitride (CM, CMB 0.1, CMB 0.25, CMp or u-CN) were mixed in a vial. The mixture was ultrasonicated at 50 amplitude for 10 minutes (2 minute portions, 5 times) to yield a dispersion. After the dispersion was transferred into a 20 mL glass vial, 0.8 g DMA and 0.06 g MBA were added. Nitrogen was flushed through the system for 3 minutes and the vial was capped. The mixture was put in front of two 50 W LED daylight source to initiate gelation. After gelation was completed, which occurs in different amount of times depending on the carbon nitride type used, the gel was removed from the vial and put into 40 mL distilled water for purification for 2 days by changing the water daily.

Synthesis of Carbon Nitride (CM) Derived *N*,*N*-Dimethylacrylamide Hydrogels without MBA addition: 9.2 g distilled water and 60 mg of CM were mixed in a vial. The mixture was ultrasonicated at 50 amplitude for 10 minutes (2 minute portions, 5 times) to yield a dispersion. After the dispersion was transferred into a 20 mL glass vial, 0.8 g DMA were added. Nitrogen was flushed through the system for 3 minutes and the vial was capped. The mixture was put in front of two 50 W LED daylight source to initiate gelation. After gelation was completed, the gel was removed from the vial and put into 40 mL distilled water for purification for 2 days by changing the water daily.

Synthesis of Poly(ethyleneglycol)methylether methacrylate 300 Reference Hydrogel: 9.2 g of water was mixed with 0.8 g PEGMEMA and 0.06 g PEGDMA in a 20 mL glass vial. 0.1 g KPS was added to the mixture and mixed until all components were dissolved. 0.5 mL 50% hydrogen peroxide was added to start the reaction, the reaction was left to stand for 3 hours until complete gelation was achieved. The gel was removed from glass vial and put into a beaker with 40 mL distilled water for 2 days for purification by changing the water daily.

Synthesis of Carbon Nitride Derived Poly(ethyleneglycol)methylether methacrylate 300 Hydrogels: 9.2 g distilled water and 60 mg of related carbon nitride (CM, CMB 0.1, CMB 0.25, CMp or u-CN) are mixed in a vial. The mixture was ultrasonicated at 50 amplitude for 10

minutes (2 minute portions, 5 times) to yield a dispersion. After the dispersion was transferred into a 20 mL glass vial, 0.8 g PEGMEMA and 0.06 g PEGDMA were added. Nitrogen was flushed through system for 3 minutes and the vial was capped. The mixture was put in front of a 50 W LED daylight source to initiate gelation. After gelation was completed, which occurs in different amount of times depending on the carbon nitride type used, the gel was removed from the vial and put into 40 mL distilled water for purification for 2 days by changing the water daily.

11.2.2. Synthesis of materials described in Chapter 5

Preparation of g-CN: 1.0 g of cyanuric acid (C) and 1.0 g of melamine (M) were mixed with 40 mL distilled water and shaked overnight. After centrifugation at 6000 rpm for 10 minutes, a precipitate was dried at 60 °C under vacuum overnight. The dried product was transferred into a capped crucible and placed to oven with N_2 atmosphere at 550 °C for 4 hours, with a heating rate of 2.3 °C /min^{-1}. CM must be well grinded prior to use.

Synthesis of Reference DMA Hydrogel with EG: 4.5 g of deionized water, 4.5 g ethylene glycol (EG), 0.8 g DMA and 0.06 g MBA crosslinker were mixed in a 20 mL glass vial. 0.1 g AscA was added to the mixture and mixed until dissolution. Addition of 1 mL 30% hydrogen peroxide was utilized to start the radical formation in the system. The glass vial was capped immediately after the hydrogen peroxide addition was completed. The reaction was left to stand for 1 hour until complete gelation occured. The gel was removed from the vial and transferred into a beaker with 40 mL distilled water; where it was left there to stand for 3 hours for purification.

Synthesis of 3% g-CN derived DMA Gels with EG: 4.45 g deionized water, 4.45 g EG and 300 mg of g-CN were mixed in a plastic centrifuge tube. The mixture was ultrasonicated at 50 amplitude for 40 minutes (2 minute portions, 20 times) to yield a dispersion. After the dispersion was transferred into a 20 mL glass vial, 0.8 g DMA and 0.06 g MBA were added. Nitrogen was flushed through the system for 3 minutes and the vial was capped. The mixture was put between 2*50 W LED daylight source (20 cm apart from each other) to initiate gelation. After gelation was completed in 20 minutes, the gel was removed from the vial and put into 40 mL deionized water for 2 hours for purification.

Synthesis of 4% g-CN derived DMA Gels with EG: 4.4 g deionized water, 4.4 g EG and 400 mg of g-CN were mixed in a plastic centrifuge tube. The mixture was ultrasonicated at 50 amplitude for 40 minutes (2 minute portions, 20 times) to yield a dispersion. After the dispersion was transferred into a 20 mL glass vial, 0.8 g DMA and 0.06 g MBA were added. Nitrogen was flushed through the system for 3 minutes and the vial was capped. The mixture was put between 2*50 W LED daylight source (20 cm apart from each other) to initiate gelation. After gelation was completed in 14 minutes, the gel was removed from the vial and put into 40 mL deionized water for 2 hours for purification.

Synthesis of 2% g-CN Derived DMA Hydrogels Without Crosslinker: 4.5 g deionized water, 4.5 g EG and 200 mg of g-CN were mixed in a plastic centrifuge tube. The mixture was ultrasonicated at 50 amplitude for 40 minutes (2 minute portions, 20 times) to yield a dispersion. After the dispersion was transferred into a 20 mL glass vial, 0.8 g DMA was added. Nitrogen was flushed through the system for 3 minutes and the vial was capped. The mixture was put between 2*50 W LED daylight source (20 cm apart from each other) to initiate gelation and reaction was completed in 4 hours by yielding viscous liquid.

Performing Gelation on Tissue Paper: Small tissue paper sample was cut from Kimtech Science lab tissue papers. It was soaked in 2% g-CN-EG monomer solution until completely wet. Tissue paper then transferred into plastic petri dish and illuminated from top for 1 hour, and washed with deionized water for the removal of unreacted portions.

Performing Gelation Under Sunlight: 2% g-CN-EG monomer mixture was poured into a vial and nitrogen was flushed through system. After capping, on a sunny day, 21.07.2017, the vial was put on the balcony of the Max Planck Institute of Colloids and Interfaces in Potsdam-Golm, Germany and gelation was completed in 1 hour.

Synthesis of Organogels With Photomask: Solution for 2% g-CN DMA gel was put into plastic petri dish and covered. On top of the transparent and plastic cover, homemade photomasks (printed and cut) were replaced and mixture was irradiated until gelation. Transfomation of patterned organogels to hydrogels can be completed in similar manner as discussed.

11.2.3. Synthesis of materials described in Chapter 6

Preparation of g-CN (CM): 1.0 g of cyanuric acid (C) and 1.0 g of melamine (M) were mixed with 40 mL distilled water and shaked overnight. After centrifugation at 6000 rpm for 10

minutes, a precipitate was dried at 60 °C under vacuum overnight. The dried product was transferred into a capped crucible and placed to oven with N_2 atmosphere at 550 °C for 4 hours, with a heating rate of 2.3 °C /min^{-1}. CM must be well grinded prior to use.

Time dependent synthesis of AHPA grafted CM: 50 mg CM was weighted in a glass vial with magnetic stirrer, 1 g AHPA solution (40% *w*/*w* in water) and 1 g deionized water were added. The mixture was sonicated for 10 minutes and nitrogen was flushed through the mixture for 3 minutes for the removal of dissolved oxygen. The mixture was put between two 50W LED daylight sources (20 cm apart from each other) and stirred continuously for the desired reaction time. Afterwards, the mixture was vacuum filtered, washed 3 times with water (3×50 mL) and washed once with acetone (20 mL). After filtration, the solid sample was dried under vacuum at 60 °C overnight and the product was obtained in nearly quantitative yield.

Synthesis of 1-decene grafted CM: 50 mg CM was weighted in a glass vial with magnetic stirrer, 1 g of 1-decene and 1 g of IPA were added. The mixture was sonicated for 10 minutes and nitrogen was flushed through the mixture for 3 minutes for the removal of dissolved oxygen. The mixture was put between two 50W LED daylight sources (20 cm apart from each other) and stirred continuously for the desired reaction times at 50 °C. Afterwards, the mixture was vacuum filtered, washed 3 times with IPA (3×40 mL) and washed once with acetone (20 mL). After filtration, the solid sample was dried under vacuum at 60 °C overnight and the product was obtained in nearly quantitative yield.

Synthesis of allylamine grafted CM: 50 mg CM was weighted in a glass vial with magnetic stirrer, 1 g allylamine and 1 g ethanol were added. The mixture was sonicated for 10 minutes and nitrogen was flushed through the mixture for 3 minutes for the removal of dissolved oxygen. The mixture was put between two 50W LED daylight sources (20 cm apart from each other) and stirred continuously for 48 hours at 40 °C. After the mixture was taken, it was vacuum filtered, washed 3 times with ethanol (3×40 mL) and washed once with acetone (20 mL). After filtration, the solid sample was dried under vacuum at 60 °C overnight, and the product was obtained in nearly quantitative yield.

Synthesis of 1*H*, 1*H*, 2*H*-perfluoro-1-decene grafted CM: 50 mg CM was weighted in a glass vial with magnetic stirrer, 1 g 1*H*,1*H*,2*H*-perfluoro-1-decene and 1 g THF were added. The mixture was sonicated for 10 minutes and nitrogen was flushed through the mixture for 3 minutes

for the removal of dissolved oxygen. The mixture was put between two 50W LED daylight sources (20 cm apart from each other) and stirred continuously for 48 hours at 50 °C. After the mixture was taken, it was vacuum filtered and washed 3 times with THF (3×40 mL) and washed once with acetone (20 mL). After filtration, the solid sample was dried under vacuum at 60 °C overnight and the product was obtained in nearly quantitative yield.

Synthesis of AHPA grafted CM with triethanolamine as hole scavenger: 50 mg CM was weighted in a glass vial with magnetic stirrer, 1 g AHPA solution (40 wt.% in water) and 1 g deionized water were added with 0.5 mL triethanolamine as hole scavenger. The mixture was sonicated for 10 minutes and nitrogen was flushed through the mixture for 3 minutes for the removal of dissolved oxygen. The mixture was put between two 50W LED daylight sources (20 cm apart from each other) and stirred continuously for 4 hours. Afterwards, the mixture was vacuum filtered, washed 3 times with water (3×50 mL) and washed once with acetone (20 mL). After filtration, the solid sample was dried under vacuum at 60 °C overnight.

Synthesis of AHPA grafted CM with hydrogen peroxide as electron scavenger: 50 mg CM was weighted in a glass vial with magnetic stirrer, 1 g AHPA solution (40 wt.% in water) and 1 g deionized water were added with 1 mL hydrogen peroxide solution (50 wt.% in water) as electron scavenger. The mixture was sonicated for 10 minutes and nitrogen was flushed through the mixture for 3 minutes for the removal of dissolved oxygen. The mixture was put between two 50W LED daylight sources (20 cm apart from each other) and stirred continuously for 4 hours. Afterwards, the mixture was vacuum filtered, washed 3 times with water (3×50 mL) and washed once with acetone (20 mL). After filtration, the solid sample was dried under vacuum at 60 °C overnight.

Control experiment of AHPA grafted CM with triethanolamine and hydrogen peroxide: 50 mg CM was weighted in a glass vial with magnetic stirrer, 1 g AHPA solution (40 wt.% in water) and 1 g deionized water were added with 1 mL hydrogen peroxide solution (50 wt.% in water) as electron scavenger and 0.5 mL triethanolamine as hole scavenger. The mixture was sonicated for 10 minutes and nitrogen was flushed through the mixture for 3 minutes for the removal of dissolved oxygen. The mixture was put between two 50W LED daylight sources (20 cm apart from each other) and stirred continuously for 4 hours. Afterwards, the mixture was vacuum

filtered, washed 3 times with water (3×50 mL) and washed once with acetone (20 mL). After filtration, the solid sample was dried under vacuum at 60 °C overnight.

UV induced grafting of 1-decene and 1*H*, 1*H*, 2*H*-perfluoro-1-decene grafted CM: Mixtures were prepared the same way as explained previously. The mixtures were put into UV illumination for 6 hours and and purified subsequently as previously reported.

11.2.4. Synthesis of materials described in Chapter 7

Synthesis of Graphitic Carbon Nitride (g-CN): g-CN was prepared from cyanuric acid-melamine (CM) complex as reported in literature.[16] In a typical process, 1.0 g of cyanuric acid and 1.0 g of melamine were mixed with 40 mL distilled water and shaked overnight. After centrifugation at 5000 rpm for 10 minutes, a precipitate was dried at 60 °C under vacuum overnight. The dried product was transferred into a capped crucible and placed to oven with N_2 atmosphere at 550 °C for 4 hours, with a heating rate of 2.3 °C /min.

Synthesis of g-CN-AHPA: g-CN was hydrophilically modified using AHPA solution as previously reported.[172] In a typical process, 200 mg g-CN was mixed with 2 g AHPA solution and 2 g distilled water and sonicated for 5 minutes. After nitrogen flow through solution for 5 minutes, the mixture was put between 2 LEDs on visible light range and stirred for 12 hours. It was then filtered, washed with distilled water (3 times – 50 mL distilled water each) for removal of unreacted portions and finally washed with 20 mL acetone. It was dried overnight in vacuum oven at 50 °C.

Synthesis of Hydrogel With 0.35% g-CN-AHPA Content: 35 mg g-CN-AHPA was mixed with 9.9 g distilled water in a plastic vessel and sonicated for 2 minutes for homogenous dispersion of g-CN-AHPA particles. 45 mg AAm, 15 mg DMA and 5 mg MBA was added to the mixture, sealed and put between 2 LED visible light sources until complete gelation (approx. 20 hours).

Synthesis of Hydrogel With 1% g-CN-AHPA Content: 100 mg g-CN-AHPA was mixed with 9.1 g distilled water in a plastic vessel and sonicated for 5 minutes for homogenous dispersion of g-CN-AHPA particles. 600 mg AAm, 200 mg DMA and 3 mg MBA was added to the mixture, sealed and put between 2 LED visible light sources until complete gelation (approx. 10 hours).

Synthesis of Hydrogel With 2% g-CN-AHPA Content: 200 mg g-CN-AHPA was mixed with 9 g distilled water in a plastic vessel and sonicated for 5 minutes for homogenous dispersion of g-CN-AHPA particles. 600 mg AAm, 200 mg DMA and 3 mg MBA was added to the mixture, sealed and put between 2 LED visible light sources until complete gelation (approx. 3 hours).

Synthesis of Hydrogel With 3.5% g-CN-AHPA Content: 350 mg g-CN-AHPA was mixed with 8.85 g distilled water in a plastic vessel and sonicated for 5 minutes for homogenous dispersion of g-CN-AHPA particles. 600 mg AAm, 200 mg DMA and 3 mg MBA was added to the mixture, sealed and put between 2 LED visible light sources until complete gelation (approx. 4 hours).

Synthesis of Hydrogel With 5% g-CN-AHPA Content: 500 mg g-CN-AHPA was mixed with 8.7 g distilled water in a plastic vessel and sonicated for 10 minutes for homogenous dispersion of g-CN-AHPA particles. 600 mg AAm, 200 mg DMA and 3 mg MBA was added to the mixture, sealed and put between 2 LED visible light sources until complete gelation (approx. 2 hours).

Synthesis of AAm Hydrogel With 2% g-CN-AHPA Content: 200 mg g-CN-AHPA was mixed with 9 g distilled water in a plastic vessel and sonicated for 5 minutes for homogenous dispersion of g-CN-AHPA particles. 800 mg AAm and 3 mg MBA was added to the mixture, sealed and put between 2 LED visible light sources until complete gelation (approx. 7 hours).

Synthesis of DMA Hydrogel With 2% g-CN-AHPA Content: 200 mg g-CN-AHPA was mixed with 9 g distilled water in a plastic vessel and sonicated for 5 minutes for homogenous dispersion of g-CN-AHPA particles. 800 mg DMA and 3 mg MBA was added to the mixture, sealed and put between 2 LED visible light sources until complete gelation (approx. 3 hours).

Investigation of Toxicity in 2% g-CN-AHPA Hydrogel: To test the biocompatibility of the hydrogel, *E. coli* cultures were grown in the presence and absence of the hydrogel. Bacterial growth was monitored over time, measuring the optical density at 600 nm (OD_{600}). In detail, a pre-culture of fast-growing *E. coli* Turbo bacteria (New England Biolabs) was grown over night (37 °C, 250 rpm) in lysogeny broth (LB; 10 g/l tryptone, 5 g/l yeast extract, 10 g/l NaCl). Using this pre-culture, two main cultures were prepared with OD_{600} = 0.1 (10 ml LB). The cultures were grown at 37°C and 250 rpm until they reached OD_{600} = 0.5-0.6. At this point, 1 g of hydrogel was added to one culture while the same amount of sterile, ultrapure water was added to the second culture as a control. In the next 5 hours, samples were taken in regular intervals for measuring

OD_{600}. The OD_{600} value measured at the time when hydrogel/water was added (t = 0 min) was subtracted from the measured OD_{600} values at the respective time points. These values were then used for plotting the growth curves to visualize the rate of cell division. The experiment was performed in triplicate/duplicate, using 3/2 independent pre-cultures.

11.2.5. Synthesis of materials described in Chapter 8

Preparation of g-CN: 2.0 g of cyanuric acid (C) and 2.0 g of melamine (M) were mixed with 40 mL distilled water and shaked overnight. After centrifugation at 6000 rpm for 10 minutes, a precipitate was dried at 60 °C under vacuum overnight. The dried product was transferred into a capped crucible and placed to oven with N_2 atmosphere at 550 °C for 4 hours, with a heating rate of 2.3 °C /min^{-1}. g-CN must be well grinded prior to use.[16]

Synthesis of g-CN Based Prepolymer: 200 mg g-CN was mixed with 4.5 g water and 4.5 g EG and ultrasonicated at 50 % amplitude for 20 minutes (10 * 2 minutes portions) to yield g-CN dispersion. Afterwards, 0.8 g DMA was added to the dispersion and mixture was put between two 50 W LED daylight sources (20 cm apart from each other) and reacted for certain times (1, 3, 6 and 12 hours, coded later as g-CN pre 1h, g-CN pre 3h, g-CN pre 6h, g-CN pre 12h) with mild stirring. For the synthesis of g-CN 2pre 3h, instead of 0.8 g, 1.6 g DMA was employed in reaction.

Exemplary Synthesis of Tough Organohydrogel (touA): 1 g g-CN pre3h was mixed with 1 g water, 2 g DMA, 100 mg MBA and mixed well for 10 minutes. Subsequently, nitrogen was flushed from system for 3 minutes and mixture was put between two 50 W LED daylight sources (20 cm apart from each other) to initiate gelation which takes place in 1 hour.

Synthesis of touB hydrogel: 1 g g-CN pre3h was mixed with 1 g water, 1 g DMA, 100 mg MBA and mixed well for 10 minutes. Subsequently, nitrogen was flushed from system for 3 minutes and mixture was put between two 50 W LED daylight sources (20 cm apart from each other) to initiate gelation which takes place in 1 hour. EG (14 wt. %) can be removed via water immersion as described.

Synthesis of touC hydrogel: 1 g g-CN pre3h was mixed with 2 g water, 1 g DMA, 100 mg MBA and mixed well for 10 minutes. Subsequently, nitrogen was flushed from system for 3 minutes and mixture was put between two 50 W LED daylight sources (20 cm apart from each

other) to initiate gelation which takes place in 1 hour. EG (10 wt. %) can be removed via water immersion as described.

Reference DMA Hydrogel Without g-CN (touRef): Mixture composed of 450 mg EG, 450 mg water and 80 mg DMA was used to replicate the content of g-CN based prepolymer. Control solution is mixed with 1 g water, 2 g DMA, 100 mg MBA, 20 mg KPS and mixed well for 10 minutes. 0.2 mL H_2O_2 was added to the mixture and gelation took place in 10 minutes. EG (10 wt. %) can be removed via water immersion as described.

Synthesis of Lubricant Organohydrogel (lubA): 1 g g-CN pre3h was mixed with 2 g water, 1 g DMA, 0.8 g SPMA, 75 mg MBA and stirred well until the dissolution of solid monomers. Nitrogen was flushed from mixture for 3 minutes and mixture was put between two 50 W LED daylight sources (20 cm apart from each other) to initiate gelation which takes place in 1 hour.

Synthesis of lubB hydrogel: 1 g g-CN pre3h was mixed with 2 g water, 1.8 g DMA, 75 mg MBA and mixed well for 10 minutes. Subsequently, nitrogen was flushed from system for 3 minutes and mixture was put between two 50 W LED daylight sources (20 cm apart from each other) to initiate gelation which takes place in 1 hour. EG can be removed via water immersion as described.

Synthesis of lubC hydrogel: 1 g g-CN pre3h was mixed with 2 g water, 1.2 g SPMA, 75 mg MBA and mixed well for 10 minutes. Subsequently, nitrogen was flushed from system for 3 minutes and mixture was put between two 50 W LED daylight sources (20 cm apart from each other) to initiate gelation which takes place in 1 hour. EG can be removed via water immersion as described.

Reference Lubricant Hydrogels Without g-CN (lubRef): Mixture composed of 450 mg EG, 450 mg water and 80 mg DMA was used to replicate the content of g-CN based prepolymer. Control solution was mixed with 2 g water, 1 g DMA, 0.8 g SPMA, 75 mg MBA, 20 mg KPS and mixed well for 10 minutes. 0.2 mL H_2O_2 was added to initiate gelation which takes place in 1 hour.

Removal of EG From Organohydrogels: All tough organohydrogel samples with different compositions were first immersed in 30 mL acetone overnight and then into 50 mL deionized water for 2 days by changing water 2 times per day. Lubricant organohydrogel can be treated in

the same way to yield highly swollen hydrogel, or it can be freeze dried after reaction, swollen in water overnight and freeze dried again, which certain amounts of water can be added to dry hydrogel for desired amount of swelling. Compression measurements were performed for hydrogels with same swelling ratios prepared through freeze drying pathway.

11.2.6. Synthesis of materials described in Chapter 9

Preparation of CMp: 2.6 g of cyanuric acid (C) and 3.6 g of 2,4-diamino-6-phenyl-1,3,5 triazine (Mp) were mixed with 50 mL distilled water and shaked overnight. After centrifugation at 5000 rpm for 5 minutes, the precipitate was dried at 70 °C under vacuum overnight. The dried product is transferred into a capped crucible and placed to oven with N_2 atmosphere at 450 °C for 2 hours, with a heating rate of 2.3 °C /min. CMp particles were well grinded prior to use. [19]

Preparation of CMB: 2.0 g of cyanuric acid (C), 2.0 g of melamine (M) and 0.2 g barbituric acid (B) were mixed with 50 mL distilled water and shaked overnight. After centrifugation at 5000 rpm for 5 minutes, the precipitate was dried at 70 °C under vacuum overnight. The dried product was transferred into a capped crucible and placed to oven with N_2 atmosphere at 550 °C for 4 hours, with a heating rate of 2.3 °C /min. CMB particles well grinded prior to use.[13]

Polymerization of vTA as control reaction: 2 mL vTA was mixed with 5 mL DMF and 30 mg AIBN until dissolution. Later, oxygen was removed from mixture via nitrogen flush and reaction was started at 90 °C for 24 hours. Afterwards, mixture was mixed with 5 mL acetone and poured into 20 mL icy water. Viscous brown phase collected and dried overnight at 60 °C for ^{1}H-NMR and SEC analysis. Product yield was less than 1%.

Grafting vTA on CMp particles: 100 mg CMp was mixed with 1 mL vTA and sonicated for 5 minutes in sonic bath. Mixture was degassed with nitrogen flux for 10 minutes and placed between 2 50W LED set ups and stirred for 3 hours under continuous visible light irradiation. For purification, mixture was filtered and washed with ethanol 3 times (20 mL each portion) and dried under vacuum at 60 °C overnight.

Grafting vTA on CMB particles: 100 mg CMB was mixed with 1 mL vTA and sonicated for 5 minutes in sonic bath. Mixture was placed between 2 50W LED set ups and stirred for 3 hours under continuous visible light irradiation. For purification, mixture was filtered and washed with ethanol 3 times (20 mL each portion) and dried under vacuum at 60 °C overnight.

Spray Coating of CMp-vTA disperions: 200 mg CMp-vTA was mixed with 5 mL chloroform and sonicated for 3 minutes. Glass slides were washed with ethanol and dried at 60 ºC. Glass slide was put under spray needle with 80 ºC heating from below. Dispersion was loaded into container and spraying was performed onto glass (1, 2 or 6 cycles).

11.3. Characterization

Zeta potential measurements of colloidal suspensions of g-CN were performed with a Zetasizer Nano ZS90 from Malvern. Zeta potential is an important phenomenon to determine colloidal stability as it is related to electrostatic repulsive forces. The measured value is based on the potential difference of dispersing media and stationary fluid attached to colloidal particle which arises from electric double layer theory. Zeta potential magnitudes more than 30 mV stands for good colloidal stability whereas magnitudes lower than 30 mV generally stand for instability. Charges of colloidal organic dispersions of g-CNs from Chapter 8 were performed with Mütek PCD 03 particle charge detector.

X-ray diffraction (XRD) patterns of powders were obtained using Bruker D8 Advance X-ray diffractometer via Cu-Kα radiation and a scintillation counter. XRD provides information about crystallinity and order of the material. Bragg law describes the diffraction of a wavelength

$$n\lambda = 2dsin\theta$$

Θ is the angle from diffraction, d is distance between planes and n represents the order of diffraction. The resulting pattern is characteristic for a sample which labels the crystalline orientation accordingly.

Scanning electron microscopy (SEM) images were obtained using SM-7500F (JEOL) equipped with an Oxford Instruments X-MAX 80 mm^2 detector. SEM records scattered electrons from sample after electron beam interaction and SEM images are used to observe the structures of samples.

Energy Dispersive X-Ray Analysis (EDX) is attached to SEM instrument. This technique presents the interaction of electron beam with inner electrons of the sample creating hole on the upper shell of sample, which emits X-ray and is specific for each atom.

Cryogenic scanning electron microscopy (Cryo-SEM) of the hydrogel samples were taken by using Jeol JSM 7500F and the cryo-chamber from Gatan (Alto 2500). Working principle is similar to SEM. In cryo-SEM, the sample is frozen before insertion for measurement to preserve the structure of the sample without drying effects.

Transmission electron microscopy (TEM) images were obtained via Zeiss EM 912 Omega microscope at 120 kV as acceleration voltage. Beam of electrons are transmitted through the sample and resulting image can be utilized to determine the structure (such as crystallinity) of material.

High resolution transmission electron microscopy (HR-TEM) measurements were acquired using a double-corrected Jeol ARM200F, equipped with a cold field emission gun and a Gatan GIF Quantum. The used acceleration voltage was 200 kV and the emission was set to 10 µA in order to reduce beam damage.

Combustive elemental analysis (EA) was performed utilizing Vario Micro device. The sample is combusted in oxygen atmosphere and decomposition products are detected to elaborate elemental ratios of C, H, N and S.

Porosity of samples was determined via nitrogen absorption of samples utilizing Quantachrome Quadrasorb. Degassed samples were employed on holders and volume of nitrogen adsorbed on surface is recorded at different pressures and investigated using BET theory.

Fourier transform infrared (FT-IR) spectra were taken on Nicolet iS 5 FT-IR spectrometer. FT-IR is non-destructive and facile method to distinguish functional groups in samples.

Solid state ultraviolet-visible (UV-Vis) spectroscopy was recorded via a Cary 500 Scan spectrophotometer equipped with an integrating sphere. It is predominantly used for determination of photo and electrical properties of materials due to light absorption. From absorption spectra band gaps can be deducted via Tauc plots.

Size exclusion chromatography (SEC) was conducted in *N*-methyl pyrrolidone (NMP, Sigma Aldrich, GC grade) with 0.05 mol·L^{-1} LiBr and BSME as internal standard using a column system by PSS GRAM 100/1000 column (8 × 300 mm, 7 µm particle size) with a PSS GRAM precolumn (8 × 50 mm) and a Shodex RI-71 detector and a calibration with PS standards from PSS. The method is utilized to determine molecular weight and molecular dispersity of polymer samples.

Nuclear magnetic resonance spectroscopy (NMR) was recorded at ambient temperature at 400 MHz using Bruker Ascend400 for ^{1}H-NMR. Thus, sample is dissolved in deuterated solvent and immersed in a magnetic field. Depending on the environment of the respective atom, chemical shifts can be measured. In the thesis, resulting spectra were investigated for determination of purity and confirmation of polymer structure.

Freeze drying of hydrogel and organohydrogel samples are applied for solid state hydrogel analysis. After standing in distilled water for 2 days; the hydrogels were cut into smaller pieces, transferred into a flask and dried by pump thaw cycles until the moisture droplets on the flask were not visible anymore. In this frozen form, they were immediately put into Lyotech GT 2E

freeze dryer overnight. Resulting products are brittle hydrogels which retain their pores on the microscopic level.

Thermogravimetric analysis (TGA) was recorded via TG 209 Libra from Netzsch in nitrogen atmosphere with a heating rate 10 K min^{-1} using aluminum crucible for samples. The sample is heated with a certain rate in defined atmosphere and mass loss with increasing temperature is measured.

Water contact angle measurement was investigated using Krüss contact angle measuring system G10 and recorded via Krüss official software. Sample with ideally flat surface is placed in front of camera which records the water drop on surface and estimates the angle between water droplet and surface. This method is useful to determine surface properties, such as hydrophilicity and hydrophobicity.

Swelling ratio is a term which specifies the water uptake of a material over defined time and can be calculated using

$$Swelling\ ratio\ = \frac{W_s - W_d}{W_d} \times 100\%$$

where W_s is the mass of swollen sample and W_d is the mass of dry sample. 100 mg of freeze-dried hydrogel samples were inserted in 10 mL distilled water and left for 24 hours to swell. Afterwards, surface of hydrogels gently dried via tissue and final masses are recorded.

Ultrasonication was performed via an ultrasonicator at 50% amplitude (Branson D450) which facilitates dispersion preparation.

Atomic force microscopy (AFM) from Digital Instruments was employed for the investigation of height profiles. Instrument consists of cantilever and ultra-fine needle which sweeps the surface of sample and the changes due to differences in height of sample is recorded.

Photoluminescent (PL) emission spectra were recorded on Jasco FP-8300 instrument with the excitation wavelength at 360 nm or at changing excitation wavelength between 300-420 nm. It is an effective method to probe electronic structure of semiconductors. Light triggers photoexcitation of sample which material is excited to higher electronic state and relaxes back to lower energy level. The emission is known as PL. Facile and non-destructive method can be employed to determine excitonic properties, evaluation of surfaces and recombination rates. Time resolved PL measures the luminescence lifetime of exciton.

X-Ray Photoelectron spectroscopy (XPS) was employed for the investigation of core levels of C1s, N1s, S2p in g-CN samples using CISSY equipment in ultra-high vacuum (UHV), with a

SPECS XR 50 X ray gun Mg Kα radiation (1254.6 eV) and Combined Lens Analyzer Module (CLAM). It is a quantitative technique which is used to analyze surface of material and provides information about elemental composition, density of electronic states and electronic state of elements. XPS operates under high vacuum and based on the irradiation of material with X-ray beams and measuring the kinetic energy and number of electrons separated from sample.

Ultraviolet Photoelectron spectroscopy (UPS) was carried out with an excitation source of He I 21.2 eV radiation and UVS 10/35 and the data were acquired at a bias -10 V. The calibration was performed by Fermi level of gold reference sample. It operates on same principles as XPS, but compared to XPS, lower energy photons are used and valance band-electronic work function of material can be calculated.

pH values of distilled water and CMp-vTA dispersion (30 mg CMp-vTA) in distilled water (6 mL) was measured via SI analytics Titro7000 and average values were taken after 3 measurements. pH is a logarithmic scale which shows the power of hydrogen in solution, therefore helps to measure acidity or basicity of aqueous solution.

Dynamic light scattering (DLS) measurements were performed on g-CN colloidal suspensions via Malvern Zetasizer Nano ZS90 with λ=633 nm at θ=90°. DLS provides information about hydrodynamic diameters of particles in solution. As all particles have Brownian motion in solution, random particle motion can be related to particle size using Stokes-Einstein equation. It assumes the particles as spheres and provides hydrodynamic diameter. Number average results were employed for g-CN dispersions.

Rheology measurements were performed on Anton Paar MCR 301 rheometer, equipped with a cone plate 12 (CP-12). Measurements were performed at constant angular frequency (10 rad s^{-1}) with strain range from 0.1-100% with 31 measuring points and 0.02 mm gap. Frequency dependent measurements were performed at constant strain (0.1%) with changing frequency in the range of 1-100 rad s^{-1}. Viscosity measurements were performed at ambient temperature with changing shear rate between 1-20 s^{-1}. Rheology stands for the deformation and flow behavior of materials. It can be applied from solids to liquids and provides information about many properties, such as viscosity and viscoelastic behavior.

Viscosity explains the resistance of liquids to flow, or a friction between fluid molecules, and one can imagine comparison of materials such as water and honey. Rheology is really helpful to determine viscosity and type of viscosity (shear thinning, shear thickening etc.). Basically, a material is replaced between two plates, where bottom plate is stationary and top plate applies

shear. Shear stress (τ) is defined as $\tau = F/A$, which F represents shear force (in Newton) and A represents area (m^2). Shear rate ($\dot{\gamma}$) is represented as v/h, which v is velocity (m/s) and h is shear gap (m). Finally, dynamic viscosity (η) can be calculated via $\eta=\tau/\dot{\gamma}$ with resulting Pa*s unit.

Viscoelastic behavior of materials represents viscous and elastic behavior upon shearing. Rheology is helpful when it comes to investigate such properties of materials. Shear stress is defined in a same manner as shown in viscosity. Shear strain (γ) can be defined as s/h where s shows deflection path (m) and h shows shear gap (m). Therefore, shear modulus (G) is represented as τ/γ with Pa unit. Complex shear modulus (G^*) is derived from oscillatory shear tests which describes viscoelastic behavior of samples. Storage modulus (G') represents elastic character and loss modulus (G'') represents viscous character of sample. In the cases where $G'>G''$, means material has solid-like character and $G'<G''$ shows that material has more liquid character.

Compression tests were measured on a Zwick mechanical tester zwickiLine Z2.5 equipped with a loadcell of 1 kN. Measurements were recorded after a preload of 0.1 N (speed pre-load 40 mm s^{-1}) and the test was performed at 0.05 mm s^{-1}. The cycling tests were performed up to different maximum forces (depending on materials from chapters) and recovered until 1 mm of strain (on specimens of 10 mm in height) before the stress was removed to restart the cycle (20-50 times). All the compression measurements were recorded using the software TestXpert II V3.71. Elastic moduli values were calculated at 10% before break.

Compression test is applied for samples for further investigation of their mechanical properties. Mostly related to mechanics, compression applies inward pushing forces to material (mainly uniaxial). Materials generally deform as elastic (recoverable) and plastic (non-recoverable) meanings. Applied force allows calculation of compressive strength and Young moduli (E_{mod}) values of materials. Typical characterization results in stress-strain curves which makes it possible to visualize elastic and plastic deformation regions of material with applied stress. Compressive strength (Pa) shows the maximum stress which material can handle (maxima of elastic deformation region) before stars to deform plastically. E_{mod} (Pa) is defined as the slope of stress-strain curve and represents materials resistance to deformation. Cyclic compression is applied to determine materials fatigue resistance within elastic deformation range.

11.4. Appendix Figures

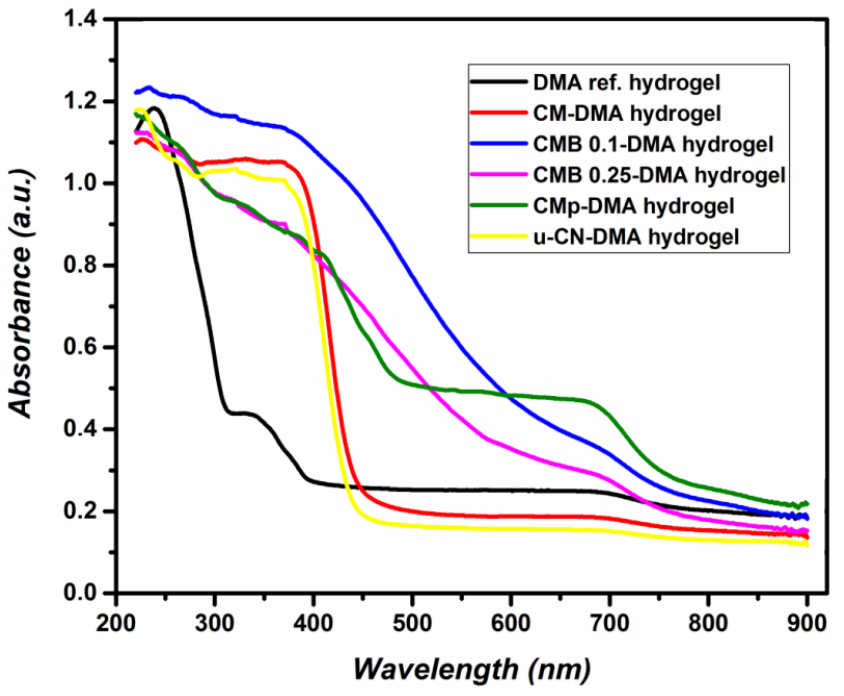

Figure A1. Solid state UV spectra of reference and carbon nitride derived DMA hydrogels.

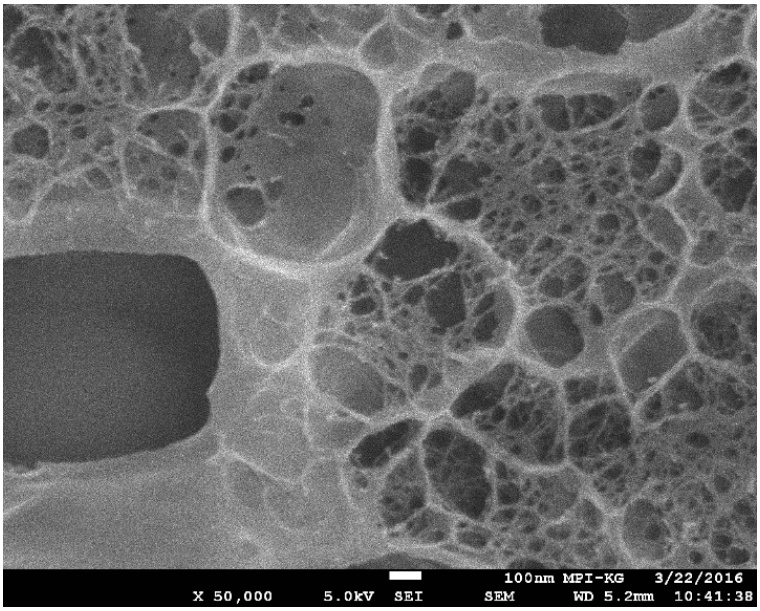

Figure A2. Cryo-SEM image of DMA reference hydrogel.

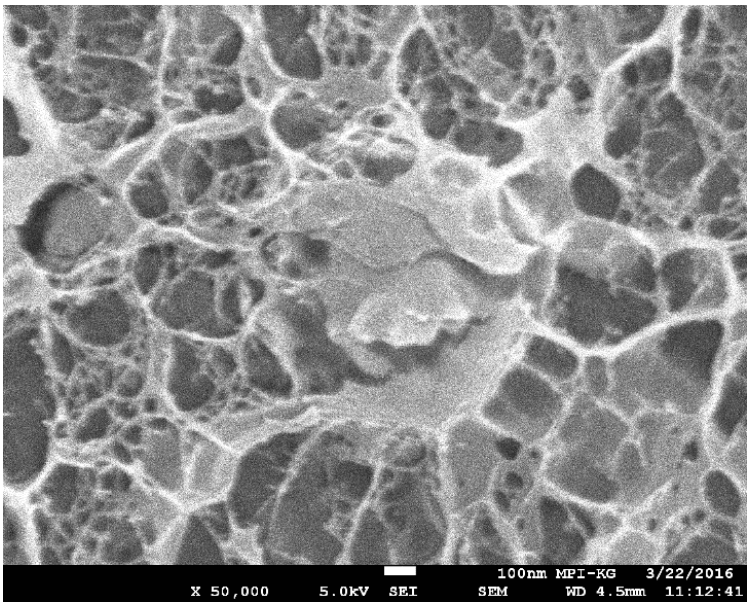

Figure A3. Cryo-SEM image of CM derived DMA hydrogel.

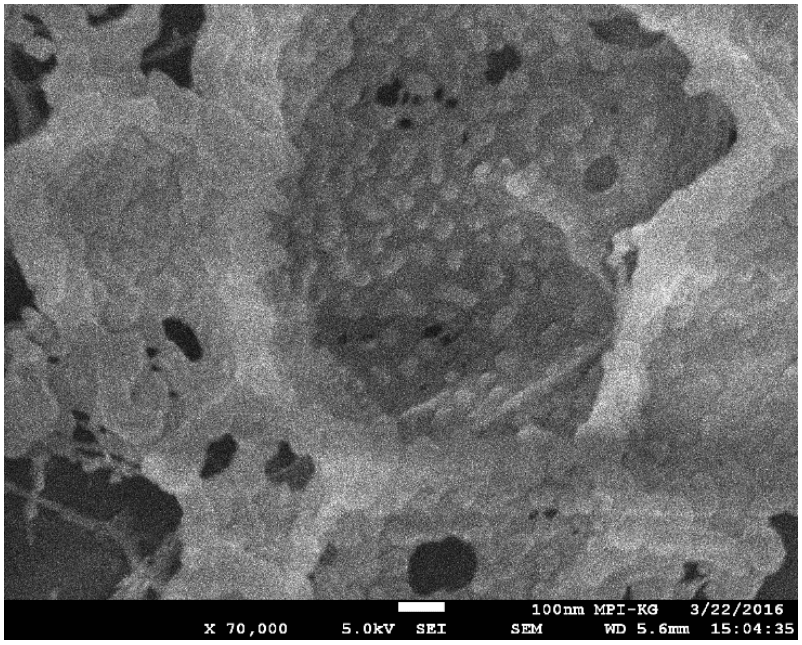

Figure A4. Cryo-SEM image of CMB 0.1 derived DMA hydrogel.

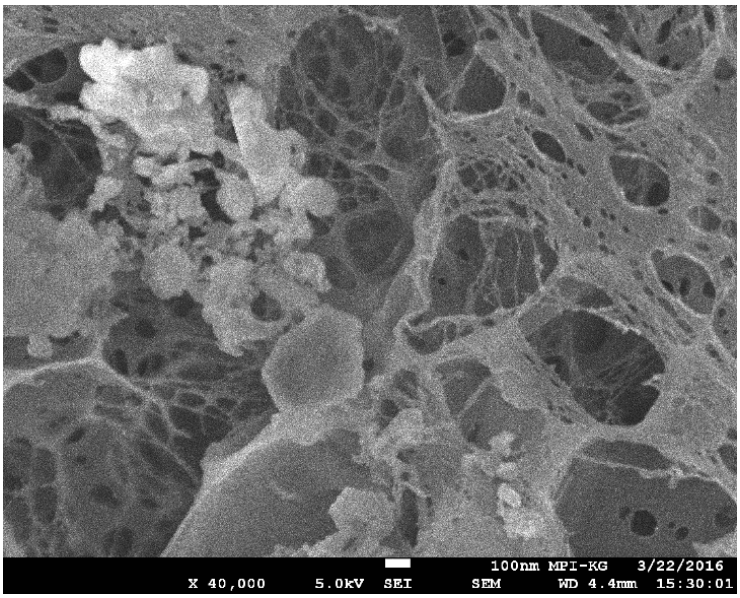

Figure A5. Cryo-SEM image of CMB 0.25 derived DMA hydrogel.

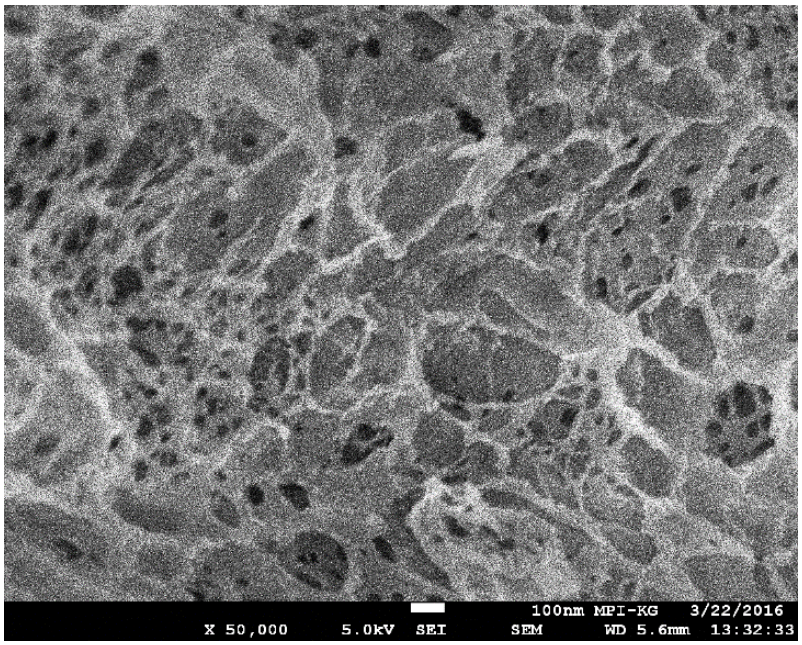

Figure A6. Cryo-SEM image of CMp derived DMA hydrogel.

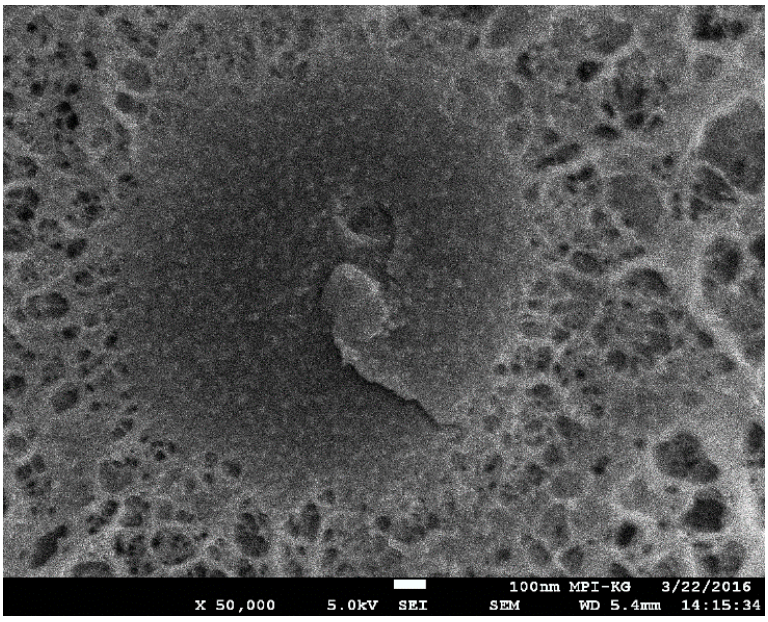

Figure A7. Cryo-SEM image of u-CN derived DMA hydrogel.

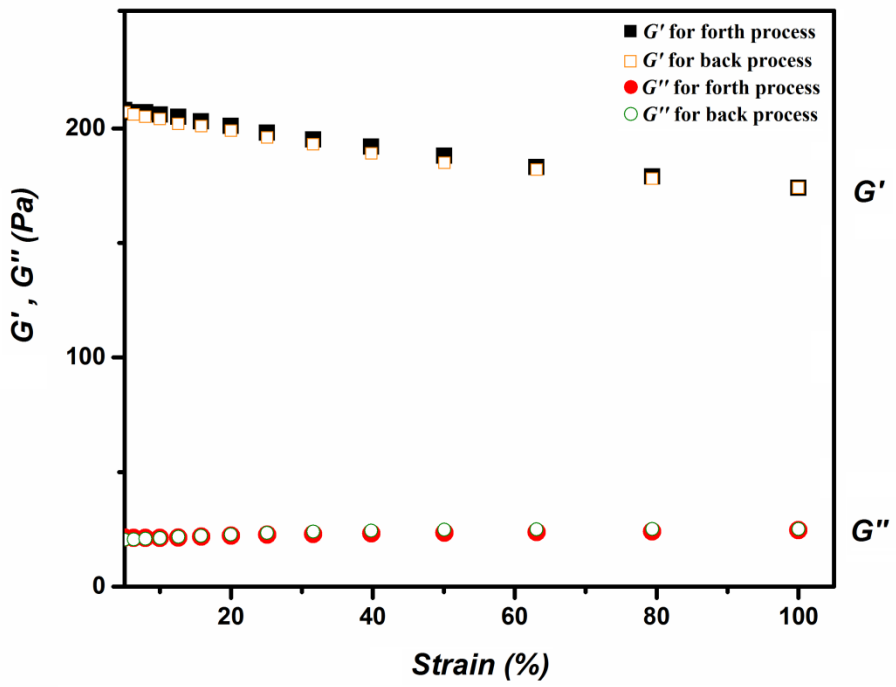

Figure A8. Rheological properties of DMA reference hydrogel with storage (*G'*) and loss moduli (*G''*) against changing strain on constant angular frequency, back (open) and forth (filled) process.

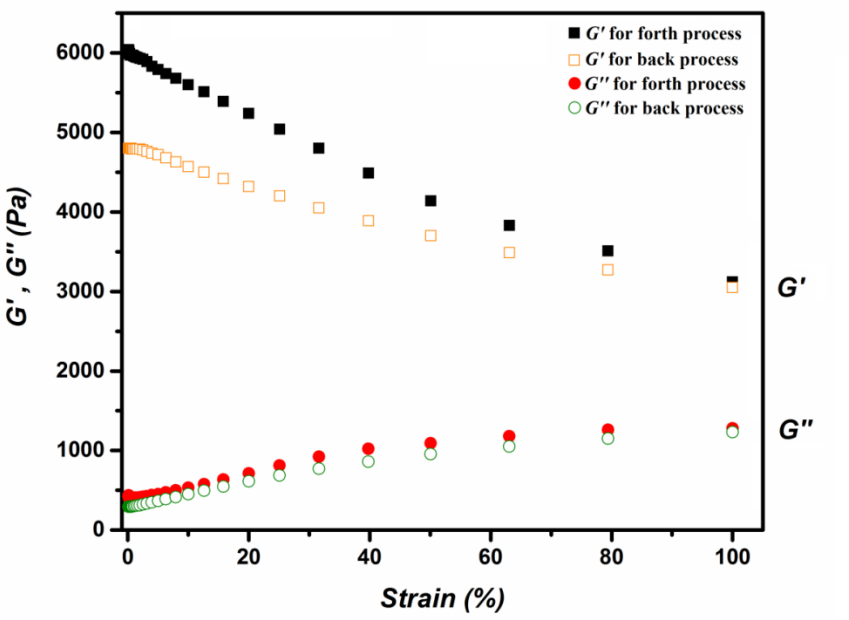

Figure A9. Rheological properties of CM-DMA reference hydrogel with storage (*G'*) and loss moduli (*G''*) against changing strain on constant angular frequency, back (open) and forth (filled) process.

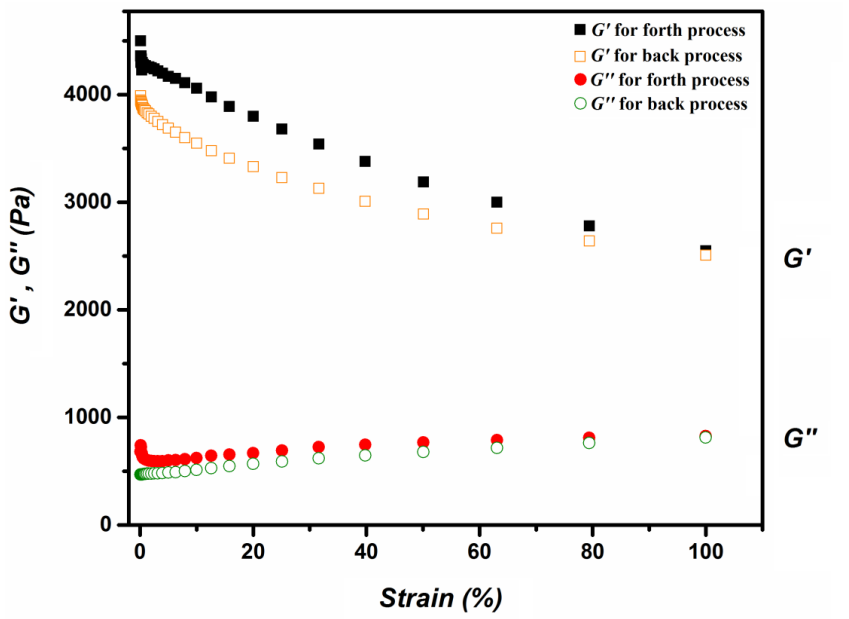

Figure A10. Rheological properties of CMB 0.1-DMA reference hydrogel with storage (*G'*) and loss moduli (*G''*) against changing strain on constant angular frequency, back (open) and forth (filled) process.

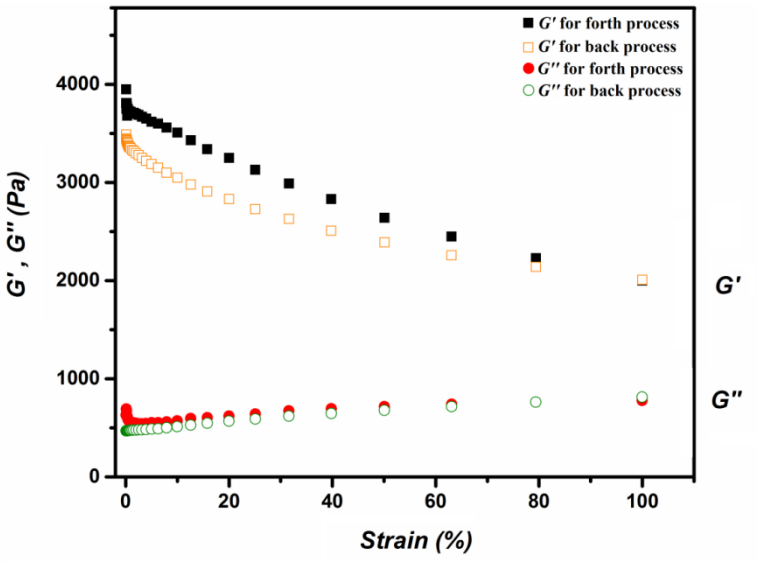

Figure A11. Rheological properties of CMB 0.25-DMA reference hydrogel with storage (*G'*) and loss moduli (*G''*) against changing strain on constant angular frequency, back (open) and forth (filled) process.

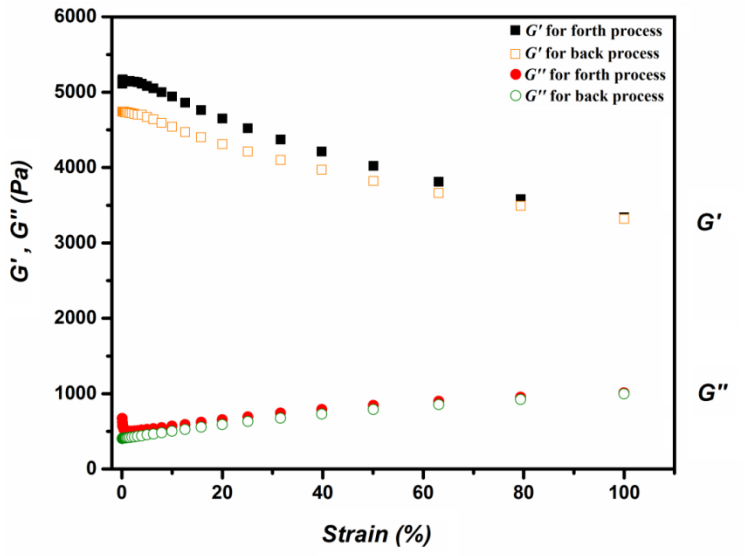

Figure A12. Rheological properties of CMp-DMA reference hydrogel with storage (*G'*) and loss moduli (*G''*) against changing strain on constant angular frequency, back (open) and forth (filled) process.

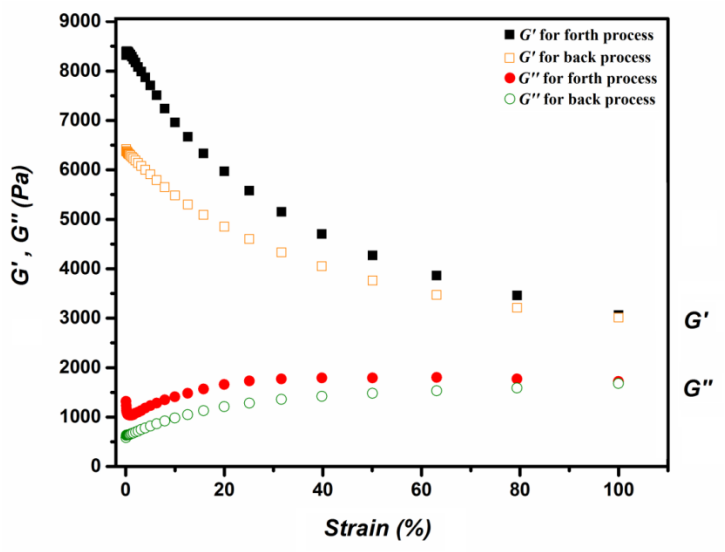

Figure A13. Rheological properties of u-CN-DMA reference hydrogel with storage (*G'*) and loss moduli (*G''*) against changing strain on constant angular frequency, back (open) and forth (filled) process.

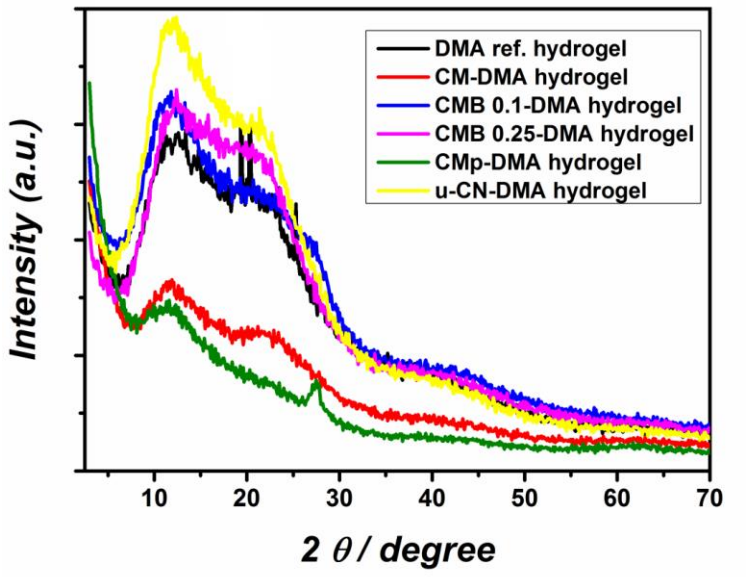

Figure A14. XRD profiles of reference and carbon nitride derived DMA hydrogels.

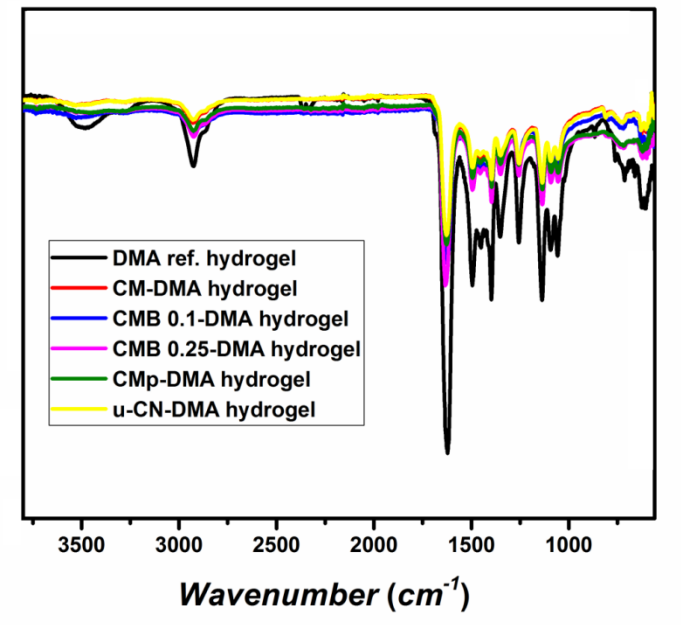

Figure A15. FT-IR spectra of reference and carbon nitride derived DMA hydrogels.

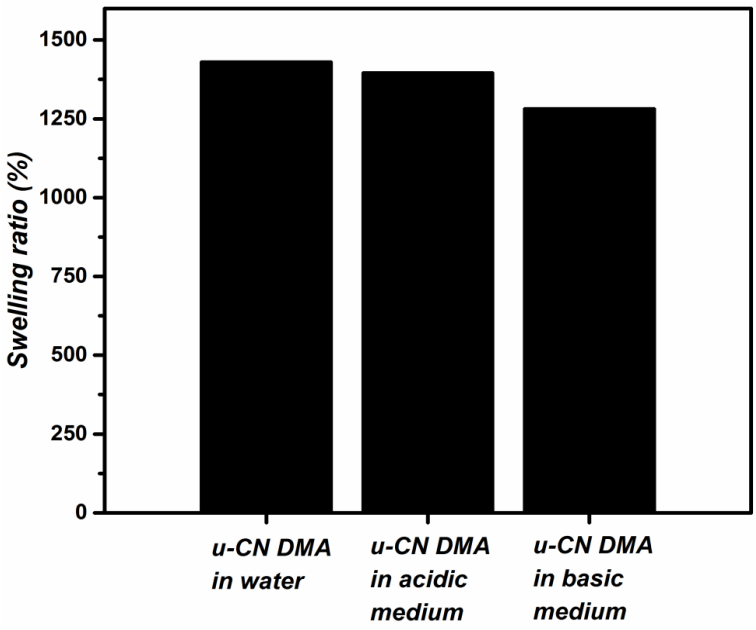

Figure A16. Swelling ratios of u-CN derived DMA hydrogels in different media.

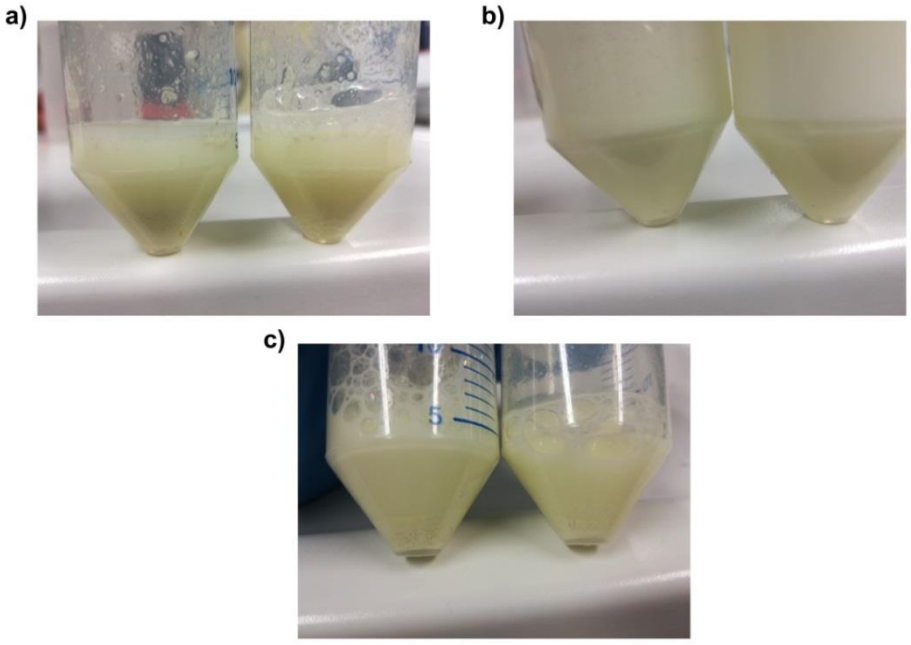

Figure A17. 2 wt.% g-CN in water with Triton X 305 (left tube) and Pluronic F127 (right tube) **(a)** before ultrasonication, **(b)** after ultrasonication and **(c)** standing after 10 minutes.

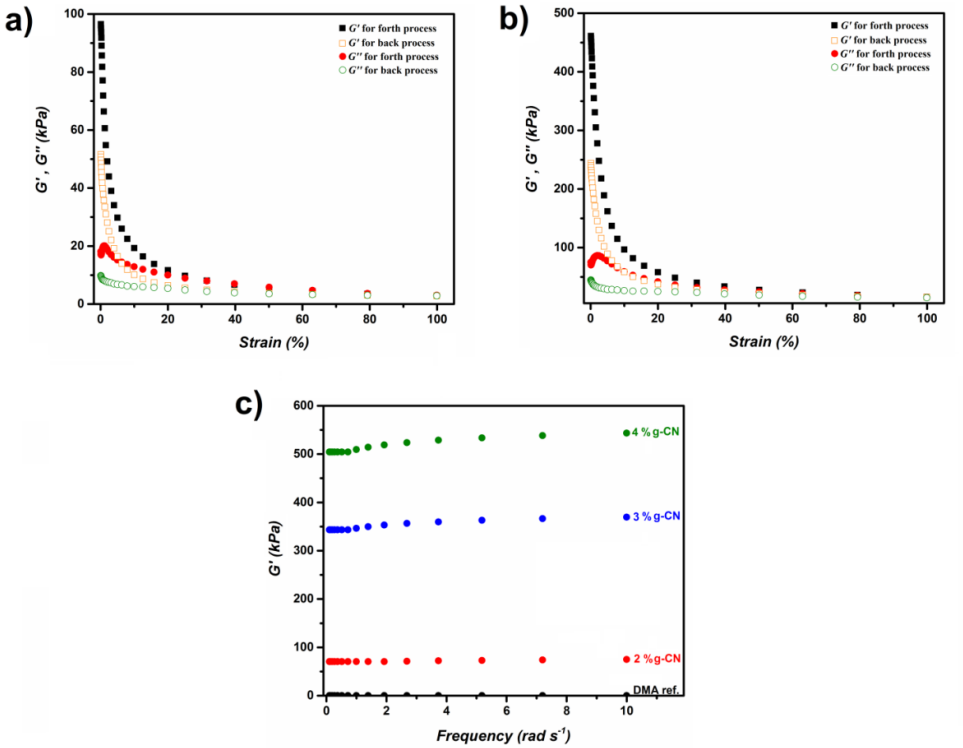

Figure A18. Comparison of storage (*G'*, black and orange squares) and loss modulus (*G''*, red and green circles) of **(a)** 2% and **(b)** 3% g-CN-EG gels against strain, back (open) and forth (filled) process and **(c)** storage moduli results of EG gels at constant strain (0.1%) against frequency.

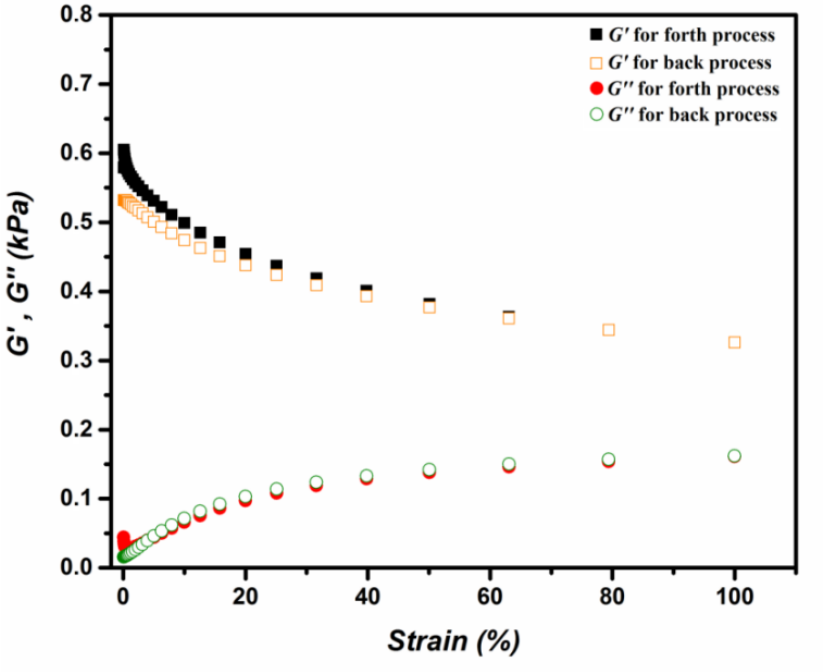

Figure A19. Rheology result of DMA reference EG gel, storage (*G'*, black and orange squares) and loss modulus (*G''*, red and green circles) against strain, back (open) and forth (filled) process.

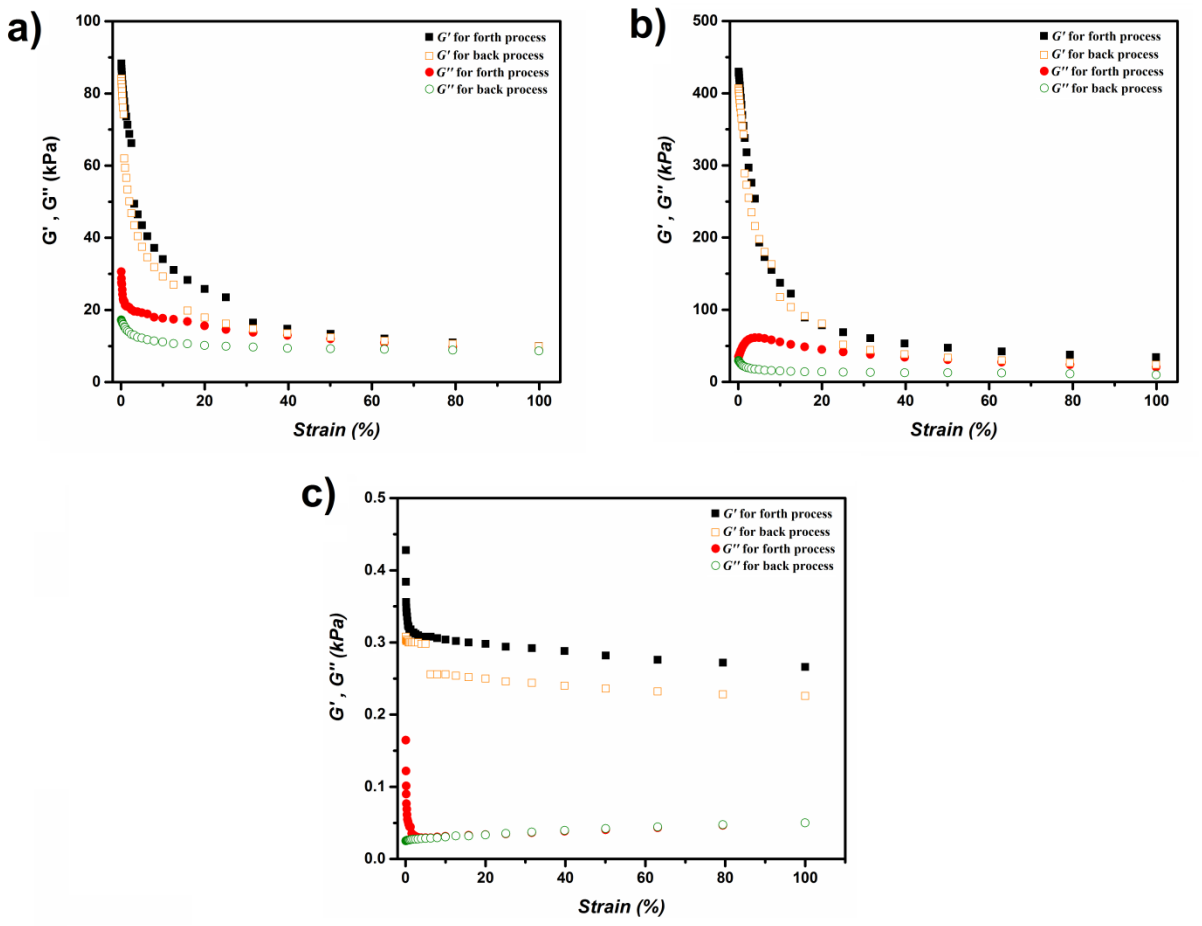

Figure A20. Comparison of storage (*G*', black and orange squares) and loss modulus (*G*'', red and green circles) of **(a)** 2% and **(b)** 3% g-CN and **(c)** reference DMA hydrogels against strain, back (open) and forth (filled) process.

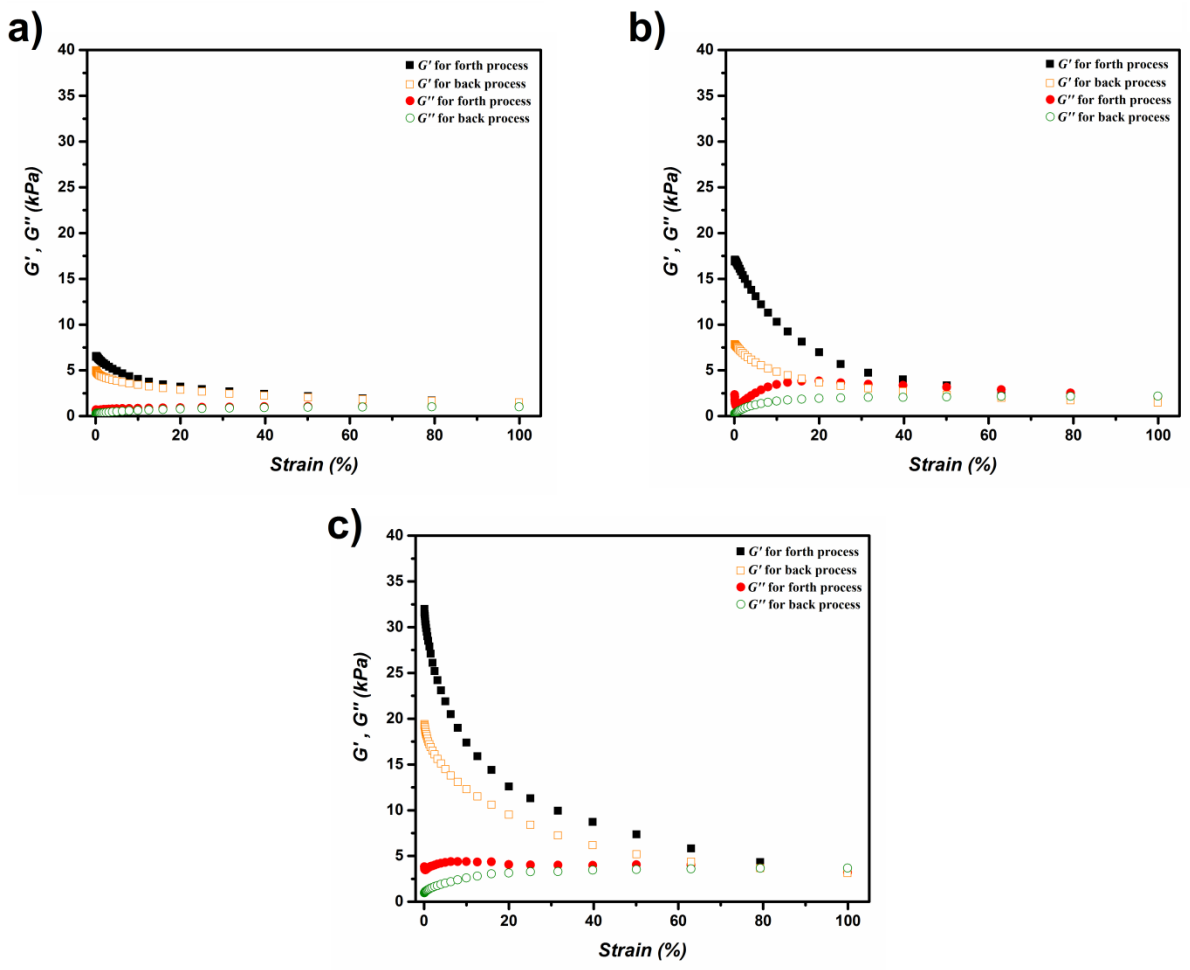

Figure A21. Comparison of storage (*G*', black and orange squares) and loss modulus (*G*'', red and green circles) of **(a)** 2% and **(b)** 3% and **(c)** 4% g-CN hydrogels initiated via redox in the dark, against strain, back (open) and forth (filled) process.

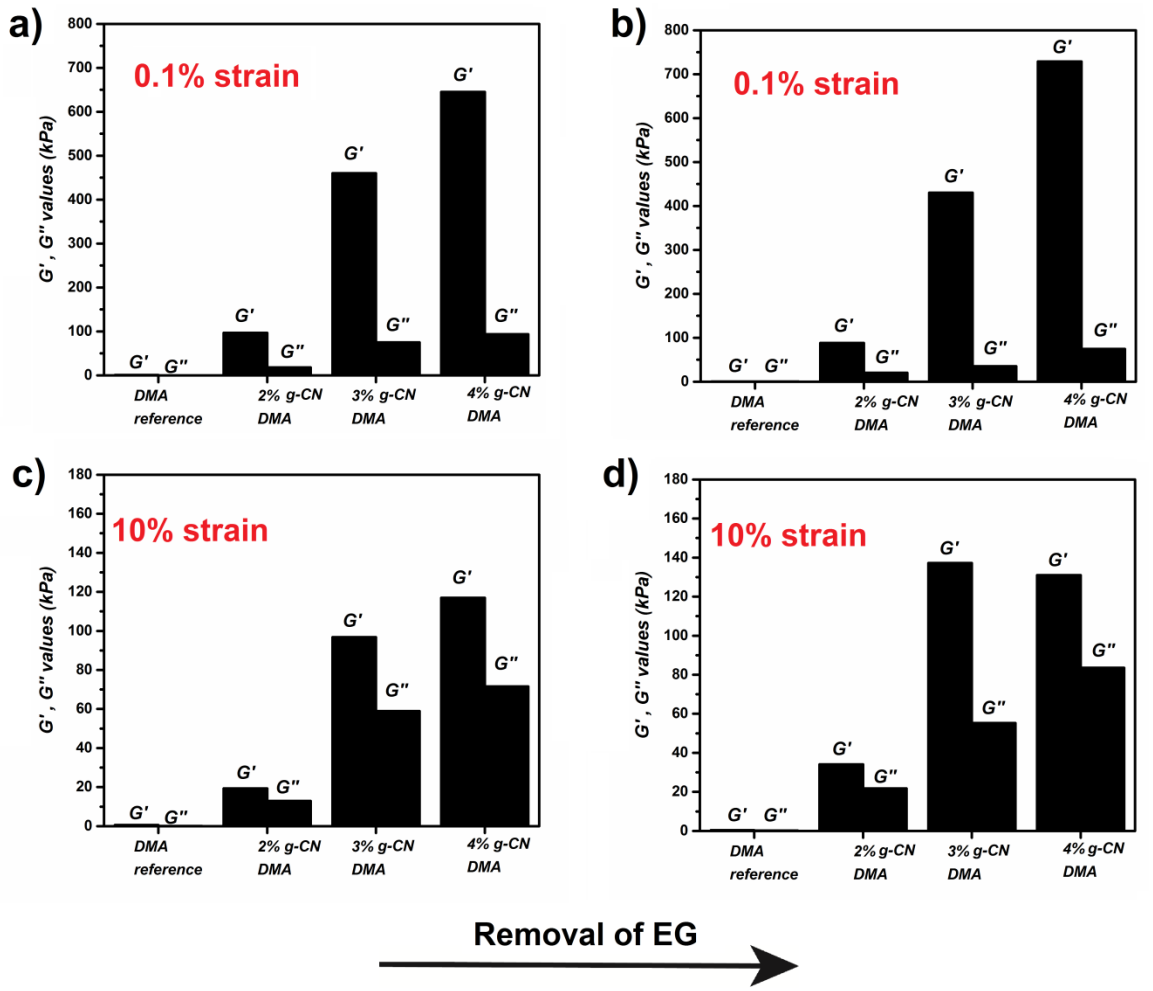

Figure A22. Comparison of storage and loss moduli for **(a)** EG gels and **(b)** hydrogels at 0.1% strain, c) EG gels and d) hydrogels at 10% strain.

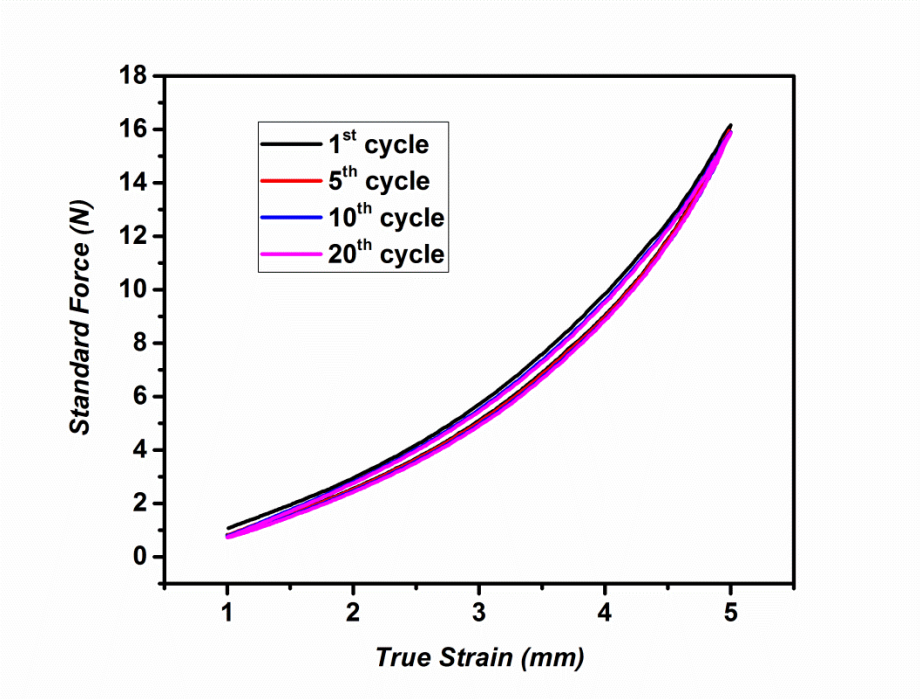

Figure A23. Cyclic compression test results of 3% g-CN EG gel.

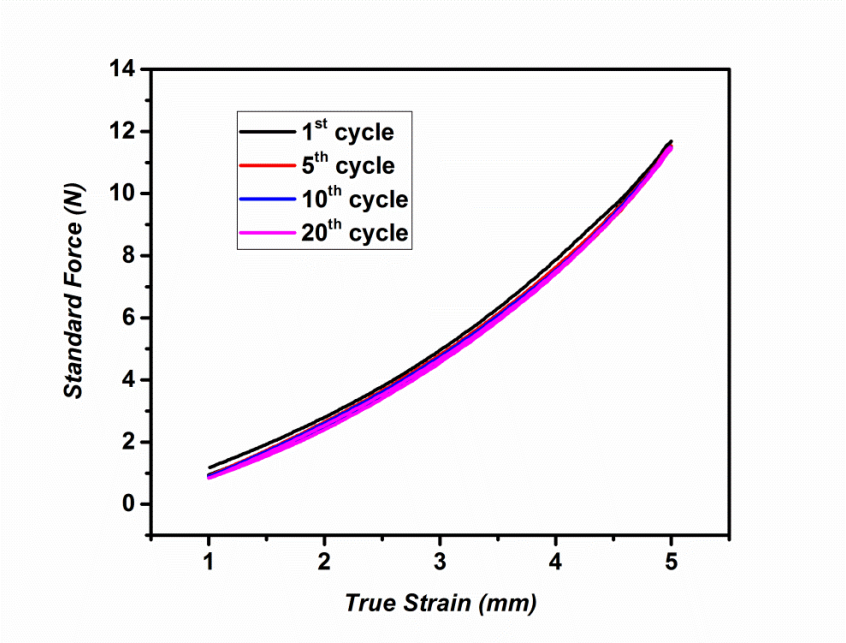

Figure A24. Cyclic compression test results of 4% g-CN EG gel.

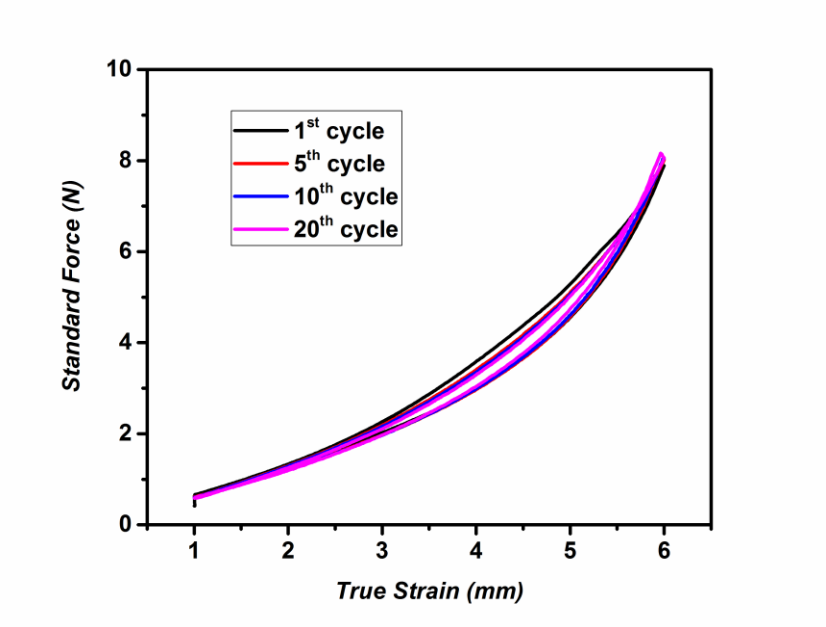

Figure A25. Cyclic compression test results of 3% g-CN hydrogel.

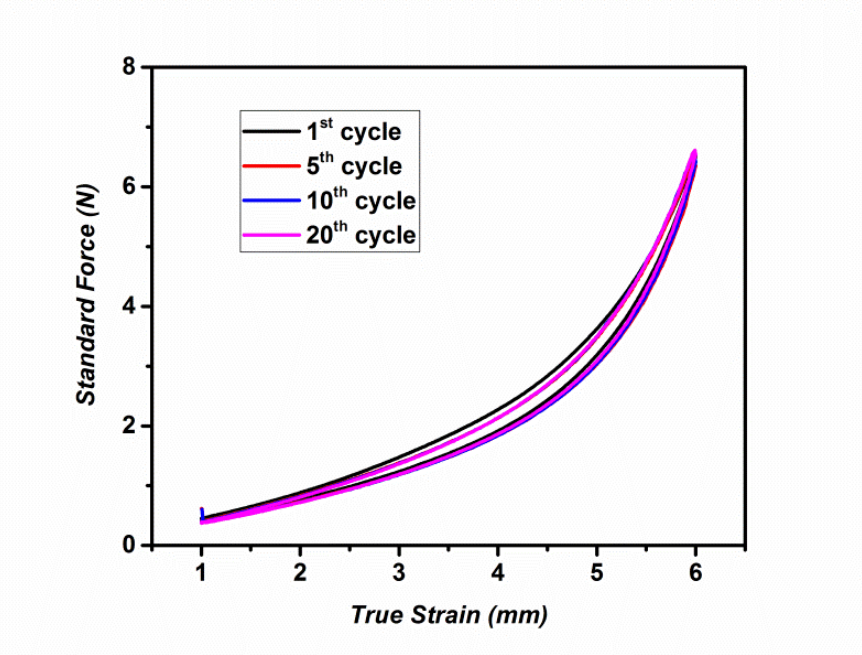

Figure A26. Cyclic compression test results of 4% g-CN hydrogel.

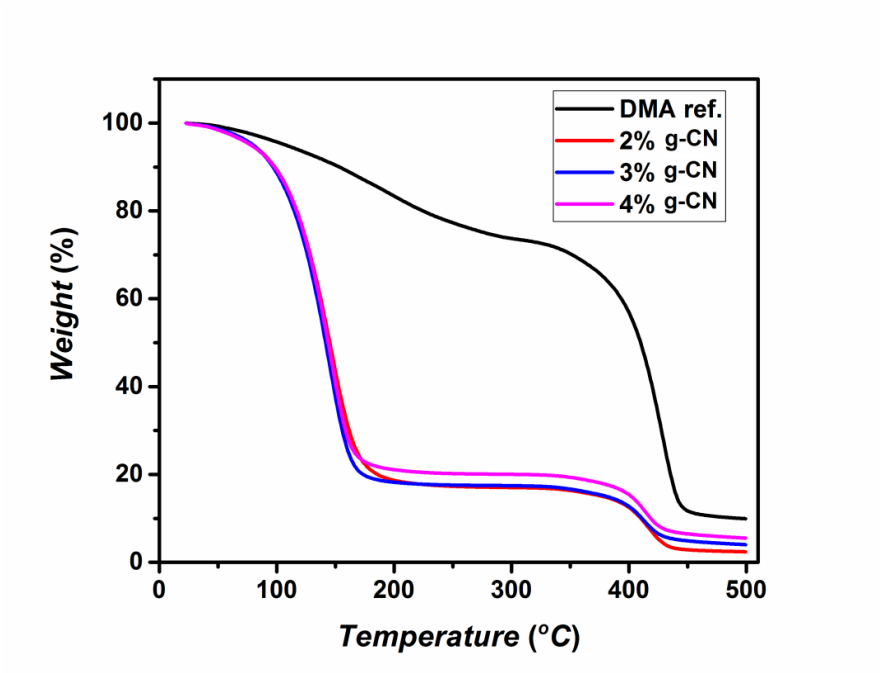

Figure A27. TGA diagrams of freeze dried g-CN EG gels.

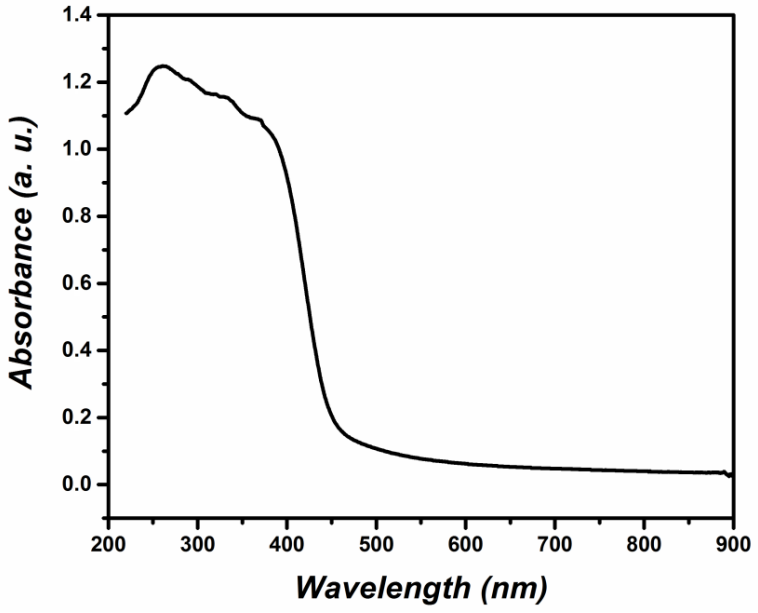

Figure A28. UV-Vis spectra of employed g-CN (synthesized from cyanuric acid-melamine precursor).

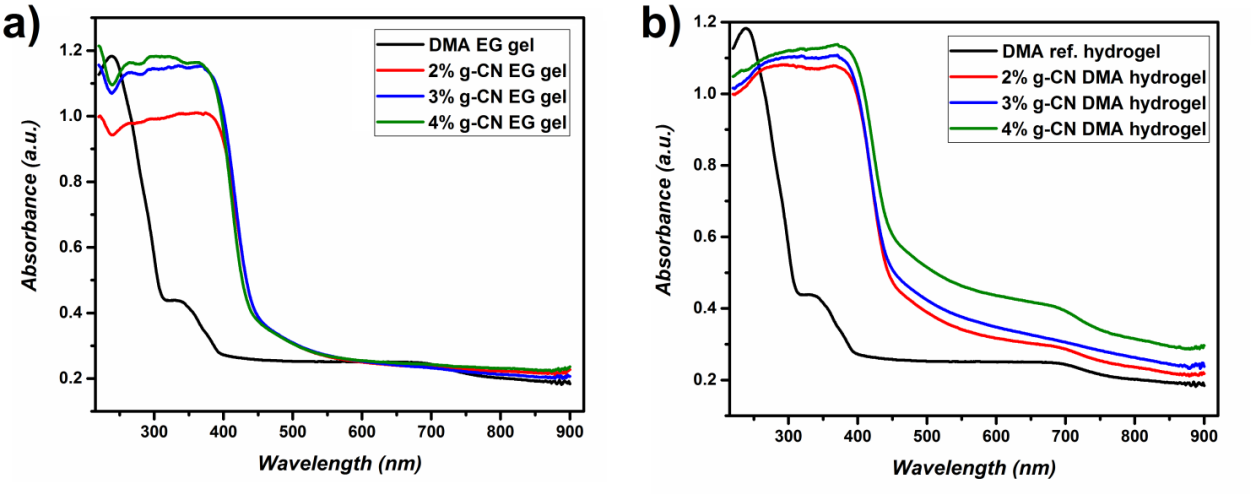

Figure A29. UV spectra of **(a)** EG gels and **(b)** hydrogels.

Figure A30. Symbols from deck of cards (spade, heart and diamond) gels synthesized via photopatterning (after rinsing with water).

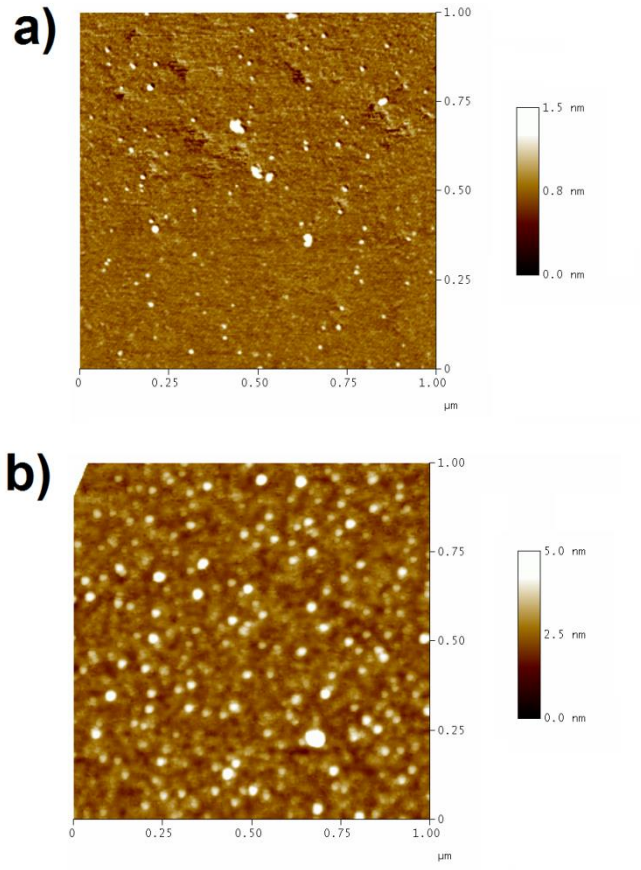

Figure A31. (a) Height profile of CM particles and **(b)** height profile of CM-AHPA24 particles on mica surface via AFM.

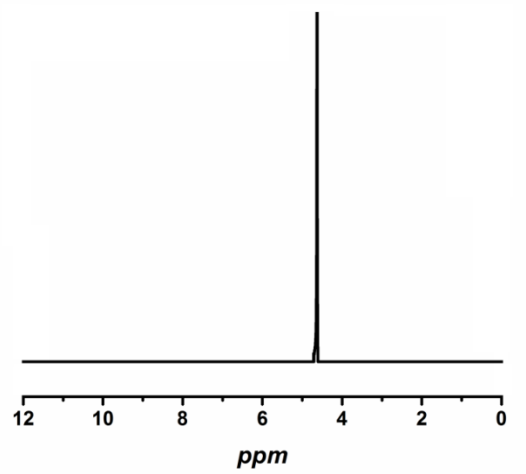

Figure A32. ^{1}H-NMR spectrum of the solvent which was yielded after mixing t6h AHPA modified CM with D_2O for 2 hours and filtering.

Table A1. Properties of unmodified and concentration dependent AHPA modified CMs. (50 mg CM+12 h reaction time).

Sample	AHPA concentration (%)	D_n (nm)[a]	Zeta Potential (mV)	S content (wt.%)[b]	C/N Ratio[b]
CM		2448	-27.5	0.712	0.6025
CM-AHPA12	10	1698	-43.5	5.411	1.0365
CM-AHPA12	20	1610	-52.2	7.345	1.0997
CM-AHPA12	40	1433	-56.1	8.686	1.5485
[a]DLS measurements were performed in water (0.05 wt.%), [b] obtained via elemental analysis. [c] reference reaction based on mixing reactants without visible light irradiation and subsequent purification					

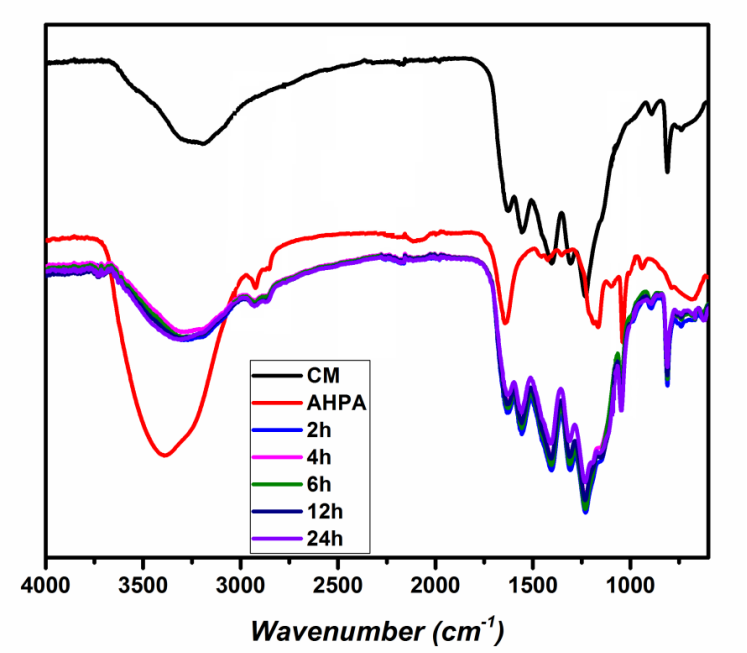

Figure A33. FT-IR spectra of unmodified and AHPA modified CM after different reaction times.

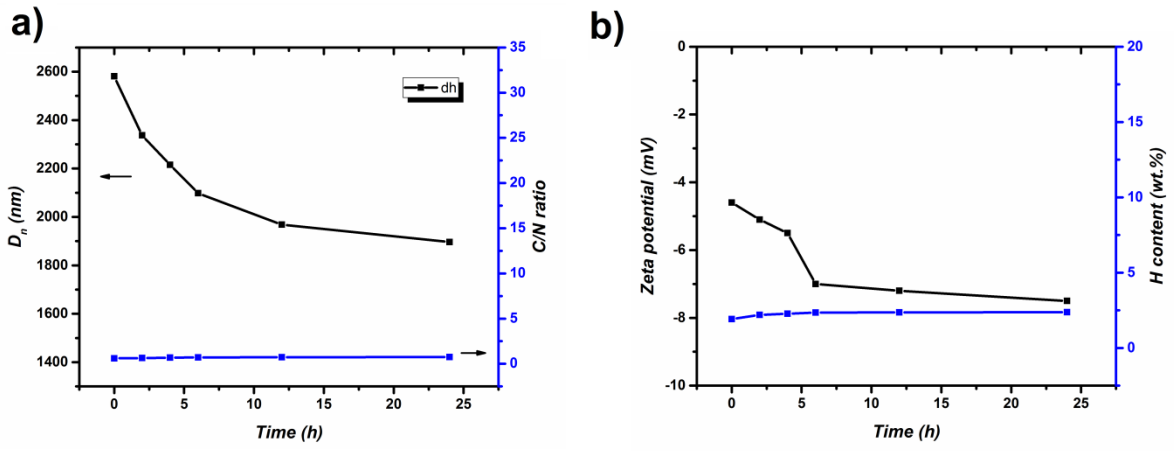

Figure A34. **(a)** The relation of reaction time with size and C/N ratio of 1-decene modified CMs, **(b)** the relation of reaction time with zeta potential and H content of 1-decene modified CMs.

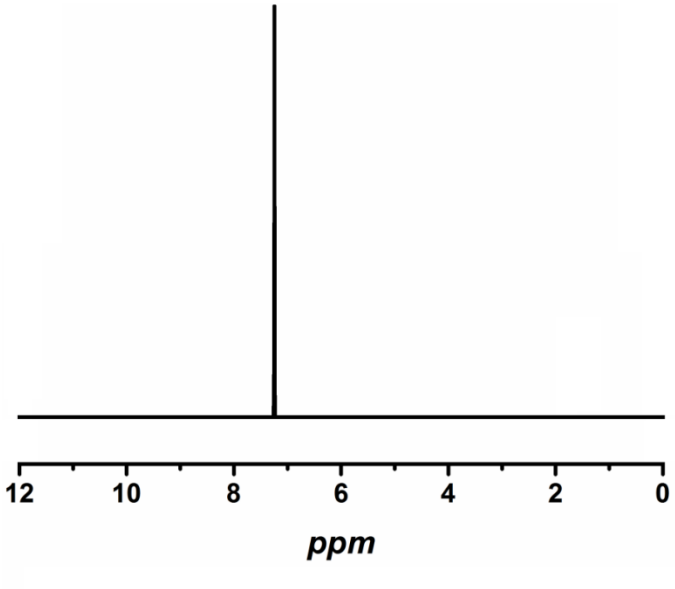

Figure A35. ^{1}H-NMR spectrum of the solvent which was yielded after mixing decene modified CM after 6 h reaction time with $CDCl_3$ for 2 hours and filtering.

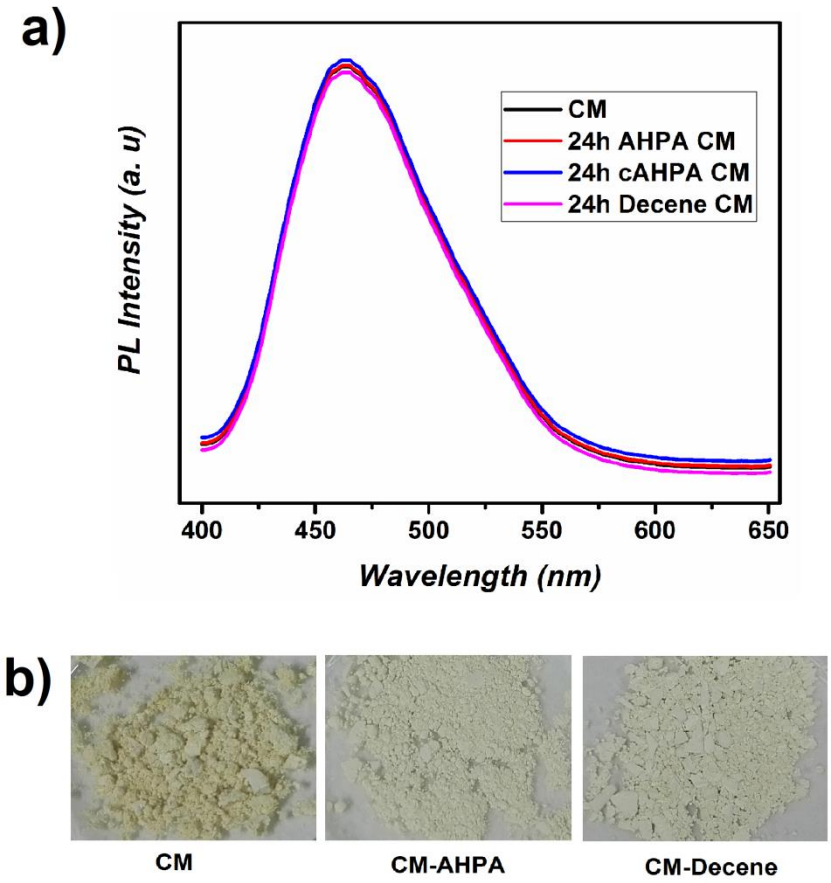

Figure A36. (a) Photoluminescence spectra of unmodified and modified CMs **(b)** Images of CM, AHPA modified CM and 1-decene modified CM.

Table A2. Properties of unmodified and AHPA modified CMs in the presence of triethanolamine (hole scavenger) and hydrogen peroxide (electron scavenger).

Sample	Time	S content (wt.%)	C/N Ratio
CM		0.712	0.6025
CM- AHPA with hole scavenger	4 h	1. 103	0.6369
CM- AHPA with electron scavenger	4 h	0. 989	0.6197
CM- AHPA with hole scavenger + electron scavenger	4 h	0. 733	0. 6043

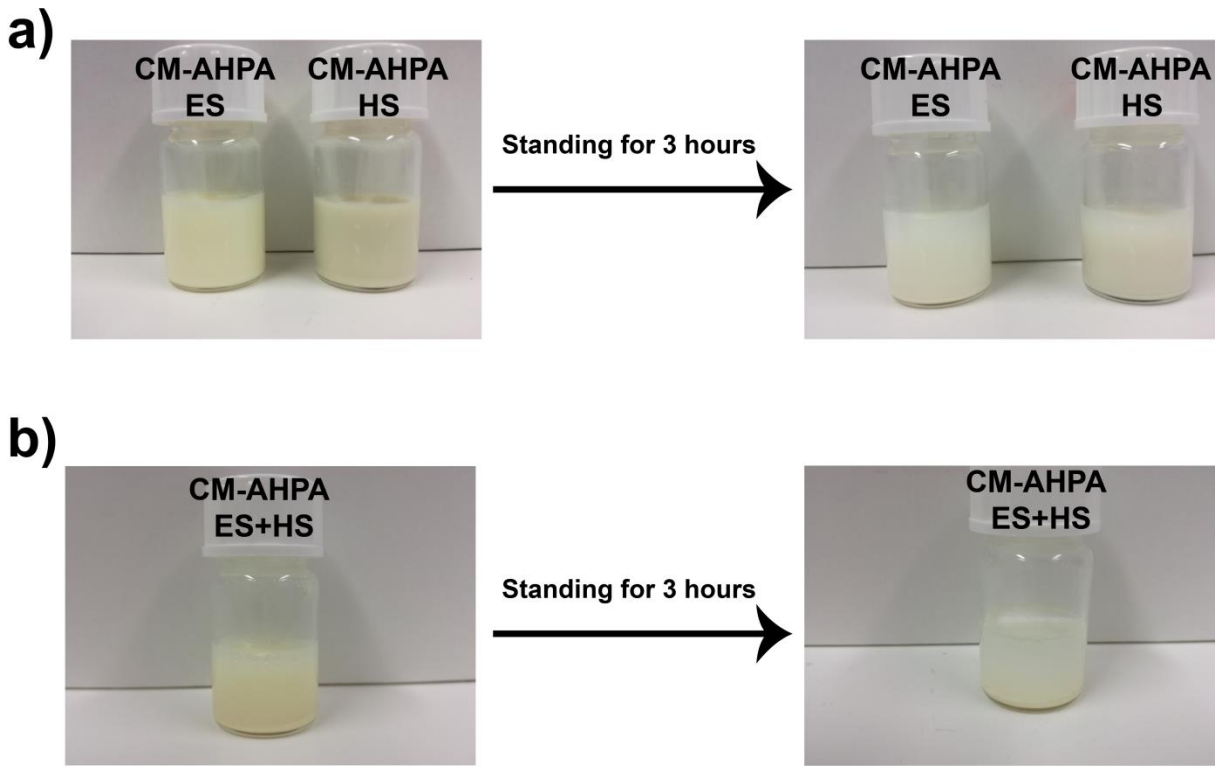

Figure A37. (a) Dispersions (1 wt.%) prepared from CM-AHPA which were synthesized in presence of electron scavenger (ES) or hole scavenger (HS) and their stability over 3 hours of standing, **(b)** Dispersion (0.5 wt.%) prepared from CM-AHPA which was synthesized in presence of both ES and HS and its sedimentation over 3 hours standing.

Table A3. Comparison of visible light and UV light induced grafting for 1-decene and fluoro modification.

Sample	Time	D_n (nm)[a]	Zeta Potential (mV)	Reaction Temperature	C/N Ratio[b]
CM		2448	-4.6		0.6025
CM-Decene[c]	12 h	1968	-7.2	50 °C	0.7372
CM-Decene[d]	6 h	2064	-6.3	R.T.	0.6644
CM-F[c]	48 h	2198	-6.4	50 °C	0.6617
CM-F[d]	6 h	2144	-6.0	R.T.	0.6376

[a] DLS measurements were performed in acetone (0.05 wt.%), [b] obtained via elemental analysis, [c] visible light induced grafting, [d] UV induced grafting.

Table A4. Properties of g-CN and g-CN-AHPA.

	Surface Zeta Potential (mV)[a]	**C:N ratio[b]**	**S content (wt. %)[b]**
g-CN	-35.5	0.6083	0.816
g-CN-AHPA	-50.8	1.0783	6.143

[a]Obtained by water dispersion of particles, [b]obtained by elemental analysis

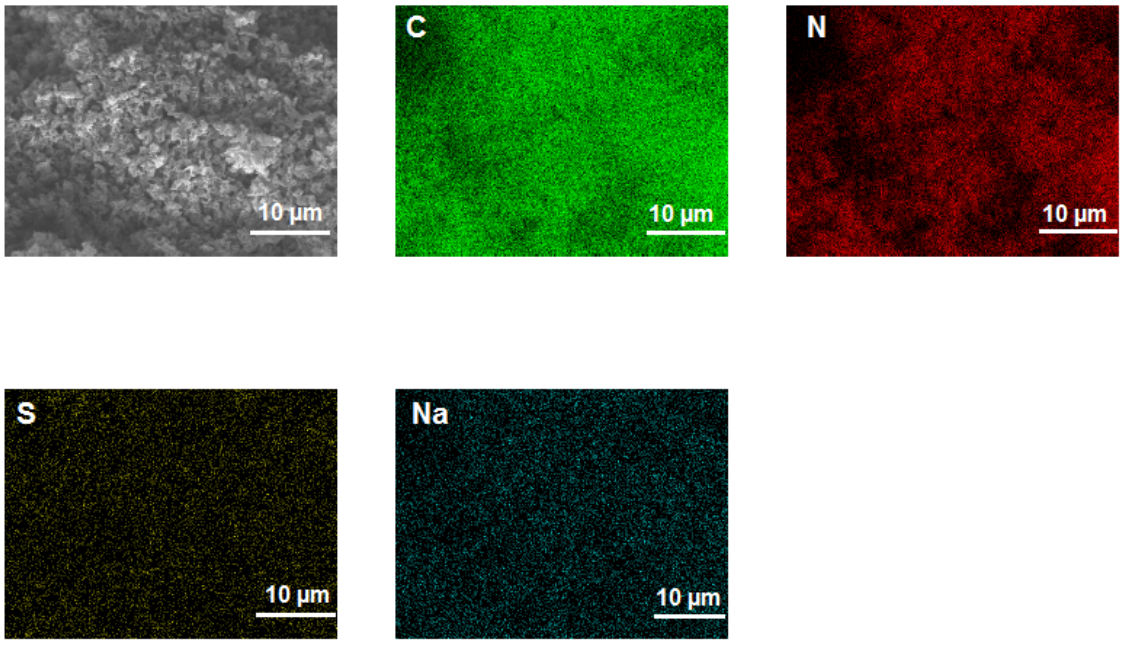

Figure A38. Elemental mapping of g-CN-AHPA via SEM.

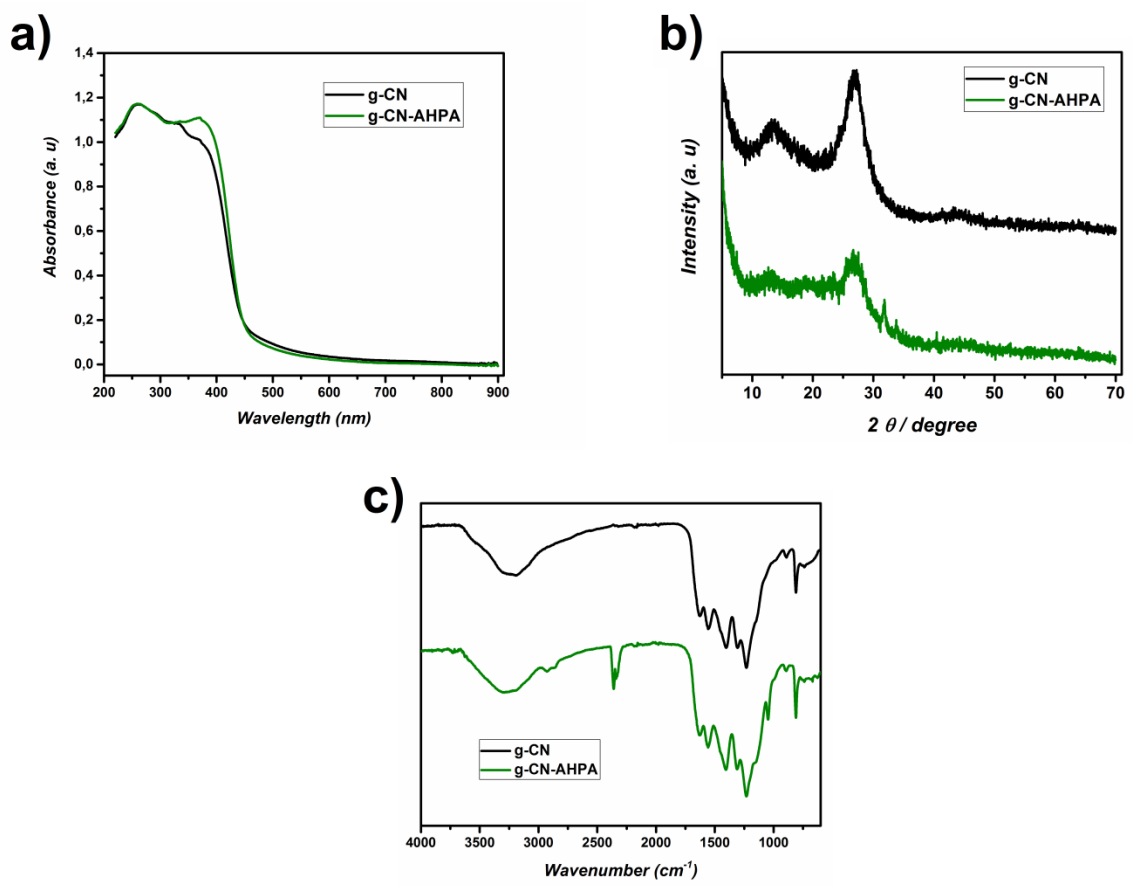

Figure A39. Solid state analysis results of g-CN and g-CN-AHPA; **(a)** UV-Vis, **(b)** XRD and **(c)** FT-IR.

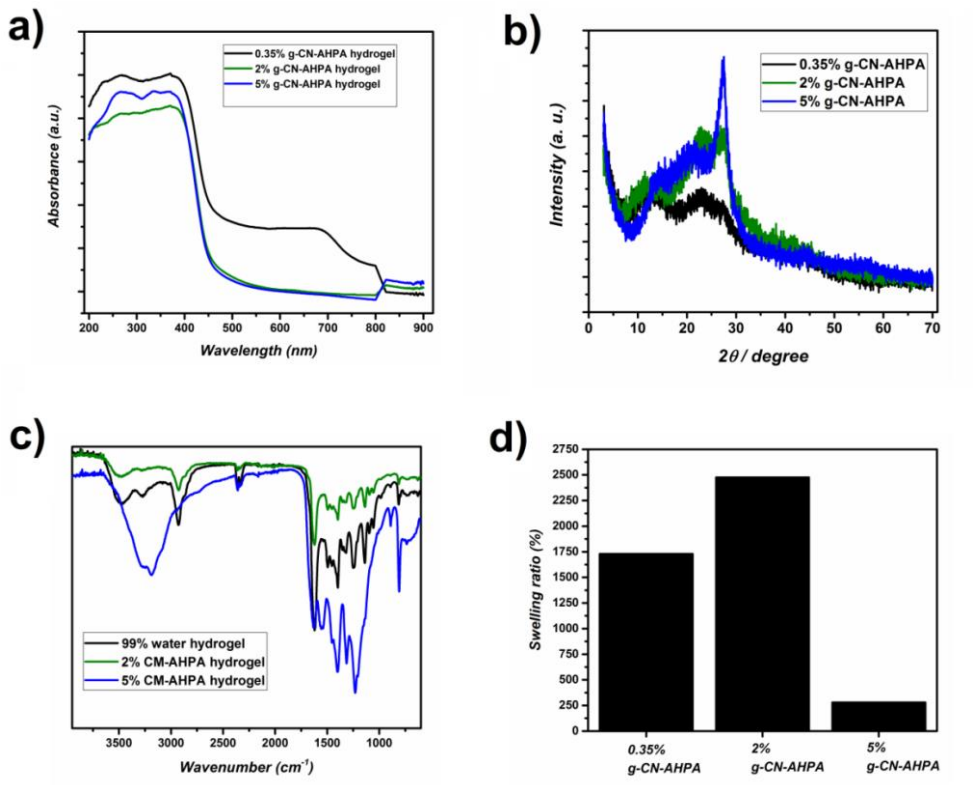

Figure A40. (a) UV-Vis spectra, **(b)** XRD profiles, **(c)** FT-IR results and **(d)** swelling ratios of g-CN-AHPA derived hydrogels.

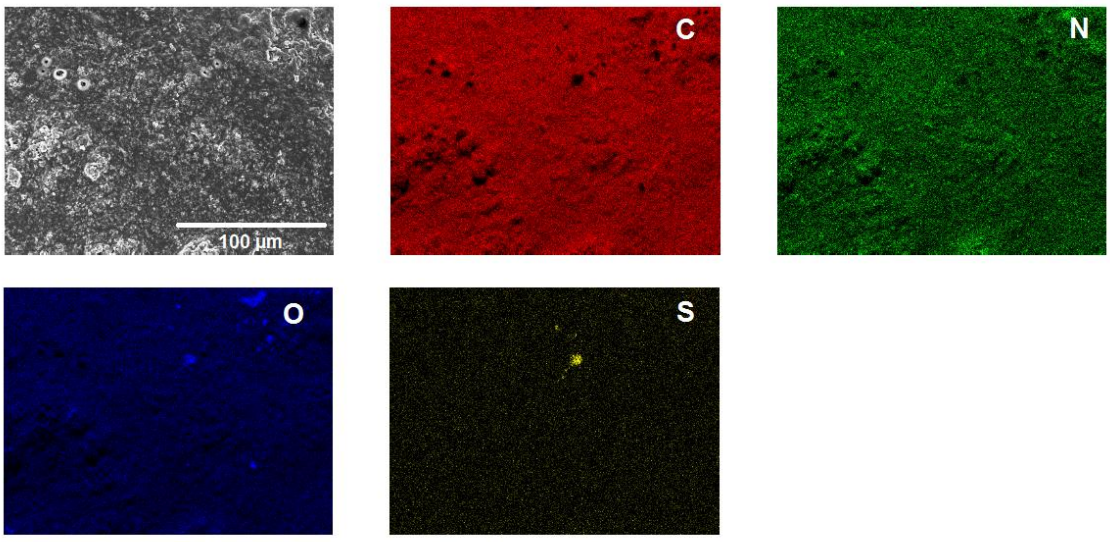

Figure A41. SEM image of freeze dried 2 wt.% g-CN-AHPA hydrogel and relative EDX mapping results.

Table A5. Elastic moduli values of hydrogels calculated right before the break or at the slope where increase starts.

g-CN-AHPA content of hydrogel (wt.%)	Strain at break (%)	Elastic moduli (MPa)	Maximum stress (MPa)
0.35	73.8	1.7	0.13
1	68.7	6.7	0.42
2	-	64.1	3.23
3.5	-	68.7	11.92
5	57.5	0.47	0.04

Figure A42. Gentle compression on 2 wt.% g-CN-AHPA hydrogel and its adhesion to finger.

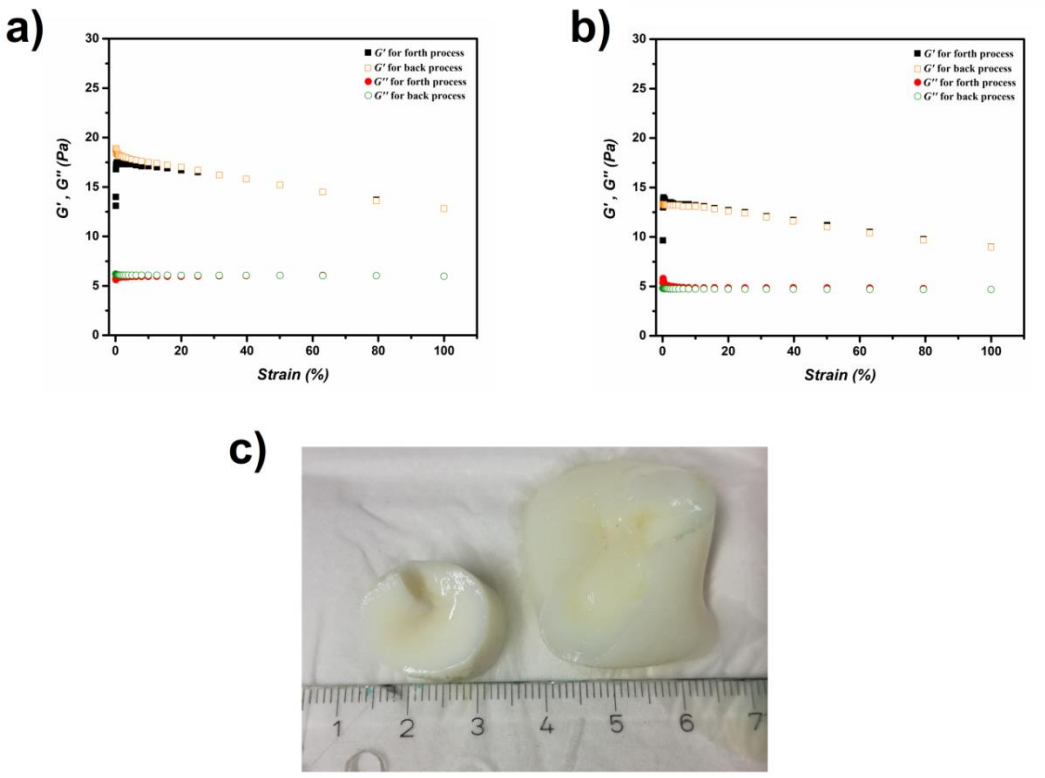

Figure A43. Rheology profiles of 2 wt.% g-CN-AHPA hydrogel swollen in **(a)** acidic and **(b)** basic media, **(c)** images of swollen hydrogels (left: swollen in acidic media; right: swollen in basic media).

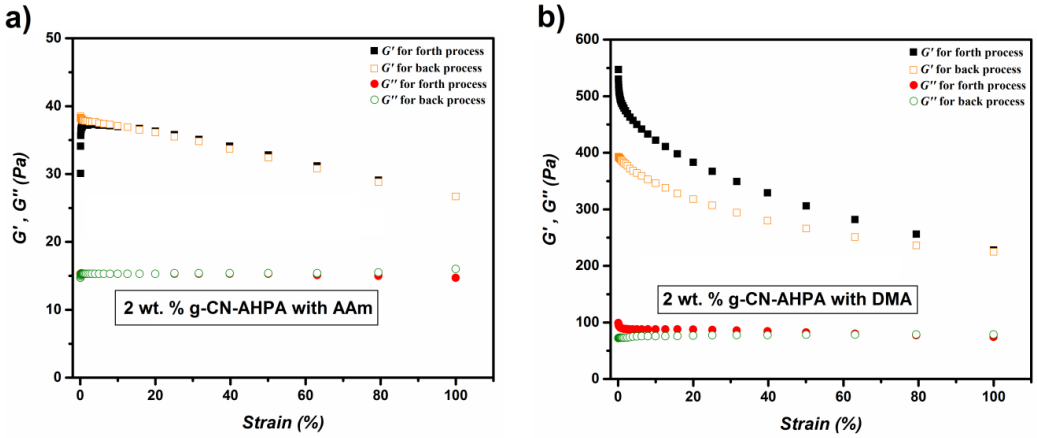

Figure A44. Comparison of storage and loss modulus values of **(a)** 2 wt.% g-CN-AHPA hydrogel synthesized from AAm, **(b)** 2 wt.% g-CN-AHPA hydrogel synthesized from DMA against strain (left, *G*' values are black and orange squares and *G*'' values are red and green circles, back (open) and forth (filled) process) and frequency (right).

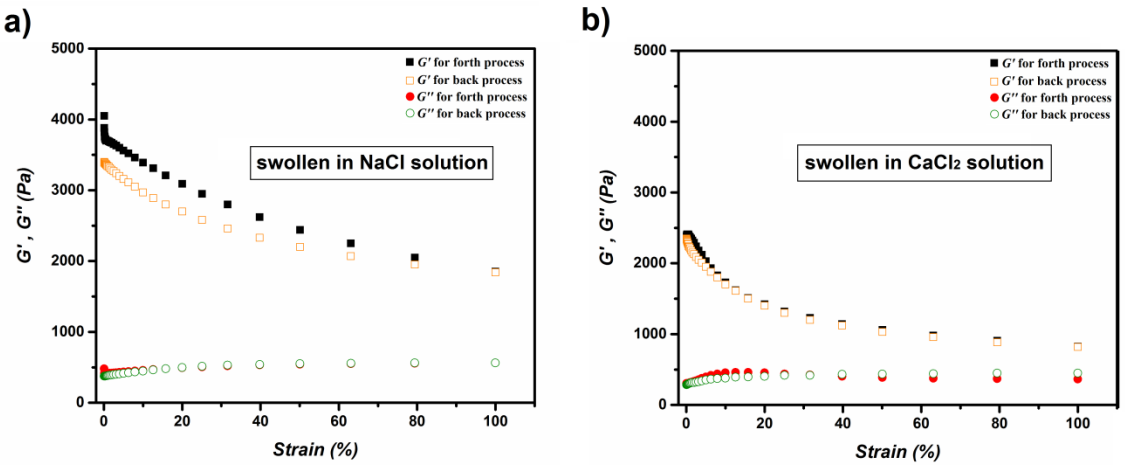

Figure A45. Comparison of storage and loss modulus values of **(a)** 2 wt.% g-CN-AHPA hydrogel swollen in NaCl solution (0.2 M) and **(b)** 2 wt. % g-CN-AHPA hydrogel swollen in $CaCl_2$ (0.2 M) solution against strain (left, *G*' values are black and orange squares and *G*'' values are red and green circles, back (open) and forth (filled) process) and frequency (right).

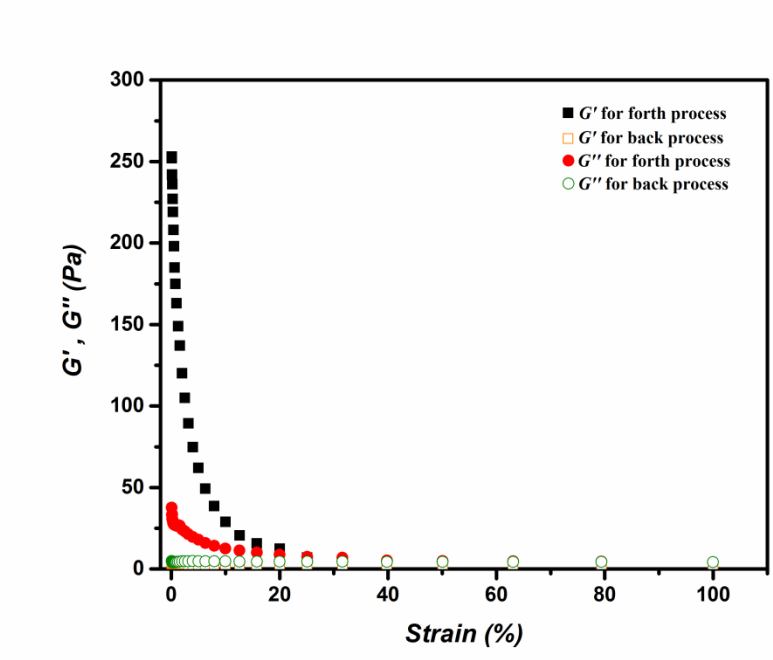

Figure A46. Rheology result of g-CN pre1h, storage (*G'*, black and orange squares) and loss modulus (*G''*, red and green circles) against strain, back (open) and forth (filled) process.

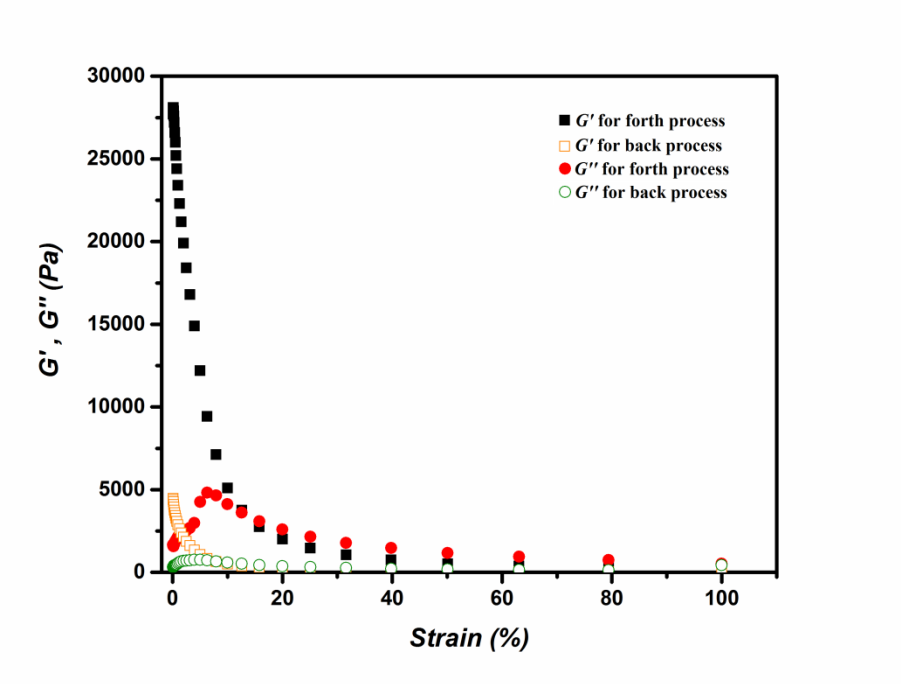

Figure A47. Rheology result of g-CN pre6h, storage (*G'*, black and orange squares) and loss modulus (*G''*, red and green circles) against strain, back (open) and forth (filled) process.

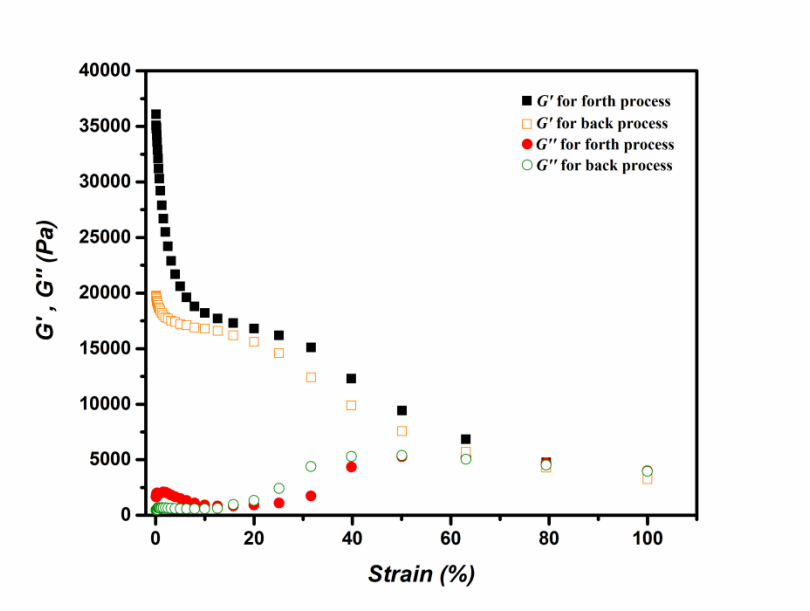

Figure A48. Rheology result of g-CN pre12h, storage (*G'*, black and orange squares) and loss modulus (*G''*, red and green circles) against strain, back (open) and forth (filled) process.

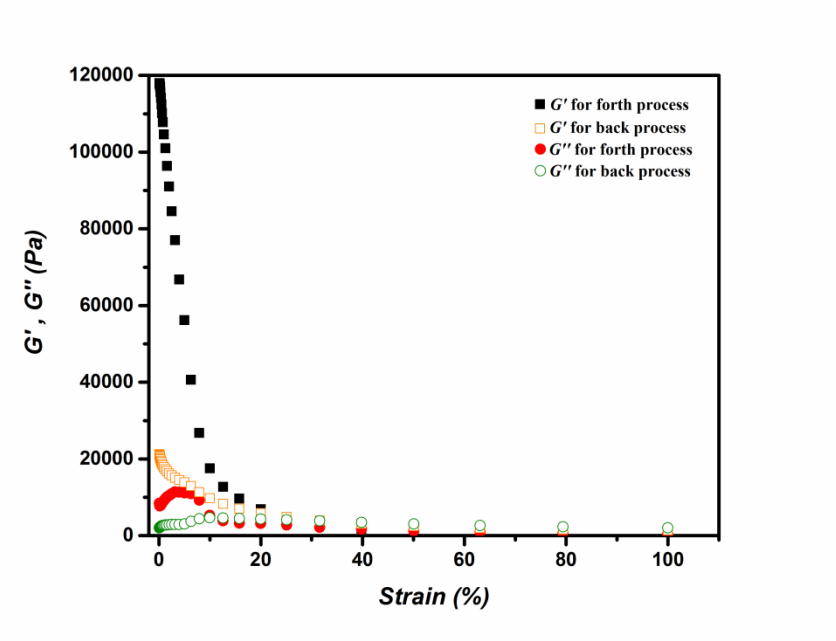

Figure A49. Rheology result of g-CN 2pre3h, storage (*G'*, black and orange squares) and loss modulus (*G''*, red and green circles) against strain, back (open) and forth (filled) process.

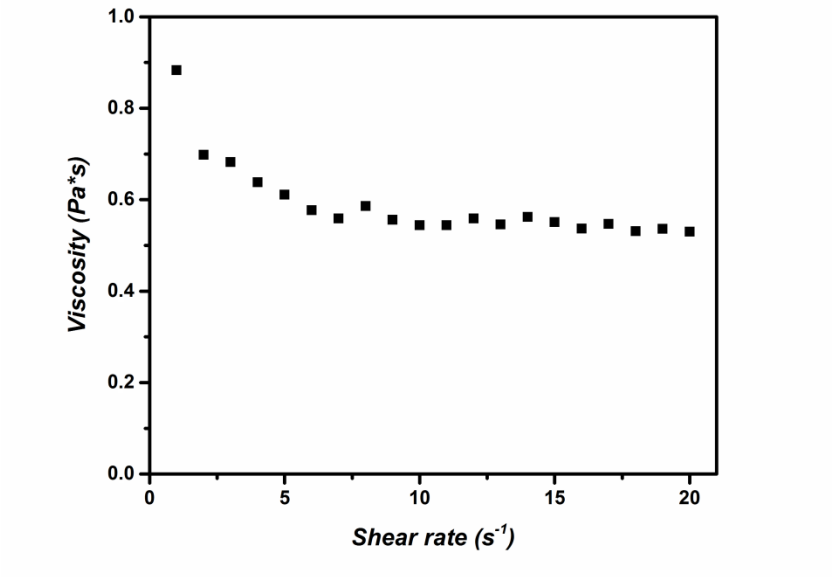

Figure A50. Viscosity profile of g-CN pre1h against shear rate between 1-20 s^{-1}.

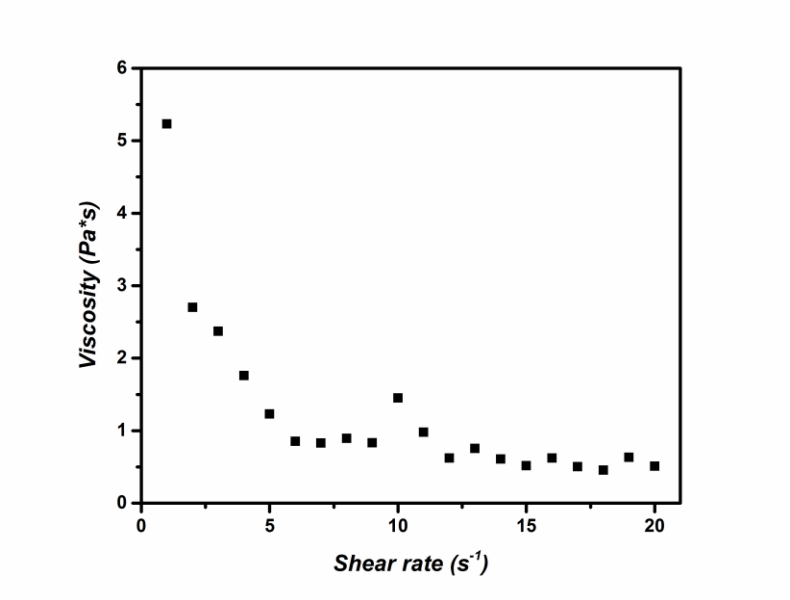

Figure A51. Viscosity profile of g-CN pre3h against shear rate between 1-20 s^{-1}.

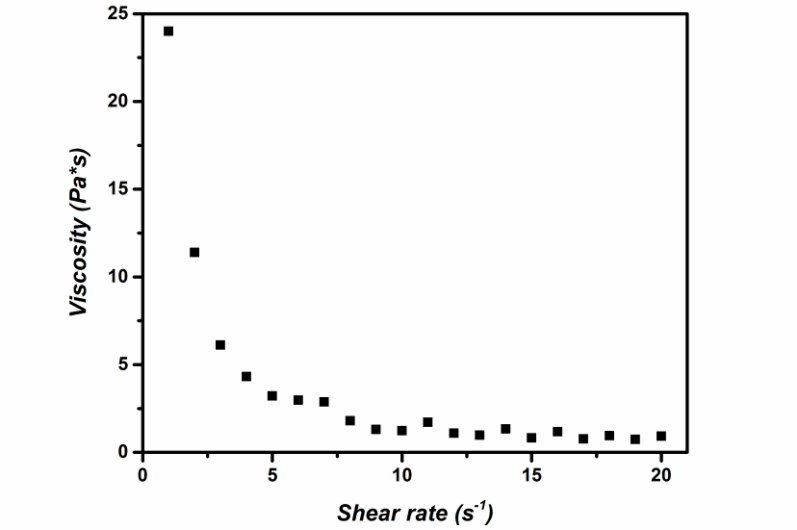

Figure A52. Viscosity profile of g-CN pre6h against shear rate between 1-20 s^{-1}.

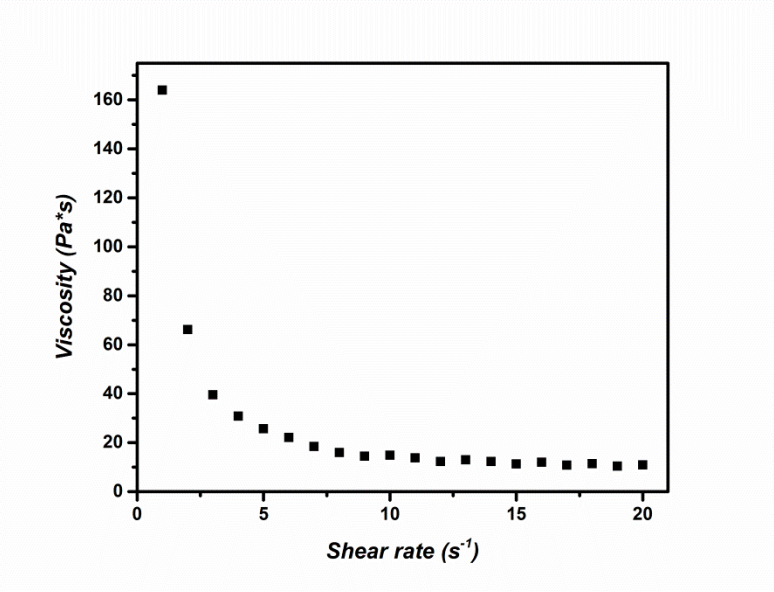

Figure A53. Viscosity profile of g-CN pre12h against shear rate between 1-20 s^{-1}.

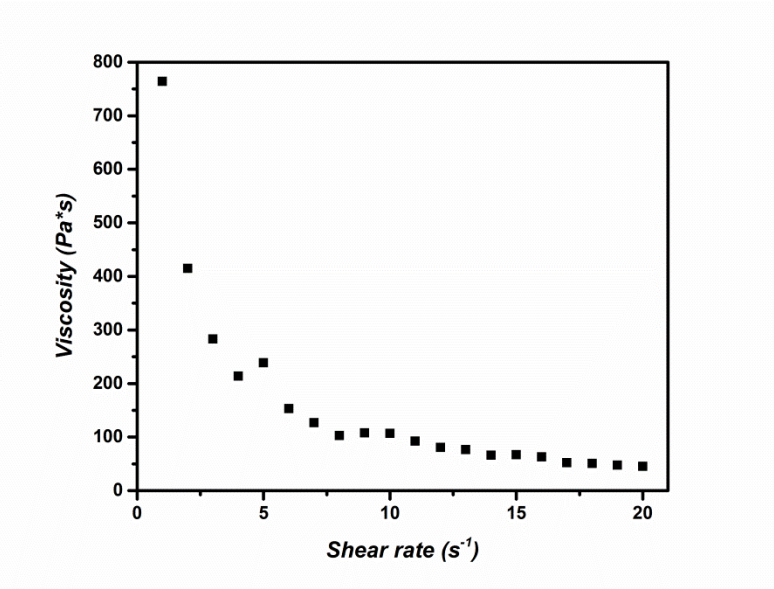

Figure A54. Viscosity profile of g-CN 2pre3h against shear rate between 1-20 s^{-1}.

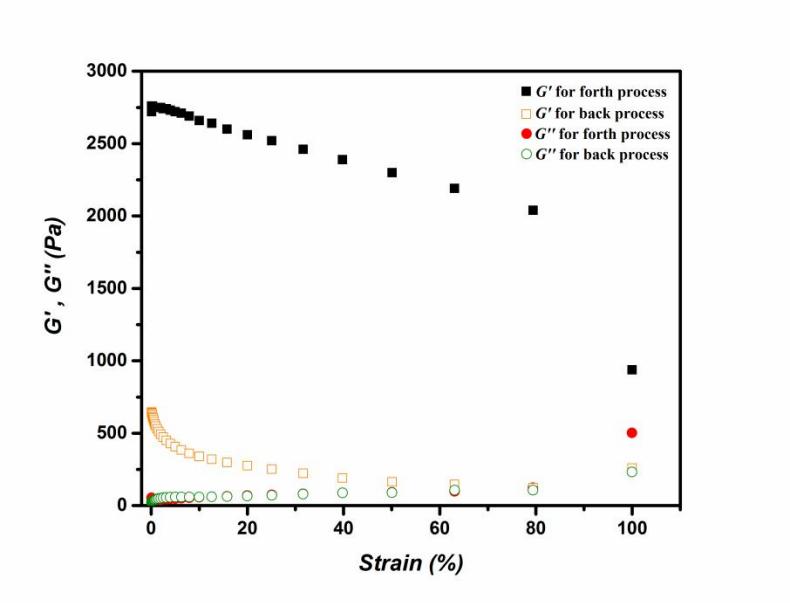

Figure A55. Rheology result of g-CN pre3h:water in 1:0.25 ratio, storage (*G'*, black and orange squares) and loss modulus (*G''*, red and green circles) against strain, back (open) and forth (filled) process.

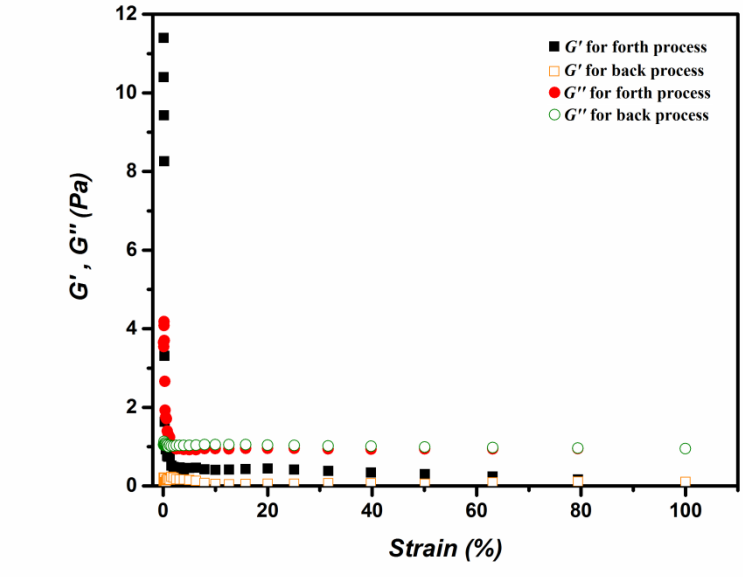

Figure A56. Rheology result of g-CN pre3h:water in 1:0.5 ratio, storage (*G'*, black and orange squares) and loss modulus (*G''*, red and green circles) against strain, back (open) and forth (filled) process.

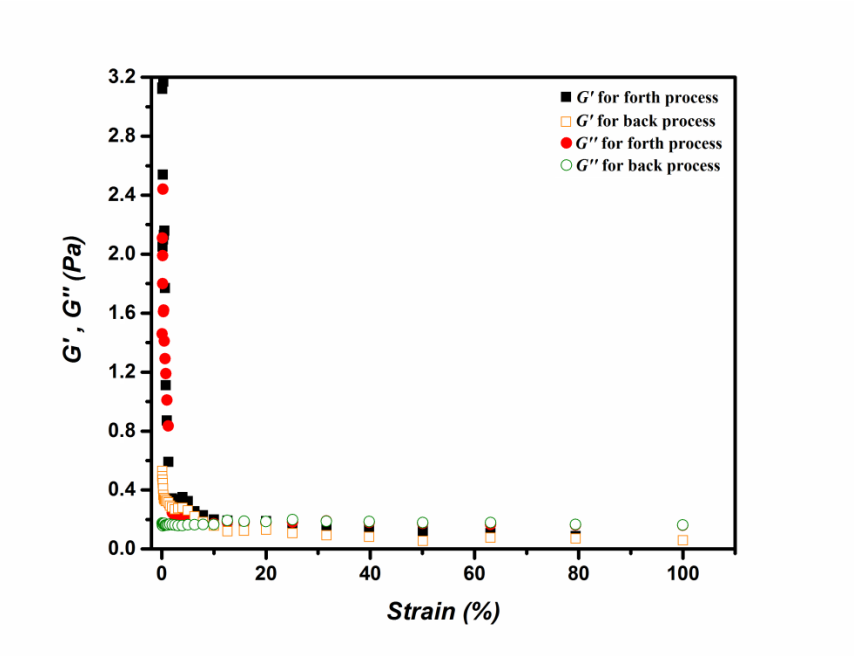

Figure A57. Rheology result of g-CN pre3h:water in 1:0.75 ratio, storage (*G'*, black and orange squares) and loss modulus (*G''*, red and green circles) against strain, back (open) and forth (filled) process.

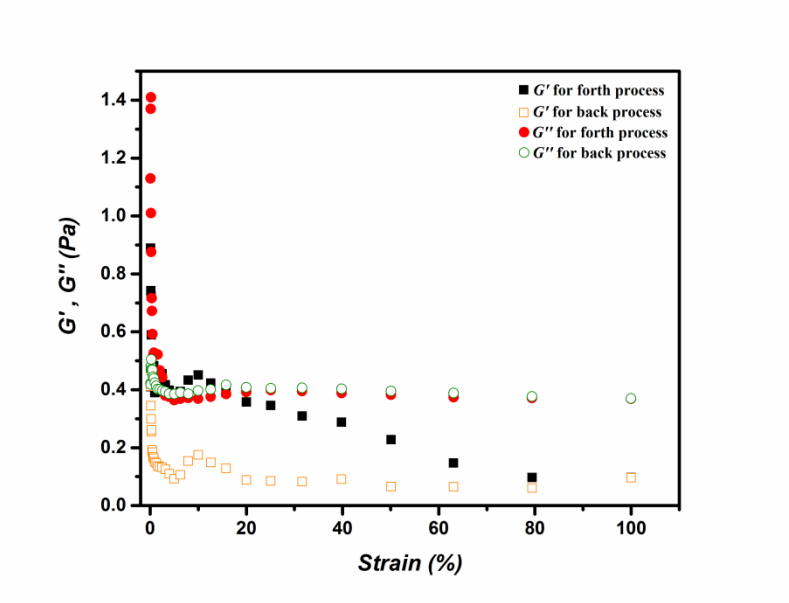

Figure A58. Rheology result of g-CN pre3h:water in 1:1 ratio, storage (*G'*, black and orange squares) and loss modulus (*G''*, red and green circles) against strain, back (open) and forth (filled) process.

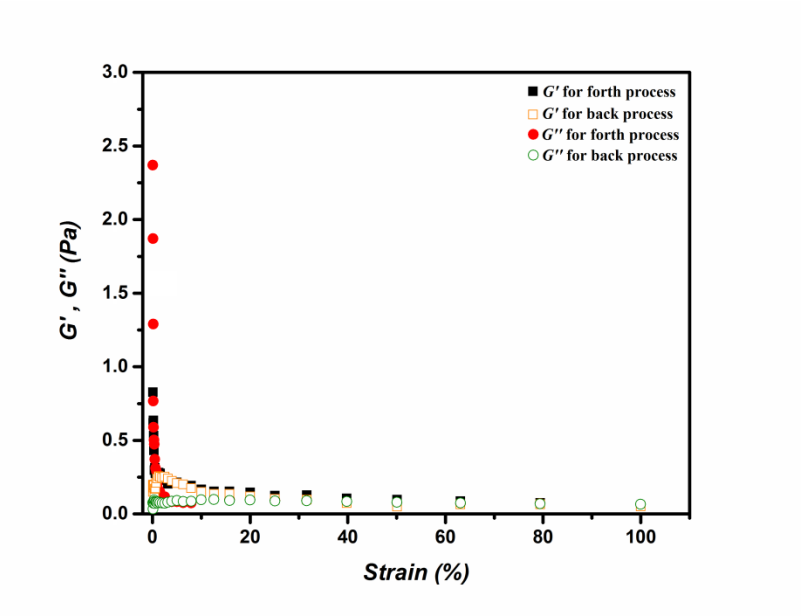

Figure A59. Rheology result of g-CN pre3h:water in 1:1.5 ratio, storage (*G'*, black and orange squares) and loss modulus (*G''*, red and green circles) against strain, back (open) and forth (filled) process.

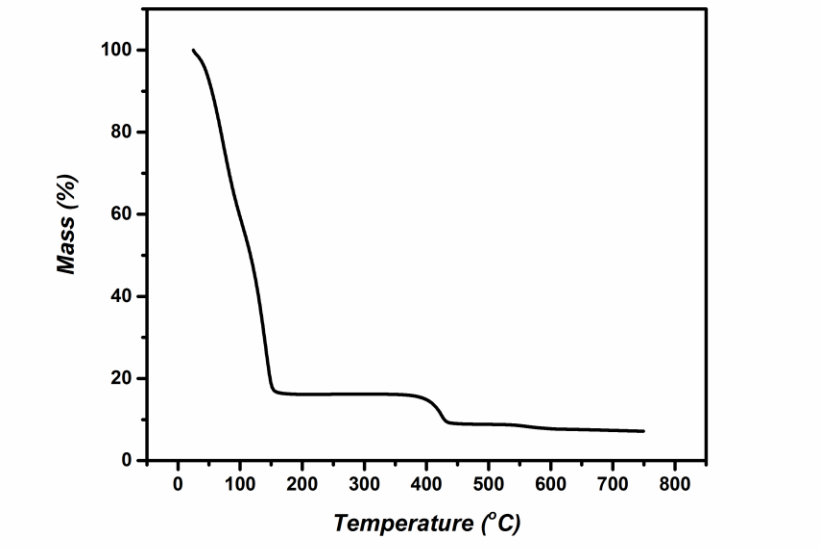

Figure A60. TGA diagram of g-CN pre3h.

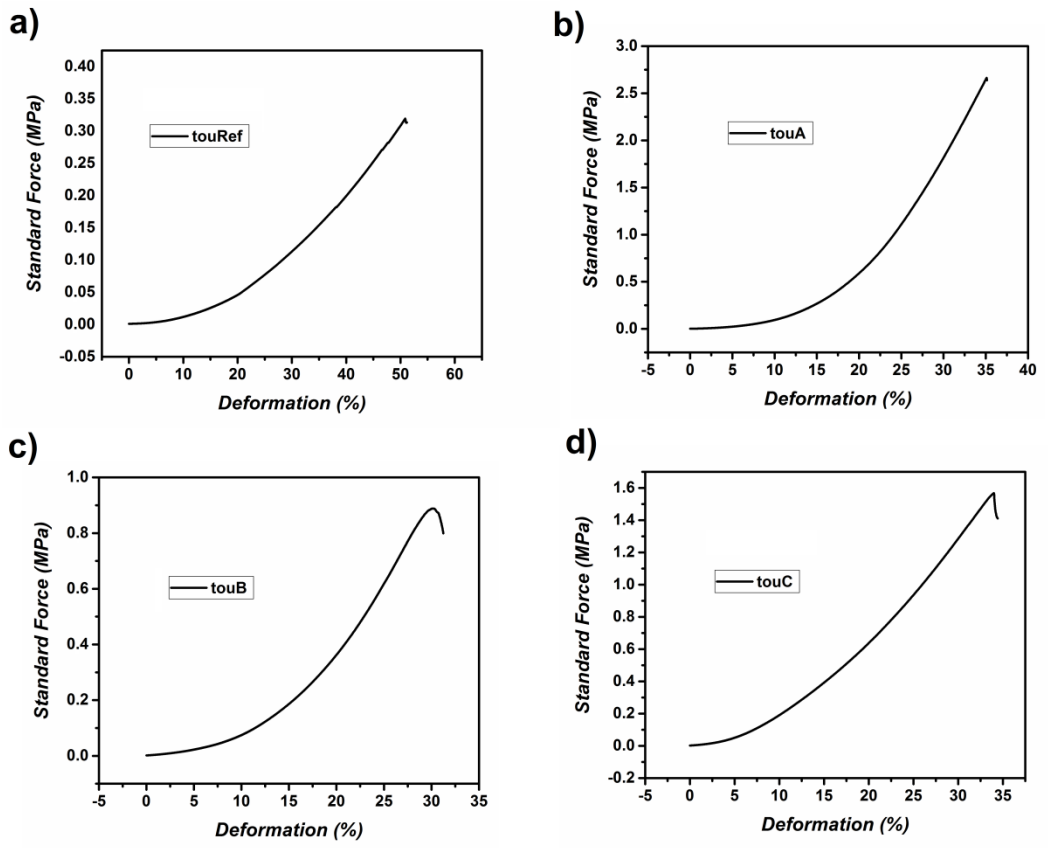

Figure A61. Compression test results of **(a)** touRef, **(b)** touA, **(c)** touB and **(d)** touC organohydrogels.

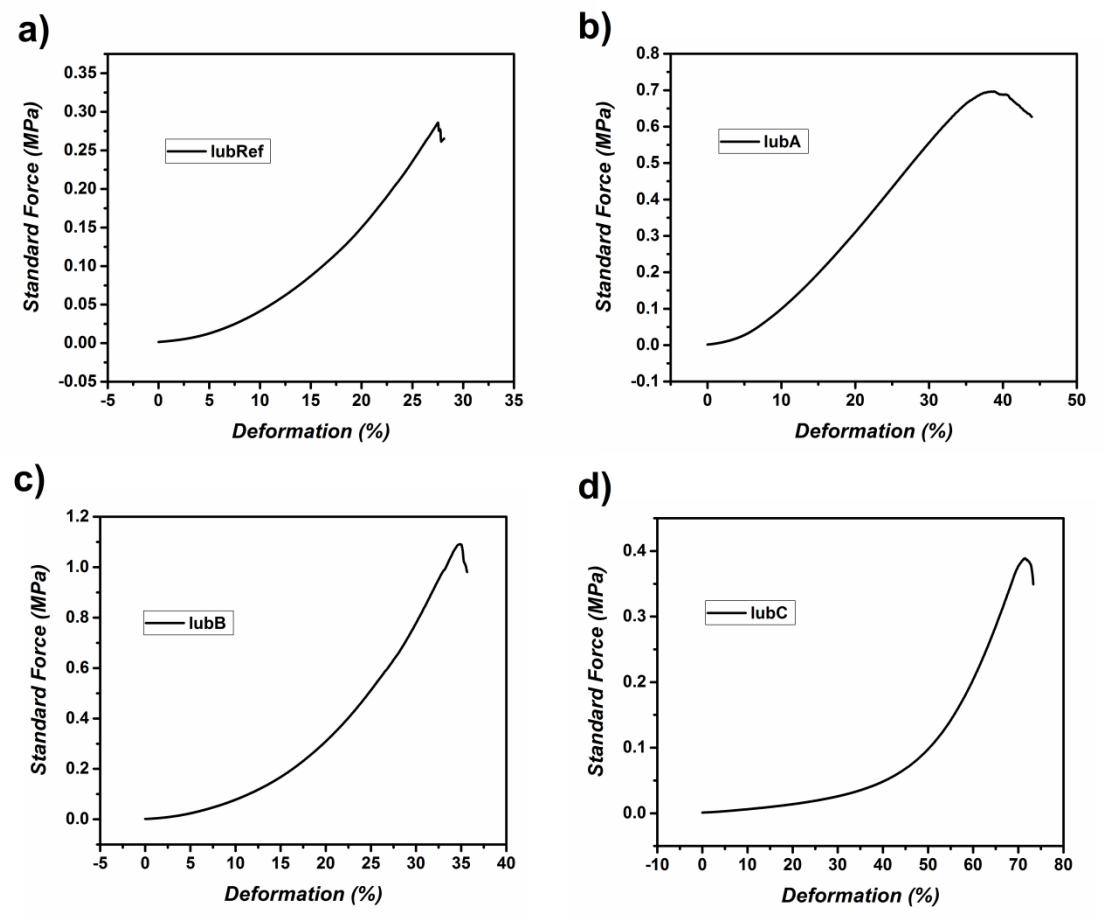

Figure A62. Compression test results of **(a)** lubRef, **(b)** lubA, **(c)** lubB and **(d)** lubC organohydrogels.

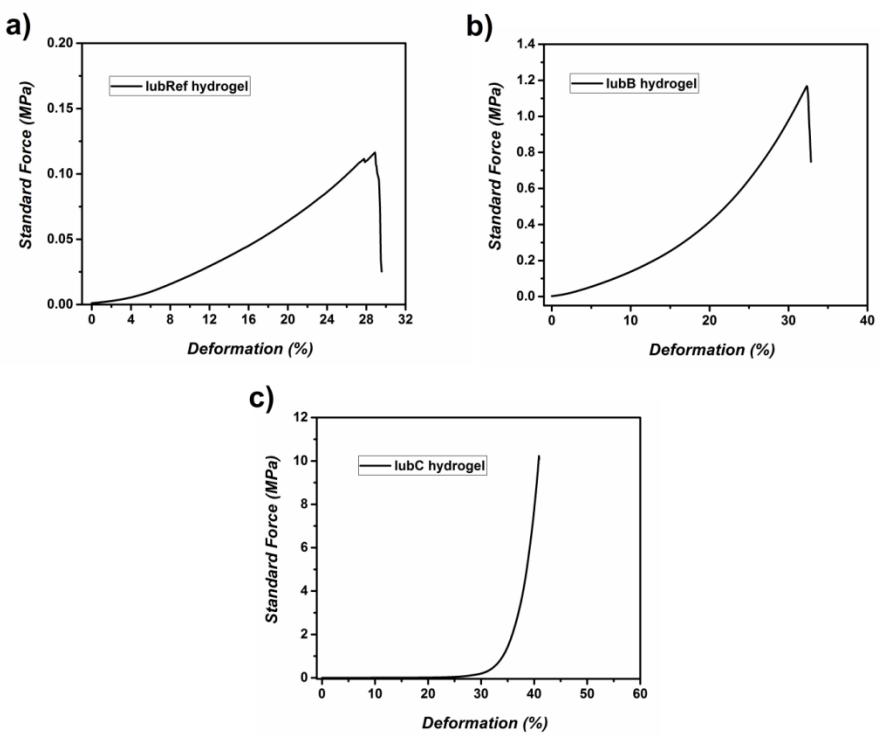

Figure A63. Compression test results of **(a)** lubRef, **(b)** lubB and **(c)** lubC hydrogels.

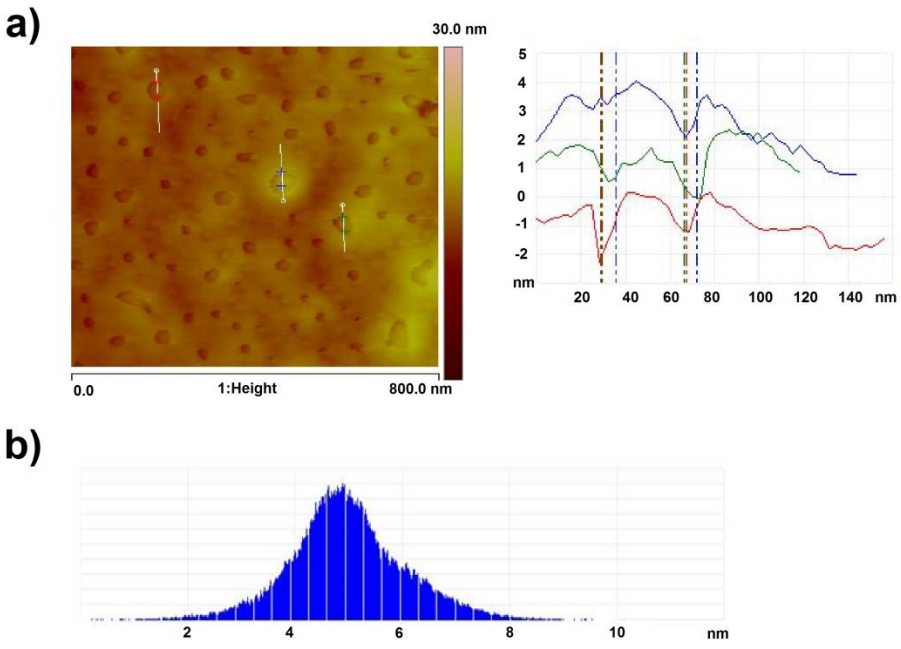

Figure A64. (a) AFM profile and particle thickness of 2 times spray coated CMp-vTA on glass substrate and **(b)** average thickness distribution of particles through AFM.

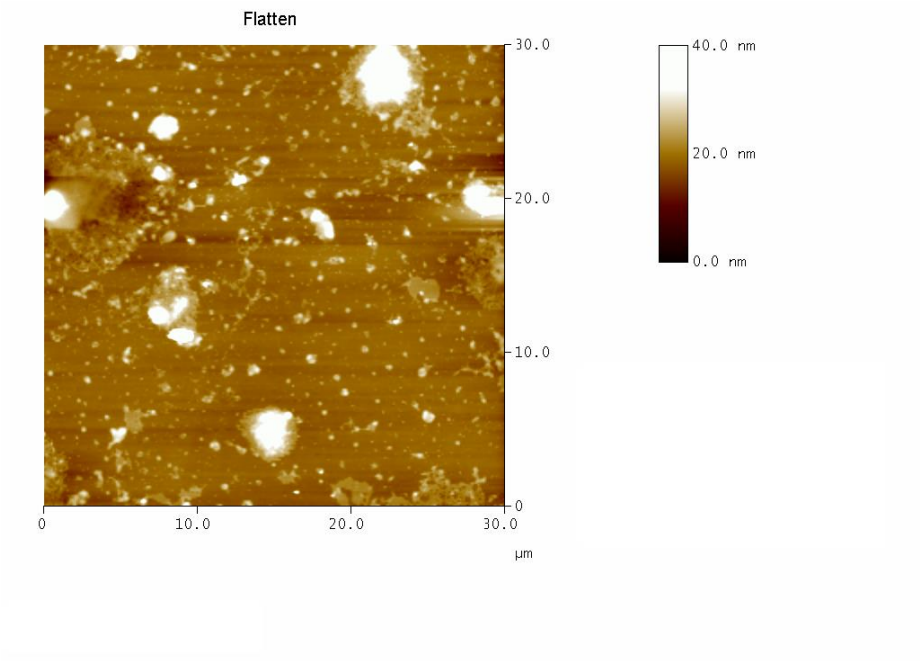

Figure A65. AFM profile of CMp-vTA sprayed from bad solvent (water) dispersion.

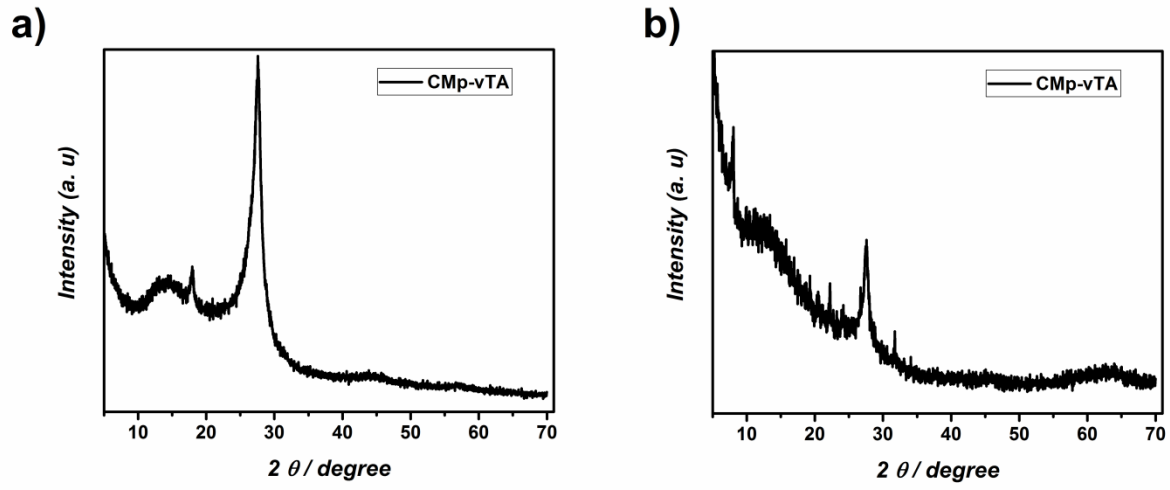

Figure A66. (a) XRD of CMp-vTA casted from bad solvent (THF), **(b)** XRD of CMp-vTA casted from mixing good solvent (DMF) dispersion with bad solvent (THF).

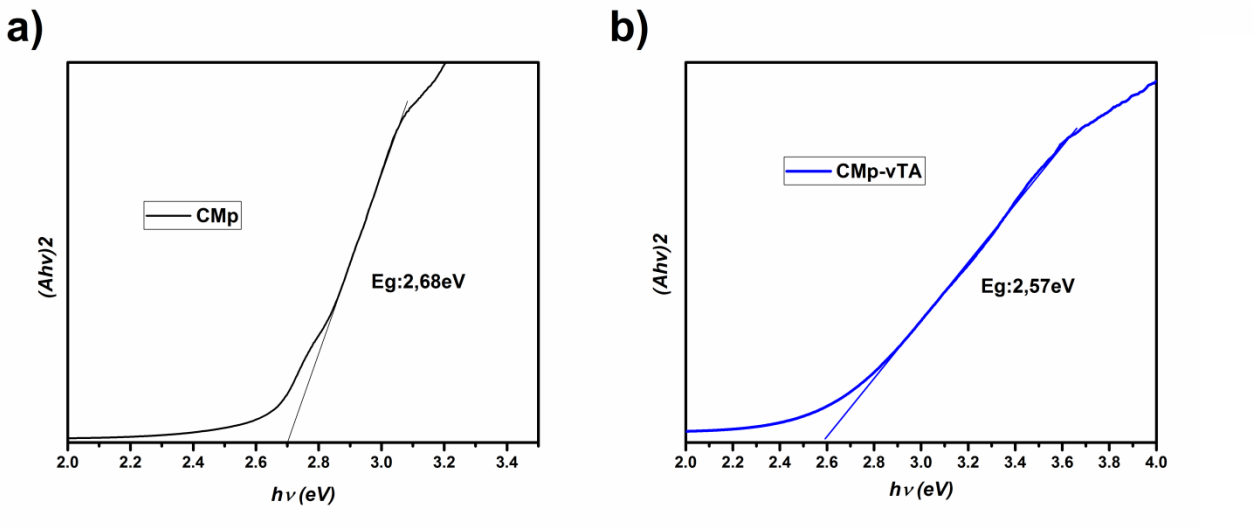

Figure A67. Tauc plots of **(a)** CMp and **(b)** CMp-vTA.

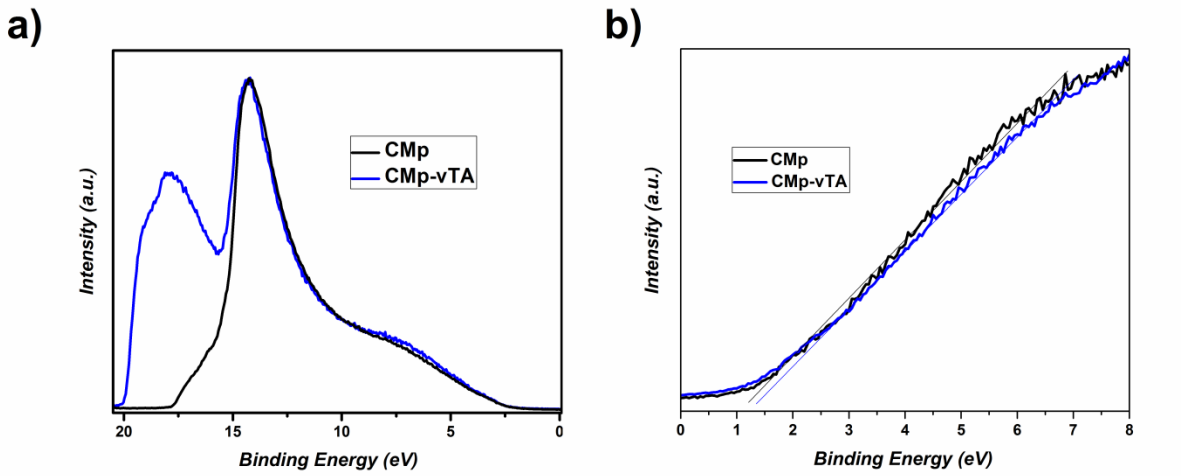

Figure A68. UPS plot of CMp and CMp-vTA over **(a)** long range (with HBEC area) and **(b)** short range.

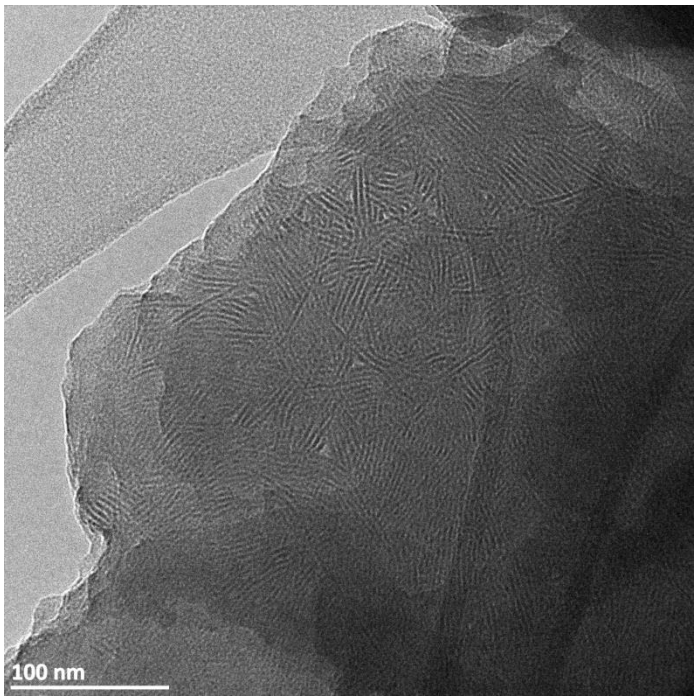

Figure A69. HR TEM image of CMp-vTA casted from bad solvent (THF).

11.5. Abbreviations

AAm	Acrylamide
AIBN	2,2′-Azobis(2-methylpropionitrile)
AHPA	3-Allyloxy-2-hydroxy-1-propanesulfonic acid sodium salt solution
ATRP	Atom transfer radical polymerization
BA	Butyl acrylate
CB	Conduction band
CM	Carbon nitride from Cyanuric acid - melamine complex
CMB	Carbon nitride from Cyanuric acid - melamine-barbituric acid complex
CMB-vTA	Vinylthiazole modified carbon nitride (from cyanuric acid - melamine-barbituric acid complex)
CMp	Carbon nitride from Cyanuric acid - 2,4-diamino-6-phenyl-1,3,5 triazine complex
CMp-vTA	Vinylthiazole modified carbon nitride (from cyanuric acid - 2,4- diamino-6-phenyl-1,3,5 triazine complex)
CN	Carbon Nitride
DCM	Dichloromethane
DMA	*N*,*N*-Dimethylacrylamide
DMF	*N*,*N* dimethylformamide
DMSO	Dimethyl sulfoxide
DN	Double network
EDL	Electric double layer
EG	Ethylene glycol
g-CN	Graphitic Carbon Nitride
GelMA	Gelatin methacrylate
GpO	Graphene peroxide
HEMA	2-hydroxyethyl methacrylate
IL	Ionic liquid
IPA	Isopropyl alcohol
IPN	Interpenetrating network
K-PHI	Potassim polyheptazine imide
KPS	Potassium persulfate
LCST	Lower critical solution temperature
LED	Light emitting diode
MA	Methyl acrylate
MBA	*N*,*N'*-methylenebis(acrylamide)
MMA	Methyl methacrylate
MO	Methyl orange
NIPAM	*N*-isopropyl acrylamide
OD_{600}	Optical density at 600 nm
PAMPS	Poly(2-acrylamido-2-methyl-1-propane sulfonic acid)
PDMAEMA	Poly(2-(dimethylamino)ethyl methacrylate)
PEG	Poly(ethyleneglycol)
PEGDMA	Poly(ethylene glycol) dimethacrylate 750

PEGMEMA	Poly(ethylene glycol) methyl ether methacrylate 300
PEO	Poly(ethylene oxide)
PET	Photoinduced electron/energy transfer
PS	Polystyrene
PP	Polypropylene
PPO	Poly(propylene oxide)
QD	Quantum dot
RAFT	Reversible addition-fragmentation transfer
RhB	Rhodamine B
SPMA	3-Sulfopropyl methacrylate potassium salt
TEOA	Triethanolamine
THF	Tetrahydrofuran
u-CN	Carbon nitride from urea
UV	Ultraviolet
VB	Valence band
vTA	4-methyl 5-vinyl thiazole

11.6. Publication List

1. Polymer Grafted Graphitic Carbon Nitride as Precursors for Reinforced Lubricant Hydrogels

   Baris Kumru, Valerio Molinari, Markus Hilgart, Florian Rummel, Michael Schaeffler, Bernhard VKJ Schmidt, **submitted**

2. Robust Carbon Nitride-Based Thermoset Coatings for Surface Modification and Photochemistry

   Baris Kumru, Jesus Barrio, Jianrui Zhang, Markus Antonietti, Menny Shalom, Bernhard VKJ Schmidt, **ACS Applied Materials&Interfaces**, 2019, 11(9), 9462-9469

3. Electrostatic Stabilization of Carbon Nitride Colloids in Organic Solvents Enables Ultrastable Dispersions and Transparent Homogeneous CN-Films for Optoelectronics

   Baris Kumru, Daniel Cruz, Tobias Heil, Bernhard V. K. J. Schmidt, Markus Antonietti, **Journal of American Chemical Society**, 2018, 140(50), 17532-17537

4. Extremely Compressible Hydrogel via Modified Graphitic Carbon Nitride Incorporation

   Baris Kumru, Valerio Molinari, Reinhild Dünnebacke, Kerstin G. Blank, Bernhard VKJ Schmidt, **Macromolecular Rapid Communications**, 2019, 40(4), 1800712

5. Thermoadaptive Supramolecular α-Cyclodextrin Crystallization-Based Hydrogels via Double Hydrophilic Block Copolymer Templating

   Tingting Li, Baris Kumru, Noah Al Nakeeb, Jochen Willersinn, Bernhard VKJ Schmidt, **Polymers**, **2018**, 10(6), 576

6. Tough high modulus hydrogels derived from carbon-nitride via an ethylene glycol co-solvent route

Baris Kumru, Valerio Molinari, Menny Shalom, Markus Antonietti, Bernhard VKJ Schmidt, **Soft Matter**, **2018**, 14, 2655-2664

7. Carbon nitride creates thioamides in high yields by the photocatalytic Kindler reaction

Bogdan Kurpil, Baris Kumru, Tobias Heil, Markus Antonietti, Aleksandr Savateev, **Green Chemistry**, **2018**, 20, 838-842

8. Enhanced Dispersibility of Graphitic Carbon Nitride Particles in Aqueous and Organic Media via a One-Pot Grafting Approach

Baris Kumru, Markus Antonietti, Bernhard VKJ Schmidt, **Langmuir**, **2017**, 33(38), 9897-9906

9. Reinforced Hydrogels via Carbon Nitride Initiated Polymerization

Baris Kumru, Menny Shalom, Markus Antonietti, Bernhard VKJ Schmidt, **Macromolecules**, **2017**, 50(5), 1862-1869

10. Polymerization of Aniline by Catalytic Air Oxidation in Microemulsion (Invited paper)

Baris Kumru, Niyazi Bicak, **Macromolecular Symposia**, **2015**, 352, 42–45

11. Synthesis of soluble poly(vinylene carbonate) by redox-initiated RAFT process in microemulsion and its aminolysis yielding snow-white polymethylol

Baris Kumru, Niyazi Bicak, **RSC Advances**, **2015**, 5, 30936

12. Regio-selective peroxybromination of poly (vinyl methyl ketone) as versatile tool for generation active ATRP initiation sites on solid surfaces)

Baris Kumru, Baris Gure, Niyazi Bicak, **Journal of Polymer Science: Part A Polymer Chemistry**, **2013**, 51(18), 3892-3900

11.7. Declaration

Die vorliegende Dissertation entstand im Zeitraum zwischen August 2016 und Oktober 2018 unter der Betreuung von Prof. Dr. Dr. h.c. Markus Antonietti am Max Planck Institut für Kolloid und Grenzflächenforschung.

Hiermit erkläre ich, dass die vorliegende Arbeit selbständig angefertigt wurde und nur keine anderen als die angegebenen Hilfsmittel und Quellen verwendet wurden.

The present work was carried out and written during August 2016 and October 2018 at the Max Planck Institute of Colloids and Interfaces under the supervision of Prof. Dr. Dr. h.c. Markus Antonietti.

I declare that I have produced all the work using only literature and other aids as described here.

BARIS KUMRU,

POTSDAM, OCTOBER 2018

12. References

1. Gong, Y.; Wang, J.; Wei, Z.; Zhang, P.; Li, H.; Wang, Y., Combination of Carbon Nitride and Carbon Nanotubes: Synergistic Catalysts for Energy Conversion. *ChemSusChem* **2014,** *7*, 2303-2309.
2. Teeter, E., *Religion and Ritual in Ancient Egypt*. Cambridge University Press: New York, 2011; p 219.
3. Black, J.; Green, A., *Gods, Demons and Symbols of Ancient Mesopotamia: An Illustrated Dictionary*. The British Museum Press: 1992; p 192.
4. Cosmos: A Spacetime Odyssey. In *Cosmos*, 20th Television: United States, 2014; p 44 minutes.
5. Fujishima, A.; Honda, K., Electrochemical Photolysis of Water at a Semiconductor Electrode *Nature* **1972,** *238*, 37-38.
6. Ong, W.-J.; Tan, L.-L.; Ng, Y. H.; Yong, S.-T.; Chai, S.-P., Graphitic carbon nitride (g-C3N4)-based photocatalysts for artificial photosynthesis and environmental remediation: are we a step closer to achieving sustainability? . *Chem. Rev.* **2016,** *116* (12), 7159-7329.
7. Liebig, J., *Ann. Pharm.* **1834,** *10* (10).
8. Zhou, Z.; Wang, J.; Yu, J.; Shen, Y.; Li, Y.; Liu, A.; Liu, S.; Zhang, Y., Dissolution and liquid crystals phase of 2D polymeric carbon nitride. *J. Am. Chem. Soc.* **2015,** *137*, 2179-2182.
9. Wang, X.; Maeda, K.; Thomas, A.; Takanabe, K.; Xin, G.; Carlsson, J. M.; Domen, K.; Antonietti, M., A metal-free polymeric photocatalyst for hydrogen production from water under visible light. *Nat. Mater.* **2009,** *8* (1), 76-80.
10. Gillan, E. G., Synthesis of Nitrogen-Rich Carbon Nitride Networks from an Energetic Molecular Azide Precursor. *Chem. Mater.* **2000,** *12*, 3906-3912.
11. Lotsch, B. V.; Doblinger, M.; Sehnert, J.; Seyfarth, L.; Senker, J.; Oeckler, O.; Schnick, W., Unmasking Melon by a Complementary Approach Employing Electron Diffraction, Solid-State NMR Spectroscopy, and Theoretical Calculations—Structural Characterization of a Carbon Nitride Polymer. *Chem. Eur. J.* **2007,** *13*, 4969-4980.
12. Algara-Siller, G.; Severin, N.; Chong, S. Y.; Bjorkman, T.; Palgrave, R. G.; Laybourn, A.; Antonietti, M.; Khimyak, Y. Z.; Krasheninnikov, A. V.; Rabe, J. P.; Kaiser, U.; Cooper, A. I.; Thomas, A.; Bojdys, M. J., Triazine-based graphitic carbon nitride: a two-dimensional semiconductor. *Angew. Chem., Int. Ed.* **2014,** *53* (29), 7450-5.
13. Shalom, M.; Guttentag, M.; Fettkenhauer, C.; Inal, S.; Neher, D.; Llobet, A.; Antonietti, M., In Situ Formation of Heterojunctions in Modified Graphitic Carbon Nitride: Synthesis and Noble Metal Free Photocatalysis. *Chem. Mater.* **2014,** *26* (19), 5812-5818.
14. Zhang, J.; Chen, X.; Takanabe, K.; Maeda, K.; Domen, K.; Epping, J. D.; Fu, X.; Antonietti, M.; Wang, X., Synthesis of a carbon nitride structure for visible-light catalysis by copolymerization. *Angew. Chem., Int. Ed.* **2010,** *49* (2), 441-4.
15. Zhang, G.; Savateev, A.; Zhao, Y.; Li, L.; Antonietti, M., Advancing the n → π* electron transition of carbon nitride nanotubes for H2 photosynthesis *J. Mater. Chem. A* **2017,** *5*, 12723-12728.
16. Shalom, M.; Inal, S.; Fettkenhauer, C.; Neher, D.; Antonietti, M., Improving carbon nitride photocatalysis by supramolecular preorganization of monomers. *J. Am. Chem. Soc.* **2013,** *135* (19), 7118-21.
17. Thaweesak, S.; Wang, S.; Lyu, M.; Xiao, M.; Peerakiatkhajohn, P.; Wang, L., Boron-doped graphitic carbon nitride nanosheets for enhanced visible light photocatalytic water splitting. *Dalton Trans.* **2017,** *46*, 10714-10720.
18. Savateev, A.; Kurpil, B.; Mishchenko, A.; Zhang, G.; Antonietti, M., A "waiting" carbon nitride radical anion: a charge storage material and key intermediate in direct C–H thiolation of methylarenes using elemental sulfur as the "S"-source. *Chem. Sci.* **2018,** *9* (14), 3584-3591.

19. Cui, Q.; Xu, J.; Wang, X.; Li, L.; Antonietti, M.; Shalom, M., Phenyl-Modified Carbon Nitride Quantum Dots with Distinct Photoluminescence Behavior. *Angew. Chem., Int. Ed.* **2016,** *55*, 3672-3676.
20. Mo, Z.; She, X.; Li, Y.; Liu, L.; Huang, L.; Chen, Z.; Zhang, Q.; Xu, H.; Li, H., Synthesis of g-C3N4 at Different Temperatures for Superior Visible/UV Photocatalytic Performance and Photoelectrochemical Sensing of MB Solution. *RSC Adv.* **2015,** *5*, 101552-101562.
21. Zhang, G.; Zhang, J.; Zhang, M.; Wang, X., Polycondensation of Thiourea into Carbon Nitride Semiconductors as Visible Light Photocatalysts. *J. Mater. Chem.* **2012,** *22*, 8083-8091.
22. Wang, Y.; Wang, X.; Antonietti, M.; Zhang, Y., Facile One-Pot Synthesis of Nanoporous Carbon Nitride Solids by Using Soft Templates. *ChemSusChem* **2010,** *3*, 435-439.
23. Paraknowitsch, J. P.; Zhang, J.; Su, D.; Thomas, A.; Antonietti, M., Ionic Liquids as Precursors for Nitrogen-Doped Graphitic Carbon. *Adv. Mater.* **2010,** *22*, 87-92.
24. Zheng, Y.; Liu, J.; Liang, J.; Jaroniec, M.; Qiao, S. Z., Graphitic carbon nitride materials: controllable synthesis and applications in fuel cells and photocatalysis. *Energy Environ. Sci.* **2012,** *5*, 6717-6731.
25. Sun, Y. S.; Hong, W. H.; Antonietti, M.; Thomas, A., Mesoporous, 2D Hexagonal Carbon Nitride and Titanium Nitride/Carbon Composites. *Adv. Mater.* **2009,** *21*, 4270-4274.
26. Hou, Y.; Laursen, A.; Zhang, J.; Zhang, G.; Zhu, Y.; Wang, X.; Dahl, S.; Chorkendorff, I., Layered Nanojunctions for Hydrogen-Evolution Catalysis. *Angew. Chem., Int. Ed.* **2013,** *52*, 3621-3625.
27. Naseri, A.; Samadi, M.; Pourjavadi, A.; Moshfegh, A. Z.; Ramakrishna, S., Graphitic carbon nitride (g-C3N4)-based photocatalysts for solar hydrogen generation: recent advances and future development directions. *J. Mater. Chem. A* **2017,** *5*, 23406-23433.
28. Jiang, Z.; Zhu, C.; Wan, W.; Qian, K.; Xie, J., Constructing Graphite-Like Carbon Nitride Modified Hierarchical Yolk-Shell TiO2 Spheres for Water Pollution Treatment and Hydrogen Production. *J. Mater. Chem. A* **2016,** *4*, 1806-1818.
29. Xu, M.; Han, L.; Dong, S., Facile Fabrication of Highly Efficient g-C3N4/Ag2O Heterostructured Photocatalysts with Enhanced Visible-Light Photocatalytic Activity. *ACS Appl. Mater. Interfaces* **2013,** *5*, 12533-12540.
30. Zhang, J.; Wang, Y.; Jin, J.; Zhang, J.; Lin, Z.; Huang, F.; Yu, J., Efficient Visible-Light Photocatalytic Hydrogen Evolution and Enhanced Photostability of Core/Shell CdS/g-C3N4 Nanowires. *ACS Appl. Mater. Interfaces* **2013,** *5*, 10317-10324.
31. Zhao, G.; Huang, X.; Fina, F.; Zhang, G.; Irvine, J. T. S., Facile Structure Design Based on C3N4 for Mediator-Free Z-Scheme Water Splitting under Visible Light *Catal. Sci. Technol.* **2015,** *5*, 3416-3422.
32. Fu, H.; Xu, T.; Zhu, S.; Zhu, Y., Photocorrosion Inhibition and Enhancement of Photocatalytic Activity for ZnO via Hybridization with C60. *Environ. Sci. Technol.* **2008,** *42*, 8064-8069.
33. Kuriki, R.; Sekizawa, K.; Ishitani, O.; Maeda, K., Visible-Light-Driven CO2 Reduction with Carbon Nitride: Enhancing the Activity of Ruthenium Catalysts. *Angew. Chem., Int. Ed.* **2015,** *54* (8), 2406-2409.
34. Qin, J.; Wang, S.; Ren, H.; Hou, Y.; Wang, X., Photocatalytic reduction of CO2 by graphitic carbon nitride polymers derived from urea and barbituric acid. *Appl. Catal., B* **2015,** *179*, 1-8.
35. Xiao, H.; Zhu, J.; Thomas, A., Graphitic carbon nitride for photocatalytic degradation of sulfamethazine in aqueous solution under simulated sunlight irradiation *RSC Adv.* **2015,** *5*, 105731-105734.
36. Cui, Y.; Huang, J.; Fu, X.; Wang, X., Metal-free photocatalytic degradation of 4-chlorophenol in water by mesoporous carbon nitride semiconductors. *Catal. Sci. Technol.* **2012,** *2*, 1396-1402.
37. Levine, I. N., *Physical Chemistry*. 5th ed.; McGraw-Hill: Boston, MA, 2001; p 955.
38. Myers, D., *Surfaces, Interfaces, and Colloids: Principles and Applications*. 2nd ed.; Wiley: 2002.
39. Napper, D. H., Colloid Stability. *Ind. Eng. Chem. Prod. Res. Develop.* **1970,** *9* (4), 467-477.
40. Li, H.-J.; Sun, B.-W.; Sui, L.; Qian, D.-J.; Chen, M., Preparation of water-dispersible porous g-C 3 N 4 with improved photocatalytic activity by chemical oxidation. *Phys. Chem. Chem. Phys.* **2015,** *17*, 3309-3315.

41. Shi, Y.; Wang, B.; Duan, L.; Zhu, Y.; Gui, Z.; Yuen, R. K. K.; Hu, Y., Processable Dispersions of Graphitic Carbon Nitride Based Nanohybrids and Application in Polymer Nanocomposites. *Ind. Eng. Chem. Res.* **2016,** *55* (28), 7646-7654.
42. Bu, X.; Li, J.; Yang, S.; Sun, J.; Deng, Y.; Yang, Y.; Wang, G.; Peng, Z.; He, P.; Wang, X.; Ding, G.; Yang, J.; Xie, X., Surface Modification of C3N4 through Oxygen-Plasma Treatment: A Simple Way toward Excellent Hydrophilicity. *ACS Appl. Mater. Interfaces* **2016,** *8* (45), 31419-31425.
43. Zhang, X.; Xie, X.; Wang, H.; Zhang, J.; Pan, B.; Xie, Y., Enhanced Photoresponsive Ultrathin Graphitic-Phase C3N4 Nanosheets for Bioimaging. *J. Am. Chem. Soc.* **2013,** *135* (1), 18-21.
44. Zhuang, Q.; Guo, P.; Zheng, S.; Lin, Q.; Lin, Y.; Wang, Y.; Ni, Y., Green synthesis of luminescent graphitic carbon nitride quantum dots from human urine and its bioimaging application. *Talanta* **2018,** *188*, 35-40.
45. Zhou, J.; Yang, Y.; Zhang, C.-Y., A low-temperature solid-phase method to synthesize highly fluorescent carbon nitride dots with tunable emission. *Chem. Comm.* **2013,** *49*, 8605-8607.
46. Zhang, Y.; Pan, Q.; Chai, G.; Liang, M.; Dong, G.; Zhang, A. Q.; Qiu, B. J., Synthesis and luminescence mechanism of multicolor-emitting g-C3N4 nanopowders by low temperature thermal condensation of melamine. *Sci. Rep.* **2013,** *3*, 1943.
47. Song, Z.; Li, Z.; Lin, L.; Zhang, Y.; Lin, T.; Chen, L.; Cai, Z.; Lin, S.; Guo, L.; Fu, F.; Wang, X., Phenyl-doped graphitic carbon nitride: photoluminescence mechanism and latent fingerprint imaging. *Nanoscale* **2017,** *9* (45), 17737-17742.
48. Xu, J.; Brenner, T. J. K.; Chabanne, L.; Neher, D.; Antonietti, M.; Shalom, M., Liquid-Based Growth of Polymeric Carbon Nitride Layers and Their Use in a Mesostructured Polymer Solar Cell with Voc Exceeding 1 V. *J. Am. Chem. Soc.* **2014,** *136* (39), 13486-13489.
49. Xu, J.; Shalom, M.; Piersimoni, F.; Antonietti, M.; Neher, D.; Brenner, T. J. K., Color-Tunable Photoluminescence and NIR Electroluminescence in Carbon Nitride Thin Films and Light-Emitting Diodes. *Adv. Opt. Mater.* **2015,** *3*, 913-917.
50. Kiskan, B.; Zhang, J.; Wang, X.; Antonietti, M.; Yagci, Y., Mesoporous Graphitic Carbon Nitride as a Heterogeneous Visible Light Photoinitiator for Radical Polymerization. *ACS Macro Lett.* **2012,** *1* (5), 546-549.
51. Dadashi-Silab, S.; Tasdelen, M. A.; Kiskan, B.; Wang, X.; Antonietti, M.; Yagci, Y., Photochemically Mediated Atom Transfer Radical Polymerization Using Polymeric Semiconductor Mesoporous Graphitic Carbon Nitride. *Macromol. Chem. Phys.* **2014,** *215* (7), 675-681.
52. Dadashi-Silab, S.; Kiskan, B.; Antonietti, M.; Yagci, Y., Mesoporous graphitic carbon nitride as a heterogeneous catalyst for photoinduced copper(I)-catalyzed azide–alkyne cycloaddition *RSC Adv.* **2014,** *4*, 52170-52173.
53. Fu, Q.; Ruan, Q.; McKenzie, T. G.; Reyhani, A.; Tang, J.; Qiao, G. G., Development of a Robust PET-RAFT Polymerization Using Graphitic Carbon Nitride (g-C3N4). *Macromolecules* **2017,** *50*, 7509-7516.
54. Xu, J.; Antonietti, M., The Performance of Nanoparticulate Graphitic Carbon Nitride as an Amphiphile. *J. Am. Chem. Soc.* **2017,** *139* (17), 6026-6029.
55. Cao, Q.; Cui, Q.; Yang, Y.; Xu, J.; Han, C.; Li, L., Graphitic Carbon Nitride as a Distinct Solid Stabilizer for Emulsion Polymerization. *Chem. Eur. J.* **2018,** *24*, 2286-2291.
56. Zhang, Y.; Zhou, Z.; Shen, Y.; Zhou, Q.; Wang, J.; Liu, A.; Liu, S.; Zhang, Y., Reversible Assembly of Graphitic Carbon Nitride 3D Network for Highly Selective Dyes Absorption and Regeneration. *ACS Nano* **2016,** *10* (9), 9036-43.
57. Ou, H.; Yang, P.; Lin, L.; Anpo, M.; Wang, X., Carbon Nitride Aerogels for the Photoredox Conversion of Water. *Angew. Chem., Int. Ed.* **2017,** *56*, 10905-10910.
58. Ko, J. W.; Choi, W. S.; Kim, J.; Kuk, S. K.; Lee, S. H.; Park, C. B., Self-Assembled Peptide-Carbon Nitride Hydrogel as a Light-Responsive Scaffold Material. *Biomacromolecules* **2017,** *18* (11), 3551-3556.
59. Zarei, M.; Ahmadzadeh, H.; Goharshadi, E. K.; Farzaneh, A., Graphitic carbon nitride embedded hydrogels for enhanced gel electrophoresis. *Anal. Chim. Acta* **2015,** *887*, 245-252.

60. Li, M.; Liao, H.; Deng, Q.; Wu, Y.; Xiao, F.; Tu, D., Preparation of an intelligent hydrogel sensor based on g-C3N4 nanosheets for selective detection of Ag+. *J. Macromol. Sci. A* **2018,** *55* (5), 408-413.
61. Sun, J.; Schmidt, B. V.; Wang, X.; Shalom, M., Self-Standing Carbon Nitride-Based Hydrogels with High Photocatalytic Activity. *ACS Appl. Mater. Interfaces* **2017,** *9* (3), 2029-2034.
62. Liu, J.; An, T.; Chen, Z.; Wang, Z.; Zhou, H.; Fan, T.; Zhang, D.; Antonietti, M., Carbon nitride nanosheets as visible light photocatalytic initiators and crosslinkers for hydrogels with thermoresponsive turbidity. *J. Mater. Chem. A* **2017,** *5* (19), 8933-8938.
63. Jiang, W.; Luo, W.; Zong, R.; Yao, W.; Li, Z.; Zhu, Y., Polyaniline/Carbon Nitride Nanosheets Composite Hydrogel: A Separation-Free and High-Efficient Photocatalyst with 3D Hierarchical Structure. *Small* **2016,** *12* (32), 4370-4378.
64. He, P.; Tang, X.; Chen, L.; Xie, P.; He, L.; Zhou, H.; Zhang, D.; Fan, T., Patterned Carbon Nitride–Based Hybrid Aerogel Membranes via 3D Printing for Broadband Solar Wastewater Remediation. *Adv. Func. Mater.* **2018,** *28* (29).
65. Cui, Q.; Xu, J.; Shen, G.; Zhang, C.; Li, L.; Antonietti, M., Hybridizing Carbon Nitride Colloids with a Shell of Water-Soluble Conjugated Polymers for Tunable Full-Color Emission and Synergistic Cell Imaging. *ACS Appl. Mater. Interfaces* **2017,** *9*, 43966-43974.
66. Kim, J. K.; Park, S.; Yoo, R. J.; Jeong, H. J.; Oh, J.; Lee, Y. J.; Park, S.; Kim, D. W., Thin PEGylated Carbon Nitrides: Water-Dispersible Organic Nanodots as Bioimaging Probes. *Chem. Eur. J.* **2018,** *24* (14), 3506-3511.
67. Yan, J.; Rodrigues, M.-T. F.; Song, Z.; Li, H.; Xu, H.; Liu, H.; Wu, J.; Xu, Y.; Song, Y.; Liu, Y.; Yu, P.; Yang, W.; Vajtai, R.; Li, H.; Yuan, S.; Ajayan, P. M., Reversible Formation of g-C3N4 3D Hydrogels through Ionic Liquid Activation: Gelation Behavior and Room-Temperature Gas-Sensing Properties. *Adv. Funct. Mater.* **2017,** *27* (22), 1700653.
68. Rivlin, R. S., Historical Perspective on the Use of Garlic. *J. Nutr.* **2001,** *131* (3), 951-954.
69. Harrison, F.; Roberts, A. E.; Gabrilska, R.; Rumbaugh, K. P.; Lee, C.; Diggle, S. P., A 1,000-Year-Old Antimicrobial Remedy with Antistaphylococcal Activity. *mBio* **2015,** *6* (4), e01129.
70. Cruz Martinez, C.; Diaz Gomez, M.; Oh, M. S., Use of traditional herbal medicine as an alternative in dental treatment in Mexican dentistry: a review. *Pharm. Biol.* **2017,** *55* (1), 1992-1998.
71. Zhou, X.; Seto, S. W.; Chang, D.; Kiat, H.; Razmovski-Naumovski, V.; Chan, K.; Bensoussan, A., Synergistic Effects of Chinese Herbal Medicine: A Comprehensive Review of Methodology and Current Research. *Front. Pharmacol.* **2016,** *7*, 201.
72. Kozlowska, W.; Wagner, C.; Moore, E. M.; Matkowski, A.; Komarnytsky, S., Botanical Provenance of Traditional Medicines From Carpathian Mountains at the Ukrainian-Polish Border. *Front. Pharmacol.* **2018,** *9*, 295-298.
73. Mahomoodally, M. F., Traditional medicines in Africa: an appraisal of ten potent african medicinal plants. *Evid. Based Complement. Alternat. Med.* **2013,** *2013*, 617459.
74. Vacanti, C., The history of tissue engineering. *J. Cell. Mol. Med.* **2006,** *1* (3), 569-576.
75. Kryuchkova-Mostacci, N.; Robinson-Rechavi, M., Tissue-Specific Evolution of Protein Coding Genes in Human and Mouse. *PLoS One* **2015,** *10* (6), e0131673.
76. Fung, Y. C., *Biomechanics: Mechanical Properties of Living Tissues*. 2 ed.; Springer: 1981.
77. Byrd, A. L.; Belkaid, Y.; Segre, J. A., The human skin microbiome. *Nat. Rev. Microbiol.* **2018,** *16* (3), 143-155.
78. Percival, N. J., Classification of Wounds and their Management. *Surgery (Oxford)* **2002,** *20* (5), 114-117.
79. Harding, K. G.; Morris, H. L.; Patel, G. K., Healing chronic wounds. *BMJ* **2002,** *324* (7330), 160-163.
80. Mustoe, T., Understanding chronic wounds: a unifying hypothesis on their pathogenesis and implications for therapy. *Am. J. Surg.* **2004,** *187*, 65S-70S.
81. Thomas, S., *Surgical Dressings and Wound Management*. Medetec: Cardiff, 2010.

82. Okan, D.; Woo, K.; Ayello, E. A.; Sibbald, G., The Role of Moisture Balance in Wound Healing. *Adv. Skin Wound Care* **2007,** *20* (1), 39-53.
83. Attinger, C. E.; Janis, J. E.; Steinberg, J.; Schwartz, J.; Al-Attar, A.; Couch, K., Clinical approach to wounds: debridement and wound bed preparation including the use of dressings and wound healing adjuvants. *Plast. Reconstr. Surg.* **2006,** *117* (7S), 72.
84. Sood, A.; Granick, M. S.; Tomaselli, N. L., Wound Dressings and Comparative Effectiveness Data. *Adv. Wound Care (New Rochelle)* **2014,** *3* (8), 511-529.
85. Morin, R. J.; Tomaselli, N. L., Interactive dressings and topical agents. *Clin. Plast. Surg.* **2007,** *34*, 643-658.
86. Boateng, J. S.; Matthews, K. H.; Stevens, H. N.; Eccleston, G. M., Wound healing dressings and drug delivery systems: a review. *J. Pharm. Sci.* **2008,** *97* (8), 2892-923.
87. Markova, A.; Mostow, E. N., US skin disease assessment: ulcer and wound care. *Dermatol. Clin.* **2012,** *30*, 107-111.
88. Liu, Y.; Pharr, M.; Salvatore, G. A., Lab-on-Skin: A Review of Flexible and Stretchable Electronics for Wearable Health Monitoring. *ACS Nano* **2017,** *11* (10), 9614-9635.
89. Hamburg, M. A.; Collins, F. S., The Path to Personalized Medicine. *N. Engl. J. Med.* **2010,** *363*, 301-304.
90. Presley, T. D., Electrical properties of the body. In *Biophysics of the Senses*, IOP Science: 2016; pp 1-7.
91. van den Brand, J.; de Kok, M.; Koetse, M.; Cauwe, M.; Verplancke, R.; Bossuyt, F.; Jablonski, M.; Vanfleteren, J., Flexible and stretchable electronics for wearable health devices. *Solid State Electron.* **2015,** *113*, 116-120.
92. Yang, Y.; Gao, W., Wearable and flexible electronics for continuous molecular monitoring. *Chem. Soc. Rev.* **2018**.
93. Mukhopadhyay, S. C., Wearable Sensors for Human Activity Monitoring: A Review. *IEEE Sens.* **2015,** *15*, 1321-1330.
94. Gubbi, J.; Buyya, R.; Marusic, S.; Palaniswami, M., Internet of Things(IoT): A vision,architectural elements,and future directions. *Future Gener. Comput. Syst.* **2013,** *29*, 1645-1660.
95. Murakami, T.; Yarimitsu, S.; Nakashima, K.; Sakai, N.; Yamaguchi, T.; Sawae, Y.; Suzuki, A., Biphasic and boundary lubrication mechanisms in artificial hydrogel cartilage: A review. *Proc. Inst. Mech. Eng. H.* **2015,** *229* (12), 864-78.
96. Murakami, T., The lubrication in natural synovial joints and joint prostheses. *JSME Int. J. III: Vib. C* **1990,** *33* (4), 465-474.
97. Brittberg, M.; Gomoll, A. H.; Canseco, J. A.; Far, J.; Lind, M.; Hui, J., Cartilage repair in the degenerative ageing knee. *Acta Orthop.* **2016,** *87* (sup363), 26-38.
98. Yarimitsu, S.; Sasaki, S.; Murakami, T.; Suzuki, A., Evaluation of lubrication properties of hydrogel artificial cartilage materials for joint prosthesis. *Biosurf. Biotribol.* **2016,** *2* (1), 40-47.
99. Liu, M.; Zeng, X.; Ma, C.; Yi, H.; Ali, Z.; Mou, X.; Li, S.; Deng, Y.; He, N., Injectable hydrogels for cartilage and bone tissue engineering. *Bone Res.* **2017,** *5*, 17014.
100. Varaprasad, K.; Raghavendra, G. M.; Jayaramudu, T.; Yallapu, M. M.; Sadiku, R., A mini review on hydrogels classification and recent developments in miscellaneous applications. *Mater. Sci. Eng. C Mater. Biol. Appl.* **2017,** *79*, 958-971.
101. Gaharwar, A. K.; Peppas, N. A.; Khademhosseini, A., Nanocomposite hydrogels for biomedical applications. *Biotechnol. Bioeng.* **2014,** *111* (3), 441-53.
102. Maitra, J.; Shukla, V. K., Cross-linking in Hydrogels - A Review. *Am. J. Polym. Sci.* **2014,** *4* (2), 25-31.
103. Lee, J.; Cuddihy, M. J.; Kotov, N. A., Three-dimensional cell culture matrices: state of the art. *Tissue Eng. Part B.* **2008,** *14* (1), 61-86.

104. Kang, J.; Miyajima, D.; Mori, T.; Inoue, Y.; Itoh, Y.; Aida, T., A rational strategy for the realization of chain-growth supramolecular polymerization. *Science* **2015,** *347* (6222), 646-651.
105. Cowie, J. M. G.; Arrighi, V., *Polymers: Chemistry and Physics of Modern Materials*. 3rd ed.; CRC Press: 2007.
106. Parhi, R., Cross-Linked Hydrogel for Pharmaceutical Applications: A Review. *Adv. Pharm. Bull.* **2017,** *7* (4), 515-530.
107. Hoffman, A. S., Hydrogels for biomedical applications. *Adv. Drug Deliv. Rev.* **2002,** *54* (1), 3-12.
108. Van Tomme, S. R.; Van Steenbergen, M. J.; De Smedt, S. C.; Van Nostrum, C. F.; Hennink, W. E., Self-gelling hydrogels based on oppositely charged dextran microspheres. *Biomaterials* **2005,** *26* (14), 2129-2135.
109. Ricciardi, R.; Gaillet, C.; Ducouret, G.; Lafuma, F.; Laupretre, F., Investigation of the relationships between the chain organization and rheological properties of atactic poly(vinyl alcohol) hydrogels. *Polymer* **2003,** *44* (11), 3375-3380.
110. Liu, L.; Gao, Q.; Lu, X.; Zhou, H., In situ forming hydrogels based on chitosan for drug delivery and tissue regeneration. *Asian J. Pharm.* **2016,** *11* (6), 673-683.
111. Kumru, B.; Bicak, N., Synthesis of soluble poly(vinylene carbonate) by redox-initiated RAFT process in microemulsion and its aminolysis yielding snow-white polymethylol. *RSC Adv.* **2015,** *5* (39), 30936-30942.
112. Escobar-Chavez, J. J.; Lopez-Cervantes, M.; Naik, A.; Kalia, Y. N.; Quintanar-Guerrero, D.; Ganem-Quintanar, A., Applications of thermo-reversible pluronic F-127 gels in pharmaceutical formulations. *J. Pharm. Pharm. Sci.* **2006,** *9* (3), 339-358.
113. Tsuji, H., Poly(lactide) Stereocomplexes: Formation, Structure, Properties, Degradation, and Applications. *Macromol. Biosci.* **2005,** *5* (7), 569-597.
114. Xu, Y.; Sheng, K.; Li, C.; Shi, G., Self-Assembled Graphene Hydrogel via a One-Step Hydrothermal Process. *ACS Nano* **2010,** *4* (7), 4324-4330.
115. Porter, T. L.; Stewart, R.; Reed, J.; Morton, K., Models of Hydrogel Swelling with Applications to Hydration Sensing. *Sensors* **2007,** *7*, 1980-1991.
116. Gupta, N. V.; Shivakumar, H. G., Investigation of Swelling Behavior and Mechanical Properties of a pH-Sensitive Superporous Hydrogel Composite. *Iran J. Pharm. Res.* **2012,** *11* (2), 481-493.
117. Montesano, F. F.; Parente, A.; Santamaria, P.; Sannino, A.; Serio, F., Biodegradable Superabsorbent Hydrogel IncreasesWater Retention Properties of Growing Media and Plant Growth. *Agric. Agric. Sci. Procedia* **2015,** *4*, 451-458.
118. Khan, S.; Ullah, A.; Ullah, K.; Rehman, N.-u., Insight into hydrogels. *Des. Monomers Polym.* **2016,** *19* (5), 456-478.
119. Gyles, D. A.; Castro, L. D.; Silva, J. O. C.; Ribeiro-Costa, R. M., A review of the designs and prominent biomedical advances of natural and synthetic hydrogel formulations. *Eur. Polym. J.* **2017,** *88*, 373-392.
120. Lim, H. L.; Hwang, Y.; Kar, M.; Varghese, S., Smart hydrogels as functional biomimetic systems. *Biomater. Sci.* **2014,** *2* (5), 603-618.
121. Ionov, L., Hydrogel-based actuators: possibilities and limitations. *Mater. Today* **2014,** *17* (10), 494-503.
122. Zhang, H.; Mardyani, S.; Chan, W. C. W.; Kumacheva, E., Design of Biocompatible Chitosan Microgels for Targeted pH-Mediated Intracellular Release of Cancer Therapeutics. *Biomacromolecules* **2006,** *7* (5), 1568-1572.
123. Zheng, J.; Xiao, P.; Le, X.; Lu, W.; Theato, P.; Ma, C.; Du, B.; Zhang, J.; Huang, Y.; Chen, T., Mimosa inspired bilayer hydrogel actuator functioning in multi-environments *J. Mater. Chem. C* **2018,** *6*, 1320-1327.
124. Phadke, A.; Zhang, C.; Arman, B.; Hsu, C. C.; Mashelkar, R. A.; Lele, A. K.; Tauber, M. J.; Arya, G.; Varghese, S., Rapid self-healing hydrogels. *Proc. Natl. Acad. Sci. U. S. A.* **2012,** *109* (12), 4383-4388.

125. Lui, F.; Urban, M. W., Recent advances and challenges in designing stimuli-responsive polymers. *Prog. Polym. Sci.* **2010,** *35*, 3-23.
126. Ruel-Gariepy, E.; Leroux, J. C., In situ-forming hydrogels –review of temperature-sensitive systems. *Eur. J. Pharm.* **2004,** *58*, 409-426.
127. Morales, D.; Palleau, E.; Dickey, M. D.; Velev, O. D., Electro-actuated hydrogel walkers with dual responsive legs. *Soft Matter* **2014,** *10* (9), 1337-48.
128. Kumar, G. S.; Neckers, D. C., Photochemistry of azobenzene-containing polymers. *Chem. Rev.* **1989,** *89*, 1915-1925.
129. Francis, W.; Dunne, A.; Delaney, C.; Florea, L.; Diamond, D., Spiropyran based hydrogels actuators—Walking in the light. *Sens. Actuators B* **2017,** *250*, 608-616.
130. Zhao, Q.; Liang, Y.; Ren, L.; Yu, Z.; Zhang, Z.; Ren, L., Bionic intelligent hydrogel actuators with multimodal deformation and locomotion. *Nano Energy* **2018,** *51*, 621-631.
131. Xu, B.; Jiang, H.; Li, H.; Zhang, G.; Zhang, Q., High strength nanocomposite hydrogel bilayer with bidirectional bending and shape switching behaviors for soft actuators. *RSC Adv.* **2015,** *5* (17), 13167-13170.
132. Gladman, A. S.; Matsumoto, E. A.; Nuzzo, R. G.; Mahadevan, L.; Lewis, J. A., Biomimetic 4D printing. *Nat. Mater.* **2016,** *15*, 413-418.
133. Dragan, E. S., Design and applications of interpenetrating polymer network hydrogels. A review. *Chem. Eng. J.* **2014,** *243*, 572-590.
134. Myung, D.; Waters, D.; Wiseman, M.; Duhamel, P. E.; Noolandi, J.; Ta, C. N.; Frank, C. W., Progress in the development of interpenetrating polymer network hydrogels. *Polym. Adv. Technol.* **2008,** *19* (6), 647-657.
135. Gong, J. P., Why are double network hydrogels so tough? *Soft Matter* **2010,** *6* (12), 2583.
136. Tsukeshiba, H.; Huang, M.; Na, Y.-H.; Kurokawa, T.; Kuwabara, R.; Tanaka, Y.; Furukawa, H.; Osada, Y.; Gong, J. P., Effect of Polymer Entanglement on the Toughening of Double Network Hydrogels. *J. Phys. Chem. B* **2005,** *109*, 16304-16309.
137. Chen, Q.; Chen, H.; Zhu, L.; Zheng, J., Fundamentals of double network hydrogels. *J. Mater. Chem. B* **2015,** *3* (18), 3654-3676.
138. Sun, J. Y.; Zhao, X.; Illeperuma, W. R.; Chaudhuri, O.; Oh, K. H.; Mooney, D. J.; Vlassak, J. J.; Suo, Z., Highly stretchable and tough hydrogels. *Nature* **2012,** *489* (7414), 133-6.
139. Gong, J. P.; Katsuyama, Y.; Kurokawa, T.; Osada, Y., Double-Network Hydrogels with Extremely High Mechanical Strength. *Adv. Mater.* **2003,** *15* (14), 1155-1158.
140. Milner, P. E.; Parkes, M.; Puetzer, J. L.; Chapman, R.; Stevens, M. M.; Cann, P.; Jeffers, J. R. T., A low friction, biphasic and boundary lubricating hydrogel for cartilage replacement. *Acta Biomater.* **2018,** *65*, 102-111.
141. Osaheni, A. O.; Finkelstein, E. B.; Mather, P. T.; Blum, M. M., Synthesis and characterization of a zwitterionic hydrogel blend with low coefficient of friction. *Acta Biomater.* **2016,** *46*, 245-255.
142. Askeland, D. R.; Phule, P. P.; Wright, W. J., *The science and engineering of materials*. 6th ed.; Cengage Learning: 2011; p 949.
143. Chen, M. H.; Wang, L. L.; Chung, J. J.; Kim, Y. H.; Atluri, P.; Burdick, J. A., Methods To Assess Shear-Thinning Hydrogels for Application As Injectable Biomaterials. *ACS Biomater. Sci. Eng.* **2017,** *3* (12), 3146-3160.
144. Sontjens, S. H. M.; Nettles, D. L.; Carnahan, M. A.; Setton, L. A.; Grinstaff, M. W., Biodendrimer-based hydrogel scaffolds for cartilage tissue repair. *Biomacromolecules* **2006,** *7* (1), 310-316.
145. Zhang, H.; Patel, A.; Gaharwar, A. K.; Mihaila, S. M.; Iviglia, G. I.; Mukundan, S.; Bae, H.; Yang, H.; Khademhosseini, A., Hyperbranched polyester hydrogels with controlled drug release and cell adhesion properties. *Biomacromolecules* **2013,** *14* (5), 1299-1310.
146. Kuilla, T.; Bhadra, S.; Yao, D.; Kim, N. H.; Bose, S.; Lee, J. H., Recent advances in graphene based polymer composites. *Prog. Polym. Sci.* **2010,** *35* (11), 1350-1375.

147. Ma, P.-C.; Siddiqui, N. A.; Marom, G.; Kim, J.-K., Dispersion and functionalization of carbon nanotubes for polymer-based nanocomposites: A review. *Comp. A Appl. Sci. Manuf.* **2010,** *41* (10), 1345-1367.
148. Shin, S. R.; Bae, H.; Cha, J. M.; Mun, J. Y.; Chen, Y.-C.; Tekin, H.; Shin, H.; Farshchi , S.; Dokmeci, M. R.; Tang, S.; Khademhosseini, A., Carbon nanotube reinforced hybrid microgels as scaffold materials for cell encapsulation. *ACS Nano* **2011,** *6* (1), 362-372.
149. Liu, J.; Chen, C.; He, C.; Zhao, J.; Yang, X.; Wang, H., Synthesis of graphene peroxide and its application in fabricating super extensible and highly resilient nanocomposite hydrogels. *ACS Nano* **2012,** *6* (9), 8194-8202.
150. Hoppe, A.; Güldal, N. S.; Boccaccini, A. R., A review of the biological response to ionic dissolution products from bioactive glasses and glassceramics. *Biomaterials* **2011,** *32* (11), 2757-2774.
151. Wang, Q.; Mynar, J. L.; Yoshida, M.; Lee, E.; Lee, M.; Okuro, K.; Kinbara, K.; Aida, T., High-water-content mouldable hydrogels by mixing clay and a dendritic molecular binder. *Nature* **2010,** *463* (7279), 339-43.
152. Liu, M.; Ishida, Y.; Ebina, Y.; Sasaki, T.; Hikima, T.; Takata, M.; Aida, T., An anisotropic hydrogel with electrostatic repulsion between cofacially aligned nanosheets. *Nature* **2015,** *517* (7532), 68-72.
153. Skardal, A.; Zhang, J.; McCoard, L.; Oottamasathien, S.; Prestwich, G. D., Dynamically crosslinked gold nanoparticle—Hyaluronan hydrogels. *Adv. Mater.* **2010,** *22* (42), 4736-4740.
154. Bhattacharya, A., Grafting: a versatile means to modify polymersTechniques, factors and applications. *Prog. Polym. Sci.* **2004,** *29* (8), 767-814.
155. Cui, Q.; Xu, J.; Wang, X.; Li, L.; Antonietti, M.; Shalom, M., Phenyl-Modified Carbon Nitride Quantum Dots with Distinct Photoluminescence Behavior. *Angew. Chem., Int. Ed.* **2016,** *55* (11).
156. Dong, F.; Wang, Z.; Sun, Y.; Ho, W. K.; Zhang, H., Engineering the nanoarchitecture and texture of polymeric carbon nitride semiconductor for enhanced visible light photocatalytic activity. *J. Colloid Interface Sci.* **2013,** *401*, 70-79.
157. Zhou, C.; Wu, Q., A novel polyacrylamide nanocomposite hydrogel reinforced with natural chitosan nanofibers. *Coll. Surf. B. Biointerfaces* **2011,** *84*, 155.
158. Liu, M.; Zhang, Y.; Li, J.; Zhou, C., Chitin-natural clay nanotubes hybrid hydrogel. *Int. J. Biol. Macromol.* **2013,** *58*, 23-30.
159. Kumru, B.; Shalom, M.; Antonietti, M.; Schmidt, B. V. K. J., Reinforced Hydrogels via Carbon Nitride Initiated Polymerization. *Macromolecules* **2017,** *50* (5), 1862-1869.
160. Wang, N.; Fan, H.; Sun, J.; Han, Z.; Dong, J.; Ai, S., Fluorine-doped carbon nitride quantum dots: Ethylene glycol-assisted synthesis, fluorescent properties, and their application for bacterial imaging. *Carbon* **2016,** *109*, 141-148.
161. Peng, G.; Xing, L.; Barrio, J.; Volokh, M.; Shalom, M., A General Synthesis of Porous Carbon Nitride Films with Tunable Surface Area and Photophysical Properties. *Angew. Chem., Int. Ed.* **2018,** *57* (5), 1186-1192.
162. Huang, C.; Chen, C.; Ye, X.; Ye, W.; Hu, J.; Xu, C.; Qiu, X., Stable colloidal boron nitride nanosheet dispersion and its potential application in catalysis. *J. Mater. Chem. A* **2013,** *1* (39), 12192.
163. She, X.; Xu, H.; Xu, Y.; Yan, J.; Xia, J.; Xu, L.; Song, Y.; Jiang, Y.; Zhang, Q.; Li, H., Exfoliated graphene-like carbon nitride in organic solvents: enhanced photocatalytic activity and highly selective and sensitive sensor for the detection of trace amounts of Cu2+. *J. Mater. Chem. A* **2014,** *2* (8), 2563-2570.
164. Sun, J.; Schmidt, B. V. K. J.; Wang, X.; Shalom, M., Self-Standing Carbon Nitride-Based Hydrogels with High Photocatalytic Activity. *ACS Appl. Mater. Interfaces* **2017,** *9* (3), 2029-2034.
165. Ju, H.; Zhu, F.; Xing, H.; Wu, Z. L.; Huang, F., Ultrastiff Hydrogels Prepared by Schiff's Base Reaction of Bis(p-Formylphenyl) Sebacate and Pillar[5]arene Appended with Multiple Hydrazides. *Macromol. Rapid Commun.* **2017,** *38* (20), 1700232.

166. Liu, M.; Li, W.; Rong, J.; Zhou, C., Novel polymer nanocomposite hydrogel with natural clay nanotubes. *Colloid Polym. Sci.* **2012,** *290* (10), 895-905.
167. Ji, J.; Wen, J.; Shen, Y.; Lv, Y.; Chen, Y.; Liu, S.; Ma, H.; Zhang, Y., Simultaneous Noncovalent Modification and Exfoliation of 2D Carbon Nitride for Enhanced Electrochemiluminescent Biosensing. *J. Am. Chem. Soc.* **2017,** *139* (34), 11698-11701.
168. Rong, Q.; Lei, W.; Chen, L.; Yin, Y.; Zhou, J.; Liu, M., Anti-freezing, Conductive Self-healing Organohydrogels with Stable Strain-Sensitivity at Subzero Temperatures. *Angew. Chem., Int. Ed.* **2017,** *56* (45), 14159-14163.
169. Huang, W.; Shen, J.; Li, N.; Ye, M., Study on a New Polymer/Graphene Oxide/Clay Double Network Hydrogel With Improved Response Rate and Mechanical Properties. *Polym. Eng. Sci.* **2015,** *55* (6), 1361-1366.
170. Nguyen, Q. T.; Hwang, Y.; Chen, A. C.; Varghese, S.; Sah, R. L., Cartilage-like mechanical properties of poly (ethylene glycol)-diacrylate hydrogels. *Biomaterials* **2012,** *33* (28), 6682-90.
171. Bhat, S.; Lidgren, L.; Kumar, A., In vitro neo-cartilage formation on a three-dimensional composite polymeric cryogel matrix. *Macromol. Biosci.* **2013,** *13* (7), 827-37.
172. Kumru, B.; Antonietti, M.; Schmidt, B., Enhanced Dispersibility of Graphitic Carbon Nitride Particles in Aqueous and Organic Media via a One-Pot Grafting Approach. *Langmuir* **2017,** *33* (38), 9897-9906.
173. Yan, S. C.; Li, Z. S.; Zou, Z. G., Photodegradation performance of g-C3N4 fabricated by directly heating melamine. *Langmuir* **2009,** *25* (17), 10397-401.
174. Yan, S. C.; Li, Z. S.; Zou, Z. G., Photodegradation of rhodamine B and methyl orange over boron-doped g-C3N4 under visible light irradiation. *Langmuir* **2010,** *26* (6), 3894-901.
175. Ehrmaier, J.; Karsili, T. N. V.; Sobolewski, A. L.; Domcke, W., Mechanism of Photocatalytic Water Splitting with Graphitic Carbon Nitride: Photochemistry of the Heptazine-Water Complex. *J. Phys. Chem. A* **2017,** *121* (25), 4754-4764.
176. Ayyaru, S.; Ahn, Y.-H., Application of sulfonic acid group functionalized graphene oxide to improve hydrophilicity, permeability, and antifouling of PVDF nanocomposite ultrafiltration membranes. *J. Membrane Sci.* **2017,** *525*, 210-219.
177. Kovtyukhova, N. I.; Ollivier, P. J.; Martin, B. R.; Mallouk, T. E.; Chizhik, S. A.; Buzaneva, E. V.; Gorchinskiy, A. D., Layer-by-Layer Assembly of Ultrathin Composite Films from Micron-Sized Graphite Oxide Sheets and Polycations. *Chem. Mater.* **1999,** *11*, 771-778.
178. Lvov, Y.; Decher, G.; Mohwald, H., Assembly, Structural Characterization, and Thermal Behavior of Layer-by-Layer Deposited Ultrathin Films of Poly(viny1 sulfate) and Poly(ally1amine). *Langmuir* **1993,** *9*, 481-486.
179. Deng, C.; Cui, Y.; Zhao, T.; Tan, M.; Huang, H.; Guo, M., Mechanically strong and stretchable polyurethane–urea supramolecular hydrogel using water as an additional in situ chain extender. *RSC Adv.* **2014,** *4* (46), 24095-24102.
180. Huang, T.; Xu, H. G.; Jiao, K. X.; Zhu, L. P.; Brown, H. R.; Wang, H. L., A Novel Hydrogel with High Mechanical Strength: A Macromolecular Microsphere Composite Hydrogel. *Adv. Mater.* **2007,** *19* (12), 1622-1626.
181. Wang, L.; Shan, G.; Pan, P., A strong and tough interpenetrating network hydrogel with ultrahigh compression resistance. *Soft Matter* **2014,** *10* (21), 3850-6.
182. Jing, M.; Fu, Y.; Fei, X.; Tian, J.; Zhi, H.; Zhang, H.; Xu, L.; Wang, X.; Wang, Y., A novel high-strength polymer hydrogel with identifiability prepared via a one-pot method. *Polym. Chem.* **2017,** *8* (23), 3553-3559.
183. Bai, T.; Zhang, P.; Han, Y.; Liu, Y.; Liu, W.; Zhao, X.; Lu, W., Construction of an ultrahigh strength hydrogel with excellent fatigue resistance based on strong dipole–dipole interaction. *Soft Matter* **2011,** *7* (6), 2825.

184. Brand, R. A., Joint Contact Stress: A Reasonable Surrogate For Biological Processes? *Iowa Orthop. J.* **2005,** *25*, 82-94.
185. Thambyah, A.; Goh, J. C.; De, S. D., Contact stresses in the knee joint in deep flexion. *Med. Eng. Phys.* **2005,** *27* (4), 329-35.
186. Li, J.; Mooney, D. J., Designing hydrogels for controlled drug delivery. *Nat. Rev. Mater.* **2016,** *1* (12).
187. Peak, C. W.; Wilker, J. J.; Schmidt, G., A review on tough and sticky hydrogels. *Colloid Polym. Sci.* **2013,** *291* (9), 2031-2047.
188. Haque, M. A.; Kurokawa, T.; Gong, J. P., Super tough double network hydrogels and their application as biomaterials. *Polymer* **2012,** *53* (9), 1805-1822.
189. Papadakis, C.; Tsitsilianis, C., Responsive Hydrogels from Associative Block Copolymers: Physical Gelling through Polyion Complexation. *Gels* **2017,** *3* (1), 3.
190. Wang, Q.; Hou, R.; Cheng, Y.; Fu, J., Super-tough double-network hydrogels reinforced by covalently compositing with silica-nanoparticles. *Soft Matter* **2012,** *8* (22), 6048.
191. Grygiel, K.; Lee, J.-S.; Sakaushi, K.; Antonietti, M.; Yuan, J., Thiazolium Poly(ionic liquid)s: Synthesis and Application as Binder for Lithium-Ion Batteries. *ACS Macro Lett.* **2015,** *4* (12), 1312-1316.
192. Grygiel, K.; Zhang, W.; Detrembleur, C.; Yuan, J., Unexpected LCST-type phase behaviour of a poly(vinyl thiazolium) polymer in acetone. *RSC Adv.* **2016,** *6* (62), 57117-57121.
193. Chen, W.; Qi, D.-C.; Huang, H.; Gao, X.; Wee, A. T. S., Organic-Organic Heterojunction Interfaces: Effect of Molecular Orientation. *Adv. Funct. Mater.* **2011,** *21* (3), 410-424.
194. Oldenburg, M.; Turshatov, A.; Busko, D.; Wollgarten, S.; Adams, M.; Baroni, N.; Welle, A.; Redel, E.; Woll, C.; Richards, B. S.; Howard, I. A., Photon Upconversion at Crystalline Organic-Organic Heterojunctions. *Adv. Mater.* **2016,** *28* (38), 8477-8482.
195. Gong, J.; Antonietti, M.; Yuan, J., Poly(Ionic Liquid)-Derived Carbon with Site-Specific N-Doping and Biphasic Heterojunction for Enhanced CO2 Capture and Sensing. *Angew. Chem., Int. Ed.* **2017,** *56* (26), 7557-7563.

13. Acknowledgements

First of all, I would like to thank Prof. Dr. Dr. Markus Antonietti for giving me a chance to conduct my research in the institute and being supportive during this period, and sharing wonderful ideas and providing beautiful insights of chemistry. He indeed influenced me about academia, how to be great scientist, how to stay motivated and how to be social, for the great 'BBQ Master' shirt and how to appreciate good wine. I hope to continue amazing collaborations with him in future.

Big thanks go to Dr. Bernhard V.K.J. Schmidt, for being amazing group leader and person. Since I started, he always provided me time for constructive discussions, teaching me a lot (from experiments to writing) and basically prepared me to be good scientist. I'm very glad for collaboration and having nice publications and I hope will be continued in future.

Thanks Prof. Dr. Menny Shalom, Dr. Valerio Molinari and Dr. Aleksandr 'Sasha' Savateev for collaborations, being friendly and supportive, discussions and underlining important parts of my projects. I thank Prof. Dr. Helmut Schlaad for providing me teaching opportunity and his valuable help with thesis reviewing and Dr. Kerstin G. Blank for collaboration. Same gratitude extends to Prof. Dr. Hans Börner for making himself available for thesis reviewing.

Of course, during my research I was not alone, but surrounded by wonderful people all the time who provided nice and friendly atmosphere with unforgettable moments. My friends which I call 'MPI family': Vale, Ralf 'Ralligalli', Paolo 'Justus', Ivan (e), Senor Cruz, Rakete Majd, Marius, Milena, Runyu, Ipek, Martin, Sandra, Jose, Martina, Nina, Alex, Steffen, Nikki, Jinyeon, Alessandro, Max, Ryan, Clemens, Bogdan, Guigang, Yubao, Qian, Jianrui, Amit, Marlies, Antje, Katharina, Heike, Irina, Ursula, Tobias, Nadja, Asad, Claudio, Tim, Jesus, Noah, Alessandro, Kook, Mike, Joao and many many more. Thanks Chez Briel for motivation and it was an honor being '*Barbeque Master*' for this period. Thanks Emrecan for friendship and support over 10 years.

Lastly, I would like to thank my mother, Mualla, for being with me and supporting me through my whole life. All these valuable moments we have spent together and all of these advices to make me better person. I'm really glad that you are my mother.